

FREIE UNIVERSITÄT BERLIN

DISSERTATION

**Field Theories of Interacting and Disordered
Dirac Fermions in Graphene**

*Zur Erlangung des akademischen Grades eines
Doktors der Naturwissenschaften*

*im Fachbereich Physik
der Freien Universität Berlin*

eingereichte Dissertation

von

Christian Fräßdorf

22. November 2018



Gutachter

Prof. Dr. Piet W. Brouwer (Freie Universität Berlin)

Prof. Dr. Felix von Oppen (Freie Universität Berlin)

Datum der Disputation: 22. März 2019



List of publications

This cumulative dissertation is based on the following first-author publications in order in which they appear in the thesis. My personal contribution to each paper is briefly explained, referring to myself in the third person as “the author” in the following.

- “*Keldysh functional renormalization group for electronic properties of graphene*”, C. Fräßdorf, J. E. M. Mosig, Phys. Rev. B **95**, 125412 (2017)
DOI: [10.1103/PhysRevB.95.125412](https://doi.org/10.1103/PhysRevB.95.125412)
The author was the main contributor of the publication. He conceptualized the study, performed all analytical calculations, was involved in the numerical solution of the equations, interpreted the data, and was responsible for the preparation of the manuscript and the response with the editors/referees.
- “*Chemical-potential flow equations for graphene with Coulomb interactions*”, C. Fräßdorf, J. E. M. Mosig, Phys. Rev. B **97**, 235415 (2018)
DOI: [10.1103/PhysRevB.97.235415](https://doi.org/10.1103/PhysRevB.97.235415)
The author was the main contributor of the publication. He conceptualized the study, performed all analytical calculations, was involved in the numerical solution of the equations, interpreted the data, and was responsible for the preparation of the manuscript and the response with the editors/referees.
- “*Abelian Chern-Simons theory for the fractional quantum Hall effect in graphene*”, C. Fräßdorf, Phys. Rev. B **97**, 115123 (2018)
DOI: [10.1103/PhysRevB.97.115123](https://doi.org/10.1103/PhysRevB.97.115123)
The author was the only contributor of the publication.
- “*Graphene pn junction in a quantizing magnetic field: Conductance at intermediate disorder strength*”, C. Fräßdorf, L. Trifunovic, N. Bogdanov, P. W. Brouwer, Phys. Rev. B **94**, 195439 (2016)
DOI: [10.1103/PhysRevB.94.195439](https://doi.org/10.1103/PhysRevB.94.195439)
The author and L. Trifunovic were the main contributors of the publication. The author performed the analytical calculations for the derivation of the effective one-dimensional model and was in equal parts with L. Trifunovic responsible for the preparation of the manuscript.

Publisher copyright:

<https://journals.aps.org/authors/transfer-of-copyright-agreement>

A second-author manuscript for a paper has been included in this dissertation with permission from the first author.

- “*Strong disorder in nodal semimetals: Schwinger-Dyson–Ward approach*”, B. Sbierski, C. Fräßdorf, arXiv:1808.09860v2, submitted to journal, peer review in progress
The author was involved in the conceptualization of the study, took part in the analytical calculations, and played an active role in the preparation of the manuscript and the response with the editors/referees.



Abstract

After its first isolation by Geim and Novoselov in 2004, graphene has grown quickly into an independent subfield of contemporary condensed matter physics, counting thousands of publications. This material has attracted so much attention not only because it is truly two-dimensional – a feature long thought to be impossible to be realized in nature – but also because it is the prime representative of a new class of condensed matter systems, the Dirac materials, whose electronic spectrum disperses linearly around isolated points in the Brillouin zone. An outstanding consequence of this linear energy-momentum dispersion is the collapse of the Fermi surface to isolated points at charge neutrality, accompanied by a vanishing single-particle density of states. While this feature of the noninteracting model is what separates graphene from most other, more conventional condensed matter systems, giving rise to many of its astounding physical properties, it leads to severe computational complications when extending the model to contain two-body interactions and/or disorder. In this thesis we consider both extensions separately.

After rigorously deriving the low-energy quantum field theory from a tight-binding model and establishing the one-particle irreducible (1PI) vertex functions as the fundamental building blocks of correlation functions, we construct a nonperturbative formalism for the calculation of these vertex functions using the well-established functional renormalization group (fRG). By combining the fRG with the Keldysh formalism, accounting for possible external electromagnetic fields and nontrivial initial correlations, this framework is capable of handling thermal equilibrium and true nonequilibrium alike. To circumvent some of the technical problems of the standard fRG formalism when treating fermionic systems at finite density, we also explore a variant of the fRG, where the chemical potential is interpreted as a flow parameter. We obtain hierarchical sets of flow equations, which describe the change of the 1PI vertex functions upon varying an artificial cutoff scale or the chemical potential, respectively. These nonperturbative formalisms have been used to calculate the renormalization of the Fermi velocity and the static dielectric function at finite temperature and density in the strong coupling regime as an explicit demonstration of their capabilities.

Since the Keldysh fRG is an exact formulation of quantum field theory, in particular when external magnetic fields are present, it should be possible to describe the fractional quantum Hall effect in this framework. However, the typical truncation schemes that are currently available to approximately solve the fRG flow equation fail to account for the nontrivial correlation effects necessary to access the fractional quantum Hall regime. To circumvent this problem we consider a modified field theory, where these correlations are implemented “by hand” via a Chern-Simons gauge field, coupling to the fermions in addition to the Coulomb interaction term. This modified field theory is analyzed in a stationary phase approximation including Gaussian fluctuations. The electromagnetic response tensor is calculated in the random phase approximation, yielding the Hall conductivities.

In the second part of this thesis we consider disordered Dirac fermions in the absence of two-particle interactions. After sketching how the most general disorder potential for Dirac fermions arises from a tight-binding model, we first consider an explicit physical scenario, a disordered graphene pn junction in the presence of a quantizing magnetic field perpendicular to the graphene sheet. We derive an effective one-dimensional theory for the chiral states that propagate along the junction interface and calculate the full conductance distribution in the crossover between the clean and the strong-disorder limit, via an exact solution of a Fokker-Planck equation. Lastly, we develop a nonperturbative approach to calculate the disorder induced self-energy that is based on exact Schwinger-Dyson equations and Ward identities, not only for graphene, but also for other paradigmatic semimetals with a nodal point dispersion.



Kurzbeschreibung

Seit der ersten Isolierung durch Geim und Novoselov im Jahr 2004 hat sich Graphene schnell in ein eigenständiges Forschungsfeld innerhalb der Physik der kondensierten Materie entwickelt, zu dem bereits Tausende von Publikationen zählen. Dieses Material hat große Aufmerksamkeit auf sich gezogen, nicht nur weil es echt zweidimensional ist – eine Besonderheit, die lange als unmöglich galt – aber auch weil es der erste Stellvertreter einer neuen Klasse von Materialien ist, deren elektronisches Spektrum linear um isolierte Punkte in der Brillouin Zone dispersiert, den Dirac-Materialien. Eine ungewöhnliche Folge der linearen Energie-Impuls Dispersion ist der Kollaps der Fermi-Fläche auf isolierte Punkte im ladungsneutralen Fall, begleitet von einer verschwindenden Zustandsdichte. Während es diese Eigenschaft des nichtwechselwirkenden Modells ist, welche Graphen von anderen, konventionellen kondensierten Materie Systemen unterscheidet, so führt sie zu schwerwiegenden Komplikationen bei der Berechnung physikalischer Observablen, sollte das Modell um Zweiteilchen-Wechselwirkungen und/oder Unordnung erweitert werden. In dieser Dissertation betrachten wir beide Fälle separat.

Nachdem wir die Niedrigenergie-Quantenfeldtheorie aus einem Tight-Binding-Modell abgeleitet und die Einteilchen-irreduziblen (1PI) Vertex-Funktionen als fundamentale Bausteine der Korrelationsfunktionen etabliert haben, konstruieren wir einen nicht-perturbativen Formalismus für die Berechnung eben dieser Vertex-Funktionen auf Basis der funktionalen Renormierungsgruppe (fRG). In Kombination mit dem Keldysh-Formalismus, erlaubt es dieser Formalismus sowohl Gleichgewichts- als auch Nichtgleichgewichtsprobleme zu behandeln. Um einige technische Probleme der fRG in ihrer Standardformulierung zu umgehen, die bei der Behandlung fermionischer Systeme bei endlicher Dichte auftreten, untersuchen wir auch eine Variation der fRG, bei der das chemische Potential als Flussparameter interpretiert wird. Wir erhalten hierarchische Gleichungssysteme, welche die Änderung der 1PI-Vertex-Funktionen unter Variation einer künstlichen Cutoff Skala beziehungsweise des chemischen Potentials beschreiben. Diese nicht-perturbativen Formalismen werden zur Berechnung der Renormierung der Fermigeschwindigkeit und der statischen dielektrischen Funktion bei endlicher Temperatur und Dichte im Regime starker Kopplung verwendet.

Da es sich bei der Keldysh-fRG um eine exakte Formulierung von Quantenfeldtheorie handelt, sollte es möglich sein mit ihrer Hilfe den fraktionierten Quanten-Hall-Effekt zu beschreiben. Mit den derzeitig verfügbaren Trunkierungsschemata gelingt es jedoch nicht die notwendigen nicht-trivialen Korrelationen mit einzubeziehen, um diesen Effekt zu beschreiben. Um dieses Problem zu umgehen betrachten wir eine modifizierte Feldtheorie, bei der diese Korrelationen “von Hand” durch ein Chern-Simons Feld implementiert werden, welches zusätzlich zur Coulomb Wechselwirkung an die Fermionen koppelt. Diese modifizierte Feldtheorie wird in Sattelpunktsnäherung mit Gauß’schen Fluktuationen analysiert. Es werden der elektromagnetische Response-Tensor, sowie die Hall Leitfähigkeiten berechnet.

Im zweiten Teil dieser Dissertation betrachten wir ungeordnete Dirac Fermionen in Abwesenheit von Zweiteilchen-Wechselwirkungen. Nachdem wir skizziert haben, wie das allgemeinste Unordnungspotential für Dirac Fermionen aus dem Tight-Binding-Modell hervorgeht, betrachten wir einen ungeordneten pn -Übergang in Anwesenheit eines magnetischen Feldes. Wir leiten eine effektive eindimensionale Theorie für die chiralen Zustände ab, welche entlang des Übergangs propagieren, und berechnen die volle Verteilung des Leitwerts mittels exakter Lösung einer Fokker-Planck-Gleichung. Zum Schluss entwickeln wir einen nicht-perturbativen Zugang um die unordnungsinduzierte Selbstenergie in Graphene und anderen paradigmatischen Semimetallen zu berechnen, welcher auf exakten Schwinger-Dyson-Gleichungen und Ward-Identitäten beruht.



Contents

1	Introduction	1
1.1	Dirac electrons in condensed matter	1
1.2	Fermi velocity renormalization	2
1.3	On the need for nonperturbative techniques	6
1.4	The fractional quantum Hall effect	10
1.5	Relativistic fermions in a random environment	17
1.6	Overview of this thesis	19
2	Electrons in graphene – A quantum field theory at low energies	33
2.1	Orbital hybridization of carbon, molecular bonding and the honeycomb lattice .	33
2.2	Tight-binding approximation for graphene	39
2.2.1	Tight-binding dispersion of noninteracting graphene electrons	40
2.2.2	The Dirac Hamiltonian	43
2.2.3	Interacting Dirac fermions	46
2.A	Appendix: Stability of Dirac cones and mass terms	51
3	Generating functionals – or how to organize the zoo of correlation functions	59
3.1	The partition function as a generator of correlation functions	59
3.2	Connected correlation functions and their generating functional	68
3.3	Effective action, vertex functions and the tree expansion of connected correlators	71
3.A	Appendix: Diagrammatic derivation of the tree expansion	79
4	Coulomb interactions in graphene	83
4.1	Paper: “ <i>Keldysh functional renormalization group for electronic properties of graphene</i> ”	85
4.2	Paper: “ <i>Chemical-potential flow equations for graphene with Coulomb interactions</i> ”	109
4.3	Paper: “ <i>Abelian Chern-Simons theory for the fractional quantum Hall effect in graphene</i> ”	121
5	Disordered Dirac fermions	143
5.1	Statistical field theory and disorder	143
5.2	A matrix-valued disorder potential	147
5.3	Paper: “ <i>Graphene pn junction in a quantizing magnetic field: Conductance at intermediate disorder strength</i> ”	151
5.A	Appendix: Manuscript: “ <i>Strong disorder in nodal semimetals: Schwinger-Dyson–Ward approach</i> ”	163
6	Conclusions	179

Chapter 1

Introduction

1.1 Dirac electrons in condensed matter

When in 1947 P. R. Wallace wrote an article on “The Band Theory of Graphite” [1] probably nobody would have believed that his findings in the introductory sections would have such a profound impact on modern-day condensed matter physics. As the title suggests, he was more concerned about the three-dimensional material graphite, rather than the single-atom thick layers from which it is made of. The investigation of these layers, which became later known as graphene, was merely a necessary intermediate step, preliminary to the analysis of graphite. The unconventional linear energy spectrum he found at the corners of the hexagonal Brillouin zone, accompanied by an unusual semimetallic behaviour, was mainly of theoretical interest, as physicists believed that an isolation of that two-dimensional material would be impossible. This belief was only reinforced when the famous Mermin-Wagner theorem was proved in the 1960’s [2–4]. The theorem essentially states that at any finite temperature there can be no spontaneous breakdown of a continuous symmetry in less than three dimensions. Hence, crystalline long-range order as the very basis for the formation of any lattice – including the honeycomb lattice – seemed to be prohibited. In light of the prevailing skepticism and prejudices at the time whether the isolation of graphene would be possible at all, further research on that material was deemed of academic value only and not much progress has been made in the following years. However, graphene is not a truly two-dimensional system, but merely a surface embedded in three-dimensional space. While the electrons are confined to the surface, the electromagnetic interactions are not. In addition, fluctuations in the displacements of the atoms normal to the surface stabilize the underlying lattice, see *e.g.* Refs. [5–8]. Nevertheless, it took almost 60 years from the early work of Wallace to overcome these prejudices, resulting in the first experimental isolation by Geim and Novoselov in 2004 [9–11]. This breakthrough entailed an enormous increase in the theoretical and experimental interest for this newly available material, still continuing to this day.

The fascination for graphene is based on several aspects, one of which being its outstanding role in the field of carbon based materials. Without exaggeration one might say that it lies at the heart of the research revolving around such materials, being the prime representative of a whole microcosmos of structures (Fig. 1.1). It can be stacked into bi-, tri- and multilayers, folded into nanotubes, curled up into buckyballs and “chemically stretched” into various graphynes [14–17]. Thus, a proper understanding of graphene is the key to the universe of carbon allotropes. Probably the most important aspect of graphene, responsible for the enormous interest in the physics community, is its bandstructure. In contrast to conventional metals and semiconductors, noninteracting graphene electrons obey a gapless and linear energy-momentum

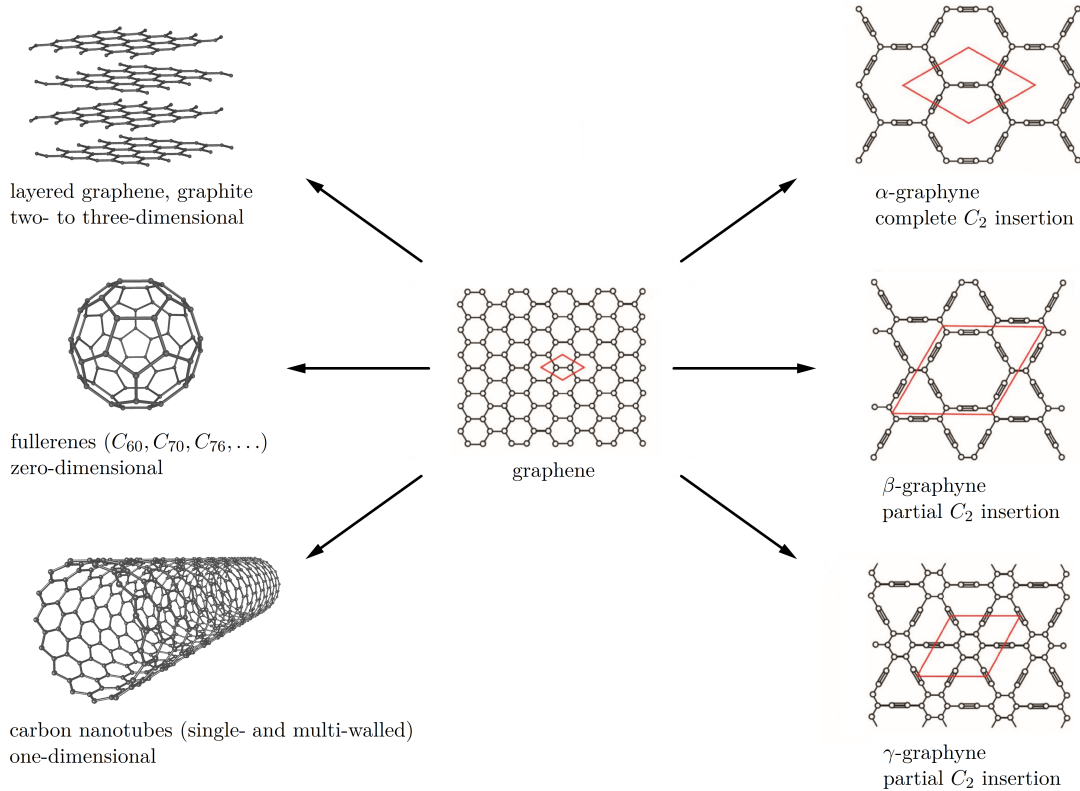


Figure 1.1: Allotropes of carbon with graphene as the central structure. The structures on the left-hand side can be constructed “mechanically” from graphene by stacking, or cutting-out a strip and curling it up into a cylindrical or ball shape, respectively. The structures on the right-hand side require chemical processing, where triple-bonded C_2 molecules are inserted completely (α -graphyne) or partially (β, γ -graphynes) into the honeycomb lattice. For graphene and the graphynes the unit cell of the lattice is indicated in red. This figure was inspired by a similar figure in Ref. [12], and created using figures from Refs. [13, 14].

dispersion at the two inequivalent corners of the hexagonal Brillouin zone, mimicking the behavior of massless relativistic Dirac particles in a condensed matter environment [1, 18–21]. As far as condensed matter systems are concerned, this rather unconventional spectrum has far-reaching implications on observable physical effects [22–26]. In fact, the investigated phenomena of graphene’s fascinating mechanical and electronic properties pervade the whole body of condensed matter physics, ranging from phonons and superconductivity [27–31] over integral and fractional quantum Hall effects [32–38], elastic strain and artificial gauge fields [39–41], disorder and defects [42–46], to a condensed matter simulation of QED_{2+1} and Dirac fermions in curved spaces [19, 39, 47, 48]. The unprecedented diversity of this (incomplete) list of topics and publications, its status as the prototype of a Dirac material in condensed matter and its central role in the study of carbon allotropes make graphene an extraordinary playground for fundamental and application-oriented research alike.

1.2 Fermi velocity renormalization

The ultimate goal of condensed matter theory – as of any other physical theory – is to describe physical reality. It should be clear, however, that a fully microscopic treatment of a generic

condensed matter system, based on first principle quantum theory, is hopeless, simply due to the overwhelmingly large number of microscopic degrees of freedom one would have to keep track of. To overcome this problem, there are in principle two very distinct strategies to pursue: Either one uses the microscopic theory as the starting point for a series of (hopefully justified) approximations until one arrives at a tractable model or one may straightaway describe the physical effects by a phenomenological model. In either case some information is lost, but the relevant degrees of freedom that characterize the system should be captured appropriately.

The outstanding feature of graphene that sets it apart from other, more conventional condensed matter systems – the pseudo-relativistic energy momentum dispersion of its quasiparticle excitations – is the result of a rather crude approximation, where the effect of Coulomb interactions between its quasiparticles is neglected. Of course, Coulomb interactions are not neglected entirely, since they are essential for the formation of the honeycomb lattice in the first place. Without Coulomb interactions there would be no lattice, and without a lattice there would be no pseudo-relativistic electrons, but their contribution to the model is restricted to the mean-field level only.¹ Correlation effects beyond the mean-field level, which is what we mean when we use the term “Coulomb interactions”, are absent. Yet, there are many instances in various condensed matter systems, where these correlation effects have been proven to play an important role in explaining physical effects. Probably the most prominent example is the fractional quantum Hall effect, which exists only because of inter-electron interactions (see Sec. 1.4 for a more detailed discussion). A lesser known example is the disorder-induced breakdown of superconductivity [49–53]. Here, the interplay of Coulomb interactions, BCS interactions and disorder is responsible for the suppression of the critical temperature in a regime that would be protected by Anderson’s theorem [54], if Coulomb interactions were absent. Lastly, the transport properties of a one-dimensional Luttinger liquid are heavily influenced by long range (Coulomb) interactions, since – among others – they lead to a strong renormalization of the propagation velocity of the quasiparticles [55, 56]. Therefore, it is only reasonable, if not to say inevitable, to estimate the influence of the Coulomb interaction on the pseudo-relativistic spectrum of graphene’s electrons and to determine under which circumstances, if at all, it is justified to neglect it.

The first instinct to gain some intuition about to-be-anticipated effects is of course to compare the system under consideration to preexisting calculations in theories that have a similar structure. For the present problem of interacting Dirac electrons in graphene, what would be closer than relativistic quantum electrodynamics? The theory, that describes the interactions of electrons and light and which has been validated time and time again with unprecedented accuracy. Here, the dynamics of electrons (and positrons) is described by the massive Dirac equation and the electromagnetic interaction is mediated by a massless vector boson – the photon – that obeys Maxwell’s equations. The Lorentz and gauge invariance of the theory put very tight constraints on the form of the correlation functions. Most notably, the vanishing rest mass of the photon is unaffected by renormalization. The polarization tensor instead leads to a renormalization of the electronic charge, which is tightly intertwined with the electron mass renormalization, coming from the fermionic selfenergy, and the vertex renormalization through Ward identities – the latter being the analogon of Noether’s theorem in a quantum field theory. Measuring mass, charge and field strengths at a certain renormalization scale removes the ultraviolet divergencies from scattering amplitudes of the theory, rendering the theory itself predictive [57–59].

Although the theory of interacting electrons in graphene and relativistic quantum electrody-

¹In fact, most if not all effective models in condensed matter theory contain the effect of a mean-field Coulomb potential disguised somewhere in their model parameters.

namics share many features, both structurally and physically, their seemingly minor differences lead to vastly different predictions. As is well-known, in graphene the low-energy dynamics of electron-like (and hole-like) quasiparticles is described by a Dirac equation as well, but here the mass term vanishes (unless it is spontaneously generated by chiral symmetry breaking, see Sec. 1.3). Borrowing the notions of *QED*, one can say the quasiparticles behave “ultra-relativistically”, propagating with the Fermi velocity v_F instead of the much larger speed of light c . The Coulomb interaction is mediated by a massless scalar boson, after decoupling the fermionic interaction in the density-density channel that is. In stark contrast to relativistic *QED*₂₊₁, however, the theory of interacting Dirac electrons in graphene is neither Lorentz invariant nor a gauge theory. (There is still a continuous $U(1)$ phase symmetry corresponding to charge conservation, but the bosonic field is not a gauge field.) In fact, the Lorentz invariance of the noninteracting model with respect to the Fermi velocity is strongly broken, due to the fact that the bare Coulomb interaction propagates instantaneously [60, 61]. In a sense it is “hyper-relativistic” in comparison to the ultra-relativistic behaviour of graphene’s quasiparticles. Dynamical retardation effects are only introduced through the polarization function, which also includes the physics of screening and collective plasmon excitations [61–65]; see the discussion in the next section. Hence, there is no reason to believe that the linear energy-momentum dispersion of the noninteracting quasiparticles would be preserved under renormalization. On the contrary, instead of mass and charge renormalization, it is the Fermi velocity that acquires momentum-dependent corrections, which are typically of a logarithmic form as a generic feature of quantum field theory. By performing a simple one-loop calculation, such a logarithmic correction has indeed been obtained in the early work of González *et al.* [60], predicting a logarithmic increase of the Fermi velocity in the infrared regime at charge neutrality. Recently, this feature has been observed in an experiment performed by Elias *et al.* [66], which clearly showed the importance of Coulomb correlation effects beyond a mean-field approximation in real-world samples and which seemed to confirm the one-loop picture.

The validity of a perturbative approach is of course limited to the weak coupling regime and even then it is fundamentally constrained to low orders only. (For an explanation of the latter statement see Sec. 1.3.) While in quantum electrodynamics the dimensionless interaction strength given by the fine structure constant α_{QED} is indeed very small, $\alpha_{QED} \approx 1/137$, in graphene it depends on the background dielectric constant ϵ_0 , $\alpha_G = e^2/\epsilon_0 v_F \approx 2.2/\epsilon_0$, which accounts for the substrate’s influence on the inter-electron interaction. There are substrates for which $\epsilon_0 \gg 1$, justifying perturbation theory, but the experimentally most relevant substrates, such as *SiO*₂ and *SiC* ($\epsilon_0 \approx 2.5$) or even the extreme case of freestanding graphene ($\epsilon_0 = 1$), lead straight into the strong coupling regime, $\alpha \gtrsim 1$ [61]. Clearly, any result obtained within a perturbative framework, such as the increase of the Fermi velocity suggested by one-loop perturbation theory, cannot be extrapolated into such a regime. Yet, the aforementioned experiment of Elias *et al.* has been performed for suspended graphene, such that the reported agreement with the perturbative result is very surprising. To resolve this issue nonperturbative methods have to be applied in such extreme conditions.

A naive way to extend perturbation theory into a nonperturbative framework is to employ resummation techniques, which give access to the strong coupling regime. As an example recall that the very concept of the self-energy is nonperturbative, based on the resummation of interaction corrections to the bare propagator as a geometric series [57–59, 67]. It is therefore not unreasonable that a similar strategy may be employed for an actual calculation of the self-energy and related quantities beyond perturbation theory. Such an approach, however, has one serious drawback. Typically, resummation techniques rely on low-order perturbation theory, where it is rather easy to analyze the structure of the diagrams order by order. In a next step, based on

the observations of the topological structure of the diagrams, the corresponding mathematical expressions are elevated to self-consistency equations, which contain contributions to all orders in perturbation theory. Since the self-consistency equations obtained by such an approach are not much more than an educated guess, they are open to systematic errors. The main problem is that low-order perturbation theory is likely to be misleading. Perturbative structures may be falsely categorized and wrongfully generalized to nonperturbative structures, and/or certain classes of diagrams may be missing or overcounted.² Even if a set of equations is found, where it could be proven that no counting errors occur, it would be rather difficult to go beyond such an approximation in a consistent and systematic way. These problems are amplified if higher level correlation functions are considered. For a specific example that illustrates these statements see the discussion in Sec. 1.5.

One of the more systematic nonperturbative methods is given by the set of self-consistent Schwinger-Dyson (SD) equations [58, 67–70]. This theoretical framework consists of an infinite hierarchy of coupled integral equations for the one-particle irreducible (1PI) vertex functions – the fundamental building blocks of n -point correlation functions. These equations resum all possible Feynman diagrams without resorting to a small expansion parameter and they are by construction free of the above systematic errors. In practice however, it is inevitable to break the hierarchy by truncating it at some finite level, which neglects certain diagrammatic contributions. Nevertheless, even a finite set of Schwinger-Dyson equations for the leftover vertices resums whole classes of diagrams without counting errors. For an application of this method in relativistic QED_{2+1} see Refs. [71, 72] and for graphene with Coulomb interactions see Ref. [73]. An alternative nonperturbative approach, that has become popular in recent years, is the functional renormalization group (fRG) [68, 74–88]. It shares some features with the celebrated Wilsonian renormalization group, but rigorously extends the concept of flowing coupling constants to 1PI vertex functions. This method features an infinite hierarchy of coupled integro-differential equations, which are closely related to the SD equations. So close in fact, that the fRG flow equations for the vertices can be interpreted as a differential form of the SD equations. The first application of the Matsubara fRG formalism to graphene has been worked out by Bauer *et al.* [89]. They studied the renormalization of the Fermi velocity and the static dielectric function at the charge neutrality point and zero temperature, finding excellent agreement with the experiment of Elias *et al.*, see Fig. 1.2. See also Ref. [90], which combines both methods, SD and fRG, to complement each other.

Albeit an impressive demonstration of the capabilities of these nonperturbative formalisms, this agreement should be taken with a grain of salt. While the theoretical calculation has been performed at zero density, resulting in a purely momentum dependent Fermi velocity, in the experiment of Elias *et al.* the logarithmic increase of the Fermi velocity was observed as a function of the charge carrier density. Strictly speaking, these two velocity functions cannot be compared directly, since they are different aspects of a more general velocity function, that is a function of momentum, chemical potential and temperature.³ Hence, it would be premature to claim that the electronic properties of graphene are fully understood. A solution of this particular problem is of fundamental importance, since many of graphene’s fascinating physical

²As a matter of fact, the representation of the exact, nonperturbative equations for the self-energy and related quantities is not unique, as there is more than one consistent framework. They all calculate the same quantities, but the structure of the individual equations differ. By trying to guess the form of the exact equations through perturbative calculations one might mix two different frameworks unknowingly and end up with inconsistencies.

³To be precise, Elias *et al.* extracted the carrier density dependence of the Fermi velocity from a measurement of the effective cyclotron mass through the temperature dependence of Shubnikov-de Haas oscillations. Since such a measurement requires nonvanishing external magnetic fields, momentum is not even a well-defined quantum number in this case.

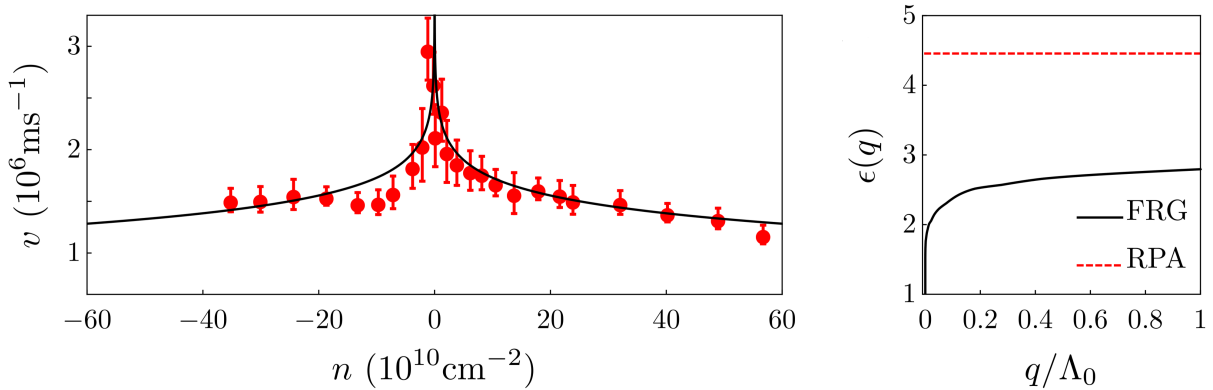


Figure 1.2: (Left) Renormalization of the Fermi velocity induced by Coulomb interactions as a function of charge carrier density n . The red dots including error bars are the experimental data of Elias *et al.* [66], and the black curve is the theoretical fit to these data, obtained by an fRG calculation at charge neutrality and zero temperature of Bauer *et al.* [89]. (Right) Static dielectric function as a function of momentum. Note that the one-loop approximation yields a trivial constant, while the fRG result logarithmically approaches unity for small momenta, due to the logarithmic divergence of the renormalized Fermi velocity. Pictures taken from Ref. [89].

effects can be directly traced back to its spectral properties near charge neutrality. Without a doubt, the prospect of possible technological applications that rely on those properties is more than enough motivation to push the boundaries of currently existing studies and to resolve this issue eventually.

1.3 On the need for nonperturbative techniques

Up until this point the use of nonperturbative techniques was mainly motivated by a strong coupling regime, where perturbative techniques cannot be applied for obvious reasons. In this section we argue that such techniques are not only superior to perturbation theory and should be applied even in a regime where a perturbative treatment seems to be viable, but also that there is a fundamental necessity to do so. To substantiate these statements we briefly discuss two physical examples. Afterwards we elaborate on the mathematical foundation of perturbation theory, or rather the lack thereof, on general grounds.

Our first example is the celebrated BCS theory of s -wave superconductivity [91–93]. For simplicity let us focus on the zero-temperature case for the moment. The BCS interaction term describes a net attraction between two electrons of different spin polarization, leading to an instability of the Fermi liquid ground state. Although the interaction strength λ is typically rather small, it is impossible to describe the superconducting ground state as a perturbation to the Fermi liquid ground state. Due to the Cooper-instability there simply is no Fermi liquid ground state. In the standard treatment of BCS theory one performs a Hubbard-Stratonovich transformation of the interaction term, integrates the fermionic fields and subsequently performs a stationary phase approximation for the effective bosonic action of the Hubbard-Stratonovich field. With this approach one is able to calculate a gap equation for the superconducting order parameter Δ , whose solution is of the form $\Delta \sim e^{-1/\lambda}$ [91–93]. This function has an essential singularity at the origin $\lambda = 0$, that means approaching the origin from the positive real axis yields zero and approaching the origin from the negative real axis yields infinite. The radius of convergence of the Taylor series around $\lambda = 0$ vanishes identically and any finite-order Taylor

expansion of this function would either yield identically zero or infinity. In other words, it is inaccessible through perturbation theory, so is the energy gap and so is superconductivity. As an extension of the standard BCS theory consider a more realistic model, where an additional disorder potential and the Coulomb interaction term are present. In particular let us consider the aforementioned suppression of the critical temperature in a weakly disordered superconductor due to Coulomb interactions. To determine the influence of disorder on the critical temperature one has to calculate the Cooper channel polarization bubble. In a calculation where the vertex correction due to Coulomb interactions is taken into account to lowest order perturbation theory, one finds – as expected – a small correction to the bare bubble [94–97]. Here, the small parameter is related to weak disorder, so it seems to be a viable strategy to use perturbation theory to calculate the disorder dependence of the critical temperature. However, the suppression of the critical temperature as a function of disorder strength one obtains from the bubble correction does not match the experiment [49–51]. Higher orders in the vertex correction, where an increasing number of virtual Coulomb-scattering processes is taken into account, approximate the experimental measurement better and better, but the critical temperature always remains finite. The complete breakdown of superconductivity at a finite but small disorder strength as observed in the experiment can only be obtained theoretically by going beyond perturbation theory [52, 53].

For the second example we want to come back to Coulomb interacting graphene, but this time we focus on a quantity we have not yet discussed in detail, the dielectric function, see Fig. 1.2. This function encodes the spectrum of collective plasmon excitations and it plays an important role in the theory of interacting Dirac fermions by renormalizing the bare Coulomb interaction. It can be derived from the polarization function mentioned earlier, which is calculated by a bubble diagram involving two fermionic propagators. To lowest order perturbation theory the fermionic propagators are the bare ones, where only the unrenormalized Fermi velocity enters [61–65]. At higher orders the renormalization of the Fermi velocity has to be taken into account, whose calculation involves the renormalized Coulomb interaction itself. So the renormalization of the Fermi velocity influences the renormalization of the Coulomb interaction and vice versa, which leads to a feedback loop that goes on ad infinitum, irrespective of the fact whether the coupling constant is strong or weak. Hence, a set of nonperturbative self-consistency equations is required to describe the full feedback correctly [89, 90]. Even if this feedback is not implemented into the theory completely – for example by treating the interaction corrections to the bosonic propagators perturbatively, while only retaining a nonperturbative equation for the fermionic propagator as done in Refs. [71–73] – particularly interesting physical effects can be studied that are beyond any finite order perturbation theory. The specific example studied in Refs. [71–73] is chiral symmetry breaking through dynamical mass generation. As was shown there, the interaction induced mass/gap is a nonanalytic function of the coupling constant/number of fermionic flavours just like the BCS gap, such that any finite order perturbation theory could not detect this feature.

With these physical examples in mind let us see why naive perturbation theory in powers of a coupling constant is fundamentally flawed. To this end we analyze the function $Z(\lambda, J)$ defined by the integral

$$Z(\lambda, J) = \int_{-\infty}^{+\infty} d\phi e^{-\frac{1}{2}\phi^2 - \lambda\phi^4 + \phi J}. \quad (1.3.1)$$

This integral is a toy model for the generating function of a zero-dimensional bosonic field theory, where λ is the aforementioned coupling constant and J is a source used to generate the moments of the probability distribution $e^{-\frac{1}{2}\phi^2 - \lambda\phi^4}$. Here, we mainly summarize some important aspects in the analysis of this function. For more details we refer to Refs. [98–101]. For a purely imaginary

source the generating function is the Fourier transform of the probability distribution,⁴ while for a purely real source it is the two-sided Laplace transform. Without loss of generality we assume $\text{Im}(J) = 0$. In general the coupling constant can be a complex number, but for now we focus on its real part only. It should be obvious, that the integral defining the generating function strongly diverges for $\lambda < 0$ irrespective of the value of the source J , whereas it converges for $\lambda \geq 0$ for any value of the source. In the latter case the generating function is analytic in the source. We can therefore expand it in a power series

$$Z(\lambda, J) = \sum_{n=0}^{\infty} \frac{1}{n!} Z^{(n)}(\lambda) J^n, \quad (1.3.2)$$

where $Z^{(n)}(\lambda) \equiv \left. \frac{\partial^n Z(\lambda, J)}{\partial J^n} \right|_{J=0}$ are the λ -dependent moments of the probability distribution. For this simple toy model the moments can be evaluated exactly in terms of special functions

$$\begin{aligned} Z^{(n)}(\lambda) &= \int_{-\infty}^{+\infty} d\phi \phi^n e^{-\frac{1}{2}\phi^2 - \lambda\phi^4} \\ &= 2^{-\frac{1}{2}(n+3)} (1 + (-1)^n) \lambda^{-\frac{1}{4}(n+1)} \Gamma\left(\frac{n+1}{2}\right) \Psi\left(\frac{n+1}{4}, \frac{1}{2}, \frac{1}{16\lambda}\right), \end{aligned} \quad (1.3.3)$$

where $\Gamma(z)$ is the Gamma function and $\Psi(\alpha, \gamma, z)$ is a confluent hypergeometric function, see Eq. (9.211.4) in Ref. [103]. The latter function has a well-defined analytic continuation to the sliced complex plane, with a branch cut along the interval $z \in (-\infty, 0)$. In the remainder of this section we focus on the zeroth order term of the expansion (1.3.2), which is nothing but the partition function $Z(\lambda, J = 0) = Z^{(0)}(\lambda) \equiv Z(\lambda)$. The features we will discuss below are representative for the finite moments. In that special case the confluent hypergeometric function is related to the modified Bessel function of the second kind $K_\alpha(z)$, yielding $Z(\lambda) = \frac{1}{2\sqrt{2\lambda}} e^{\frac{1}{32\lambda}} K_{\frac{1}{4}}\left(\frac{1}{32\lambda}\right)$, Eqs. (3.469.1) and (8.485) Ref. [103]. This form of the partition function highlights the fundamental flaw of perturbation theory, as it contains a factor of $e^{1/\lambda}$ we encountered before. The remaining factors, involving the modified Bessel function and the inverse square root of the coupling, tame the essential singularity at the origin, but the nonanalytic features remain. In fact, they become even worse, since the inverse square root introduces the branch cut along the negative real axis.

Now let us see what happens, if despite these facts we apply the standard routine of perturbation theory to the partition function, assuming λ to be small. In the standard perturbative treatment of the integral (1.3.1) one would separate the kinetic term, proportional to ϕ^2 in the exponent, from the interaction term, proportional to ϕ^4 . The exponentiated quartic term would be expanded in a Taylor series and the order of integration and summation would be interchanged. We are left with a simple calculation of the moments of a Gaussian probability distribution, leading to the series representation

$$\begin{aligned} Z(\lambda) &= \int_{-\infty}^{+\infty} d\phi e^{-\frac{1}{2}\phi^2 - \lambda\phi^4}, \\ &= \int_{-\infty}^{+\infty} d\phi e^{-\frac{1}{2}\phi^2} \sum_{n=0}^{\infty} \frac{(-\lambda\phi^4)^n}{n!} \\ &= \sum_{n=0}^{\infty} (-1)^n \frac{\sqrt{2\pi}(4n)!}{2^{2n}(2n)!n!} \lambda^n \end{aligned} \quad (1.3.4)$$

⁴In that case the moment generating function would actually be called characteristic function [102], but we do not make a distinction here.

So far each step seems to be viable, but the last equality is actually incorrect. Due to the branch cut of $Z(\lambda)$ along the negative real axis the order of integration and summation must not be interchanged. Since we ignored that fact, the radius of convergence of the power series is identically zero, such that for any positive finite value of the coupling the series is at best asymptotic. If we were only given the series representation of $Z(\lambda)$, without already knowing about the branch cut, we could deduce the asymptotic divergence just as easily. To this end consider sufficiently large orders n of the power series. Then we may use Stirling's formula to estimate the growth rate of its coefficients $\frac{\sqrt{2\pi}(4n)!}{2^{2n}(2n)!n!} \approx \sqrt{\frac{2}{n}} \left(\frac{n}{e}\right)^n 4^{2n}$. (In a realistic field theory this huge number corresponds to the rapidly increasing number of perturbative Feynman diagrams.) Now it is an elementary exercise to prove that the sum diverges. No matter how small the coupling constant, the complete perturbative series will diverge, since consecutive terms grow too quickly. The alternating factor $(-1)^n$ delays the onset of the divergence, but only for the first few partial sums. A physically intuitive picture why such power series diverge was put forward by Dyson for the theory of quantum electrodynamics already in 1952 [104]. The same arguments apply for our toy model and pretty much any other quantum field theory as well. He argued that the vacuum state would be unstable if the sign of the fine-structure constant would be reversed. The energy could be lowered indefinitely by creating more and more particles, which is unphysical. In the end, his arguments led to the same conclusion. A power series in terms of the fine-structure constant cannot be analytic and thus not convergent.

Admittedly, the above arguments paint a very bleak picture of perturbation theory, but it is not as bad as one might think. If one would consider a truncated power series, that is cut off at a certain order N ,

$$Z_N(\lambda) = \sum_{n=0}^N (-1)^n \frac{\sqrt{2\pi}(4n)!}{2^{2n}(2n)!n!} \lambda^n, \quad (1.3.5)$$

it is possible to obtain excellent approximations to the exact result as long as the coupling is sufficiently small and N does not exceed a critical value. To illustrate this rather unexpected, almost miraculous behavior, we compared the exact result of the partition function with the first few orders of the truncated perturbation series (1.3.5) in Fig. 1.3. Since the critical order at which the truncated series actually starts to diverge from the exact result is rather large, it is unlikely to encounter the asymptotic divergence when performing perturbative calculations for realistic models. Even though we typically do not have the luxury of an exact solution to compare or estimate when a truncated perturbation series should be stopped, the first few orders of perturbation theory should be safe. Due to this fact, and because of the possibility to use resummation methods to gain access to the nonperturbative regime as explained earlier in Sec. 1.2⁵, perturbation theory is at least partially remedied and certainly has its value. In any case, the analysis of our toy model has shown that all the problems arise from the nonanalyticity of the partition function in the complex plane and our ignorance about that fact when we tried to organize a perturbation expansion in powers of the coupling constant around zero. So, loosely speaking, as long as we stay away from this essential singularity we should be safe from an asymptotic divergence. This is precisely the approach taken by the manifestly nonperturbative techniques, such as Schwinger-Dyson equations and the functional renormalization group. Here, one does not need to assume anything about the magnitude of the coupling constants and the typical truncation schemes yield highly nonlinear integral or integro-differential equations, which

⁵In addition to those resummation methods, there are other mathematical resummation methods which can extract finite results from such asymptotic series, for example by Borel summation or Kleinert's variational perturbation theory. While the former method attempts to construct a converging series from the coefficients of the asymptotic series, the latter method transforms the diverging weak-coupling series into converging strong-coupling series. See Refs. [98, 99, 105] for more details.

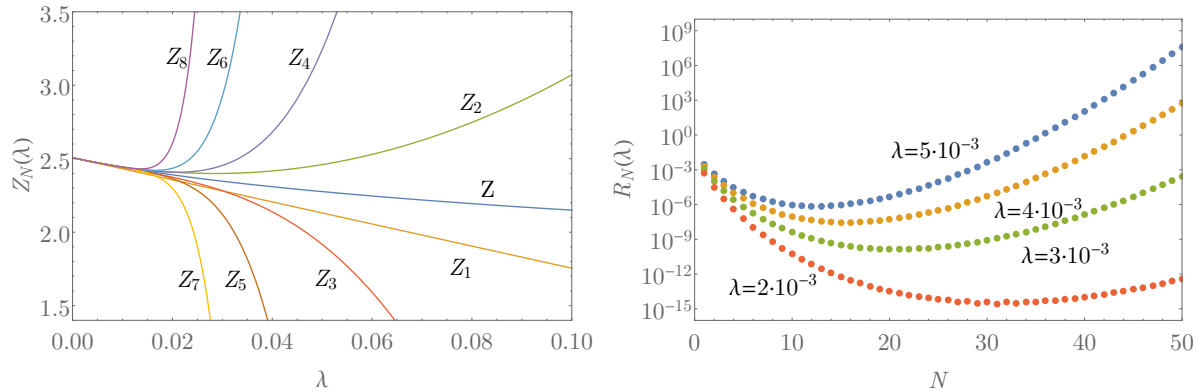


Figure 1.3: (Left) Exact result for the partition function $Z(\lambda)$, Eqs. (1.3.2) and (1.3.3), as well as the first eight orders of the asymptotic series $Z_N(\lambda)$, Eq. (1.3.4), as functions of the coupling constant λ . The behaviour of the moments is similar and not shown explicitly. (Right) Residual error $R_N(\lambda) = |Z(\lambda) - Z_N(\lambda)|$ for different values of the coupling constant as a function of the order N . For small values of the coupling constant perturbation theory can approximate the exact result very well, if stopped at an early stage. The perturbative order at which the optimal approximation is obtained depends on the coupling constant, shifting towards larger orders the smaller the coupling.

already implement some sort of resummation.

1.4 The fractional quantum Hall effect

Before we dive into the quantum theory of electrons moving in the presence of external magnetic fields let us briefly recall some of the predictions a classical treatment of that problem has to offer [106–110]. Classically, an electron is regarded as a point charge following a well-defined trajectory. The Lorentz force, acting perpendicular to both the magnetic field vector and the velocity vector of the moving charge, forces it into a circular cyclotron orbit. Applying an additional bias voltage in, say, the x -direction causes the electrons in a two-dimensional sample to be deflected into the y -direction (assuming the magnetic field points in the z -direction, perpendicular to the plane of the sample). This deflection results in a voltage drop across the width of the sample, the Hall voltage, that can be measured easily. The Hall voltage is directly proportional to the magnetic field, causing the Hall resistance – the quotient of Hall voltage and current – to be directly proportional to the magnetic field as well. Based on this classical analysis, when measuring the Hall resistance in an actual experiment as a function of the external magnetic field one would expect to see a simple linear behaviour. For small magnetic fields and large temperatures this classical expectation matches the experiments. However, the low-temperature experiments of von Klitzing published in 1980 painted a very different picture when the magnetic fields were tuned to large enough values [111]. He observed several plateaus, which became more and more pronounced for increasing values of the magnetic field, following a simple and extraordinarily precise quantization rule, see Fig. 1.4. This observation, for which he was ultimately awarded the Nobel prize in physics, is in strong contradiction to the classical prediction, requiring a fully quantum mechanical treatment of the problem.

Upon treating the electron as a quantum mechanical object, which obeys the Schrödinger equation, the trajectory concept of classical mechanics loses its meaning. Free electrons are described by plane waves or wave packets, with an associated momentum quantum number. As

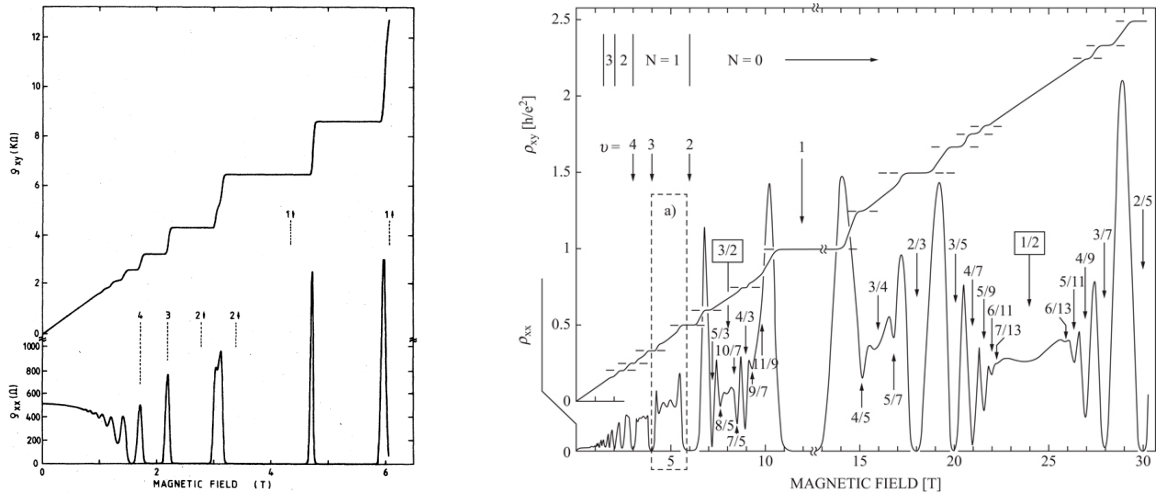


Figure 1.4: Diagonal resistivity ρ_{xx} and Hall resistivity ρ_{xy} of a GaAs/AlGaAs heterostructure as a function of the external magnetic field. (Left) Measurement of the integer quantum Hall effect. For small values of the magnetic field, $B \lesssim 1\text{T}$, the Hall resistivity increases linearly as expected from the classical analysis, whereas for larger magnetic field strengths, $B \gtrsim 1\text{T}$, the plateau structure mentioned in the main text emerges. Picture taken from Ref. [112], see also Ref. [113]. (Right) Measurement of the fractional quantum Hall effect. Again, the Hall resistivity increases linearly as a function of the magnetic field, but improvements on the sample quality and measurement techniques reveal new plateaus at certain fractional values of the filling, in addition to the known integer fillings. Note that the plateaus of the integer quantum Hall effect of the left measurement do not appear at the same numerical value of the external magnetic field. A possible explanation is that the samples used for the left and right experiments have slightly different carrier densities. Picture taken from Ref. [114].

soon as the electronic system is subjected to an external magnetic field its spectrum and physical properties change drastically. The energy eigenvalues are no longer continuous functions of a momentum quantum number, simply because “momentum” is not a well-defined concept for quantum mechanical particles in magnetic fields. Instead, the spectrum collapses to highly degenerate discrete energy levels, called Landau levels, featuring equidistant energy gaps between two successive levels [115–118]. As a consequence there is only a single cyclotron resonance – a dipole transition from the n -th to the $(n + 1)$ -st Landau level – which may be observed in a transmission spectroscopy experiment [112, 116]. For the degeneracy of the Landau levels as well as their energetic separation one finds a linear dependence on the magnetic field. Quite remarkably, these features of the noninteracting model are (almost) sufficient to explain the exact integer quantization of the Hall resistance found by von Klitzing [112, 116, 118]. Whenever the filling of the spectrum, controlled by either the strength of the external field or a gate voltage, is such that the Fermi level lies in the gap between two Landau levels – meaning that an integer number of Landau levels is occupied – the Hall resistance/conductance shows a plateau. The missing piece to fully explain the quantum Hall effect is disorder. In a nutshell, for the Fermi level to lie in between two successive Landau levels there have to be states, which can be occupied by the electrons, but which do not contribute to the conductivity. Disorder leads to a broadening of the otherwise sharp Landau levels due to degeneracy breaking, and it provides such localized states in the “tails” of the broadened levels [112, 116, 118]. To quote Tong: “There’s a wonderful irony in this: the glorious precision with which these integers ν are

measured is due to the dirty, crappy physics of impurities.” [118].⁶

In light of renormalization theory one may wonder how “stable” these predictions are, once Coulomb interactions are taken into account. As we have discussed in the previous section, using the example of the Fermi velocity in graphene, interaction terms typically alter the features and predictions of a noninteracting theory. For the present case of a two-dimensional electron gas in a magnetic field one might expect that the single cyclotron resonance will be renormalized, or perhaps the equidistance of the Landau levels may be broken, such that more than one resonance could be observed. It turns out however that this is not the case, due to Kohn’s theorem [121]. Albeit this highly nontrivial result may come as a surprise, Kohn’s theorem admits a very intuitive physical interpretation: if all electrons collectively perform a cyclotron motion, their mutual interactions cancel each other and, hence, do not matter. As a result, the noninteracting model is an even better description of the integer quantum Hall regime than the naive expectation would suggest.

The linear energy-momentum dispersion in a (pseudo-)relativistic electron system has some rather dramatic consequences on the Landau level structure. In sharp contrast to Schrödinger theory, relativistic Landau levels are not equidistantly separated, since their dispersion involves the square root of the Landau level index n [21, 38]. This feature leads to a multitude of cyclotron resonances, which depend explicitly on n , becoming more and more dense the higher the level index [122, 123]. Furthermore, since Kohn’s theorem requires Galilei invariance, it does not apply in graphene, such that these resonances are not protected from renormalization through electron-electron interactions [38, 124–128]. Lastly, the spectrum exhibits an anomaly inasmuch the degeneracy of the zero-energy Landau level – which is exactly half-filled at charge neutrality – is only half the size of the other Landau levels. These features have some intriguing consequences for the quantum Hall effect. While the breakdown of Kohn’s theorem in graphene is not as severe as one might expect, the spectral anomaly leads to an anomalous quantization of the Hall conductivity [32]. Each one of the four fermionic flavours – two spin degrees of freedom for each of the two valleys – contributes a half-integer to the total Hall conductivity, such that plateaus can only be observed at the fillings $\nu = \pm 2, \pm 6, \pm 10, \dots$ (Interactions in combination with the spectral anomaly can lead to additional plateaus for example at $\nu = \pm 1$, see Refs. [38, 124] and references therein.) As mentioned previously, the integer quantum Hall effect typically requires rather low temperatures close to absolute zero to be observed, since the Landau level structure is quickly washed out by thermal fluctuations. Not so in graphene, where the single Landau level at the charge neutrality point is quite robust against those fluctuations, being well-separated from the rest of the spectrum due to the high velocity of the charge carriers. Astonishingly, this feature allows for an observation of the integer quantum Hall effect even at room temperature [33]. In fact, all of the features mentioned above the multiple cyclotron resonances, the anomalous Hall quantization, as well as the room temperature quantum Hall effect have already been observed in experiments. They are perhaps the most striking evidences for the relativistic nature of graphene’s quasiparticles.

Only two years after the discovery of von Klitzing, experiments on high quality samples performed by Tsui and Störmer revealed the existence of additional plateaus, occurring at distinct fractional values of the conductance quantum [129], see Fig. 1.4. Hence, we can immediately conclude that this “fractional quantum Hall effect” can no longer be explained by a simple noninteracting theory, but fundamentally requires electron-electron interactions. In fact, the fractional quantum Hall effect is the prime example of strongly correlated matter. To under-

⁶There is an alternative way to fix the Fermi energy in between two Landau levels, which does not rely on disorder [119, 120]. However, since the samples used in actual experiments are always disordered, even if only by a small amount, the disorder mechanism to fix the Fermi energy is a more realistic depiction of the phenomenon.

stand this – at first glance seemingly unrelated – conclusion, recall that the noninteracting Landau levels have no dispersion. They are “flat bands”, which exhibit an enormous energetic degeneracy. For large enough magnetic fields the degeneracy becomes so huge that all electrons occupy the lowest energy level only. As a result, the kinetic energy is completely quenched and only the Coulomb interaction term remains [116].⁷ Since there is no small parameter in the problem and due to the macroscopically large ground state degeneracy in the absence of interactions, all conventional approaches to treat interacting quantum systems that have been developed over the years are doomed to fail.

Our short discussion should have made it clear that interactions are single-handedly responsible for the existence of Hall plateaus in a partially filled Landau level. We are now in a position, where we know cause and effect, but the actual mechanism, which could answer the questions why and where those plateaus form, is still missing. This is especially frustrating, since the formal calculational tools we have at our disposal to deal with a purely interacting Hamiltonian are limited. For example, the numerical method of exact diagonalization is limited to small system sizes, due to the exponential growth of the Hilbert space. Fortunately, despite these obstacles and the technical limitations at the time, the few clues that were available about the nature of the fractional quantum Hall groundstates were sufficient for Laughlin to come up with his celebrated wavefunction [130]. The Laughlin wavefunction describes the $\nu = 1/m$ (m being an odd integer) fractional quantum Hall states as a uniform and incompressible electron liquid, similar to the high density plasma phase of a Coulomb gas. Probably its most remarkable feature is that it is a trial wavefunction with an extraordinarily simple mathematical structure, that does not contain any free/adjustable parameters.⁸ Yet it approximates the exact $\nu = 1/m$ groundstates extraordinarily well. Based on the seminal work of Laughlin, Jain pushed forward the ingenious idea that the fractional quantum Hall effect can be understood as an integer quantum Hall effect of a new type of quasiparticle, the so-called composite fermion [116, 131]. It is a charge-flux bound state of an electron and an even number of magnetic flux quanta. The intuitive idea is that the composite fermions feel a weakened effective magnetic field, since part of the external magnetic field is captured by the electrons to form the bound state. As a consequence, a new set of composite fermion Landau levels is formed that is less degenerate than the original one. As it turned out, a large class of the “magical” fractional fillings that have been observed in the experiment map precisely to an integer filling of those composite fermion Landau levels. Hence, the integer quantum Hall effect of composite fermions explains the fractional quantum Hall effect of ordinary electrons.

From a purely methodological point of view the fractional quantum Hall effect is highly interesting, since its investigation challenges the well-established approaches of quantum field theory, requiring the development of new calculational techniques. For some this fact alone may be enough motivation to study this effect, but it certainly cannot explain why quantum Hall physics has grown into a separate subfield of condensed matter theory. Without exaggeration the discovery of the fractional quantum Hall effect shook the very foundations of condensed matter theory, as it broke the longstanding paradigm of the Landau symmetry breaking theory as the cornerstone of phase transitions. Before its discovery it was believed that the Landau

⁷For nonrelativistic electrons the low-energy Hilbert space does not contain transitions into neighboring Landau levels, known as Landau level mixing, since the energy gap between two successive levels is proportional to the magnetic field. Hence, the physics is entirely constrained to the lowest Landau level. Even for intermediate magnetic field strengths, where the lowest level is completely filled and the next level is partially filled, it is a good approximation to neglect Landau level mixing [116].

⁸Sometimes the Laughlin wavefunction is referred to as a variational wavefunction (even Laughlin himself did refer to it as such [130]), but since there are no free parameters to be varied, such a description would hardly be justified, if not misleading.

theory of phase transitions accounts for all possible phases of matter [92, 99]. In this framework two different phases of matter can be distinguished by their symmetries, a symmetric phase and a symmetry broken phase, and the transition itself is understood as a symmetry breaking process. Furthermore, one defines an order parameter, which vanishes in the symmetric phase, but assumes a finite value in the symmetry broken phase. The symmetric phase with vanishing order parameter is also called disordered phase, while the symmetry broken phase is the ordered one. This assignment may sound counterintuitive at first, but think of the solid-gas transition as a prime example to clarify this terminology. The solid state with its periodic arrangement of atoms is certainly more ordered than a gas, where the atoms just fly around in space randomly. At the same time, however, the solid is less symmetric than a gas, because the former only allows for discrete lattice translations, while the latter can be translated continuously. Another example where Landau’s theory has proven to be useful is the BCS theory of superconductivity we mentioned earlier [92, 93, 99]. In the metallic phase, the action of the electronic system obeys a global $U(1)$ symmetry, which, according to Noether’s theorem, yields a conserved charge. In this case the conserved charge coincides with the electric charge of the electrons, which is equivalent to the particle number. If the system is cooled down below the critical temperature, a gap (serving as an order parameter) opens up, which breaks the $U(1)$ symmetry. As a consequence, the particle number is not conserved anymore, since the spin-up and spin-down electrons form bound states, so-called Cooper pairs, which behave as bosonic quasiparticles. This is a manifestation of Goldstone’s theorem, according to which a spontaneously broken continuous symmetry is accompanied by a massless/gapless bosonic excitation [58, 92, 99, 132, 133]. The superconducting state can then be described as a Bose-Einstein condensate, supporting a dissipationless superfluid flow of electric charge. In the fractional quantum Hall effect, however, there is no symmetry breaking mechanism involved. Yet, it is frequently stated that the fractional quantum Hall state corresponding to one of those magical filling fractions represents a new phase of matter [116, 117, 134, 135]. But why is that? Since there is no spontaneous or explicit symmetry breaking, why should that statement be justified, and what is so different in comparison to the integer quantum Hall effect?

The answer to these questions is rather subtle and requires a thorough analysis of the topological properties of the state, which is quite abstract and hard to grasp. Possibly the easiest way to understand the fundamental difference between a fractional quantum Hall liquid and an “ordinary” Fermi liquid is by investigating its excitations. Fractional quantum Hall states in general feature a different kind of collective excitation that is neither fermionic nor bosonic. Instead, the excitations obey anyonic statistics with distinct topological properties. In addition, their charge is not an integer multiple of the elementary charge, but only a fraction of it, which was thought to be impossible for a long time.⁹ These features are induced solely by the structure of the respective fractional quantum Hall state itself and cannot be realized in a Fermi liquid, Fermi gas, in an integer quantum Hall state or any other “conservative” phase of matter. In that sense, the fractional quantum Hall states represent topological phases of matter that are beyond the Landau symmetry breaking theory.¹⁰

Due to the enormous impact of the nonrelativistic fractional quantum Hall effect on condensed matter theory, it goes without saying that it is worthwhile to study its relativistic analogon in graphene. As we have stated above, the linearity of the pseudo-relativistic graphene

⁹Quarks in the theory of quantum chromodynamics similarly feature a fractional elementary charge, but they cannot be observed as free particles due to confinement [58].

¹⁰In this context we should also mention the Berezinskii-Kosterlitz-Thouless transition [136–138], which is an infinite order phase transition in the two-dimensional XY -model. In fact, it was the first topological phase transition to be discovered. Long before the discovery of the fractional quantum Hall effect, it was the first hint into the new world of topological phases of matter.

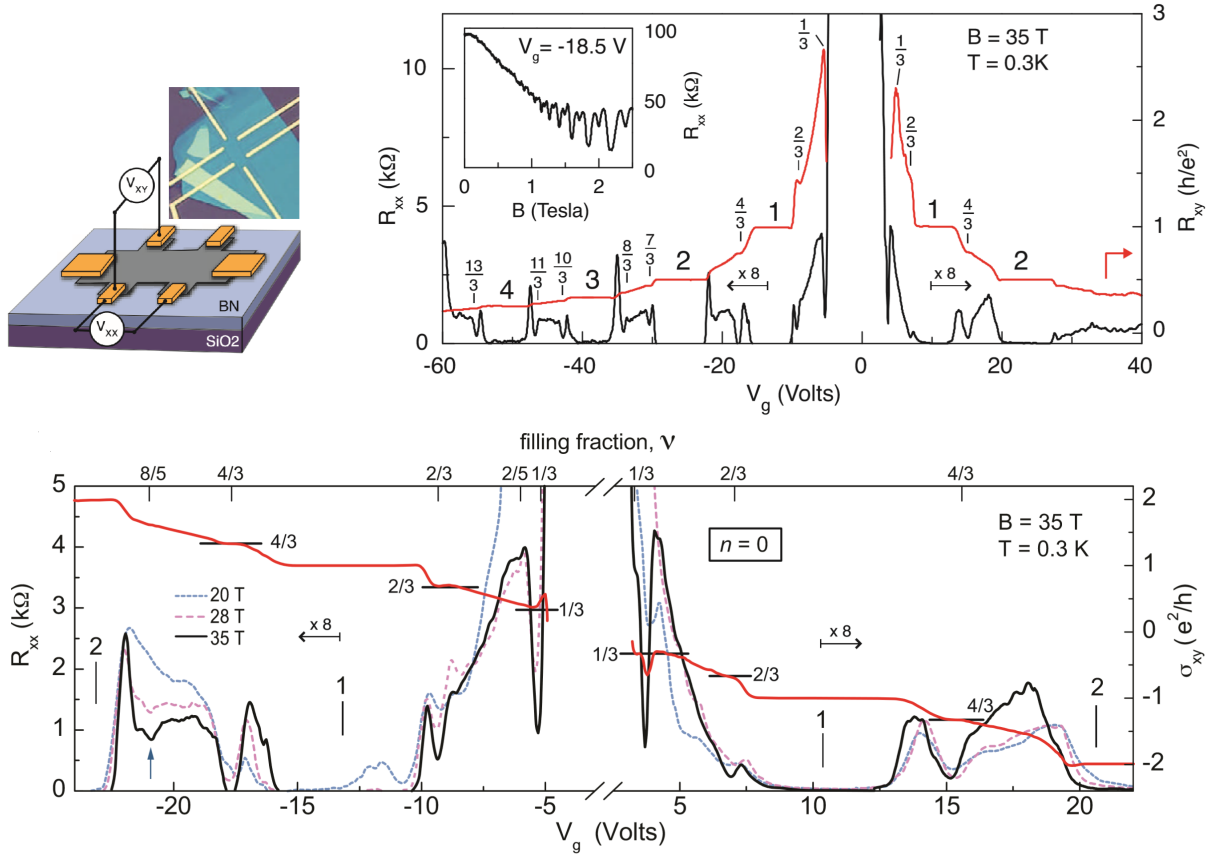


Figure 1.5: (Top left) Schematic of the Hall device and optical image of the experimental realization. (Top right) Diagonal resistance R_{xx} and Hall resistance R_{xy} of graphene as a function of the gate voltage at constant value of the magnetic field. Integer and fractional fillings are indicated explicitly. Note that the data do not lie symmetrically around zero gate voltage, since even at vanishing gate voltage there is always a finite amount of charge carriers in the system, either due to impurities, external contacts or the substrate. Apart from that the data show an approximate particle-hole symmetry as expected from graphene. (Bottom) Diagonal resistance R_{xx} and Hall conductivity σ_{xy} of graphene as a function of the gate voltage at constant value of the magnetic field. The Hall conductivity shows the plateau structure at fractional fillings very clearly. Pictures taken from Ref. [139] with minor adaptations.

spectrum has some intriguing consequences for the integer quantum Hall effect, so it is not unreasonable to expect similar consequences to occur in the fractional quantum Hall regime. In particular, since the nonrelativistic fractional quantum Hall effect is interpreted as an integer quantum Hall effect of composite particles, there should be a footprint of composite Dirac fermions in the relativistic fractional quantum Hall effect. Furthermore, being a genuine multi-component system – the quasiparticles come in four different flavours – quantum Hall physics in graphene has much more to offer than spin-polarized single-component systems, that are typically studied. At the time of this writing there is already a plethora of theoretical studies on this topic [37, 140–149]. Even first measurements have been performed, showing the signature plateau structure of the fractional quantum Hall effect [36, 139, 150–152], together with an approximate particle-hole-symmetry as expected from graphene, see Fig. 1.5. Yet, this area of research is still in its infancy and there is potentially a lot left to be discovered.

To access the fractional quantum Hall effect theoretically there are essentially two complementary approaches. There is the aforementioned method of exact diagonalization of projected Hamiltonians, which is typically combined with an educated guess of trial wavefunctions in the spirit of Laughlin's and Jain's original works, and then there are field theoretical methods. The latter study the fractional quantum Hall effect either by phenomenological Ginzburg-Landau/hydrodynamic type of models, or truly microscopically [153–164], but they all have one feature in common: the use of Chern-Simons gauge fields. In this thesis the microscopic field theory approach of Lopez and Fradkin is of particular relevance, Refs. [161, 163, 164], so let us briefly explain its main features. As has been proven by Lopez and Fradkin, in the presence of an external magnetic field there is not only a single theory of two-dimensional interacting electrons, but a whole family of theories, where an additional Chern-Simons gauge field is minimally coupled to the fermions. By restricting the level of the Chern-Simons theory – a constant in the kinetic term of the gauge field – to assume only certain values, they were able to show that the theories with and without Chern-Simons fields are equivalent as they yield the same physical amplitudes. The role of the Chern-Simons field is to attach magnetic flux quanta to the physical electrons, transforming them into composite fermions, which experience a reduced effective magnetic field, confirming the picture painted by Jain. They went on to show, that these microscopic Chern-Simons theories are able to access the fractional quantum Hall regime even in an approximative treatment, using a stationary phase approximation with Gaussian fluctuations.¹¹ This feature has to be contrasted with the original formulation of the theory that does not employ Chern-Simons gauge fields. Here, a stationary phase approximation does not yield fractional quantum Hall physics. The modified field theory of Lopez and Fradkin allowed for a calculation of the Hall conductivities of the Jain sequence, the spectrum of collective excitations as well as the corresponding wavefunctions, and even corrections thereof.

Despite these major successes of the microscopic Chern-Simons approach, it is unsatisfactory that such gauge fields are needed in the first place. Since the nonperturbative methods discussed in the previous sections are exact reformulations of the quantum field theory of interacting fermions, it has to be possible to describe the fractional quantum Hall effect in these frameworks, even without explicitly introducing such gauge fields. Besides, the projected Hamiltonians used in exact diagonalization do not need them either, which already proves that it is indeed possible to avoid Chern-Simons fields altogether. However, the typical truncation schemes that are currently available to approximatively solve the exact equations of the Schwinger-Dyson formalism or the functional renormalization group are incapable of accounting for the necessary correlations needed to describe the fractional quantum Hall regime. Therefore, as unsatisfactory as it is, for the time being it seems to be inevitable to consider Chern-Simons theory. For the case of graphene such microscopic Chern-Simons theories have already been considered in Refs. [144, 145], but the scope of these analyses were rather limited and by far not as comprehensive as that of Lopez and Fradkin. Focussing only on the filling fractions this framework predicts, they did not properly address several important aspects, which distinguish relativistic composite fermions from nonrelativistic ones. To name a few examples: (i) the fate of the spectral anomaly of (composite) Dirac fermions – such a discussion was avoided by prescribing a flux attachment to the physical electrons/holes measured from the bottom/top of the lowest Landau

¹¹In this context recall the standard treatment of BCS theory we discussed earlier. The stationary phase approximation is able to capture truly nonperturbative effects such as instantonic/solitonic field configurations [98–101], since it is not a naive power series expansion of a coupling constant. Nonetheless, we would still ascribe it to the class of perturbative techniques, since the classical action within the functional integral is expanded in fluctuations around a possibly nonvanishing mean field. Truly nonperturbative techniques do not operate on the level of the classical action, but rather on the level of the quantum effective action, see chapter 3 and the papers in Secs. 4.1, 4.2 and 5.A.

level; (ii) particle-hole symmetry breaking due to the Chern-Simons fields and how it might be restored; (iii) the spectrum of collective excitations; (iv) the breakdown of Kohn's theorem for relativistic systems and its implications on the renormalization of the composite fermion spectrum and excitation spectrum; (v) and lastly Landau level mixing, which in graphene is a substantially more severe problem than for nonrelativistic systems. In conclusion, despite the plethora of already existing publications, there are still a lot of questions that demand an answer.

1.5 Relativistic fermions in a random environment

The assumption of an absolutely clean and perfect crystal is a highly idealized abstraction of physical reality, which is impossible to manufacture in a laboratory. There will always be dislocations, disclinations and vacancies in the crystal as well as impurities at which the electrons can scatter. Such imperfections can be conveniently modeled by a complicated potential landscape in which the electrons move [92, 93, 165]. Yet, calculating the correlation functions for a particular realization of such a disorder potential can be a rather difficult, if not impossible task. Even if one would succeed in finding a solution, it would be of little to no use, since there is almost no way to determine, let alone control, the exact impurity potential on atomic scales. In other words, there is always a certain kind of ignorance or randomness involved. A way out of this dilemma is to take this randomness seriously by manifestly implementing our ignorance about the microscopic details of the disorder potential into the theory. To this end one should consider not one, but many realizations of distinct disorder potentials and describe their effect on the correlation functions and measurable quantities with statistical methods [92, 93]. The set of disorder potentials form a statistical ensemble, whose statistical properties are defined by a certain probability distribution, and the correlation functions should be averaged with respect to that ensemble.

A very prominent and for practical applications and calculations well-suited probability distribution is a Gaussian. It is uniquely defined by only two cumulants, the mean value of the potential, typically assumed to vanish, and its variance, which determines the autocorrelation of the ensemble. Formulating the theory in the functional integral language, it becomes obvious why the Gaussian probability distribution is so attractive for practical calculations: it is possible to perform the impurity average on the level of the partition function exactly. As a result one obtains a fermionic pseudo-interaction term, that can be analyzed by standard methods of quantum field theory. As it turns out, the so-defined averaged partition function is the generating functional for disorder-averaged correlation functions, being the desired quantities to calculate.¹² It has to be emphasized that this pseudo-interaction has to be distinguished from a "true" interaction, since the former only involves a momentum transfer but no energy transfer, in contrast to a real interaction process. Apart from that difference, however, the pseudo-interaction term is open to the whole machinery of quantum field theory, most importantly perturbation theory in terms of Feynman diagrams and renormalization theory.

In ordinary Fermi gases, liquids, superconductors and quantum Hall systems such field theoretical techniques have been applied with great success [52–54, 167–169]. For example, in the analysis of the disorder averaged two-point Green function one encounters a disorder induced self-energy, which describes the influence of the random environment on the quasiparticle spectrum. Its diagrammatic perturbation expansion is shown in Fig. 1.6. As it turns out when calculating the second order contribution to the self-energy – those diagrams, which possess

¹²To be precise, for this statement to be true one either has to use the Keldysh formalism, or, when using the Matsubara formulation, a replicated partition function prior to ensemble averaging [92, 93, 166].

$$\Sigma = \text{[diagram 1]} + \text{[diagram 2]} + \text{[diagram 3]} + \dots$$

$$\Sigma_{SCBA} = \text{[diagram 4]}$$

$$= \text{[diagram 5]} + \text{[diagram 6]} + \text{[diagram 7]} + \dots$$

Figure 1.6: (Top) Perturbative expansion of the disorder induced self-energy for the impurity averaged two-point Green function. The solid lines with an arrow denote the bare (disorder free) two-point Green function and the dashed line corresponds to an “impurity propagator”, which is nothing but a diagrammatic representation of the variance of the disorder potential. (Bottom) Disorder induced self-energy in the self-consistent Born approximation (SCBA), which takes into account all rainbow-like diagrams, that have no crossing impurity lines. Here, the double solid line in the first line of the equation corresponds to the SCBA self-energy dressed two-point Green function.

two disorder lines – the relative weight of the rainbow and crossing diagrams is proportional to $k_F \ell$, where k_F is the Fermi momentum and ℓ is the elastic mean free path. Assuming the inverse of the Fermi momentum to be small against the elastic mean free path, $k_F^{-1} \ll \ell$, which is typically fulfilled in a weakly disordered metal, one can neglect the parametrically smaller crossing diagrams and calculate the self-energy via a nonperturbative self-consistency equation (see the bottom of Fig. 1.6). This approximation, known as self-consistent Born approximation (SCBA) or non-crossing approximation, is widely used in the theory of disordered metals to explain diffusion in the realm of quantum theory, and to calculate the quantum corrections to Drude conductivity and other related transport phenomena.

In the case of graphene the above condition, which is necessary for the SCBA to be a controlled approximation, is not always fulfilled. Since the Fermi momentum is directly proportional to the chemical potential, $k_F = \mu/v_F$, it depends on the filling relative to the charge neutrality point whether or not $(k_F \ell)^{-1} \ll 1$ holds. Upon approaching the charge neutrality point from large filling, one enters a strong coupling regime, which is reminiscent of the Coulomb problem in freestanding graphene. With the lack of a small parameter to organize a perturbation expansion, new methods have to be explored to tackle the problem of disorder near or at charge neutrality. One possible route would be to include the missing crossing diagrams. However, this is easier said than done. Since the SCBA is already a nonperturbative approximation, which combines perturbation theory with resummation techniques, it is difficult to go beyond it in a consistent and systematic way. A perturbative treatment in the number of crossings, even if formulated in a self-consistent way such that these crossings appear infinitely often, should not be sufficient [170]. Furthermore, as discussed previously, a naive extension of the SCBA based on resummed perturbation theory is likely to either miss or overcount certain classes of diagrams, which disqualifies such a method as a viable strategy. These problems are amplified if one wants to calculate conductivities, which require knowledge of the disorder averaged four-

point function. Here the SCBA resums all diagrams with a ladder-like structure, particle-hole ladders to describe diffusons and particle-particle ladders to describe cooperons. Any extension of the SCBA on the level of the self-energy should also be incorporated on the level of the four-point Green function/vertex function, otherwise the approximations would be inconsistent, but it would be significantly more complicated to incorporate such an extension manually for higher level Green/vertex functions and check for consistency. Therefore, as far as field theory techniques are considered, the only proper way to extend the SCBA is to resort to one of the nonperturbative formalisms mentioned before, Schwinger-Dyson equations or the functional RG.

1.6 Overview of this thesis

This thesis is written in a modular form. Since the included papers are written in a self-contained way for the most part, we provide additional background information that are not or only shortly covered there. Depending on the knowledge of the reader about graphene and/or the general formalism of quantum field theory it is admissible to skip certain sections. The thesis is organized as follows.

In chapter 2 we explain the physical mechanism that is responsible for the formation of the honeycomb crystal lattice structure. Based on this analysis we motivate the form of the interacting tight-binding Hamiltonian for the π -electrons, which describes a two-band system. We show that its noninteracting part leads to two inequivalent band touching points around which the spectrum disperses linearly, giving rise to the pseudo-relativistic Dirac nature of graphene's quasiparticles. The stability of the Dirac cones against lattice deformations is briefly investigated and a short discussion about gap opening variations of the two-dimensional Dirac Hamiltonian is given. Lastly, we analyze the Coulomb interactions between such quasiparticles, identifying those contributions that have to be kept to arrive at a consistent low-energy theory.

After having obtained the desired low-energy Hamiltonian, which is the starting point for all the papers on which this thesis is based, in chapter 3 we explain the basic working tools of real-time quantum field theory by using a real bosonic field theory – the proper finite dimensional generalization of the toy model discussed in Sec. 1.3. This simple theory only serves as a prototype field theory to illustrate the inner workings and mathematical structures of a general formalism, whose main features are shared by almost all quantum field theories. Only minor adjustments are necessary to apply this formalism to the theory of interest. Yet, the bosonic field theory is not completely unrelated to the physics of graphene, since a real bosonic field arises in the form of a Hubbard-Stratonovich field when decoupling the interaction in the density-density channel. We explain the connection between correlation functions, connected correlation functions and vertex functions, motivating the calculations performed in chapters 4 and 5.

The two aforementioned introductory chapters are followed by the main body of this thesis. Chapter 4 contains the three papers that revolve around graphene's Dirac electrons interacting via Coulomb interactions. In the first paper entitled "*Keldysh functional renormalization group for electronic properties of graphene*" we construct a nonperturbative framework in the Keldysh formalism to calculate the vertex functions of the theory in and out of thermal equilibrium. As a first application this framework has been used to calculate the renormalization of the static dielectric function and the Fermi velocity at charge neutrality and finite temperatures, extending the results of Ref. [89]. The second paper called "*Chemical-potential flow equations for graphene with Coulomb interactions*" builds upon the ideas of the first paper, reinterpreting the chemical potential as a flow parameter in the sense of the functional renormalization group. In contrast to standard fRG, the flow in this framework is entirely physical, describing the change of the vertex

functions upon changing the charge carrier density. This formalism has been used to extend the finite temperature results for the static dielectric function and Fermi velocity obtained in the first paper to finite densities, in order to substantiate the theoretical fit of the Fermi velocity renormalization of Ref. [89] to the experimental data of Ref. [66]. In the third and last paper of this chapter, “*Abelian Chern-Simons theory for the fractional quantum Hall effect in graphene*”, we consider an extension of the field theory considered in the preceding sections that is capable of describing the fractional quantum Hall regime of the pseudo-relativistic Dirac electrons in graphene. In that work we limited our analysis to much simpler perturbative techniques, because the Chern-Simons transformation already takes care of most of the nontrivial correlation effects, but also due to the greater complexity of the theory. We calculated the finite temperature electromagnetic response tensor in the random phase approximation from which we extracted the Hall conductivities. Our results clearly show the hallmark of the fractional quantum Hall effect: quantized plateaus at fractional filling factors.

In the last chapter we turn our attention to the problem of noninteracting disordered Dirac fermions. First, we sketch how the most general form of a disorder potential in the continuum Dirac theory – being a Hermitean matrix coupling the individual spinor components to one another – arises from the more fundamental tight-binding model of hopping electrons on the honeycomb lattice. Next, we present a paper, “*Graphene pn junction in a quantizing magnetic field: Conductance at intermediate disorder strength*”, which deals with the chiral modes that are formed at the pn junction interface in a uniform magnetic field normal to the graphene sheet in the presence of disorder. Starting from the two-dimensional Dirac model, we first derive an effective one-dimensional Hamiltonian for the chiral interface modes, incorporating the effect of the bulk disorder potential on the interface states. This effective model is then analyzed by a scattering matrix approach, which avoids the problems of the field theory approach altogether. We obtain a Fokker-Planck equation for the probability distribution of scattering angles that can be solved analytically exactly. This solution allows for a calculation of the full conductance distribution in the crossover between the clean limit and the strong disorder limit. Lastly, we present a manuscript for a paper, “*Strong disorder in nodal semimetals: Schwinger-Dyson–Ward approach*”, which is under peer review at the time of this writing. In this paper we combine the nonperturbative Schwinger-Dyson equation for the disorder induced self-energy at charge neutrality with a Ward identity to approximately eliminate the three-vertex contribution. The now closed equation for the self-energy is solved numerically and the validity of the approximation is tested against exact numerical reference data, showing excellent agreement in the strong disorder regime. In this work we did not focus on graphene exclusively, but we also investigated other paradigmatic semimetals at nodal point filling for the special case of a band-diagonal disorder potential.

Bibliography

- [1] P. R. Wallace, “The Band Theory of Graphite,” *Phys. Rev.*, vol. 71, pp. 622–634, May 1947.
- [2] N. D. Mermin and H. Wagner, “Absence of Ferromagnetism or Antiferromagnetism in One- or Two-Dimensional Isotropic Heisenberg Models,” *Phys. Rev. Lett.*, vol. 17, pp. 1133–1136, Nov 1966.
- [3] P. C. Hohenberg, “Existence of Long-Range Order in One and Two Dimensions,” *Phys. Rev.*, vol. 158, pp. 383–386, Jun 1967.
- [4] S. Coleman, “There are no Goldstone bosons in two dimensions,” *Communications in Mathematical Physics*, vol. 31, pp. 259–264, Dec 1973.
- [5] Nelson, D.R. and Peliti, L., “Fluctuations in membranes with crystalline and hexatic order,” *J. Phys. France*, vol. 48, no. 7, pp. 1085–1092, 1987.
- [6] P. Le Doussal and L. Radzihovsky, “Self-consistent theory of polymerized membranes,” *Phys. Rev. Lett.*, vol. 69, pp. 1209–1212, Aug 1992.
- [7] J. C. Meyer, A. K. Geim, M. I. Katsnelson, K. S. Novoselov, T. J. Booth, and S. Roth, “The structure of suspended graphene sheets,” *Nature*, vol. 446, pp. 60–63, Mar 2007.
- [8] Nelson, D. and Piran, T. and Weinberg, S., *Statistical mechanics of membranes and surfaces*. World Scientific, 2004.
- [9] K. S. Novoselov, A. K. Geim, S. V. Morozov, D. Jiang, Y. Zhang, S. V. Dubonos, I. V. Grigorieva, and A. A. Firsov, “Electric Field Effect in Atomically Thin Carbon Films,” *Science*, vol. 306, no. 5696, pp. 666–669, 2004.
- [10] K. S. Novoselov, A. K. Geim, S. V. Morozov, D. Jiang, M. I. Katsnelson, I. V. Grigorieva, S. V. Dubonos, and A. A. Firsov, “Two-dimensional gas of massless Dirac fermions in graphene,” *Nature*, vol. 438, p. 197, 2005.
- [11] K. S. Novoselov, D. Jiang, F. Schedin, T. J. Booth, V. V. Khotkevich, S. V. Morozov, and A. K. Geim, “Two-dimensional atomic crystals,” *Proceedings of the National Academy of Sciences*, vol. 102, no. 30, pp. 10451–10453, 2005.
- [12] Z. Li, M. Smeu, A. Rives, V. Maraval, R. Chauvin, M. A. Ratner, and E. Borguet, “Towards graphyne molecular electronics,” *Nature Communications*, vol. 6, no. 6321, 2015.
- [13] M. Ströck https://commons.wikimedia.org/wiki/File:Eight_Allotropes_of_Carbon.png, 2006.

- [14] B. G. Kim and H. J. Choi, “Graphyne: Hexagonal network of carbon with versatile Dirac cones,” *Phys. Rev. B*, vol. 86, p. 115435, Sep 2012.
- [15] R. H. Baughman, H. Eckhardt, and M. Kertesz, “Structure-property predictions for new planar forms of carbon: Layered phases containing sp² and sp atoms,” *The Journal of Chemical Physics*, vol. 87, no. 11, pp. 6687–6699, 1987.
- [16] N. Narita, S. Nagai, S. Suzuki, and K. Nakao, “Optimized geometries and electronic structures of graphyne and its family,” *Phys. Rev. B*, vol. 58, pp. 11009–11014, Oct 1998.
- [17] A. N. Enyashin and A. L. Ivanovskii, “Graphene allotropes,” *Physica Status Solidi B Basic Research*, vol. 248, pp. 1879–1883, Aug. 2011.
- [18] J. C. Slonczewski and P. R. Weiss, “Band Structure of Graphite,” *Phys. Rev.*, vol. 109, pp. 272–279, Jan 1958.
- [19] G. W. Semenoff, “Condensed-Matter Simulation of a Three-Dimensional Anomaly,” *Phys. Rev. Lett.*, vol. 53, pp. 2449–2452, Dec 1984.
- [20] V. P. Gusynin, S. G. Sharapov, and J. P. Carbotte, “Ac Conductivity of Graphene: from Tight-Binding Model to 2 + 1-DIMENSIONAL Quantum Electrodynamics,” *International Journal of Modern Physics B*, vol. 21, pp. 4611–4658, 2007.
- [21] A. H. Castro Neto, F. Guinea, N. M. R. Peres, K. S. Novoselov, and A. K. Geim, “The electronic properties of graphene,” *Reviews of Modern Physics*, vol. 81, pp. 109–162, Jan. 2009.
- [22] O. Klein, “Die Reflexion von Elektronen an einen Potentialsprung nach der relativistischen Dynamik von Dirac,” *Z. Phys.*, vol. 53, p. 157, 1929.
- [23] V. V. Cheianov and V. I. Falko, “Selective transmission of Dirac electrons and ballistic magnetoresistance of n-p junctions in graphene,” *Phys. Rev. B*, vol. 74, p. 041403(R), 2006.
- [24] M. I. Katsnelson, K. S. Novoselov, and A. K. Geim, “Chiral tunnelling and the Klein paradox in graphene,” *Nat. Phys.*, vol. 2, p. 620, 2006.
- [25] M. I. Katsnelson, “Zitterbewegung, chirality, and minimal conductivity in graphene,” *Eur. Phys. J. B*, vol. 51, p. 1434, 2006.
- [26] C. W. J. Beenakker, “Colloquium: Andreev reflection and Klein tunneling in graphene,” *Rev. Mod. Phys.*, vol. 80, p. 1337, 2008.
- [27] E. Mariani and F. von Oppen, “Flexural Phonons in Free-Standing Graphene,” *Phys. Rev. Lett.*, vol. 100, p. 076801, Feb 2008.
- [28] D. L. Nika and A. A. Balandin, “Phonons and thermal transport in graphene and graphene-based materials,” *Reports on Progress in Physics*, vol. 80, no. 3, p. 036502, 2017.
- [29] B. Roy and V. Juričić, “Strain-induced time-reversal odd superconductivity in graphene,” *Phys. Rev. B*, vol. 90, p. 041413, Jul 2014.

-
- [30] F. K. Kunst, C. Delerue, C. M. Smith, and V. Juričić, “Kekule versus hidden superconducting order in graphene-like systems: Competition and coexistence,” *Phys. Rev. B*, vol. 92, p. 165423, Oct 2015.
- [31] A. di Bernardo, O. Millo, M. Barbone, H. Alpern, Y. Kalcheim, U. Sassi, A. K. Ott, D. de Fazio, D. Yoon, M. Amado, A. C. Ferrari, J. Linder, and J. W. A. Robinson, “p-wave triggered superconductivity in single-layer graphene on an electron-doped oxide superconductor,” *Nature Communications*, vol. 8, p. 14024, Jan. 2017.
- [32] V. P. Gusynin and S. G. Sharapov, “Unconventional Integer Quantum Hall Effect in Graphene,” *Phys. Rev. Lett.*, vol. 95, p. 146801, Sep 2005.
- [33] K. S. Novoselov, Z. Jiang, Y. Zhang, S. V. Morozov, H. L. Stormer, U. Zeitler, J. C. Maan, and G. S. Boebinger, “Room-Temperature Quantum Hall Effect in Graphene,” *Science*, vol. 315, p. 1379, 2007.
- [34] Y. Zhang, Z. Jiang, J. P. Small, M. S. Purewal, Y.-W. Tan, M. Fazlollahi, J. D. Chudow, J. A. Jaszczak, H. L. Stormer, and P. Kim, “Landau-Level Splitting in Graphene in High Magnetic Fields,” *Phys. Rev. Lett.*, vol. 96, p. 136806, Apr 2006.
- [35] Z. Jiang, Y. Zhang, H. L. Stormer, and P. Kim, “Quantum Hall States near the Charge-Neutral Dirac Point in Graphene,” *Phys. Rev. Lett.*, vol. 99, p. 106802, Sep 2007.
- [36] K. I. Bolotin, F. Ghahari, M. D. Shulman, H. L. Stormer, and P. Kim, “Observation of the fractional quantum Hall effect in graphene,” *Nature*, vol. 462, pp. 196–199, Nov. 2009.
- [37] C. Tóke, P. E. Lammert, V. H. Crespi, and J. K. Jain, “Fractional quantum Hall effect in graphene,” *Phys. Rev. B*, vol. 74, p. 235417, Dec 2006.
- [38] M. O. Goerbig, “Electronic properties of graphene in a strong magnetic field,” *Rev. Mod. Phys.*, vol. 83, pp. 1193–1243, Nov 2011.
- [39] M. Vozmediano, M. Katsnelson, and F. Guinea, “Gauge fields in graphene,” *Physics Reports*, vol. 496, no. 4, pp. 109 – 148, 2010.
- [40] A. Marzoli and G. Palumbo, “BF-theory in graphene: A route toward topological quantum computing?,” *EPL (Europhysics Letters)*, vol. 99, p. 10002, July 2012.
- [41] B. Amorim, A. Cortijo, F. de Juan, A. G. Grushin, F. Guinea, A. Gutiérrez-Rubio, H. Ochoa, V. Parente, R. Roldán, P. San-José, J. Schiefele, M. Sturla, and M. A. H. Vozmediano, “Novel effects of strains in graphene and other two dimensional materials,” *ArXiv e-prints*, Mar. 2015.
- [42] P. M. Ostrovsky, I. V. Gornyi, and A. D. Mirlin, “Electron transport in disordered graphene,” *Phys. Rev. B*, vol. 74, p. 235443, Dec 2006.
- [43] I. L. Aleiner and K. B. Efetov, “Effect of Disorder on Transport in Graphene,” *Physical Review Letters*, vol. 97, p. 236801, Dec. 2006.
- [44] A. Altland, “Low-Energy Theory of Disordered Graphene,” *Phys. Rev. Lett.*, vol. 97, p. 236802, Dec 2006.
- [45] P. M. Ostrovsky, I. V. Gornyi, and A. D. Mirlin, “Quantum Criticality and Minimal Conductivity in Graphene with Long-Range Disorder,” *Physical Review Letters*, vol. 98, p. 256801, June 2007.

- [46] K. Kechedzhi, O. Kashuba, and V. I. Fal'ko, "Quantum kinetic equation and universal conductance fluctuations in graphene," *Phys. Rev. B*, vol. 77, p. 193403, May 2008.
- [47] A. Cortijo and M. A. H. Vozmediano, "Minimal conductivity of rippled graphene with topological disorder," *Phys. Rev. B*, vol. 79, p. 184205, May 2009.
- [48] A. Sinner, A. Sedrakyan, and K. Ziegler, "Optical conductivity of graphene in the presence of random lattice deformations," *Phys. Rev. B*, vol. 83, p. 155115, Apr 2011.
- [49] J. M. Graybeal and M. R. Beasley, "Localization and interaction effects in ultrathin amorphous superconducting films," *Phys. Rev. B*, vol. 29, pp. 4167–4169, Apr 1984.
- [50] J. Graybeal, "Competition between superconductivity and localization in two-dimensional ultrathin a-MoGe films," *Physica B+C*, vol. 135, no. 1, pp. 113 – 119, 1985.
- [51] A. Frydman, "The superconductor insulator transition in systems of ultrasmall grains," *Physica C: Superconductivity*, vol. 391, no. 2, pp. 189 – 195, 2003.
- [52] A. Finkel'stein, "Superconducting transition temperature in amorphous films," *Sov. Phys. JETP Lett.*, vol. 45, p. 46, 1987.
- [53] A. Finkel'stein, "Suppression of superconductivity in homogeneously disordered systems," *Physica B: Condensed Matter*, vol. 197, no. 1, pp. 636 – 648, 1994.
- [54] P. Anderson, "Theory of dirty superconductors," *Journal of Physics and Chemistry of Solids*, vol. 11, no. 1, pp. 26 – 30, 1959.
- [55] Giamarchi, T., *Quantum Physics in One Dimension*. Oxford Science Publications, 2003.
- [56] J. von Delft and H. Schoeller, "Bosonization for beginners - refermionization for experts," *Annalen der Physik*, vol. 510, pp. 225–305, Nov. 1998.
- [57] Kaku, M., *An Introduction to Quantum Field Theory*. Oxford University Press, 1993.
- [58] Peskin, M. E. and Schroeder, D. V., *An Introduction to Quantum Field Theory*. Westview Press, 1995.
- [59] Greiner, W. and Reinhardt, J., *Quantum Electrodynamics*. Springer, 2003.
- [60] J. González, F. Guinea, and M. A. H. Vozmediano, "Non-Fermi liquid behavior of electrons in the half-filled honeycomb lattice (A renormalization group approach)," *Nuclear Physics B*, vol. 424, pp. 595–618, Aug. 1994.
- [61] V. N. Kotov, B. Uchoa, V. M. Pereira, F. Guinea, and A. H. Castro Neto, "Electron-Electron Interactions in Graphene: Current Status and Perspectives," *Reviews of Modern Physics*, vol. 84, pp. 1067–1125, July 2012.
- [62] K. W. K. Shung, "Dielectric function and plasmon structure of stage-1 intercalated graphite," *Phys. Rev. B*, vol. 34, pp. 979–993, Jul 1986.
- [63] B. Wunsch, T. Stauber, F. Sols, and F. Guinea, "Dynamical polarization of graphene at finite doping," *New Journal of Physics*, vol. 8, p. 318, Dec. 2006.
- [64] E. H. Hwang and S. Das Sarma, "Dielectric function, screening, and plasmons in two-dimensional graphene," *Phys. Rev. B*, vol. 75, p. 205418, May 2007.

-
- [65] M. Schütt, P. M. Ostrovsky, I. V. Gornyi, and A. D. Mirlin, “Coulomb interaction in graphene: Relaxation rates and transport,” *Phys. Rev. B*, vol. 83, p. 155441, Apr 2011.
- [66] D. C. Elias, R. V. Gorbachev, A. S. Mayorov, S. V. Morozov, A. A. Zhukov, P. Blake, L. A. Ponomarenko, I. V. Grigorieva, K. S. Novoselov, F. Guinea, and A. K. Geim, “Dirac cones reshaped by interaction effects in suspended graphene,” *Nature Physics*, vol. 7, p. 701, 2011.
- [67] Greiner, W. and Reinhardt, J., *Field Quantization*. Springer, 1996.
- [68] Kopietz, P. and Bartosch, L. and Schütz, F., *Introduction to the Functional Renormalization Group*. Springer, 2010.
- [69] F. J. Dyson, “The S Matrix in Quantum Electrodynamics,” *Phys. Rev.*, vol. 75, pp. 1736–1755, Jun 1949.
- [70] J. Schwinger, “On the Green’s functions of quantized fields. I,” *Proceedings of the National Academy of Sciences*, vol. 37, no. 7, pp. 452–455, 1951.
- [71] T. W. Appelquist, M. Bowick, D. Karabali, and L. C. R. Wijewardhana, “Spontaneous chiral-symmetry breaking in three-dimensional QED,” *Phys. Rev. D*, vol. 33, pp. 3704–3713, Jun 1986.
- [72] T. Appelquist, D. Nash, and L. C. R. Wijewardhana, “Critical Behavior in (2+1)-Dimensional QED,” *Phys. Rev. Lett.*, vol. 60, pp. 2575–2578, Jun 1988.
- [73] C. Popovici, C. S. Fischer, and L. von Smekal, “Fermi velocity renormalization and dynamical gap generation in graphene,” *Phys. Rev. B*, vol. 88, p. 205429, Nov 2013.
- [74] C. Wetterich, “Average action and the renormalization group equations,” *Nuclear Physics B*, vol. 352, no. 3, pp. 529 – 584, 1991.
- [75] C. Wetterich, “Effective Average Action in Statistical Physics and Quantum Field Theory,” *International Journal of Modern Physics A*, vol. 16, pp. 1951–1982, 2001.
- [76] H. Gies and C. Wetterich, “Renormalization flow from UV to IR degrees of freedom,” *ArXiv High Energy Physics - Phenomenology e-prints*, May 2002.
- [77] J. Berges, N. Tetradis, and C. Wetterich, “Non-perturbative renormalization flow in quantum field theory and statistical physics,” *Physics Reports*, vol. 363, pp. 223–386, June 2002.
- [78] R. Gezzi, T. Pruschke, and V. Meden, “Functional renormalization group for nonequilibrium quantum many-body problems,” *Phys. Rev. B*, vol. 75, p. 045324, Jan. 2007.
- [79] F. Schütz and P. Kopietz, “Functional renormalization group with vacuum expectation values and spontaneous symmetry breaking,” *Journal of Physics A Mathematical General*, vol. 39, pp. 8205–8219, June 2006.
- [80] S. G. Jakobs, V. Meden, and H. Schoeller, “Nonequilibrium Functional Renormalization Group for Interacting Quantum Systems,” *Physical Review Letters*, vol. 99, p. 150603, Oct. 2007.
- [81] P. Strack, R. Gersch, and W. Metzner, “Renormalization group flow for fermionic superfluids at zero temperature,” *Phys. Rev. B*, vol. 78, p. 014522, Jul 2008.

- [82] T. Gasenzer and J. M. Pawłowski, “Functional renormalisation group approach to far-from-equilibrium quantum field dynamics,” *ArXiv e-prints*, Oct. 2007.
- [83] J. Berges and G. Hoffmeister, “Nonthermal fixed points and the functional renormalization group,” *Nuclear Physics B*, vol. 813, pp. 383–407, June 2009.
- [84] S. G. Jakobs, M. Pletyukhov, and H. Schoeller, “Nonequilibrium functional renormalization group with frequency-dependent vertex function: A study of the single-impurity Anderson model,” *Phys. Rev. B*, vol. 81, p. 195109, May 2010.
- [85] T. Kloss and P. Kopietz, “Nonequilibrium time evolution of bosons from the functional renormalization group,” *Phys. Rev. B*, vol. 83, p. 205118, May 2011.
- [86] J. Berges and D. Mesterházy, “Introduction to the nonequilibrium functional renormalization group,” *Nuclear Physics B Proceedings Supplements*, vol. 228, pp. 37–60, July 2012.
- [87] W. Metzner, M. Salmhofer, C. Honerkamp, V. Meden, and K. Schönhammer, “Functional renormalization group approach to correlated fermion systems,” *Rev. Mod. Phys.*, vol. 84, pp. 299–352, Mar 2012.
- [88] Y. Tanizaki, G. Fejős, and T. Hatsuda, “Fermionic functional renormalization group approach to superfluid phase transition,” *Progress of Theoretical and Experimental Physics*, vol. 2014, p. 043I01, Apr. 2014.
- [89] C. Bauer, A. Rückriegel, A. Sharma, and P. Kopietz, “Nonperturbative renormalization group calculation of quasiparticle velocity and dielectric function of graphene,” *Phys. Rev. B*, vol. 92, p. 121409, Sept. 2015.
- [90] A. Sharma and P. Kopietz, “Multilogarithmic velocity renormalization in graphene,” *Phys. Rev. B*, vol. 93, p. 235425, June 2016.
- [91] Tinkham, M., *Introduction to Superconductivity*. Dover Publications, 1996.
- [92] Altland, A. and Simons, B., *Condensed Matter Field Theory*. Cambridge University Press, 2010.
- [93] A. Kamenev, *Field Theory of Non-Equilibrium Systems*. Cambridge University Press, 2011.
- [94] H. Takagi and Y. Kuroda, “Anderson localization and superconducting transition temperature in two-dimensional systems,” *Solid State Communications*, vol. 41, no. 9, pp. 643 – 648, 1982.
- [95] S. Maekawa, H. Ebisawa, and H. Fukuyama, “Upper Critical Field in Two-Dimensional Superconductors,” *Journal of the Physical Society of Japan*, vol. 52, no. 4, pp. 1352–1360, 1983.
- [96] R. A. Smith, B. S. Handy, and V. Ambegaokar, “Upper critical field in disordered two-dimensional superconductors,” *Phys. Rev. B*, vol. 61, pp. 6352–6359, Mar 2000.
- [97] R. A. Smith, B. S. Handy, and V. Ambegaokar, “Width and magnetic-field dependence of the transition temperature in ultranarrow superconducting wires,” *Phys. Rev. B*, vol. 63, p. 094513, Feb 2001.

-
- [98] M. Flory, R. C. Helling, and C. Sluka, “How I Learned to Stop Worrying and Love QFT,” *ArXiv e-prints*, Jan. 2012.
- [99] Negele, J. W. and Orland, H., *Quantum Many-Particle Systems*. Westview Press, 1998.
- [100] D. I. Kazakov and D. V. Shirkov, “Asymptotic Series of Quantum Field Theory and Their Summation,” *Fortschritte der Physik*, vol. 28, no. 8-9, pp. 465–499, 1980.
- [101] V. V. Belokurov, E. T. Shavgulidze, and Y. P. Solovoyov, “New Perturbation Theory for Quantum Field Theory: Convergent Series Instead of Asymptotic Expansions,” *Acta Applicandae Mathematica*, vol. 68, pp. 71–104, Aug 2001.
- [102] Billingsley, P., *Probability and Measure*. John Wiley & Sons, Inc., 2012.
- [103] Gradshteyn, I. S. and Ryzhik, I. M., *Table of Integrals, Series, and Products*. Elsevier, 2007.
- [104] F. J. Dyson, “Divergence of Perturbation Theory in Quantum Electrodynamics,” *Phys. Rev.*, vol. 85, pp. 631–632, Feb 1952.
- [105] Kleinert, H., *Path Integrals in Quantum Mechanics, Statistics, Polymer Physics, and Financial Markets*. World Scientific, 2009.
- [106] Griffiths, D. J., *Introduction to Electrodynamics*. Cambridge University Press, 2017.
- [107] Jackson, J. D., *Classical Electrodynamics*. Hamilton Printing Company, 1999.
- [108] Landau, L. D. and Lifschitz, E. M., *Elektrodynamik der Kontinua*. Akademie-Verlag Berlin, 1990.
- [109] Kittel, C., *Introduction to Solid State Physics*. John Wiley & Sons, 2006.
- [110] Ashcroft, N. W. and Mermin, N. D., *Festkörperphysik*. Oldenbourg, 2005.
- [111] K. v. Klitzing, G. Dorda, and M. Pepper, “New Method for High-Accuracy Determination of the Fine-Structure Constant Based on Quantized Hall Resistance,” *Phys. Rev. Lett.*, vol. 45, pp. 494–497, Aug 1980.
- [112] K. von Klitzing, “The quantized Hall effect,” *Rev. Mod. Phys.*, vol. 58, pp. 519–531, Jul 1986.
- [113] G. Ebert, K. Klitzing, C. Probst, and K. Ploog, “Magneto-quantumtransport on GaAs-Al_xGa_{1-x}As heterostructures at very low temperatures,” *Solid State Communications*, vol. 44, no. 2, pp. 95 – 98, 1982.
- [114] R. Willett, J. P. Eisenstein, H. L. Störmer, D. C. Tsui, A. C. Gossard, and J. H. English, “Observation of an even-denominator quantum number in the fractional quantum Hall effect,” *Phys. Rev. Lett.*, vol. 59, pp. 1776–1779, Oct 1987.
- [115] Schwabl, F., *Quantenmechanik*. Springer, 2007.
- [116] Jain, J. K., *Composite Fermions*. Cambridge University Press, 2007.
- [117] Fradkin, E., *Field Theories of Condensed Matter Physics*. Cambridge University Press, 2013.

- [118] D. Tong, “Lectures on the Quantum Hall Effect,” *ArXiv e-prints*, June 2016.
- [119] G. A. Baraff and D. C. Tsui, “Explanation of quantized-Hall-resistance plateaus in heterojunction inversion layers,” *Phys. Rev. B*, vol. 24, pp. 2274–2277, Aug 1981.
- [120] T. Toyoda, V. Gudmundsson, and Y. Takahashi, “The plateau widths of the quantized Hall conductance,” *Physics Letters A*, vol. 102, no. 3, pp. 130 – 132, 1984.
- [121] W. Kohn, “Cyclotron Resonance and de Haas-van Alphen Oscillations of an Interacting Electron Gas,” *Phys. Rev.*, vol. 123, pp. 1242–1244, Aug 1961.
- [122] M. L. Sadowski, G. Martinez, M. Potemski, C. Berger, and W. A. de Heer, “Landau Level Spectroscopy of Ultrathin Graphite Layers,” *Phys. Rev. Lett.*, vol. 97, p. 266405, Dec 2006.
- [123] Z. Jiang, E. A. Henriksen, L. C. Tung, Y.-J. Wang, M. E. Schwartz, M. Y. Han, P. Kim, and H. L. Stormer, “Infrared Spectroscopy of Landau Levels of Graphene,” *Phys. Rev. Lett.*, vol. 98, p. 197403, May 2007.
- [124] S. Das Sarma, S. Adam, E. H. Hwang, and E. Rossi, “Electronic transport in two-dimensional graphene,” *Rev. Mod. Phys.*, vol. 83, pp. 407–470, May 2011.
- [125] Y. A. Bychkov and G. Martinez, “Magnetoplasmon excitations in graphene for filling factors $\nu \leq 6$,” *Phys. Rev. B*, vol. 77, p. 125417, Mar 2008.
- [126] R. Roldán, J.-N. Fuchs, and M. O. Goerbig, “Spin-flip excitations, spin waves, and magnetoexcitons in graphene Landau levels at integer filling factors,” *Phys. Rev. B*, vol. 82, p. 205418, Nov 2010.
- [127] K. Shizuya, “Many-body corrections to cyclotron resonance in monolayer and bilayer graphene,” *Phys. Rev. B*, vol. 81, p. 075407, Feb 2010.
- [128] A. A. Sokolik, A. D. Zabolotskiy, and Y. E. Lozovik, “Many-body effects of Coulomb interaction on Landau levels in graphene,” *Phys. Rev. B*, vol. 95, p. 125402, Mar 2017.
- [129] D. C. Tsui, H. L. Stormer, and A. C. Gossard, “Two-Dimensional Magnetotransport in the Extreme Quantum Limit,” *Phys. Rev. Lett.*, vol. 48, pp. 1559–1562, May 1982.
- [130] R. B. Laughlin, “Anomalous Quantum Hall Effect: An Incompressible Quantum Fluid with Fractionally Charged Excitations,” *Phys. Rev. Lett.*, vol. 50, pp. 1395–1398, May 1983.
- [131] J. K. Jain, “Composite-fermion approach for the fractional quantum Hall effect,” *Phys. Rev. Lett.*, vol. 63, pp. 199–202, Jul 1989.
- [132] J. Goldstone, “Field theories with « Superconductor » solutions,” *Il Nuovo Cimento (1955-1965)*, vol. 19, pp. 154–164, Jan 1961.
- [133] J. Goldstone, A. Salam, and S. Weinberg, “Broken Symmetries,” *Phys. Rev.*, vol. 127, pp. 965–970, Aug 1962.
- [134] C. Nayak, S. H. Simon, A. Stern, M. Freedman, and S. Das Sarma, “Non-Abelian anyons and topological quantum computation,” *Rev. Mod. Phys.*, vol. 80, pp. 1083–1159, Sep 2008.

-
- [135] A. Stern, “Anyons and the quantum Hall effect—A pedagogical review,” *Annals of Physics*, vol. 323, no. 1, pp. 204 – 249, 2008. January Special Issue 2008.
- [136] V. L. Berezinskii, “Destruction of Long-range Order in One-dimensional and Two-dimensional Systems having a Continuous Symmetry Group I. Classical Systems,” *Soviet Journal of Experimental and Theoretical Physics*, vol. 32, p. 493, 1971.
- [137] V. L. Berezinskii, “Destruction of Long-range Order in One-dimensional and Two-dimensional Systems Possessing a Continuous Symmetry Group. II. Quantum Systems,” *Soviet Journal of Experimental and Theoretical Physics*, vol. 34, p. 610, 1972.
- [138] J. M. Kosterlitz and D. J. Thouless, “Ordering, metastability and phase transitions in two-dimensional systems,” *Journal of Physics C: Solid State Physics*, vol. 6, no. 7, p. 1181, 1973.
- [139] C. R. Dean, A. F. Young, P. Cadden-Zimansky, L. Wang, H. Ren, K. Watanabe, T. Taniguchi, P. Kim, J. Hone, and K. L. Shepard, “Multicomponent fractional quantum Hall effect in graphene,” *Nature Physics*, vol. 7, pp. 693–696, Sept. 2011. ArXiv: arXiv:1010.1179v1
- [140] C. Tóke and J. K. Jain, “SU(4) composite fermions in graphene: Fractional quantum Hall states without analog in GaAs,” *Phys. Rev. B*, vol. 75, p. 245440, Jun 2007.
- [141] M. O. Goerbig and N. Regnault, “Analysis of a SU(4) generalization of Halperin’s wave function as an approach towards a SU(4) fractional quantum Hall effect in graphene sheets,” *Phys. Rev. B*, vol. 75, p. 241405, Jun 2007.
- [142] Z. Papić, M. O. Goerbig, and N. Regnault, “Theoretical expectations for a fractional quantum Hall effect in graphene,” *Solid State Communications*, vol. 149, no. 27, pp. 1056 – 1060, 2009. Recent Progress in Graphene Studies.
- [143] Z. Papić, M. O. Goerbig, and N. Regnault, “Atypical Fractional Quantum Hall Effect in Graphene at Filling Factor 1/3,” *Phys. Rev. Lett.*, vol. 105, p. 176802, Oct 2010.
- [144] D. V. Khveshchenko, “Composite Dirac fermions in graphene,” *Phys. Rev. B*, vol. 75, p. 153405, Apr 2007.
- [145] S. Modak, S. S. Mandal, and K. Sengupta, “Fermionic Chern-Simons theory of SU(4) fractional quantum Hall effect,” *Phys. Rev. B*, vol. 84, p. 165118, Oct 2011.
- [146] A. Jellal and B. Malika, “FRACTIONAL QUANTUM HALL STATES IN GRAPHENE,” *International Journal of Geometric Methods in Modern Physics*, vol. 07, no. 01, pp. 143–164, 2010.
- [147] M. R. Peterson and C. Nayak, “More realistic Hamiltonians for the fractional quantum Hall regime in GaAs and graphene,” *Phys. Rev. B*, vol. 87, p. 245129, Jun 2013.
- [148] M. R. Peterson and C. Nayak, “Effects of Landau Level Mixing on the Fractional Quantum Hall Effect in Monolayer Graphene,” *Phys. Rev. Lett.*, vol. 113, p. 086401, Aug 2014.
- [149] I. Sodemann and A. H. MacDonald, “Landau level mixing and the fractional quantum Hall effect,” *Phys. Rev. B*, vol. 87, p. 245425, Jun 2013.

- [150] X. Du, I. Skachko, F. Duerr, A. Luican, and E. Y. Andrei, “Fractional quantum Hall effect and insulating phase of Dirac electrons in graphene,” *Nature*, vol. 462, pp. 192–195, Nov. 2009.
- [151] I. Skachko, X. Du, F. Duerr, A. Luican, D. A. Abanin, L. S. Levitov, and E. Y. Andrei, “Fractional quantum Hall effect in suspended graphene probed with two-terminal measurements,” *Philosophical Transactions of the Royal Society of London A: Mathematical, Physical and Engineering Sciences*, vol. 368, no. 1932, pp. 5403–5416, 2010.
- [152] D. A. Abanin, I. Skachko, X. Du, E. Y. Andrei, and L. S. Levitov, “Fractional quantum Hall effect in suspended graphene: Transport coefficients and electron interaction strength,” *Phys. Rev. B*, vol. 81, p. 115410, Mar 2010.
- [153] S. C. Zhang, T. H. Hansson, and S. Kivelson, “Effective-Field-Theory Model for the Fractional Quantum Hall Effect,” *Phys. Rev. Lett.*, vol. 62, pp. 82–85, Jan 1989.
- [154] X. G. Wen and Q. Niu, “Ground-state degeneracy of the fractional quantum Hall states in the presence of a random potential and on high-genus Riemann surfaces,” *Phys. Rev. B*, vol. 41, pp. 9377–9396, May 1990.
- [155] J. Fröhlich and A. Zee, “Large scale physics of the quantum hall fluid,” *Nuclear Physics B*, vol. 364, no. 3, pp. 517 – 540, 1991.
- [156] X. G. Wen and A. Zee, “Classification of Abelian quantum Hall states and matrix formulation of topological fluids,” *Phys. Rev. B*, vol. 46, pp. 2290–2301, Jul 1992.
- [157] B. I. Halperin, P. A. Lee, and N. Read, “Theory of the half-filled Landau level,” *Phys. Rev. B*, vol. 47, pp. 7312–7343, Mar 1993.
- [158] X.-G. Wen, “Topological orders and edge excitations in fractional quantum Hall states,” *Advances in Physics*, vol. 44, pp. 405–473, Sept. 1995.
- [159] X.-G. Wen, “Projective construction of non-Abelian quantum Hall liquids,” *Phys. Rev. B*, vol. 60, pp. 8827–8838, Sep 1999.
- [160] Heinonen, O., *Composite Fermions*. World Scientific, 1998.
- [161] A. Lopez and E. Fradkin, “Fractional quantum Hall effect and Chern-Simons gauge theories,” *Phys. Rev. B*, vol. 44, pp. 5246–5262, Sep 1991.
- [162] A. Balatsky and E. Fradkin, “Singlet quantum Hall effect and Chern-Simons theories,” *Phys. Rev. B*, vol. 43, pp. 10622–10634, May 1991.
- [163] A. Lopez and E. Fradkin, “Response functions and spectrum of collective excitations of fractional-quantum-Hall-effect systems,” *Phys. Rev. B*, vol. 47, pp. 7080–7094, Mar 1993.
- [164] A. Lopez and E. Fradkin, “Fermionic Chern-Simons theory for the fractional quantum Hall effect in bilayers,” *Phys. Rev. B*, vol. 51, pp. 4347–4368, Feb 1995.
- [165] H. Bruus and K. Flensberg, *Many-body quantum theory in condensed matter physics*. Oxford University Press, 2009.
- [166] K.-c. Chou, Z.-b. Su, B.-l. Hao, and L. Yu, “Equilibrium and Nonequilibrium Formalisms Made Unified,” *Phys. Rept.*, vol. 118, p. 1, 1985.

- [167] M. V. Feigel'man, A. I. Larkin, and M. A. Skvortsov, "Keldysh action for disordered superconductors," *Phys. Rev. B*, vol. 61, pp. 12361–12388, May 2000.
- [168] G. Schwiete and A. M. Finkel'stein, "Keldysh approach to the renormalization group analysis of the disordered electron liquid," *Phys. Rev. B*, vol. 89, p. 075437, Feb. 2014.
- [169] G. Schwiete and A. M. Finkel'stein, "Renormalization group analysis of thermal transport in the disordered Fermi liquid," *Phys. Rev. B*, vol. 90, p. 155441, Oct. 2014.
- [170] B. Sbierski, G. Pohl, E. J. Bergholtz, and P. W. Brouwer, "Quantum Transport of Disordered Weyl Semimetals at the Nodal Point," *Phys. Rev. Lett.*, vol. 113, p. 026602, Jul 2014.

Chapter 2

Electrons in graphene – A quantum field theory at low energies

In this chapter we want to obtain an effective low-energy model to describe the dynamics of electron-like quasiparticles in the vicinity of the charge neutrality point. Starting from a single carbon atom we explain the microscopic mechanism behind the formation of the honeycomb crystal lattice structure. Due to the predominantly covalent nature of bonding in graphene, the π -bands are approximated by a tight-binding model that describes the electron dynamics as a “discretized” hopping from lattice site to lattice site. After transforming the discrete lattice model to momentum space and keeping only long wavelength contributions, we perform a continuum limit by considering very large system sizes, turning the discrete model into a continuum quantum field theory for the quasiparticles.

2.1 Orbital hybridization of carbon, molecular bonding and the honeycomb lattice

It is well-known that the extraordinary electronic properties of graphene derive from the honeycomb crystal lattice structure. Since the microscopic mechanism that leads to the formation of any crystal is undoubtedly rooted in the atomic structure of its constituents, we briefly analyze an isolated carbon atom first, in order to understand why a macroscopic amount of carbon atoms arrange themselves in a honeycomb structure. Neglecting relativistic corrections, such as spin-orbit coupling, the Hamiltonian of a single carbon atom is given by [1–3]

$$H_{atom}(\vec{R}) = \sum_{\alpha=1}^6 \left(-\frac{\hbar}{2m} \frac{\partial^2}{\partial \vec{r}_\alpha^2} + V_{en}(\vec{r}_\alpha - \vec{R}) \right) + \frac{1}{2} \sum_{\substack{\alpha, \beta \\ \alpha \neq \beta}} V_{ee}(\vec{r}_\alpha - \vec{r}_\beta). \quad (2.1.1)$$

Here, lower (upper) case vectors describe electron (nuclear) coordinates in three-dimensional Euclidean space. The first term in brackets, containing the partial derivative with respect to the electronic coordinates, is the kinetic energy of the electrons in position representation, while the remaining two terms describe the two-body interactions between an electron and a nucleus, and between two electrons. Their interaction amplitudes are given by the Coulomb interaction

$$V_{en}(\vec{r}_\alpha - \vec{R}) = -\frac{6e^2}{|\vec{r}_\alpha - \vec{R}|}, \quad V_{ee}(\vec{r}_\alpha - \vec{r}_\beta) = \frac{e^2}{|\vec{r}_\alpha - \vec{r}_\beta|}. \quad (2.1.2)$$

Note, however, that the electron-nucleus interaction $V_{en}(\vec{r}_\alpha - \vec{R})$ effectively reduces to a single-particle potential, one for each of the six electrons, since the nucleus is assumed to be fixed in space. Thus, the only true two-particle potential in the problem is the electron-electron interaction, which prevents us from diagonalizing Eq. (2.1.1) analytically exactly. Its approximative treatment is the real challenge of atomic and molecular physics, requiring rather involved analytical and numerical techniques. A thorough discussion of these techniques is beyond the scope of this chapter, but neglecting the effect of the electron-electron interaction on the atomic spectrum and wavefunctions entirely is not an option either, since precise knowledge of the latter is crucial to understand chemical bonding. Therefore, as a compromise we neglect the electron-electron interaction for the moment and briefly discuss its influence on the structures we find, referring to the literature for details [1–8].

For vanishing electron-electron interaction the atomic Hamiltonian (2.1.1) decouples into six hydrogen-like Hamiltonians, each of which is diagonalized by the normalized single-electron wavefunction [1, 3]

$$\psi_{nlm}(r, \theta, \varphi) = \sqrt{\left(\frac{2Z}{na_0}\right)^3 \frac{(n-l-1)!}{2n(n+l)!}} e^{-Zr/na_0} \left(\frac{2Zr}{na_0}\right)^l L_{n-l-1}^{2l+1}\left(\frac{2Zr}{na_0}\right) Y_l^m(\theta, \varphi), \quad (2.1.3)$$

where $a_0 = 4\pi\epsilon_0\hbar^2/me^2$ is the Bohr radius, L_{n-l-1}^{2l+1} are generalized Laguerre polynomials and Y_l^m are spherical harmonics. Here, we neglected the spin degree of freedom for brevity. The spherical coordinates r , θ and φ are measured relative to the position of the nucleus, and the quantum numbers n , l and m are well-known from the hydrogen problem, being the principal, orbital angular momentum and magnetic quantum number, respectively. Note that the atomic number $Z = 6$ appears explicitly in the wavefunction, due to the enlarged charge of the carbon nucleus in comparison to the hydrogen nucleus, which effectively reduces the spatial extent of the electron cloud, cf. Eq. (2.1.2). Since the electrons are assumed to be noninteracting, the wavefunction for the entire electron system can be written as a Slater determinant[1, 4],

$$\Psi_{n_1l_1m_1\dots n_6l_6m_6}(\vec{r}_1, \dots, \vec{r}_6) = \frac{1}{\sqrt{6!}} \begin{vmatrix} \psi_{n_1l_1m_1}(\vec{r}_1) & \psi_{n_2l_2m_2}(\vec{r}_1) & \cdots & \psi_{n_6l_6m_6}(\vec{r}_1) \\ \psi_{n_1l_1m_1}(\vec{r}_2) & \psi_{n_2l_2m_2}(\vec{r}_2) & \cdots & \psi_{n_6l_6m_6}(\vec{r}_2) \\ \vdots & \vdots & \ddots & \vdots \\ \psi_{n_1l_1m_1}(\vec{r}_6) & \psi_{n_2l_2m_2}(\vec{r}_6) & \cdots & \psi_{n_6l_6m_6}(\vec{r}_6) \end{vmatrix}, \quad (2.1.4)$$

which accounts for the correct (anti-)symmetry of the wavefunction under particle permutation according to the Pauli principle. As a consequence, the energy eigenvalue of the entire system is just the sum of the single-particle energy eigenvalues, giving rise to a large degeneracy. If the electron spin is properly taken into account and using spectroscopic notation, the electron configuration of the ground state is given by $(1s)^2(2s)^2(2p)^2$.

As soon as Coulomb interactions are taken into account it should be clear that the energy spectrum is altered, partially lifting the degeneracies of the noninteracting model [1]. Furthermore, the above Slater determinant states can no longer be the exact energy eigenstates of the interacting electron system. Nevertheless, since these states still form a basis of the fermionic multiparticle Hilbert space, the exact energy eigenstates can be represented as a linear combination, where the expansion coefficients have to be determined from the Schrödinger equation of the interacting problem. Although this diagonalization strategy in principle works, there is no reason to believe that the matrix elements of the Coulomb interaction, which occur in the calculation of the expansion coefficients, are in any way small. Hence, we expect the linear combination to be rather complex, containing a lot of terms to even approximate the exact eigenstates. A more promising approach is to keep the form of the Slater determinant as an

ansatz, but to modify the single-particle states (2.1.3) within it in such way that the influence of the Coulomb interaction is minimized, for example by the introduction of several variational parameters. This idea leads to the well-known Hartree-Fock mean-field theory of multi-electron atoms [1–8]. Possibly its greatest feature is that the relevant physics can be described in terms of single-particle quantum mechanics to a good approximation, even though we are dealing with a strongly interacting multi-particle system. For instance, in this theory it still makes sense to use the single-particle quantum numbers n, l and m for a classification of states and to say that the ground state of carbon is given by the electron configuration $(1s)^2(2s)^2(2p)^2$, although they are not well-defined in the presence of a two-body interaction. As mentioned previously, here we do not want to go into detail on how to formalize this idea, and how to derive and solve the equations that follow. Instead, we refer to the literature listed above, and we continue our discussion under the assumption that the Hartree-Fock wavefunctions have been obtained.

Now let us consider the case of N_c interacting carbon atoms whose nuclei are pinned to the positions $\vec{\mathbf{R}} = (\vec{R}_1, \dots, \vec{R}_{N_c})$. Such a scenario is described by the Hamiltonian [7, 9–11]

$$H_{el}(\vec{\mathbf{R}}) = \sum_{i=1}^{N_c} H_{atom}(\vec{R}_i) + \frac{1}{2} \sum_{\substack{i,j \\ i \neq j}} \left(\sum_{\alpha,\beta} V_{ee}(\vec{r}_{\alpha i} - \vec{r}_{\beta j}) + 2 \sum_{\alpha} V_{en}(\vec{r}_{\alpha i} - \vec{R}_j) + \sum_{\alpha,\beta} V_{nn}(\vec{R}_i - \vec{R}_j) \right), \quad (2.1.5)$$

where the first term represents the isolated atoms, Eq. (2.1.1), and the remaining three terms describe their mutual interactions, that is, the electron-electron, electron-nuclei and nuclei-nuclei Coulomb interactions between the constituents of two different atoms. Here, the nuclear positions $\vec{\mathbf{R}}$ only enter as parameters, since the nuclear kinetic energies do not appear. As a consequence, the energy eigenvalues of Eq. (2.1.5) are functions of $\vec{\mathbf{R}}$, which can be thought of as surfaces or landscapes in the space of nuclear configurations. Their local minima define the possible equilibrium positions of the atoms and, hence, determine the crystal lattice structure, encoding all the information about chemical bonding.¹ For carbon based materials there is a plethora of local minima with the honeycomb lattice being only one of them, cf. Fig. 1.1. However, now that we have understood the structure of an isolated carbon atom we can at least motivate why the honeycomb crystal lattice should be one of those minima.

To diagonalize the above Hamiltonian one might be tempted to construct its energy eigenfunctions from linear combinations of tensor products of atomic orbitals. Albeit a viable strategy – the atomic orbitals form a basis of the Hilbert space [1, 2] – it is inefficient, due to the same reason we encountered before. Intuitively, the “bare” atomic orbitals of one atom do not account for the presence of another nearby atom. Once again, a better approach to construct molecular orbitals is to consider modified atomic orbitals, which precisely account for that fact. This idea, which is actually not so different from the Hartree-Fock approach mentioned above, dates back to Linus Pauling in his explanation of the geometrical structure of methane [12], culminating in the theory of hybridization [3–5, 7, 8, 13, 14]. In its simplest form the hybridization of atomic orbitals can be understood as follows. (In the following consideration we can forget about the

¹The above parametric Hamiltonian for the electrons also appears in a first principle calculation, where the general many-body Hamiltonian of interacting electrons and nuclei is considered as a starting point [5, 9]. In a full treatment one would isolate the nuclear kinetic energies from the remainder of the full Hamiltonian – the remainder being Eq. (2.1.5) – and separate the electron dynamics from the nuclear dynamics by virtue of the adiabatic movement of the nuclei. Employing the Born-Oppenheimer approximation, one obtains a Schrödinger equation for the nuclear wavefunction, in addition to the electronic Schrödinger equation implied by Eq. (2.1.5). Within the nuclear Schrödinger equation the electronic energy eigenvalues appear as a background potential in which the nuclei move, leading to the physics of phonons. This aspect of condensed matter theory in general and of graphene in particular will not be covered here.

inner shell $1s$ electrons, since they are tightly bound to their nucleus. Only the valence shell electrons matter for chemical bonding.)

In the presence of interatomic Coulomb interactions the individual atomic orbitals are deformed such that the Coulomb repulsion is minimized, while at the same time the overlap of the single electron wavefunctions that form a molecular bond is maximized. This competition results in a certain directedness, which can be achieved by linearly combining the $2s$ - and $2p$ -wavefunctions into hybrid-wavefunctions [4, 5, 13, 14]. It helps to visualize orbital hybridization and molecular bonding as a process, involving excitation and relaxation, albeit it is only a virtual one that is not accessible through experiments.² First, one of the two $2s$ -electrons is excited to the $2p$ -state, resulting in the electronic configuration $(1s)^2(2s)(2p)^3$ with four unpaired valence shell electrons. The wavefunction of the remaining $2s$ -electron then “hybridizes” with the wavefunction(s) of the $2p$ -electron(s), meaning the single-particle states $2s$ and $2p$ form new hybrid orbitals that are linear combinations of the two, which are then occupied by the electrons. Since there are three $2p$ -orbitals available for the $2s$ -orbital to form quantum superpositions, there are three possible hybridization schemes,³ sp^1 , sp^2 and sp^3 , which have a linear, trigonal planar and tetrahedral geometry respectively. These three basic geometrical structures can be viewed as the fundamental building blocks of carbon-based materials. Since they can be arranged in a sheer endless number of ways, it becomes clear why carbon plays such a distinguished role in chemistry, to the extent that an entire branch – organic chemistry – is devoted to the study of its compounds. The preferred type of hybridization depends on the environment, that is, which and how many other atoms are present, but also other external influences, such as temperature and pressure, play a role. The honeycomb lattice of graphene is the result of a pure sp^2 -hybridization, with single-particle wavefunctions [4, 5]

$$\psi_{sp^2,1} = \frac{1}{\sqrt{3}} \left(\psi_s + \sqrt{2}\psi_{p_x} \right), \quad (2.1.6a)$$

$$\psi_{sp^2,2} = \frac{1}{\sqrt{3}} \left(\psi_s + \sqrt{\frac{3}{2}}\psi_{p_x} - \frac{1}{\sqrt{2}}\psi_{p_y} \right), \quad (2.1.6b)$$

$$\psi_{sp^2,3} = \frac{1}{\sqrt{3}} \left(\psi_s - \sqrt{\frac{3}{2}}\psi_{p_x} - \frac{1}{\sqrt{2}}\psi_{p_y} \right), \quad (2.1.6c)$$

where neighboring atoms are oriented in an alternating pattern see Fig. 2.1. The three-dimensional material graphite has the structure of stacked graphene sheets that are loosely bound by the p_z orbitals, and diamond – another three-dimensional crystal lattice with pure sp^3 -hybridization – can be manufactured from graphite by applying large temperatures and pressures. At first glance it seems to be a bad idea to consider a set of excited atoms to describe the low-energy sector of the Hilbert space, but here is where the inter-atom interactions come into play. The “initial investment” of exciting the atoms that participate in molecular structure formation pays off by the bonding energy that is gained in the final step of the virtual process: the formation and occupation of molecular orbitals as superpositions of the two partially overlapping hybrid orbitals that are directly facing each other, see Figs. 2.1 and 2.2. If the inter-atom interactions would be neglected entirely, one would expect the ground state atoms

²Virtual processes are a common terminology in quantum many-body systems and quantum field theories. For instance, in quantum electrodynamics the scattering process between two electrons or between an electron and a positron to lowest order perturbation theory involves a virtual photon to be exchanged. The latter has to be distinguished from a real photon, since it does not lie on the mass shell – it is not restricted to have a vanishing rest mass – and, hence, cannot be measured in a laboratory [15–18].

³Actually, there is an entire hybridization spectrum sp^r with $r \in \mathbb{R}$. The p -character in the hybrid orbitals is not necessarily restricted to integers [13].

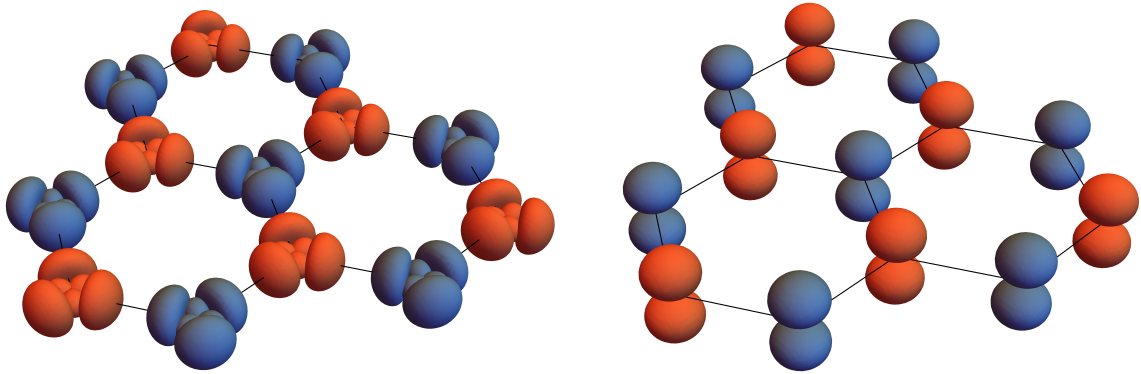


Figure 2.1: Carbon atoms arranged in a honeycomb lattice. The sp^2 - and p_z -orbitals of the individual atoms are shown separately (left and right) for clarity. To plot these orbitals we used the single-particle wavefunctions (2.1.3) and (2.1.6). A honeycomb lattice can be described as two triangular Bravais lattices (see below), which are shifted against each other. The atoms are coloured in red and blue to indicate their affiliation to one of these two Bravais sublattices. Note the relative orientation of the sp^2 -orbitals of neighboring carbon atoms, which alternates between the sublattices. The orbitals that are directly facing each other partially overlap and form molecular bonds, so-called σ -bonds, see Fig. 2.2, which explains the hexagonal lattice structure.

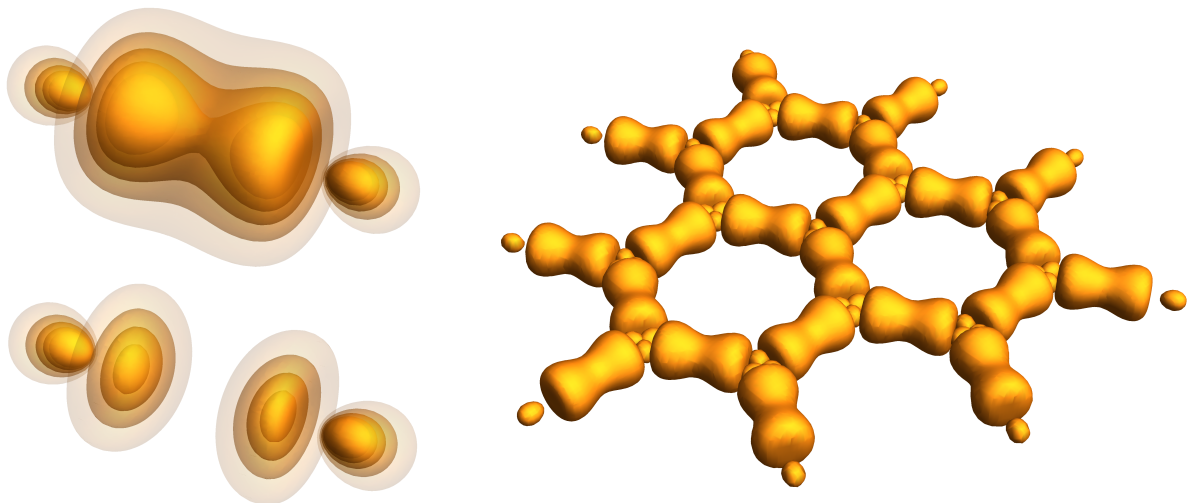


Figure 2.2: (Left) Surfaces of constant probability density for bonding (top left) and anti-bonding molecular orbitals (bottom left), that are formed from the two linear combinations of overlapping sp^2 wavefunctions of two nearby carbon atoms. (Right) Honeycomb lattice of graphene in terms of bonding molecular orbitals.

with electron configuration $(1s)^2(2s)^2(2p)^2$ to form the low-energy sector of the Hilbert space. Such an electron configuration, however, would lead to very different geometrical structures for micro- and macro-molecules in violation to observations.

Having understood the microscopic mechanism that leads to the formation of the honeycomb structure, we have all the ingredients necessary to come up with an effective model that captures the relevant low-energy degrees of freedom of interacting electrons in graphene. Before we do so let us first describe the honeycomb structure properly. Mathematically, a lattice – more precisely a Bravais lattice – is defined as a periodic array of discrete points $\vec{R}_{\text{Bravais}}^{n_1 n_2 \dots n_d}$ in a d -dimensional vector space, that is spanned by a set of d linearly independent lattice basis vectors, or primitive translation vectors $\vec{a}_1, \vec{a}_2, \dots, \vec{a}_d$ [9–11]

$$\vec{R}_{\text{Bravais}}^{n_1 n_2 \dots n_d} = n_1 \vec{a}_1 + n_2 \vec{a}_2 + \dots + n_d \vec{a}_d, \quad n_1, n_2, \dots, n_d \in \mathbb{Z}. \quad (2.1.7)$$

The set of integers n_1, n_2, \dots, n_d uniquely define each point in the lattice, and any integral translation of the whole set of points with respect to the primitive translation vectors maps the lattice onto itself. In two dimensions there are precisely five such lattices [9–11], but none of them describes the honeycomb structure directly. Instead, one has to construct it as a triangular lattice with two atoms per unit cell, or, equivalently, as two triangular Bravais lattices that are shifted against each other by a constant vector $\vec{\delta}$

$$\vec{R}_{0, n_1 n_2 m} = \vec{R}_{\text{triang}}^{n_1 n_2} + \vec{R}_{\text{shift}}^m = n_1 \vec{a}_1 + n_2 \vec{a}_2 + m \vec{\delta}. \quad (2.1.8)$$

Here, m is either 0 or 1, distinguishing the two sublattices. The lattice basis vectors are not uniquely defined, leaving a certain freedom of choice. We use the following convention

$$\vec{a}_1 = \frac{a}{2} (3, \sqrt{3}), \quad \vec{a}_2 = \frac{a}{2} (3, -\sqrt{3}), \quad (2.1.9)$$

where $a \approx 1.42 \text{ \AA}$ is the equilibrium distance between two neighboring atoms [19, 20]. For the shift vector itself there are three natural choices

$$\vec{\delta}_1 = \frac{a}{2} (1, \sqrt{3}), \quad \vec{\delta}_2 = \frac{a}{2} (1, -\sqrt{3}), \quad \vec{\delta}_3 = -a (1, 0), \quad (2.1.10)$$

each of which points towards one of the three nearest neighbors and yields the same honeycomb structure. In addition to the discrete translation symmetry of the underlying Bravais lattice, the honeycomb crystal lattice shows two more discrete symmetries, a rotation and a reflection symmetry. A rotation of the entire crystal by $60^\circ = 2\pi/6$ around an axis perpendicular to the sheet and centered at one hexagon maps the crystal onto itself, while the A and B Bravais sublattices are interchanged. A straight line connecting two nearest neighbor atoms defines a reflection axis, which not only maps the crystal lattice onto itself, but also leaves the individual sublattices invariant. Since the three nearest neighbors are equivalent there are three of those reflection symmetry axes.⁴

The basis vectors of the reciprocal lattice – the discrete Fourier transform of the real space Bravais lattice [9–11] – are given by

$$\vec{b}_1 = \frac{2\pi}{3a} (1, \sqrt{3}), \quad \vec{b}_2 = \frac{2\pi}{3a} (1, -\sqrt{3}). \quad (2.1.11)$$

As one can easily check, they fulfill the reciprocity relation $\vec{a}_i \cdot \vec{b}_j = 2\pi \delta_{ij}$. In Fig. 2.3 we show a schematic representation of the real space lattice of graphene with primitive translation and shift vectors, as well as the reciprocal lattice basis vectors and the associated first Brillouin zone

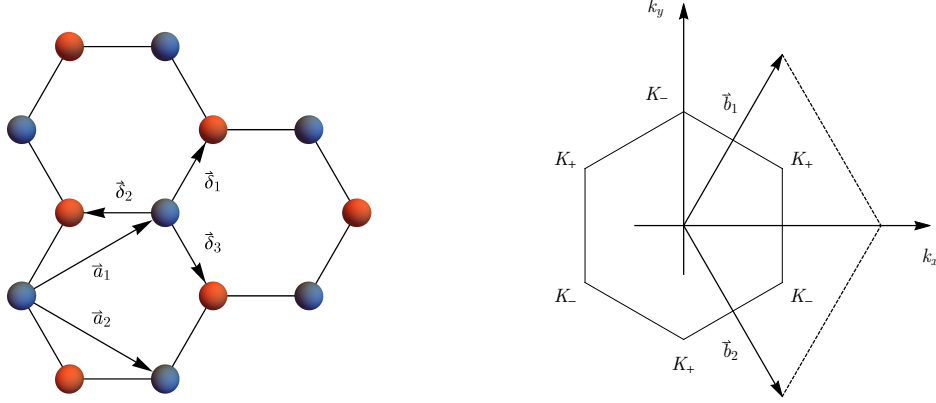


Figure 2.3: (Left) Lattice structure of graphene in real space with primitive translation vectors \vec{a}_1 and \vec{a}_2 , and shift vectors $\vec{\delta}_1$, $\vec{\delta}_2$ and $\vec{\delta}_3$. (Right) Reciprocal lattice vectors \vec{b}_1 and \vec{b}_2 and first Brillouin zone with indicated K -points in momentum space. Note that the first Brillouin zone has a hexagonal shape just like the real space crystal structure, but we emphasize that this fact is a mere coincidence. See also Refs. [19, 20] for similar depictions of the real-space lattice and the Brillouin zone.

in momentum space. The six corners of the Brillouin zone, the so-called K -points, are given by

$$\vec{K}_+ = \frac{2\pi}{3a} (1, 1/\sqrt{3}) \cong \frac{2\pi}{3a} (-1, 1/\sqrt{3}) \cong \frac{2\pi}{3a} (0, -2/\sqrt{3}), \quad (2.1.12a)$$

$$\vec{K}_- = \frac{2\pi}{3a} (1, -1/\sqrt{3}) \cong \frac{2\pi}{3a} (0, 2/\sqrt{3}) \cong \frac{2\pi}{3a} (-1, -1/\sqrt{3}), \quad (2.1.12b)$$

where the equivalence relation “ \cong ” indicates that they are identical up to integral reciprocal lattice vector translations (note the symmetry relation $\vec{K}_- \cong -\vec{K}_+$). In other words, only two out of the six K -points are truly inequivalent. As we will see in the next section, these points play a crucial role in the low-energy dynamics of electrons in graphene.

2.2 Tight-binding approximation for graphene

To gain a microscopic understanding for the formation of the honeycomb lattice it was beneficial to write the electronic Hamiltonian (2.1.5) in a first quantized form, that emphasizes the individual atoms. Mathematically, the infinite number of energy eigenstates of a single atom merge into an infinite number of energy bands in a lattice array of atoms. For practical band structure calculations however, this form is not the best starting point. Since by definition a crystal lattice is spatially periodic, Bloch’s theorem applies [9–11, 21]. Hence, the many-body Hamiltonian may be cast in a second quantized form in terms of ladder operators that create/annihilate Bloch waves – plane waves modulated by a function with the periodicity of the lattice. Although the use of this basis is accompanied by significant simplifications, the resulting Hamiltonian is still intractable, since it still contains an infinite number of energy bands and a rather complicated two-body interaction term. To proceed, it is inevitable to make approximations, which at first glance seem to be quite radical. We have to truncate the infinite dimensional Hilbert space to

⁴There is another set of reflection axes, which would interchange the two sublattices, but they do not represent an additional symmetry.

contain only a selected few energy bands instead of infinitely many. Yet, such a truncation is justified, because most of the energy bands are irrelevant for a low-energy theory, being far away from the Fermi energy.

Based on the analysis of the preceding section we already know which energy bands should be kept: the σ - and π -bands that are formed from the sp^2 - and p_z -orbitals, respectively. The inner shell $1s$ -electrons would lead to an energy band that is fully occupied and deep below the Fermi energy. Similarly, the other high-energy atomic orbitals we have not discussed previously would lead to high energy bands far above the Fermi energy. Luckily, there is a single-particle basis conjugate to the Bloch basis, which implements the idea of constructing energy bands from localized atomic orbitals in a mathematically precise way, while respecting the symmetries of the crystal lattice, the Wannier basis [9–11, 22]. In analogy to the position eigenstates, being the conjugate basis to ordinary plane waves and localized at a single point in space, the Wannier states are maximally localized at one lattice site. Since there are two atoms per unit cell and four orbitals per atom, a model Hamiltonian constructed from the sp^2 - and p_z -orbitals contains eight bands in total, six of them coming from the three sp^2 -orbitals per atom and the remaining two coming from the p_z -orbitals. We can truncate the Hilbert space even further by neglecting the σ bands as well. Figuratively speaking, the sp^2 -electrons are already busy in holding the lattice together, while only the p_z electrons are free to move. All of these considerations culminate in the following second quantized Hamiltonian [9]

$$\begin{aligned}
 H_{el}(\vec{R}_0) &\approx H_{hop} + H_{int} \\
 &= - \sum_{i,j} t_{\vec{R}_{0,i}\vec{R}_{0,j}} c_{\vec{R}_{0,i}}^\dagger c_{\vec{R}_{0,j}} + \frac{1}{2} \sum_{\substack{i,j \\ i \neq j}} c_{\vec{R}_{0,i}}^\dagger c_{\vec{R}_{0,i}} V(\vec{R}_{0,i} - \vec{R}_{0,j}) c_{\vec{R}_{0,j}}^\dagger c_{\vec{R}_{0,j}}. \quad (2.2.1)
 \end{aligned}$$

The operators $c_{\vec{R}_{0,i}}^\dagger$ and $c_{\vec{R}_{0,i}}$ are fermionic ladder operators that create/annihilate an electron at the discrete position $\vec{R}_{0,i}$ in the honeycomb lattice. The first term describes the propagation of electrons as a hopping from lattice site $\vec{R}_{0,j}$ to lattice site $\vec{R}_{0,i}$ with an amplitude $t_{\vec{R}_{0,i}\vec{R}_{0,j}}$, and the second term describes the density-density interaction of electrons located at sites i and j with the long-range Coulomb interaction amplitude $V(\vec{R}_{0,i} - \vec{R}_{0,j}) = e^2/|\vec{R}_{0,i} - \vec{R}_{0,j}|$. The remainder of this chapter is devoted to the analysis of this Hamiltonian.

2.2.1 Tight-binding dispersion of noninteracting graphene electrons

To get a feeling for the low-energy physics of electrons in graphene, we neglect the Coulomb interaction in the tight-binding Hamiltonian (2.2.1) for the moment, focussing only on the hopping term. In its present form, the transition amplitudes $t_{\vec{R}_{0,i}\vec{R}_{0,j}}$ are nonvanishing for any distance between two sites i and j . However, since the atomic p_z -orbitals are fairly localized at one site only, the absolute value of the hopping amplitudes rapidly decrease with increasing distance between the atoms. For this reason it is advisable to organize a perturbative expansion of the full hopping Hamiltonian into a series of successively decreasing amplitudes, that is, nearest-neighbor hopping, next-nearest-neighbor hopping, and so on [9]

$$H_{hop} = H_{hop}^{nn} + H_{hop}^{n nn} + H_{hop}^{nnnn} + \dots \quad (2.2.2)$$

From the structure of the graphene lattice it is obvious that nearest-neighbor hopping requires an electron to change the sublattice, while for next-nearest-neighbor hopping it remains in the same sublattice, see Fig. 2.4. This alternating pattern continues for higher orders in the

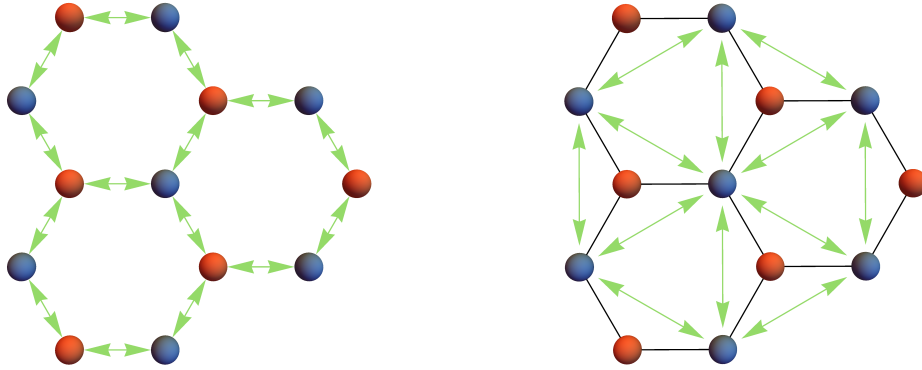


Figure 2.4: (Left) Nearest-neighbor hopping and (right) next-nearest-neighbor hopping of electrons indicated by green arrows. The former process requires an electron to change the sublattice, whereas for the latter process the electron stays within the same sublattice.

“neighbor-expansion”. Hence, the expansion (2.2.2) assumes the form

$$H_{hop} = - \sum_{\langle i,j \rangle} \left(t_{ij}^{nn} a_i^\dagger b_j + \text{h.c.} \right) + \sum_{\langle\langle i,j \rangle\rangle} \left(t_{ij}^{nnn} \left(a_i^\dagger a_j + b_i^\dagger b_j \right) + \text{h.c.} \right) + \dots, \quad (2.2.3)$$

where a_i^\dagger (b_i^\dagger) and a_i (b_i) are the creation and annihilation operators for an electron in sublattice A (B) at site i , and t_{ij}^{nn} and t_{ij}^{nnn} are nearest-neighbor and next-nearest-neighbor hopping amplitudes, respectively. Since here we consider the lattice to be static and all the atoms to be of the same kind, we can forget about their indices and simply write $t_{ij}^{nn} = t$ and $t_{ij}^{nnn} = t'$. Furthermore, without loss of generality we can choose the matrix elements t and t' to be real, because a possible complex phase could always be absorbed into the operators without changing their commutation relations. We note that such a simplification would not occur if magnetic fields were present. In a semiclassical picture, an electrically charged particle, travelling in an external magnetic field from point \vec{r}_1 to point \vec{r}_2 , picks up a phase that is proportional to the line integral of the vector potential \vec{A} . This fact can be proven easily in the path integral formalism by calculating the single-particle transition amplitude [23, 24]. Considering slowly varying magnetic fields in a tight-binding model – slow with respect to the underlying lattice – such a phase factor can be taken care of by the Peierls substitution [25], where the hopping matrix element t_{ij} of the zero field case is replaced by $t_{ij} \exp \left(ie \int_{\vec{R}_i}^{\vec{R}_j} \vec{A} \cdot d\vec{r} \right)$ [9, 26–28]. Although finite external magnetic fields are of interest in this thesis, we will omit the Peierls phase in the following discussion. Instead, we will include external electromagnetic fields on the level of the low-energy continuum theory via a minimal coupling prescription, where ordinary partial derivatives are substituted by gauge covariant derivatives [1, 2, 18].⁵

Since the next-nearest-neighbor hopping matrix element t' is already about an order of magnitude smaller than nearest-neighbor hopping [19, 20], we can neglect even higher order hopping in the further analysis. Choosing an arbitrary site as a reference point, we can write

⁵In fact, the result of the minimal coupling prescription is nothing but the lowest-order contribution of a gradient approximation of the Peierls phase.

the two hopping terms as follows

$$H_{hop}^{nn} = -t \sum_{\vec{R}_A} \left(a_{\vec{R}_A}^\dagger b_{\vec{R}_A + \vec{\delta}_1} + a_{\vec{R}_A}^\dagger b_{\vec{R}_A + \vec{\delta}_2} + a_{\vec{R}_A}^\dagger b_{\vec{R}_A + \vec{\delta}_3} + \text{h.c.} \right), \quad (2.2.4a)$$

$$\begin{aligned} H_{hop}^{nnp} &= -t' \frac{1}{2} \sum_{\vec{R}_A} \sum_{\substack{n_1, n_2 = -1, 0, 1 \\ |n_1 \vec{a}_1 + n_2 \vec{a}_2| = a}} \left(a_{\vec{R}_A}^\dagger a_{\vec{R}_A + n_1 \vec{a}_1 + n_2 \vec{a}_2} + \text{h.c.} \right) \\ &\quad - t' \frac{1}{2} \sum_{\vec{R}_B} \sum_{\substack{n_1, n_2 = -1, 0, 1 \\ |n_1 \vec{a}_1 + n_2 \vec{a}_2| = a}} \left(b_{\vec{R}_B}^\dagger b_{\vec{R}_B + n_1 \vec{a}_1 + n_2 \vec{a}_2} + \text{h.c.} \right). \end{aligned} \quad (2.2.4b)$$

Note that nearest-neighbor hopping only involves a summation over one sublattice, while next-nearest-neighbor hopping requires a separate summation for each sublattice. The two remaining hopping Hamiltonians (2.2.4a) and (2.2.4b) can be diagonalized simultaneously by a standard Bogoliubov transformation. The corresponding energy eigenvalues are functions of the crystal momentum \vec{k} , assuming the form [19, 20]

$$E_{\pm}(\vec{k}) = \pm t \sqrt{3 + f(\vec{k})} - t' f(\vec{k}), \quad (2.2.5a)$$

$$f(\vec{k}) = 2 \cos(\sqrt{3} k_y a) + 4 \cos(\sqrt{3} k_y a / 2) \cos(3 k_x a / 2). \quad (2.2.5b)$$

Here, the plus (minus) sign refers to the conduction (valence) band. We note that at charge neutrality and zero temperature the valence band is completely filled, whereas the conduction band is completely empty. In Fig. 2.5 we show the full band structure in the first Brillouin zone for the two cases of vanishing and nonvanishing next-nearest-neighbor hopping amplitude t' . An expansion to second order in the momentum around the two inequivalent Dirac points \vec{K}_{\pm} yields

$$E_{\pm}(\vec{K}_{+} + \delta\vec{k}) \approx \pm t \left(\frac{3a}{2} \delta k - \frac{3a^2}{8} \sin(3 \arctan(\delta k_x / \delta k_y)) \delta k^2 \right) + t' \left(3 - \frac{9a^2}{4} \delta k^2 \right), \quad (2.2.6a)$$

$$E_{\pm}(\vec{K}_{-} + \delta\vec{k}) \approx \pm t \left(\frac{3a}{2} \delta k + \frac{3a^2}{8} \sin(3 \arctan(\delta k_x / \delta k_y)) \delta k^2 \right) + t' \left(3 - \frac{9a^2}{4} \delta k^2 \right). \quad (2.2.6b)$$

The second order term proportional to t describes the trigonal warping of the spectrum [20, 29, 30], which breaks chirality. If next-nearest-neighbor hopping is taken into account, $t' \neq 0$, the global particle-hole symmetry is broken, since the conduction and valence bands are deformed asymmetrically, see Fig. 2.5, but the spectrum remains gapless. The touching points of the bands are shifted downwards in energy, while the linear energy-momentum dispersion is preserved. Since the particle-hole symmetry breaking only shows up at second order in the momentum expansion, the low-energy excitations to linear order still respect a particle-hole symmetry. In Fig. 2.6 we show a contour plot of the spectrum in the first Brillouin zone for $t' = 0$, where the trigonal warping around the two Dirac points becomes clearly visible. In addition, this figure shows a zoom-in of the spectrum around the Dirac point K_{+} for the two cases $t' = 0$ and $t' = 0.1t$. We emphasize that the conical structure of the spectrum in the vicinity of the band touching points is not a mere coincidence caused by the low-order truncation of the hopping Hamiltonian. To any order in the neighbor expansion, the spectrum would feature such Dirac cones, since they are a consequence of the crystal symmetries of the honeycomb lattice (translation, rotation and reflection) and time-reversal symmetry, as has been shown in Refs. [31] and [32] for example. (See also Ref. [33] for a symmetry classification of energy bands

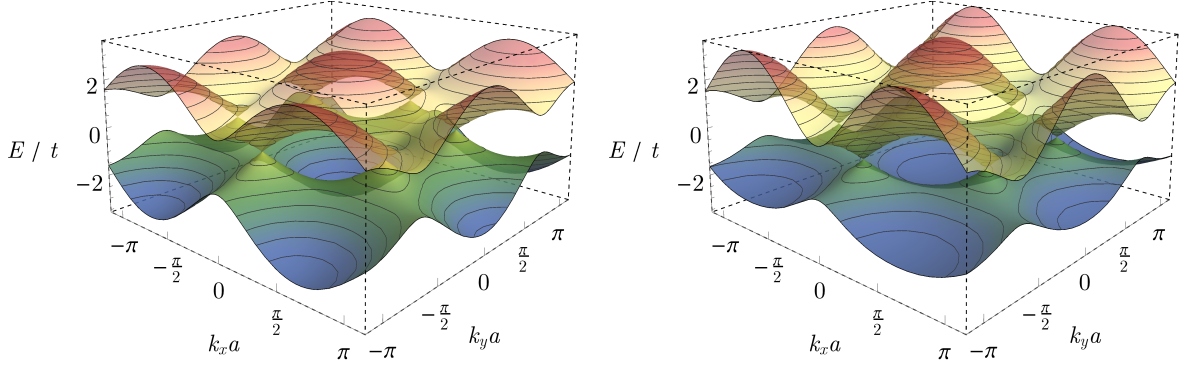


Figure 2.5: (Left) Tight-binding spectrum with vanishing next-nearest-neighbor hopping. The spectrum is symmetric around $E = 0$, which yields an emergent particle-hole symmetry for the quasiparticle excitations near half filling. The two bands touch at the six corners of the Brillouin zone, see Eq. (2.1.12b), around which the energy disperses linearly as a function of momentum. (Right) Tight-binding spectrum with finite next-nearest-neighbor hopping $t' = -0.1t$. The spectrum is no longer symmetric around zero energy, showing a flattened valence band and a steepened conduction band, which breaks the global particle-hole symmetry. Additionally, the band touching occurs at a finite energy $E = 3t'$. Nevertheless, low-energy excitations to linear order in momentum around the shifted touching points would still feature a particle-hole symmetry, since the symmetry breaking terms only appear at order δk^2 , see Eq. (2.2.6b) and Fig. 2.6.

in graphene using group theory and Refs. [34–37] for further reading, regarding the connection between massless Dirac fermions and discrete symmetries.) This finding immediately leads to the question: how stable are the cones against perturbations, which break those symmetries? We will come back to this issue in a separate appendix at the end of this chapter.

2.2.2 The Dirac Hamiltonian

Now that we have understood the band structure of the noninteracting tight-binding model and identified the reason why the corners of the Brillouin zone play such a distinguished role in the low-energy physics of graphene, we can continue to develop an actual low-energy continuum theory for the quasiparticle excitations around these points. In the remainder of this chapter we only deal with the nearest-neighbor contribution to the hopping Hamiltonian, Eq. (2.2.4a), setting $t' = 0$.

As a first step we transform from real space to momentum space by expanding the creation and annihilation operators in a Fourier series

$$a_i = \frac{1}{\sqrt{N}} \sum_{\vec{k} \in 1.\text{BZ}} e^{i\vec{k} \cdot \vec{R}_i} a_{\vec{k}}, \quad a_{\vec{k}} = \frac{1}{\sqrt{N}} \sum_{\vec{R}_i} e^{-i\vec{k} \cdot \vec{R}_i} a_i, \quad (2.2.7a)$$

$$b_i = \frac{1}{\sqrt{N}} \sum_{\vec{k} \in 1.\text{BZ}} e^{i\vec{k} \cdot \vec{R}_i} b_{\vec{k}}, \quad b_{\vec{k}} = \frac{1}{\sqrt{N}} \sum_{\vec{R}_i} e^{-i\vec{k} \cdot \vec{R}_i} b_i. \quad (2.2.7b)$$

Here, N is the number of unit cells⁶ and the momenta \vec{k} are constrained to the first Brillouin

⁶Note that N is very large but finite, due to the periodic boundary conditions we implicitly assumed.

2.2. Tight-binding approximation for graphene

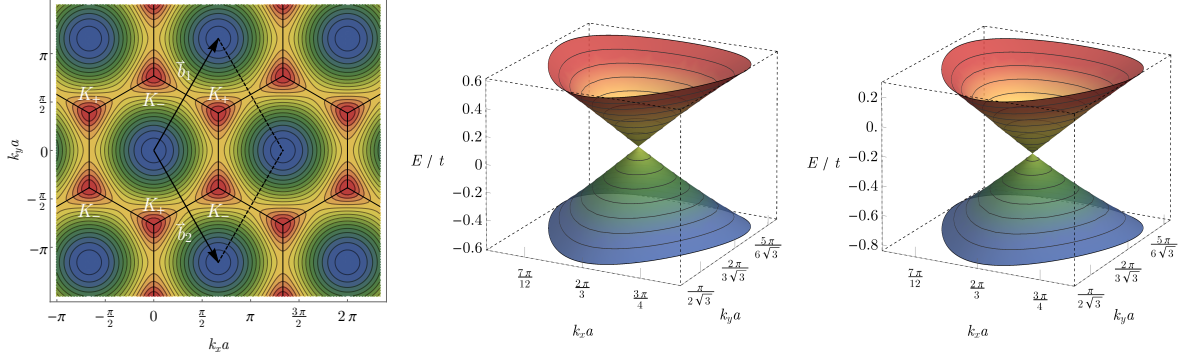


Figure 2.6: (Left) Contour plot of the tight-binding spectrum with vanishing next-nearest-neighbor hopping. The first Brillouin zone, reciprocal lattice vectors and K -points are indicated. Note that the trigonal warping around \vec{K}_+ and \vec{K}_- are mirror images of each other. (Middle and right) Zoom-in of the tight-binding spectrum around the Dirac point \vec{K}_+ for vanishing and nonvanishing next-nearest-neighbor hopping, respectively.

zone, due to the periodicity of the lattice. Inserting this expansion into Eq. (2.2.4a) yields

$$H_{hop}^{nn} = -t \sum_{\vec{k} \in 1.BZ} \begin{pmatrix} a_{\vec{k}}^\dagger & b_{\vec{k}}^\dagger \\ \gamma_{\vec{k}}^* & 0 \end{pmatrix} \begin{pmatrix} 0 & \gamma_{\vec{k}} \\ \gamma_{\vec{k}}^* & 0 \end{pmatrix} \begin{pmatrix} a_{\vec{k}} \\ b_{\vec{k}} \end{pmatrix}, \quad (2.2.8)$$

with the momentum-space matrix elements

$$\gamma_{\vec{k}} = e^{i\vec{k} \cdot \vec{\delta}_1} + e^{i\vec{k} \cdot \vec{\delta}_2} + e^{i\vec{k} \cdot \vec{\delta}_3} = e^{-ik_x a} + 2e^{ik_x a/2} \cos \frac{\sqrt{3}}{2} k_y a. \quad (2.2.9)$$

Since we are interested in the low-energy sector of the theory, we only keep those momentum components that are close to the two inequivalent Dirac points \vec{K}_+ and \vec{K}_-

$$\begin{aligned} H_{hop}^{nn} &\approx -t \sum_{\delta \vec{k}} \begin{pmatrix} a_{\vec{K}_+ + \delta \vec{k}}^\dagger & b_{\vec{K}_+ + \delta \vec{k}}^\dagger \\ \gamma_{\vec{K}_+ + \delta \vec{k}}^* & 0 \end{pmatrix} \begin{pmatrix} 0 & \gamma_{\vec{K}_+ + \delta \vec{k}} \\ \gamma_{\vec{K}_+ + \delta \vec{k}}^* & 0 \end{pmatrix} \begin{pmatrix} a_{\vec{K}_+ + \delta \vec{k}} \\ b_{\vec{K}_+ + \delta \vec{k}} \end{pmatrix} \\ &- t \sum_{\delta \vec{k}} \begin{pmatrix} a_{\vec{K}_- + \delta \vec{k}}^\dagger & b_{\vec{K}_- + \delta \vec{k}}^\dagger \\ \gamma_{\vec{K}_- + \delta \vec{k}}^* & 0 \end{pmatrix} \begin{pmatrix} 0 & \gamma_{\vec{K}_- + \delta \vec{k}} \\ \gamma_{\vec{K}_- + \delta \vec{k}}^* & 0 \end{pmatrix} \begin{pmatrix} a_{\vec{K}_- + \delta \vec{k}} \\ b_{\vec{K}_- + \delta \vec{k}} \end{pmatrix}. \end{aligned} \quad (2.2.10)$$

Here, the absolute value of the momenta $\delta \vec{k}$ is assumed to be small compared to the absolute value of \vec{K}_\pm . Because of this restriction and since the two K -points are well-separated in momentum space, there are no terms mixing the two valleys. Expanding the matrix elements $\gamma_{\vec{K}_\pm + \delta \vec{k}}$ around each of the two K -points to second order in the deviation $\delta \vec{k}$ we obtain

$$\gamma_{\vec{K}_+ + \delta \vec{k}} = e^{+i\pi/3} \frac{3a}{2} \left[(i\delta k_x - \delta k_y) + \frac{a}{4} (\delta k_x^2 - \delta k_y^2 - 2i\delta k_x \delta k_y) \right] + \mathcal{O}(\delta k^3), \quad (2.2.11a)$$

$$\gamma_{\vec{K}_- + \delta \vec{k}} = e^{-i\pi/3} \frac{3a}{2} \left[(i\delta k_x + \delta k_y) + \frac{a}{4} (\delta k_x^2 - \delta k_y^2 + 2i\delta k_x \delta k_y) \right] + \mathcal{O}(\delta k^3). \quad (2.2.11b)$$

After inserting this expansion into Eq. (2.2.10) we find

$$\begin{aligned} H_{hop}^{nn} &\approx + \sum_{\delta \vec{k}} \begin{pmatrix} a_{\vec{K}_+ + \delta \vec{k}}^\dagger & b_{\vec{K}_+ + \delta \vec{k}}^\dagger \\ \gamma_{\vec{K}_+ + \delta \vec{k}}^* & 0 \end{pmatrix} (\mathcal{H}_D + \mathcal{H}_{\text{Warp}})_{\vec{K}_+ + \delta \vec{k}} \begin{pmatrix} a_{\vec{K}_+ + \delta \vec{k}} \\ b_{\vec{K}_+ + \delta \vec{k}} \end{pmatrix} \\ &+ \sum_{\delta \vec{k}} \begin{pmatrix} b_{\vec{K}_- + \delta \vec{k}}^\dagger & a_{\vec{K}_- + \delta \vec{k}}^\dagger \\ \gamma_{\vec{K}_- + \delta \vec{k}}^* & 0 \end{pmatrix} (\mathcal{H}_D + \mathcal{H}_{\text{Warp}})_{\vec{K}_- + \delta \vec{k}} \begin{pmatrix} b_{\vec{K}_- + \delta \vec{k}} \\ a_{\vec{K}_- + \delta \vec{k}} \end{pmatrix}, \end{aligned} \quad (2.2.12)$$

with the Hamiltonian densities

$$\mathcal{H}_{D, \vec{K}_\pm + \delta \vec{k}} = \mp \frac{3ta}{2} \begin{pmatrix} 0 & e^{i\pi/3} (i\delta k_x - \delta k_y) \\ e^{-i\pi/3} (-i\delta k_x - \delta k_y) & 0 \end{pmatrix}, \quad (2.2.13)$$

and

$$\mathcal{H}_{\text{Warp}, \vec{K}_\pm + \delta \vec{k}} = -\frac{3ta^2}{8} \begin{pmatrix} 0 & e^{+i\pi/3} (\delta k_x^2 - \delta k_y^2 - 2i\delta k_x \delta k_y) \\ e^{-i\pi/3} (\delta k_x^2 - \delta k_y^2 + 2i\delta k_x \delta k_y) & 0 \end{pmatrix}. \quad (2.2.14)$$

The term linear in momentum is the celebrated Dirac Hamiltonian, while the term quadratic in momentum is the warping correction. The latter contribution to the low-energy Hamiltonian only becomes relevant at large fillings. In the vicinity of the charge neutrality point it may safely be neglected, but we kept it for now for completeness' sake. Note that we reorganized the matrix representation of the hopping Hamiltonian for the \vec{K}_- valley, interchanging the operators $a_{\vec{K}_- + \delta \vec{k}}$ and $b_{\vec{K}_- + \delta \vec{k}}$ in the two-component spinor. This choice was motivated by the relation $\vec{K}_- \cong -\vec{K}_+$, since in this representation the Hamiltonian densities of the two valleys are structurally identical and their chiral and time-reversal symmetry relations assume the simple form $\mathcal{H}_{D, \vec{K}_- + \delta \vec{k}} = -\mathcal{H}_{D, \vec{K}_+ + \delta \vec{k}} = \mathcal{H}_{D, \vec{K}_+ - \delta \vec{k}}$. The phases $e^{\pm i\pi/3}$ in Eqs. (2.2.13) and (2.2.14) are irrelevant, since they can be absorbed into the ladder operators without changing their commutation relations.

By collecting the two-component spinors of the two Dirac points \vec{K}_+ and \vec{K}_- into a single four-component spinor

$$\Psi_{\delta \vec{k}} \equiv \begin{pmatrix} a_{\vec{K}_+ + \delta \vec{k}} & b_{\vec{K}_+ + \delta \vec{k}} & b_{\vec{K}_- + \delta \vec{k}} & a_{\vec{K}_- + \delta \vec{k}} \end{pmatrix}^\top, \quad (2.2.15)$$

as well as interchanging δk_x and δk_y , we can write the two low-energy contributions to the nearest-neighbor hopping Hamiltonian in the compact form [20, 29, 30]

$$\begin{aligned} H_D &= \sum_{\delta \vec{k}} \Psi_{\delta \vec{k}}^\dagger \begin{pmatrix} \mathcal{H}_{D, \vec{K}_+ + \delta \vec{k}} & 0 \\ 0 & \mathcal{H}_{D, \vec{K}_- + \delta \vec{k}} \end{pmatrix} \Psi_{\delta \vec{k}} \\ &= v_F \sum_{\delta \vec{k}} \Psi_{\delta \vec{k}}^\dagger \tau_3 \otimes \vec{\sigma} \cdot \delta \vec{k} \Psi_{\delta \vec{k}}, \end{aligned} \quad (2.2.16)$$

$$\begin{aligned} H_{\text{Warp}} &= \sum_{\delta \vec{k}} \Psi_{\delta \vec{k}}^\dagger \begin{pmatrix} \mathcal{H}_{\text{Warp}, \vec{K}_+ + \delta \vec{k}} & 0 \\ 0 & \mathcal{H}_{\text{Warp}, \vec{K}_- + \delta \vec{k}} \end{pmatrix} \Psi_{\delta \vec{k}} \\ &= \lambda \sum_{\delta \vec{k}} \Psi_{\delta \vec{k}}^\dagger \tau_0 \otimes (\sigma_1 (\delta k_x^2 - \delta k_y^2) - 2\sigma_2 \delta k_x \delta k_y) \Psi_{\delta \vec{k}}. \end{aligned} \quad (2.2.17)$$

Here, τ and σ are the standard Pauli matrices, acting in valley and sublattice space respectively, $v_F = 3ta/2$ is the Fermi velocity and $\lambda = -v_F a/4 = -3ta^2/8$ is the warping coefficient.

We may now perform the continuum limit by considering large system sizes. In this limit the discrete momenta of the finite system with periodic boundary conditions become continuous, such that we can substitute the momentum sums by integrals

$$\frac{1}{V} \sum_{\delta \vec{k}} \longrightarrow \int \frac{d^2 k}{(2\pi)^2} \equiv \int_{\vec{k}}. \quad (2.2.18)$$

2.2. Tight-binding approximation for graphene

Here, the volume factor V is needed for dimensional reasons, because the sum itself is dimensionless, but the integral has the dimension of an inverse volume. To get a well-defined continuum limit we also need to attach a volume factor to the operators $\Psi_{\delta\vec{k}}$,

$$\sqrt{V}\Psi_{\delta\vec{k}} \longrightarrow \Psi(\vec{k}). \quad (2.2.19)$$

To understand this substitution recall the nontrivial commutation relation of fermionic ladder operators: $\{\psi_{i,\delta\vec{k}_1}^\dagger, \psi_{j,\delta\vec{k}_2}\} = \delta_{ij}\delta_{\delta\vec{k}_1\delta\vec{k}_2}$. In particular, note the Kronecker delta, involving the two momenta $\delta\vec{k}_{1/2}$. For any finite volume this anticommutator is perfectly well-defined, but its infinite volume limit does not converge to the known commutation relation of continuum field operators: $\{\psi_i^\dagger(\vec{k}_1), \psi_j(\vec{k}_2)\} = \delta_{ij}(2\pi)^2\delta(\vec{k}_1 - \vec{k}_2)$. Here, the Dirac delta distribution appears as the appropriate generalization of the Kronecker delta to continuous variables. To obtain the correct result one has to multiply the discrete commutation relation by a volume factor first, and only then perform the limit,

$$\{\sqrt{V}\psi_{i,\delta\vec{k}_1}^\dagger, \sqrt{V}\psi_{j,\delta\vec{k}_2}\} = \delta_{ij}V\delta_{\delta\vec{k}_1\delta\vec{k}_2} \longrightarrow \{\psi_i^\dagger(\vec{k}_1), \psi_j(\vec{k}_2)\} = \delta_{ij}(2\pi)^2\delta(\vec{k}_1 - \vec{k}_2), \quad (2.2.20)$$

where we have used Eq. (2.2.19) and $\lim_{V \rightarrow \infty} V\delta_{\delta\vec{k}_1\delta\vec{k}_2} = (2\pi)^2\delta(\vec{k}_1 - \vec{k}_2)$.

The final outcome of these considerations is the continuum Hamiltonian

$$H_{hop}^{nn} \approx H_D + H_{Warp} \\ = \int_{\vec{k}} \Psi^\dagger(\vec{k}) \left(v_F \tau_3 \otimes \vec{\sigma} \cdot \vec{k} + \lambda \tau_0 \otimes \left(\sigma_1(k_x^2 - k_y^2) - 2\sigma_2 k_x k_y \right) \right) \Psi(\vec{k}). \quad (2.2.21)$$

A Fourier transformation to real space finally yields

$$H_D + H_{Warp} = \int_{\vec{r}} \Psi^\dagger(\vec{r}) \left(-iv_F \tau_3 \otimes \vec{\sigma} \cdot \vec{\nabla} - \lambda \tau_0 \otimes \left(\sigma_1(\partial_x^2 - \partial_y^2) - 2\sigma_2 \partial_x \partial_y \right) \right) \Psi(\vec{r}). \quad (2.2.22)$$

With this result we already succeeded in deriving a low-energy quantum field theory for the electrons in graphene, albeit it is only a noninteracting one. To obtain an interacting theory we still need to analyze the lattice Coulomb interaction term in Eq. (2.2.1).

2.2.3 Interacting Dirac fermions

For the analysis of the tight-binding Coulomb interaction we can play the same game as before, that is, transform to momentum space, only keep the small momentum components around the Dirac points and perform the continuum limit in the end. This program is straightforward, except for the identification of the low-energy contributions, which demands special care due to the long-range and nonlocal nature of the Coulomb interaction.

Accounting for the two triangular sublattices of graphene, the lattice Coulomb interaction decomposes into four terms

$$H_{int} = \frac{1}{2} \sum_{\substack{i,j \\ i \neq j}} \left(a_i^\dagger a_i + b_i^\dagger b_i \right) V(\vec{R}_i - \vec{R}_j) \left(a_j^\dagger a_j + b_j^\dagger b_j \right) \\ = H_{int}^{AA} + H_{int}^{AB} + H_{int}^{BA} + H_{int}^{BB}. \quad (2.2.23)$$

The individual terms describe the interactions between electrons within the same sublattice (H_{int}^{AA} and H_{int}^{BB}) and in different sublattices (H_{int}^{AB} and H_{int}^{BA}). In the following discussion we

will focus on the term H_{int}^{AA} . Once its low-energy contributions are understood, it is straightforward to adapt the arguments for the remaining three terms. Just like we did in the previous subsection, we expand the ladder operators in a Fourier series, Eq. (2.2.7a). For the density of electrons in sublattice A we obtain

$$a_i^\dagger a_i = \frac{1}{N} \sum_{\vec{k}_1, \vec{k}_2} e^{-i(\vec{k}_1 - \vec{k}_2) \cdot \vec{R}_i} a_{\vec{k}_1}^\dagger a_{\vec{k}_2} = \frac{1}{N} \sum_{\vec{k}, \vec{q}} e^{-i\vec{q} \cdot \vec{R}_i} a_{\vec{k} + \vec{q}}^\dagger a_{\vec{k}}, \quad (2.2.24)$$

with $\vec{q} = \vec{k}_1 - \vec{k}_2$ and $\vec{k} = \vec{k}_2$. Inserting this expression into the interaction Hamiltonian (2.2.23) we find

$$H_{int}^{AA} = \frac{1}{2} \frac{1}{N^2} \sum_{\vec{k}_1, \vec{k}_2, \vec{q}_1, \vec{q}_2} a_{\vec{k}_1 + \vec{q}_1}^\dagger a_{\vec{k}_1} a_{\vec{k}_2} V(\vec{q}_1, \vec{q}_2) a_{\vec{k}_2 + \vec{q}_2}^\dagger a_{\vec{k}_2}, \quad (2.2.25)$$

with the two-body interaction amplitude

$$V(\vec{q}_1, \vec{q}_2) = \sum_{\substack{i,j \\ i \neq j}} e^{-i\vec{q}_1 \cdot \vec{R}_i - i\vec{q}_2 \cdot \vec{R}_j} V(\vec{R}_i - \vec{R}_j) \propto \delta_{\vec{q}_1, -\vec{q}_2} \frac{1}{|\vec{q}_1|}. \quad (2.2.26)$$

We will prove a continuum version of this result and determine the proportionality constant at a later stage, once we have identified the low energy contributions of the interaction term. For now it suffices to know that the Fourier transform of the Coulomb interaction amplitude conserves momentum, which is expressed by the Kronecker delta, and that it is inversely proportional to the transferred momentum.

For the further analysis we want to switch to a diagrammatic representation of the interaction term, since it illustrates the scattering process very clearly, allowing us to focus on its essential features. To this end we represent an annihilation operator $a_{\vec{k}}$ with ingoing momentum \vec{k} as a solid line with an ingoing arrow, a creation operator $a_{\vec{k}}^\dagger$ with outgoing momentum \vec{k} as a solid line with an outgoing arrow, and the interaction amplitude as a wiggly line, transferring the momentum \vec{q} . Absorbing all the distracting prefactors into the diagram, the interaction term becomes

$$H_{int}^{AA} = \sum_{\vec{k}_1, \vec{k}_2, \vec{q}} \begin{array}{c} \vec{k}_1 + \vec{q} \quad \vec{k}_2 - \vec{q} \\ \nearrow \quad \nearrow \\ \text{---} \text{wiggly line} \text{---} \\ \searrow \quad \searrow \\ \vec{k}_1 \quad \vec{k}_2 \end{array} . \quad (2.2.27)$$

Note that we already made use of momentum conservation, which can be immediately read off of the diagram. To find those contributions of the Coulomb interaction that are part of the low energy sector of the theory, we have to demand that all external momenta are close to the Dirac points. Only then it is sensible to speak of ‘‘interacting Dirac fermions’’. To this end, we first expand \vec{k}_1 and \vec{k}_2 around the two Dirac points, which yields four separate interaction terms

$$\begin{aligned}
 H_{int}^{AA} \approx & \sum'_{\delta\vec{k}_1, \delta\vec{k}_2} \sum_{\vec{q}} \\
 & \begin{array}{c} \vec{K}_+ + \delta\vec{k}_1 + \vec{q} \quad \vec{K}_+ + \delta\vec{k}_2 - \vec{q} \\ \nearrow \quad \nwarrow \\ \text{---} \vec{q} \text{---} \\ \nwarrow \quad \nearrow \\ \vec{K}_+ + \delta\vec{k}_1 \quad \vec{K}_+ + \delta\vec{k}_2 \end{array} + \begin{array}{c} \vec{K}_+ + \delta\vec{k}_1 + \vec{q} \quad \vec{K}_- + \delta\vec{k}_2 - \vec{q} \\ \nearrow \quad \nwarrow \\ \text{---} \vec{q} \text{---} \\ \nwarrow \quad \nearrow \\ \vec{K}_+ + \delta\vec{k}_1 \quad \vec{K}_- + \delta\vec{k}_2 \end{array} \\
 & + \begin{array}{c} \vec{K}_- + \delta\vec{k}_1 + \vec{q} \quad \vec{K}_+ + \delta\vec{k}_2 - \vec{q} \\ \nearrow \quad \nwarrow \\ \text{---} \vec{q} \text{---} \\ \nwarrow \quad \nearrow \\ \vec{K}_- + \delta\vec{k}_1 \quad \vec{K}_+ + \delta\vec{k}_2 \end{array} + \begin{array}{c} \vec{K}_- + \delta\vec{k}_1 + \vec{q} \quad \vec{K}_- + \delta\vec{k}_2 - \vec{q} \\ \nearrow \quad \nwarrow \\ \text{---} \vec{q} \text{---} \\ \nwarrow \quad \nearrow \\ \vec{K}_- + \delta\vec{k}_1 \quad \vec{K}_- + \delta\vec{k}_2 \end{array} .
 \end{aligned} \tag{2.2.28}$$

Here, the prime at the k -sum indicates that $|\delta\vec{k}_{1/2}| \ll |\vec{K}_\pm|$. Note, however, that the momentum transfer \vec{q} can still be large, such that $\delta\vec{k}_1 + \vec{q}$ and $\delta\vec{k}_2 - \vec{q}$ need not be small. To fulfill the requirement that all external momenta are close to the Dirac points, it therefore seems that we are forced to demand the absolute value of \vec{q} to be small against the absolute value of \vec{K}_\pm as well. Such processes describe forward scattering and – as we will substantiate below – they are indeed the dominant contribution to the Coulomb interaction in the low-energy regime. However, it would be premature to conclude that forward scattering is the only possible contribution allowed at low energies. To see that the sum over momentum transfers \vec{q} contains additional low-energy contributions, we need to consider very large momentum transfers, being of the order \vec{K}_\pm .⁷ As it turns out, for such large momentum transfers the “valley identity” of the incoming fermions – whose momenta are initially close to a certain Dirac point – is not conserved. In other words, a \vec{K}_+ -fermion can become a \vec{K}_- -fermion and vice versa or a fermion’s affiliation to a certain Dirac point may be lost entirely, see Fig. 2.7. (In the latter case the corresponding process belongs to the high-energy sector.) To estimate whether these additional contributions have to be taken into account recall that the Coulomb interaction amplitude (2.2.26) is inversely proportional to the transferred momentum. Hence, for small \vec{q} the flavour-changing processes are suppressed by a factor of $|\vec{q}|/|\vec{K}_\pm - \vec{q}|$ compared to forward scattering, such that they can safely be neglected. As a result, the leading order interaction Hamiltonian is given by Eq. (2.2.28) with \vec{q} assumed to be small. Now all the external momenta are close to a Dirac point \vec{K}_\pm and it is legitimate to assign a well-defined valley index for each of the ingoing and outgoing solid lines, and speak of interacting Dirac fermions.

Repeating the analysis for the remaining interaction terms and switching back to an analytic representation, the low-energy interaction Hamiltonian can be written in the concise form

$$H_{int} \approx \frac{1}{2} \frac{1}{N^2} \sum_{\delta\vec{k}_1, \delta\vec{k}_2, \vec{q}_1, \vec{q}_2} \Psi_{\delta\vec{k}_1 + \vec{q}_1}^\dagger \Psi_{\delta\vec{k}_1} V(\vec{q}_1, \vec{q}_2) \Psi_{\delta\vec{k}_2 + \vec{q}_1}^\dagger \Psi_{\delta\vec{k}_2} . \tag{2.2.29}$$

⁷Since \vec{K}_\pm is of the order of a reciprocal lattice it can happen that the fermions are scattered out of the first Brillouin zone. Such processes are called umklapp scattering and they are typically discussed in the context of electron-phonon scattering [9–11], but they also appear for electron-electron interactions.

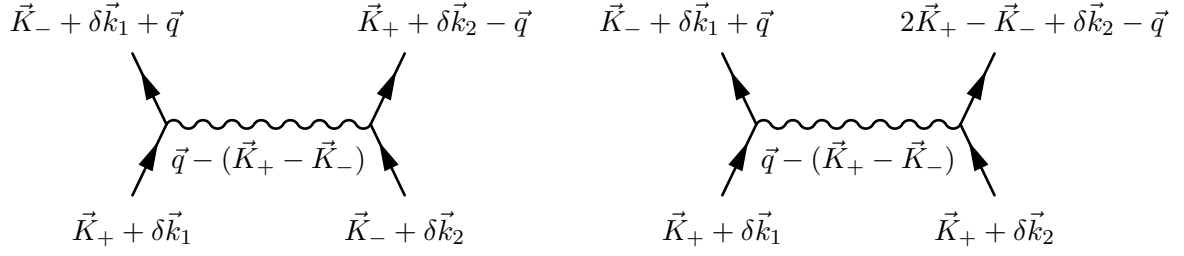


Figure 2.7: (Left) A low-energy contribution of the Coulomb interaction, where the valley affiliation of both fermions changes through the scattering process. Since all external momenta are close to a Dirac point (\vec{q} is assumed to be small) it is a valid contribution to the low-energy sector of the theory. (Right) An example of a high-energy contribution of the Coulomb interaction as a consequence of large momentum transfers. Note that $2\vec{K}_+ - \vec{K}_-$ lies well outside the first Brillouin zone. Yet, since the momentum quantum number of a fermion in a crystal is only defined up to reciprocal lattice vectors, it can be “folded back” into the first Brillouin zone [9]. As a result, this outgoing fermion resides close to the Γ -point ($2\vec{K}_+ - \vec{K}_- \simeq 0$).

We may now perform the continuum limit in just the same way as in the previous section, see Eqs. (2.2.18) and (2.2.19). We obtain

$$H_{int} = \frac{1}{2} \int_{\vec{k}_1, \vec{k}_2, \vec{q}_1, \vec{q}_2} \Psi^\dagger(\vec{k}_1 + \vec{q}_1) \Psi(\vec{k}_1) V(\vec{q}_1, \vec{q}_2) \Psi^\dagger(\vec{k}_2 + \vec{q}_2) \Psi(\vec{k}_2), \quad (2.2.30)$$

with the continuum form of the interaction amplitude⁸

$$V(\vec{q}_1, \vec{q}_2) = \int_{\vec{r}_1, \vec{r}_2} e^{-i\vec{q}_1 \cdot \vec{r}_1 - i\vec{q}_2 \cdot \vec{r}_2} V(\vec{r}_1 - \vec{r}_2). \quad (2.2.31)$$

Transforming to the center-of-mass frame by introducing relative and center-of-mass coordinates, we can solve this integral exactly

$$\begin{aligned} V(\vec{q}_1, \vec{q}_2) &= \int_{\vec{r}} e^{-i(\vec{q}_1 + \vec{q}_2) \cdot \vec{r}} \int_{\Delta\vec{r}} e^{-i\frac{1}{2}(\vec{q}_1 - \vec{q}_2) \cdot \Delta\vec{r}} \frac{e^2}{|\Delta\vec{r}|} \\ &= (2\pi)^2 \delta(\vec{q}_1 + \vec{q}_2) e^2 \int_0^\infty d\Delta r J_0(q_1 \Delta r) \\ &= (2\pi)^2 \delta(\vec{q}_1 + \vec{q}_2) \frac{2\pi e^2}{q_1}. \end{aligned} \quad (2.2.32)$$

In the second line J_0 is the Bessel function of the first kind [38], which occurs after transforming the integral over $\Delta\vec{r}$ to polar coordinates. The above interaction amplitude is the proper continuum limit of Eq. (2.2.26). Inserting this result into Eq. (2.2.30) and going back to a real-space representation we find

$$H_{int} = \frac{1}{2} \int_{\vec{r}, \vec{r}'} \Psi^\dagger(\vec{r}) \Psi(\vec{r}) \frac{e^2}{|\vec{r} - \vec{r}'|} \Psi^\dagger(\vec{r}') \Psi(\vec{r}'). \quad (2.2.33)$$

Putting everything together we arrive at the low-energy quantum field theory that describes spin polarized interacting electrons in a honeycomb lattice

$$H_D + H_{int} = -iv_F \int_{\vec{r}} \Psi^\dagger(\vec{r}) \tau_3 \otimes \vec{\sigma} \cdot \vec{\nabla} \Psi(\vec{r}) + \frac{1}{2} \int_{\vec{r}, \vec{r}'} \Psi^\dagger(\vec{r}) \Psi(\vec{r}) \frac{e^2}{|\vec{r} - \vec{r}'|} \Psi^\dagger(\vec{r}') \Psi(\vec{r}'). \quad (2.2.34)$$

⁸Note that, while performing the continuum limit, Eq. (2.2.26) is multiplied by the volume of the unit cell squared, which accounts for the correct physical dimension in the substitution $V_{EZ}^2 \sum_{i,j} \rightarrow \int_{\vec{r}_1, \vec{r}_2}$.

The electron spin is straightforward to implement by doubling the degrees of freedom of the spinor (2.2.15) to contain eight components instead of four. The structure of the kinetic and interaction term remain the same. In comparison to Eq. (2.2.22) we neglected the warping term that describes the deviations from the isotropic Dirac spectrum. Since it is of second order in the spatial derivative/momentum, trigonal warping is irrelevant for the physics near charge neutrality. As long as the filling is sufficiently small compared to the band cutoff, it would only lead to minor corrections to the fermionic self-energy and bosonic polarization function, which can safely be neglected. Significant contributions of trigonal warping to those quantities would only occur for intermediate to large fillings, cf. Figs. 2.5 and 2.6, which is not covered in this thesis.

2.A Appendix: Stability of Dirac cones and mass terms

In section 2.2.1 we have seen explicitly that the linear energy-momentum dispersion is stable against the next-nearest-neighbor hopping perturbation. We mentioned that higher order terms in the neighbor expansion cannot lead to a gap in the spectrum, since such terms respect the discrete symmetries of the honeycomb crystal lattice. In fact, any perturbation which respects these symmetries cannot generate a gap in the spectrum. But what if they are broken, say, by a distortion of the crystal lattice? Would the Dirac cones survive?

The proper framework to address this kind of question is group theory and topology, but its results are oftentimes rather abstract statements. Here, we prefer to investigate a concrete and experimentally relevant example, uniaxially strained graphene [39–41]. Depending on the direction in which the strain is applied, the primitive translation vectors $\vec{a}_{1/2}$ and nearest neighbor shift vectors $\vec{\delta}_{1/2/3}$ are modified, compared to the symmetric lattice, Eqs. (2.1.9) and (2.1.10). As a consequence of the Bravais lattice distortion, the reciprocal lattice is distorted as well. In particular, the corners of the Brillouin zone drift away from their original position in momentum space. The corresponding tight-binding description to nearest-neighbor hopping approximation, however, is very similar in structure to the symmetric honeycomb lattice. It is merely a generalization of the Hamiltonian (2.2.4a), where the hopping amplitudes t_1, t_2 and t_3 among the three neighbors of an individual atom do not need to be identical, due to the modified bond lengths $|\vec{\delta}_i|$,

$$H_{Strain} = - \sum_{\vec{R}_A} \left(t_1 a_{\vec{R}_A}^\dagger b_{\vec{R}_A + \vec{\delta}_1} + t_2 a_{\vec{R}_A}^\dagger b_{\vec{R}_A + \vec{\delta}_2} + t_3 a_{\vec{R}_A}^\dagger b_{\vec{R}_A + \vec{\delta}_3} + \text{h.c.} \right). \quad (2.A.1)$$

Despite the modification of the reciprocal lattice it is straightforward to diagonalize this Hamiltonian, which yields the energy eigenvalues

$$E_{\pm}(\vec{k}) = \pm \left| t_1 e^{i\vec{k} \cdot \vec{\delta}_1} + t_2 e^{i\vec{k} \cdot \vec{\delta}_2} + t_3 e^{i\vec{k} \cdot \vec{\delta}_3} \right|. \quad (2.A.2)$$

For $t_i = t$ and $\vec{\delta}_i$ being identical to Eq. (2.1.10), the spectrum reduces to the nearest-neighbor tight-binding spectrum of unstrained graphene we have obtained previously. To isolate the effects of lattice distortion and hopping amplitude distortion from one another, we may neglect the former feature and use Eq. (2.1.10) in what follows. It is clear that such a simplification is not realistic for graphene, since strain always influences both the lattice and the hoppings, but it can be realized in optical lattices as proposed in Ref. [40]. Furthermore, as was argued in Ref. [41], this simplification does not affect the general features we are about to discuss.

Following Ref. [41] we may assume $t_1 = t_2 = t \neq t_3$. The tight-binding spectrum (2.A.2) calculated for that special case is shown in Fig. 2.8 for a few values of the ratio t_3/t . One can easily see that the spectrum still features two inequivalent Dirac cones as long as the asymmetry in the hopping is sufficiently small. However, the Dirac points do not occur at the corners of the Brillouin zone anymore, but they drift away to the points

$$\vec{K}_{D,\pm} = \left(0, \pm \frac{2}{\sqrt{3}a} \arccos \left(-\frac{t_3}{2t} \right) \right), \quad (2.A.3)$$

up to reciprocal lattice vectors. This result is valid up to the critical value $t_3 = 2t$, where the two Dirac points merge and a gap opens up if t_3 is increased beyond that point. As mentioned above, the deformation of the lattice would alter the Brillouin zone and potentially influence the location of the Dirac points, but the general features of drifting, merging and gap-opening are not invalidated. Thus, we can conclude that for weak strain the Dirac cones are stable. Other

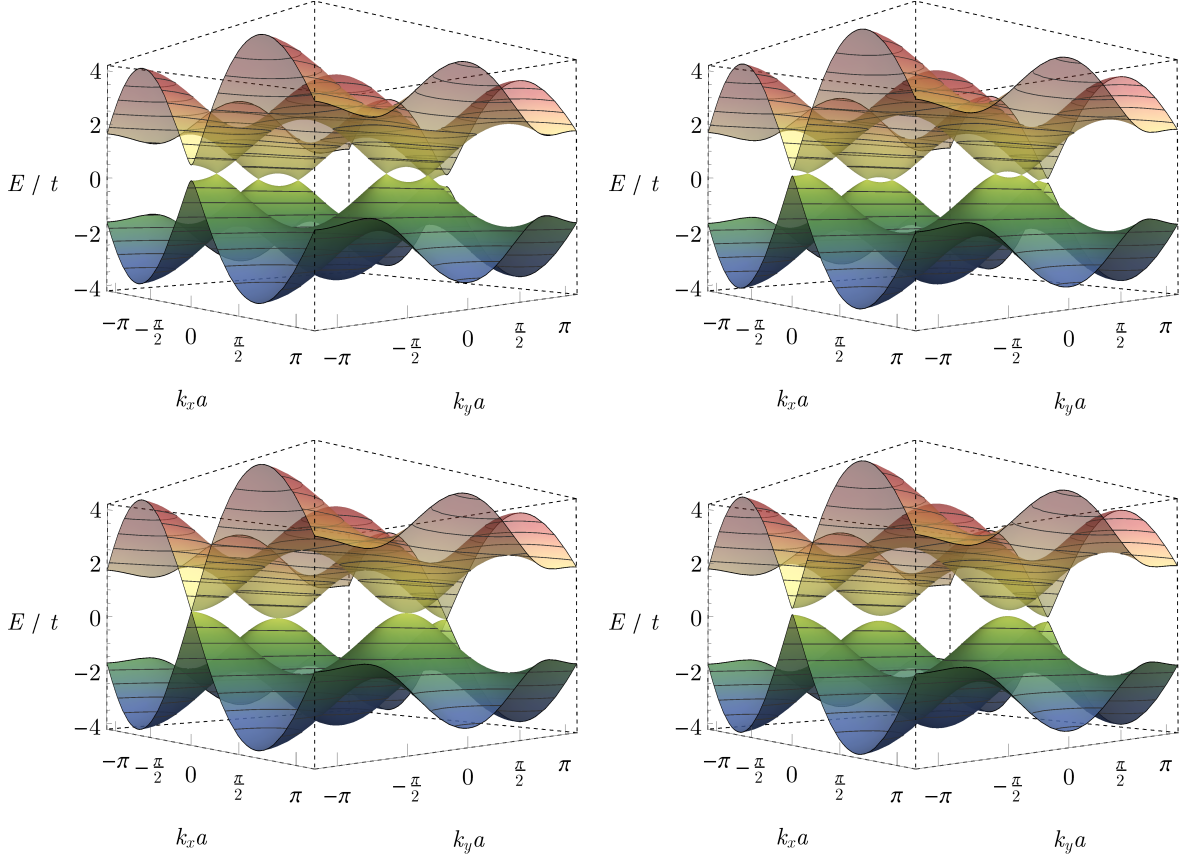


Figure 2.8: Merging of the Dirac cones due to an asymmetry in the hopping amplitudes, $t_1 = t_2 = t \neq t_3$. From top left to bottom right: $t_3 = 1.75t$, $t_3 = 1.9t$, $t_3 = 2t$, $t_3 = 2.1t$. For $t_3 < 2t$ the Dirac cones move toward each other until they merge at the M -point of the Brillouin zone with the gap threshold $t_3 = 2t$. Increasing the hopping t_3 beyond this critical value turns the system into an ordinary semiconductor.

studies, which include bending of the sheet, the coupling to phonons or even random distortions of lattice have also shown the robustness of Dirac cones in graphene. See Refs. [32, 42, 43] for further reading. These findings immediately lead to the question: if weak lattice distortions cannot create a gap in the spectrum, what else would be necessary?

As a first example that leads to a gap, let us consider a perturbation to the hopping Hamiltonian that introduces a charge carrier imbalance between the two sublattices [44]

$$H_{CDW} = -m \sum_{\vec{R}_A} \left(a_{\vec{R}_A}^\dagger a_{\vec{R}_A} - b_{\vec{R}_A + \vec{\delta}_1}^\dagger b_{\vec{R}_A + \vec{\delta}_1} \right). \quad (2.A.4)$$

Here, m is a real-valued parameter which will play the role of a mass. It may be interpreted as a staggered chemical potential, which has the opposite sign for the two sublattices and describes a charge-density-wave (CDW) phase. As explained in the original work of Semenoff, Ref. [44], such a term arises naturally in a two-dimensional layer of hexagonal boron nitride (hBN). This material has a honeycomb structure as well, but the sublattices are inequivalent, due to the two distinct atoms in the unit cell. After Fourier transforming to momentum space and keeping

only the momentum components close to the inequivalent Dirac points, we find

$$\begin{aligned}
 H_{CDW} &= - \sum_{\vec{\delta k}} \Psi_{\vec{\delta k}}^\dagger \begin{pmatrix} m & 0 & 0 & 0 \\ 0 & -m & 0 & 0 \\ 0 & 0 & -m & 0 \\ 0 & 0 & 0 & m \end{pmatrix} \Psi_{\vec{\delta k}} \\
 &= - \sum_{\vec{\delta k}} \Psi_{\vec{\delta k}}^\dagger m \tau_3 \otimes \sigma_3 \Psi_{\vec{\delta k}}.
 \end{aligned} \tag{2.A.5}$$

Here, $\Psi_{\vec{\delta k}}$ is the same four-component spinor we have introduced before. A diagonalization of the Dirac Hamiltonian with this perturbation yields the energy eigenvalues $E_\pm(\vec{\delta k}) = \pm \sqrt{v_F^2 \delta \vec{k}^2 + m^2}$ and a gap of size $2m$.

Another example for a perturbation that leads to a gap is the so-called Kekulé distortion [45, 46]. Here, the hopping is altered by a periodic modulation that mixes the two valleys

$$H_{Kek} = - \sum_{\vec{R}_A} \left(\sum_{i=1}^3 \delta t_{\vec{R}_A, i} a_{\vec{R}_A}^\dagger b_{\vec{R}_A + \vec{\delta}_i} + \text{h.c.} \right), \tag{2.A.6}$$

with

$$\delta t_{\vec{R}_A, i} = \frac{1}{3} \left(\Delta_0 e^{i\vec{K}_+ \cdot \vec{\delta}_i} e^{i(\vec{K}_+ - \vec{K}_-) \cdot \vec{R}_A} + \Delta_0^* e^{-i\vec{K}_+ \cdot \vec{\delta}_i} e^{-i(\vec{K}_+ - \vec{K}_-) \cdot \vec{R}_A} \right). \tag{2.A.7}$$

The strength of the modulation is parametrized by the complex parameter Δ_0 . Using the same strategy as before we obtain the low energy Hamiltonian

$$\begin{aligned}
 H_{Kek} &= - \sum_{\vec{\delta k}} \Psi_{\vec{\delta k}}^\dagger \begin{pmatrix} 0 & 0 & \Delta & 0 \\ 0 & 0 & 0 & \Delta \\ \Delta^* & 0 & 0 & 0 \\ 0 & \Delta^* & 0 & 0 \end{pmatrix} \Psi_{\vec{\delta k}} \\
 &= - \sum_{\vec{\delta k}} \Psi_{\vec{\delta k}}^\dagger \left(\text{Re} \Delta_0 \tau_1 \otimes \sigma_0 - \text{Im} \Delta_0 \tau_2 \otimes \sigma_0 \right) \Psi_{\vec{\delta k}},
 \end{aligned} \tag{2.A.8}$$

which yields the energy spectrum $E_\pm(\vec{\delta k}) = \pm \sqrt{v_F^2 \delta \vec{k}^2 + |\Delta_0|^2}$.

For spinless fermions there is a fourth mass term – the Kekulé distortion counts twice due to its real and imaginary part – with the low energy Hamiltonian

$$\begin{aligned}
 H_{HQHE} &= - \sum_{\vec{\delta k}} \Psi_{\vec{\delta k}}^\dagger \begin{pmatrix} m & 0 & 0 & 0 \\ 0 & -m & 0 & 0 \\ 0 & 0 & m & 0 \\ 0 & 0 & 0 & -m \end{pmatrix} \Psi_{\vec{\delta k}} \\
 &= - \sum_{\vec{\delta k}} \Psi_{\vec{\delta k}}^\dagger m \tau_3 \otimes \sigma_3 \Psi_{\vec{\delta k}}
 \end{aligned} \tag{2.A.9}$$

In a tight-binding model such a term would emerge from a next-nearest neighbor hopping term with a rather peculiar hopping amplitude, that describes a directed motion due to a lattice periodic magnetic field, but with zero magnetic flux through the unit cell. It was proposed by Haldane as a condensed matter simulation of the parity anomaly, realizing a quantum Hall effect without Landau levels, Ref. [47].

The above list exhausts all possible mass terms in graphene, if the spin degree of freedom is neglected that is. Once the electronic spin is taken into account, the number of possible mass

terms increases drastically from four to 36. All of these terms have been classified and physically interpreted in Ref. [48]. We do not bother to repeat this extensive analysis here again, but at least we want to sketch how these mass terms can be found systematically following Ref. [48]. First, it is convenient to introduce a Nambu-spinor $\Psi = (\Psi_\uparrow, \Psi_\downarrow, \Psi_\uparrow^\dagger, \Psi_\downarrow^\dagger)$ and write the massive Dirac Hamiltonian in Bogoliubov-de Gennes (BdG) form

$$H = \frac{1}{2} \int_{\vec{r}} \Psi^\dagger \begin{pmatrix} \mathcal{H}_{pp} & \mathcal{H}_{ph} \\ \mathcal{H}_{ph}^\dagger & -\mathcal{H}_{pp}^\dagger \end{pmatrix} \Psi. \quad (2.A.10)$$

Here, \mathcal{H}_{pp} and \mathcal{H}_{ph} are the particle-particle and particle-hole Hamilton densities respectively. The structure of the BdG Hamilton density is determined by hermiticity and the Fermi-Dirac statistics of the field operators. The massless Dirac kinetic energy only appears in the diagonal and reads $\mathcal{H}_D = -iv_F \tau_0^N \otimes \sigma_0^s \otimes \tau_3 \otimes \sigma_1 \partial_x - iv_F \tau_3^N \otimes \sigma_0^s \otimes \tau_3 \otimes \sigma_2 \partial_y$, where τ^N are the Pauli matrices (including the identity) in Nambu space and σ_0^s is the identity matrix in spin space.

A gap in the spectrum opens up if a BdG mass matrix $\hat{\mathcal{M}}$ anticommutes with the Dirac Hamiltonian. Since a general BdG matrix is sixteen-dimensional – two sublattices, two valleys, two spins and particle-hole space – there are 64 matrices that fulfill this requirement. Not all of them are allowed, however, due to the particle-hole symmetry in Nambu space $\tau_1^N \otimes \sigma_0^s \otimes \tau_0 \otimes \sigma_0 \hat{\mathcal{M}}^\top \tau_1^N \otimes \sigma_0^s \otimes \tau_0 \otimes \sigma_0 = -\hat{\mathcal{M}}$. This constraint reduces the number of linearly independent mass matrices to 36, sixteen of them being insulating and the remaining twenty being superconducting. The latter classification into insulating and superconducting mass terms is due to their Nambu space structure, depending on whether they are on the diagonal or off-diagonal of the BdG Hamiltonian. A mass matrix is called insulating, if it commutes with the particle number operator – its associated BdG matrix is given by $\tau_3^N \otimes \sigma_0^s \otimes \tau_0 \otimes \sigma_0$ – and, thus, describes an insulating/semiconducting phase. On the other hand, a mass is called superconducting, if it does not commute with the number operator, yielding a finite expectation value of two creation/annihilation operators. This feature is reminiscent of an ordinary BCS superconductor and, thus, describes a superconducting phase.

Bibliography

- [1] Schwabl, F., *Quantenmechanik*. Springer, 2007.
- [2] Schwabl, F., *Quantenmechanik für Fortgeschrittene*. Springer, 2008.
- [3] Haken, H. and Wolf, H. C., *Atom- und Quantenphysik*. Springer, 2004.
- [4] Haken, H. and Wolf, H. C., *Molekülphysik und Quantenchemie*. Springer, 2006.
- [5] Demtröder, W., *Molecular Physics*. Wiley-VCH, 2005.
- [6] Atkins, P. W. and Friedman, R. S., *Molecular Quantum Mechanics*. Oxford University Press, 1997.
- [7] Lowe, J. P. and Peterson, K. A., *Quantum Chemistry*. Elsevier, 2006.
- [8] Weinhold, F. and Landis, C., *Valency and Bonding*. Cambridge University Press, 2005.
- [9] Czycoll, G., *Theoretische Festkörperphysik*. Springer, 2008.
- [10] Ashcroft, N. W. and Mermin, N. D., *Festkörperphysik*. Oldenbourg, 2005.
- [11] Kittel, C., *Introduction to Solid State Physics*. John Wiley & Sons, 2006.
- [12] L. Pauling, “THE NATURE OF THE CHEMICAL BOND. APPLICATION OF RESULTS OBTAINED FROM THE QUANTUM MECHANICS AND FROM A THEORY OF PARAMAGNETIC SUSCEPTIBILITY TO THE STRUCTURE OF MOLECULES,” *Journal of the American Chemical Society*, vol. 53, no. 4, pp. 1367–1400, 1931.
- [13] Ballhausen, C. J. and Gray, H. B., *Molecular Orbital Theory*. W. A. Benjamin, Inc., 1964.
- [14] Sutton, L. J., *Chemische Bindung und Molekülstruktur*. Springer, 1961.
- [15] Greiner, W. and Reinhardt, J., *Quantum Electrodynamics*. Springer, 2003.
- [16] Greiner, W. and Reinhardt, J., *Field Quantization*. Springer, 1996.
- [17] Kaku, M., *An Introduction to Quantum Field Theory*. Oxford University Press, 1993.
- [18] Peskin, M. E. and Schroeder, D. V., *An Introduction to Quantum Field Theory*. Westview Press, 1995.
- [19] A. H. Castro Neto, F. Guinea, N. M. R. Peres, K. S. Novoselov, and A. K. Geim, “The electronic properties of graphene,” *Reviews of Modern Physics*, vol. 81, pp. 109–162, Jan. 2009.

- [20] M. O. Goerbig, “Electronic properties of graphene in a strong magnetic field,” *Rev. Mod. Phys.*, vol. 83, pp. 1193–1243, Nov 2011.
- [21] F. Bloch, “Über die Quantenmechanik der Elektronen in Kristallgittern,” *Zeitschrift für Physik*, vol. 52, pp. 555–600, Jul 1929.
- [22] G. H. Wannier, “The Structure of Electronic Excitation Levels in Insulating Crystals,” *Phys. Rev.*, vol. 52, pp. 191–197, Aug 1937.
- [23] Feynman, R. P. and Hibbs, A. R., *Quantum Mechanics and Path Integrals*. Dover Publications, Inc., 2005.
- [24] Kleinert, H., *Path Integrals in Quantum Mechanics, Statistics, Polymer Physics, and Financial Markets*. World Scientific, 2009.
- [25] R. Peierls, “Zur Theorie des Diamagnetismus von Leitungselektronen,” *Zeitschrift für Physik*, vol. 80, pp. 763–791, Nov 1933.
- [26] J. M. Luttinger, “The Effect of a Magnetic Field on Electrons in a Periodic Potential,” *Phys. Rev.*, vol. 84, pp. 814–817, Nov 1951.
- [27] W. Kohn, “Theory of Bloch Electrons in a Magnetic Field: The Effective Hamiltonian,” *Phys. Rev.*, vol. 115, pp. 1460–1478, Sep 1959.
- [28] G. H. Wannier, “Dynamics of Band Electrons in Electric and Magnetic Fields,” *Rev. Mod. Phys.*, vol. 34, pp. 645–655, Oct 1962.
- [29] E. McCann, K. Kechedzhi, V. I. Fal’ko, H. Suzuura, T. Ando, and B. L. Altshuler, “Weak-Localization Magnetoresistance and Valley Symmetry in Graphene,” *Phys. Rev. Lett.*, vol. 97, p. 146805, Oct 2006.
- [30] K. Kechedzhi, O. Kashuba, and V. I. Fal’ko, “Quantum kinetic equation and universal conductance fluctuations in graphene,” *Phys. Rev. B*, vol. 77, p. 193403, May 2008.
- [31] J. L. Mañes, F. Guinea, and M. A. H. Vozmediano, “Existence and topological stability of Fermi points in multilayered graphene,” *Phys. Rev. B*, vol. 75, p. 155424, Apr 2007.
- [32] M. Vozmediano, M. Katsnelson, and F. Guinea, “Gauge fields in graphene,” *Physics Reports*, vol. 496, no. 4, pp. 109 – 148, 2010.
- [33] E. Kogan and V. U. Nazarov, “Symmetry classification of energy bands in graphene,” *Phys. Rev. B*, vol. 85, p. 115418, Mar 2012.
- [34] L. M. Malard, M. H. D. Guimarães, D. L. Mafra, M. S. C. Mazzoni, and A. Jorio, “Group-theory analysis of electrons and phonons in n -layer graphene systems,” *Phys. Rev. B*, vol. 79, p. 125426, Mar 2009.
- [35] C.-H. Park and S. G. Louie, “Making Massless Dirac Fermions from a Patterned Two-Dimensional Electron Gas,” *Nano Letters*, vol. 9, no. 5, pp. 1793–1797, 2009. PMID: 19338276.
- [36] R. Winkler and U. Zülicke, “Invariant expansion for the trigonal band structure of graphene,” *Phys. Rev. B*, vol. 82, p. 245313, Dec 2010.

-
- [37] J.-M. Hou and W. Chen, “Hidden symmetry and protection of Dirac points on the honeycomb lattice,” *Scientific Reports*, vol. 5, p. 17571, Dec. 2015.
- [38] Gradshteyn, I. S. and Ryzhik, I. M., *Table of Integrals, Series, and Products*. Elsevier, 2007.
- [39] Y. Hasegawa, R. Konno, H. Nakano, and M. Kohmoto, “Zero modes of tight-binding electrons on the honeycomb lattice,” *Phys. Rev. B*, vol. 74, p. 033413, Jul 2006.
- [40] B. Wunsch, F. Guinea, and F. Sols, “Dirac-point engineering and topological phase transitions in honeycomb optical lattices,” *New Journal of Physics*, vol. 10, no. 10, p. 103027, 2008.
- [41] V. M. Pereira, A. H. Castro Neto, and N. M. R. Peres, “Tight-binding approach to uniaxial strain in graphene,” *Phys. Rev. B*, vol. 80, p. 045401, Jul 2009.
- [42] A. Cortijo and M. A. H. Vozmediano, “Minimal conductivity of rippled graphene with topological disorder,” *Phys. Rev. B*, vol. 79, p. 184205, May 2009.
- [43] A. Sinner, A. Sedrakyan, and K. Ziegler, “Optical conductivity of graphene in the presence of random lattice deformations,” *Phys. Rev. B*, vol. 83, p. 155115, Apr 2011.
- [44] G. W. Semenoff, “Condensed-Matter Simulation of a Three-Dimensional Anomaly,” *Phys. Rev. Lett.*, vol. 53, pp. 2449–2452, Dec 1984.
- [45] C. Chamon, “Solitons in carbon nanotubes,” *Phys. Rev. B*, vol. 62, pp. 2806–2812, Jul 2000.
- [46] C.-Y. Hou, C. Chamon, and C. Mudry, “Electron Fractionalization in Two-Dimensional Graphenelike Structures,” *Phys. Rev. Lett.*, vol. 98, p. 186809, May 2007.
- [47] F. D. M. Haldane, “Model for a Quantum Hall Effect without Landau levels: Condensed-Matter Realization of the “Parity Anomaly”,” *Phys. Rev. Lett.*, vol. 61, pp. 2015–2018, Oct 1988.
- [48] S. Ryu, C. Mudry, C.-Y. Hou, and C. Chamon, “Masses in graphenelike two-dimensional electronic systems: Topological defects in order parameters and their fractional exchange statistics,” *Phys. Rev. B*, vol. 80, p. 205319, Nov 2009.

Chapter 3

Generating functionals – or how to organize the zoo of correlation functions

In this chapter we explain the elementary statistical methods used in quantum field theory to calculate the quantities of interest, the correlation functions. Using a prototype quantum field theory – a real scalar boson – as a working basis, we discuss how correlation functions are obtained in an efficient way from a superior mathematical structure, the generating functional. We explicitly calculate the correlation functions for the case of a free field theory, that is, when the action is assumed to be quadratic in the fields. We then proceed to introduce a new functional, the generating functional for connected correlation functions, and work out the relation between these two types of correlation functions. It is shown that the connected correlators are the “atomic” building blocks of the correlation functions, reducing the calculational effort by a large extent. We finally introduce the effective action as the Legendre transform of the connected functional, and the one-particle irreducible vertex functions as the corresponding type of correlation functions. We show that the connected n -point correlation functions, with $n > 2$, can be expanded into “trees” with connected two-point functions as branches and vertex functions as branching points, resolving the “subatomic” structure of the connected correlators. These relations further condense the calculations down to the truly fundamental objects, which need to be investigated in order to understand the properties of the physical system.

3.1 The partition function as a generator of correlation functions

Although we derived the effective low-energy Hamiltonian of interacting electrons in graphene in the previous chapter, which is the starting point for the papers included in this thesis, here we want to explain the statistical methods of quantum field theory using a much simpler theory: a single scalar boson. The main reason for this choice is that a bosonic field theory, without any internal degrees of freedom, is the simplest kind of field theory one could possibly study. There are no distractions one would have to deal with, like certain symmetries and other system specific details, or even just minus signs when commuting fermionic field operators. Such a simple theory, instead, allows us to focus on very general features that are shared by almost all quantum field theories. The results presented in this chapter are straightforward to generalize and easy to adapt to the physical system one actually wants to study. In that sense the real

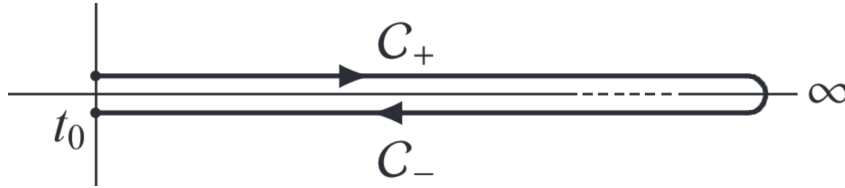


Figure 3.1: Schwinger-Keldysh closed time contour, with initial time t_0 , forward (\mathcal{C}_+) and backward branch (\mathcal{C}_-). The contour-time ordering operator $\mathcal{T}_{\mathcal{C}}$ is defined with respect to this contour. Any time t_- on the backward branch is considered to be larger than any other time t_+ on the forward branch, although it may be the case that their numerical values satisfy $t_- < t_+$.

scalar boson is – at least for the purpose of this chapter – a prototypical field theory, and we care little about the physics and physical systems it describes. Nevertheless, we want to mention that such a theory has, in fact, plenty of applications, namely as a Ginzburg-Landau type of effective field theory in such diverse physical fields as magnetism, superconductivity and Bose-Einstein condensation, and even standard model physics to model the Higgs sector [1–4]. In the present context of interacting Dirac fermions in graphene, a real scalar boson emerges as a Hubbard-Stratonovich field that is associated to the charge carrier density [1–3, 5–7]. Hence, although it is not our main focus in this chapter, the real scalar field is intimately related to the physics of graphene.

The primary objects of interest in a quantum field theory are correlation functions. We may first introduce them thoroughly before we further motivate their importance for physics. The n -point correlation function or n -point Green function $G_{\mathcal{C}}(x_1, \dots, x_n)$, is defined as the time-ordered expectation value of n bosonic field operators in the Heisenberg picture [1, 2, 7–16]¹

$$G_{\mathcal{C}}(x_1, \dots, x_n) \equiv (-i)^{n-1} \langle \mathcal{T}_{\mathcal{C}} \hat{\phi}(x_1) \cdots \hat{\phi}(x_n) \rangle. \quad (3.1.1)$$

Here, the label $x = (t, \vec{r})$ is a short notation, combining temporal and spatial degrees of freedom. The time arguments are defined on the Schwinger-Keldysh contour – a closed time contour in complex time space, which starts at an initial time t_0 , extends into the remote future ($t = +\infty$) along the real time axis and returns to the initial time along the same path [7, 8, 10–18], see Fig. 3.1. Furthermore, $\mathcal{T}_{\mathcal{C}}$ is the time ordering operator, putting operators with larger contour-time to the left of operators with smaller contour-time, and the angular brackets define the quantum mechanical expectation value as a trace over the states in Fock space with respect to a density matrix $\rho(t_0)$

$$\langle \cdots \rangle \equiv \text{Tr}(\rho(t_0) \cdots). \quad (3.1.2)$$

The density matrix is defined at the initial time t_0 , specifying the initial state of the system. If the system is initially prepared in a thermal equilibrium state, the Schwinger-Keldysh contour can be extended downwards, by adding a finite imaginary time branch that connects t_0 and $t_0 - i\beta$, with β being the inverse temperature [10, 14–16]. This is possible, because the equilibrium density matrix, $\rho(t_0) \propto e^{-\beta H}$, has the structure of a time evolution operator that evolves the system along such an imaginary time branch, implementing the nontrivial initial correlations of the thermal state. Such an extension is useful, if one is interested in studying the transient regime upon perturbing the equilibrium. If instead one is interested in the fully equilibrated system, one could send the initial time t_0 to the remote past ($t_0 = -\infty$), which effectively gets rid of the finite imaginary time branch, since then all nontrivial initial correlations would

¹The prefactor in the definition of Eq. (3.1.1) is pure choice. Many authors use a different convention, but none of them became uniformly accepted. So we may stick to the convention of Ref. [11] for now.

have already decayed. More formally, any correlation function which possesses two kinds of time arguments, imaginary and real time, is typically suppressed at least algebraically or even exponentially, if the system thermalizes that is. But since the imaginary branch is infinitely far away with respect to any of the real time arguments, the limit $t_0 \rightarrow -\infty$ would cause these correlations to vanish. It seems that the extension of the Schwinger-Keldysh contour into the imaginary regime is restricted to the equilibrium density matrix, but this is not necessarily the case as has been discussed in Refs. [10, 14–16]. There is more than one way to implement the effect of nontrivial initial density matrices into the theory, but of course all of them are equivalent. The specific implementation we use here is discussed below.

Now that we have rigorously introduced the Green functions, we may further motivate their importance for physics. In (nonrelativistic) quantum theory the equation governing the dynamics of particles is the Schrödinger equation. Its solutions define a Hilbert space and they contain all the information that could possibly be extracted from the quantum mechanical system. For a quantum many-body system it is convenient to formulate this theory in a second quantized form, which expresses all the physical observables in terms of field operators, whose expectation values are the Green functions introduced above. In that sense, knowing all the correlation functions of a theory is equivalent to solving the many-body Schrödinger equation, since all expectation values of physical observables can be expressed in terms of correlation functions. In an actual experiment, there are two common strategies to extract information from a many-body system. Either the system is probed by perturbing it externally and investigating its response to the perturbation, which is encoded in the response functions [1, 3, 7, 8], or one performs a scattering experiment, whose scattering amplitudes can be extracted from the n -point Green functions by the LSZ (Lehmann-Symanzik-Zimmermann) reduction [4, 9]. Hence, although the n -point correlation functions may seem to be rather abstract mathematical objects, they actually contain all the physical informations one could possibly be interested in. Therefore, we have to calculate these functions as accurately as possible to match existing experiments or even be able to make predictions. In order to do so and come up with suitable and consistent approximations, we need to understand their internal mathematical structures first, which is precisely what this chapter aims for. In this context recall our discussion about asymptotic series on the basis of the zero-dimensional toy model field theory in Sec. 1.3. In that case we were able to solve the integral defining the moment generating function exactly. If we would not have been able to solve this toy model exactly, probably the first idea to analyze this theory would have been to restrict the coupling constant to small values and use perturbation theory. However, we found that a naive perturbation theory in terms of a power series of a small coupling constant is asymptotically divergent, due to a branch cut of the moment generating function along the negative real axis. Away from the cut the generating function and all its associated moments are a perfectly well-defined, analytic functions of the coupling constant, admitting a series expansion with a finite radius of convergence. Since the field theory we consider here is nothing but a generalization of the toy model to the case of a finite dimensional base manifold, the same arguments apply. To avoid an asymptotic divergence we must avoid any weak-coupling expansion, even if the coupling happens to be small against the kinetic term. Although an exact solution of this generalized case is impossible, we can still analyze the topological structures of the correlation functions exactly. This analysis will naturally lead us to a formulation of quantum field theory, that circumvents the above problems altogether and which allows for systematical studies in the nonperturbative regime.

As a final remark before we continue our discussion, we want to mention that the use of the Schwinger-Keldysh contour, either in its original or in its extended form, is very convenient, because it allows for a compact notation. It is this feature, which is important for the purpose

of this chapter. Physically meaningful are only real-time correlation functions. At any point in the upcoming calculations one could map the abstract contour-time to the physical real-time by assigning fields to each branch of the contour. This procedure would be accompanied by a doubling – in the case of the extended Schwinger-Keldysh contour even tripling – of degrees of freedom [7, 8, 10–16], which we want to avoid here in favour of the more compact notation.

With the analysis of the zero-dimensional field theory fresh in mind it should be clear how to proceed. Instead of trying to perform the quantum mechanical average for each correlation function individually, it is beneficial to introduce a mathematical object that contains all of these amplitudes in a unified manner. To this end, we employ the methods of statistical physics. In particular, we make use of the concept of generating functions, or rather their generalization to functionals [1, 2, 9–13, 19]. We introduce the generating functional of correlation functions, or partition function as we will call it shortly,² as the expectation value of a contour-time ordered exponential, containing the to-be-averaged field operator $\hat{\phi}$ and a source field J , which we may use to generate the desired correlation function

$$Z[J, \rho] = \left\langle \mathcal{T}_C \exp \left(i \int_x \hat{\phi}(x) J(x) \right) \right\rangle. \quad (3.1.3)$$

The n -point Green functions can then be obtained as the n -fold derivative of the partition function with respect to the source field $J(x)$ evaluated at vanishing source,

$$G(x_1, \dots, x_n) = i(-1)^n \frac{\delta^n Z[J, \rho]}{\delta J(x_1) \cdots \delta J(x_n)} \Big|_{J=0}. \quad (3.1.4)$$

In some cases it can be useful to consider a generalization of Eq. (3.1.3), where the exponential contains a local or bilocal two-particle source coupling to a field bilinear, either instead of or in addition to the single-particle source, see Refs. [1, 7, 13, 20] for instance. We use this technique in chapter 4.3 to calculate the physical response of fermions to an external electromagnetic perturbation, but we will not cover it here in detail. Once we have understood how to deal with the single-particle source, the relations we will obtain are easy to generalize to n -particle sources. Assuming the partition function to be an analytic functional of the source field, it can be expanded in a Taylor series, which in the context of functionals is also known as Volterra expansion [9],

$$\begin{aligned} Z[J, \rho] &= \sum_{n=0}^{\infty} \frac{1}{n!} \int_{x_1, \dots, x_n} \frac{\delta^n Z[J, \rho]}{\delta J(x_1) \cdots \delta J(x_n)} \Big|_{J=0} J(x_1) \cdots J(x_n) \\ &= 1 + \sum_{n=1}^{\infty} \frac{(-1)^{n-1}}{n!} \int_{x_1, \dots, x_n} G(x_1, \dots, x_n) J(x_1) \cdots J(x_n). \end{aligned} \quad (3.1.5)$$

Note the similarity with Eq. (1.3.2). Besides of being a convenient tool to generate correlation functions, the use of the partition function – and the other generating functionals we will introduce later on – has another great advantage. Whenever one performs a certain approximation on the level of a generating functional it immediately affects all correlation functions that are derived from it. Think of the stationary phase approximation as one such example. Thus, the

²Strictly speaking, one should distinguish the generating functional from the partition function, since the latter is actually just a normalization constant, $Z = \text{Tr} \rho(t_0)$, that ensures the probabilistic interpretation of quantum theory [1, 2]. The probability for the system to be in some microstate, no matter which one, must be equal to 1. For the important case of an equilibrium density matrix, however, their mathematical structures are so similar, that we do not make a distinction here.

approximation is implemented into the theory throughout all correlators in a manifestly consistent way. For comparison, if the correlation functions would be calculated one at a time, one would have to implement the same approximation for each correlation function individually and explicitly check for consistency. As long as low-order perturbation theory for a few low-level correlation functions is considered, the latter strategy may be feasible, but as soon as non-perturbative effects and/or higher level correlation function are important it should be obvious that the use of generating functionals is indeed superior to any other strategy.

Although the above definition of the partition function is sufficient to continue with our discussion, it is beneficial to cast the quantum mechanical expectation value into a functional integral representation. In principle, all the calculations could be performed in the operator formalism equally likely, but in many instances the functional integral formalism is superior, allowing for powerful approximation schemes that are difficult to implement using field operators and Heisenberg equations of motion. In the end, however, the formulation one chooses is a matter of taste. To translate the theory into functional integral language, we first introduce a set of time-dependent eigenstates of the Heisenberg field operator,

$$\hat{\phi}(t, \vec{x})|\phi, t\rangle = \phi(\vec{x})|\phi, t\rangle, \quad (3.1.6)$$

which form a complete basis of the Hilbert space at every instant in time [9, 12, 13, 21, 22]

$$\int \mathcal{D}\phi |\phi, t\rangle \langle \phi, t| = \mathbb{1}. \quad (3.1.7)$$

Note that the eigenvalue field $\phi(\vec{x})$ is a static field configuration specified by the state $|\phi, t\rangle$ at the initial time $t = t_0$. Nevertheless, Eq. (3.1.6) holds for all times. We furthermore emphasize that the functional integral in the above completeness relation covers static field configurations only, which is reflected by the integral measure $\mathcal{D}\phi = \prod_{\vec{x}} d\phi(\vec{x})$.³ Next, the trace involved in the definition of the partition function, Eqs. (3.1.2) and (3.1.3), is expressed as a functional integral with respect to initial time states, for which we may write

$$\hat{\phi}(t_0, \vec{x})|\phi_{\pm}\rangle = \phi_{\pm}(\vec{x})|\phi_{\pm}\rangle, \quad (3.1.8)$$

with $|\phi_{\pm}\rangle \equiv |\phi_{\pm}, t_0\rangle$. The choice of the plus/minus indices will become clear momentarily. In terms of these states the partition function acquires the form [11–13, 22]

$$\begin{aligned} Z[J, \rho] &= \text{Tr} \left(\rho(t_0) \mathcal{T}_C \exp \left(i \int_x \hat{\phi}(x) J(x) \right) \right) \\ &= \int \mathcal{D}\phi_+ \mathcal{D}\phi_- \langle \phi_+ | \rho(t_0) | \phi_- \rangle \langle \phi_- | \mathcal{T}_C \exp \left(i \int_x \hat{\phi}(x) J(x) \right) | \phi_+ \rangle, \end{aligned} \quad (3.1.9)$$

where we inserted a resolution of the identity in between the density matrix and the contour time ordered exponential. Note that the matrix element $\langle \phi_+ | \rho(t_0) | \phi_- \rangle$, which contains all the information about the initial state of the system, is time independent, since it involves initial-time states only. Furthermore, since the density matrix could in principle be expressed in terms of field operators at time t_0 , its matrix element is a functional of the initial-time field configurations $\phi_{\pm}(\vec{x})$, which we parametrize as follows [13, 22]

$$\langle \phi_+ | \rho(t_0) | \phi_- \rangle = e^{iK[\phi_+, \phi_-]}. \quad (3.1.10)$$

³The states (3.1.6) are related to coherent states, but the way they are introduced here and in Refs. [9, 12, 13, 22] is a bit sloppy. We refer to Ref. [21] for a rigorous discussion.

3.1. The partition function as a generator of correlation functions

The functional $K[\phi_+, \phi_-]$, we may call correlation functional, admits a Taylor expansion similar to the Taylor expansion of the partition function, *cf.* Eq. (3.1.5),

$$K[\phi_+, \phi_-] = \sum_{n=0}^{\infty} \frac{1}{n!} \sum_{\alpha_1, \dots, \alpha_n = \pm} \int_{\vec{x}_1, \dots, \vec{x}_n} K^{\alpha_1, \dots, \alpha_n}(\vec{x}_1, \dots, \vec{x}_n) \phi_{\alpha_1}(\vec{x}_1) \cdots \phi_{\alpha_n}(\vec{x}_n). \quad (3.1.11)$$

It translates the information about the initial state of system, that is contained in the density matrix, to initial correlations, that are contained in the kernels $K^{\alpha_1, \dots, \alpha_n}(\vec{x}_1, \dots, \vec{x}_n)$. Hence, instead of specifying the initial density matrix explicitly, it would be equivalently viable to specify all the initial correlations [13, 22, 20].

The remaining matrix element, involving the contour-time ordered exponential source term, describes the actual dynamics of the system. It can be cast into functional integral form by a standard procedure, see Refs. [1, 3, 4, 7, 9, 23]. Starting from the initial state $|\phi_+\rangle$ at the beginning of the Schwinger-Keldysh contour, where t_0 is interpreted to lie on the forward branch \mathcal{C}_+ , we follow the system's unitary time evolution along the contour into the final state $|\phi_-\rangle$ at the end of the Schwinger-Keldysh contour. The end of this contour coincides with the initial time t_0 , but now it is approached on the backward branch \mathcal{C}_- . Along the way we divide the contour time evolution into several short intervals, and we successively insert a resolution of the identity in terms of the above states, Eqs. (3.1.6) and (3.1.7), at each time slice. Performing the limiting procedure of infinitely small and infinitely many times slices then yields the integral representation

$$\langle \phi_- | \mathcal{T}_{\mathcal{C}} \exp \left(i \int_x \hat{\phi}(x) J(x) \right) | \phi_+ \rangle = \int' \mathcal{D}\phi e^{iS[\phi] + i \int_x \phi(x) J(x)}. \quad (3.1.12)$$

Here, the functional integral covers the dynamical field configurations for all contour times excluding the initial time, $\mathcal{D}\phi = \prod_{t \in \mathcal{C} \setminus t_0, \vec{x}} d\phi(t, \vec{x})$. The prime at the integral symbol indicates that it has to be solved with the boundary conditions $\phi(t_0 \in \mathcal{C}_+, \vec{x}) = \phi_+(\vec{x})$ and $\phi(t_0 \in \mathcal{C}_-, \vec{x}) = \phi_-(\vec{x})$. Note the appearance of the action $S[\phi]$, which derives from the unitary time evolution generated by the Hamiltonian. [1, 3, 4, 7, 9, 23]

Putting everything together, we can write the partition function in the condensed form

$$\begin{aligned} Z[J, \rho] &= \int \mathcal{D}\phi_+ \mathcal{D}\phi_- e^{iK[\phi_+, \phi_-]} \int' \mathcal{D}\phi e^{iS[\phi] + i \int_x \phi(x) J(x)} \\ &= \int \mathcal{D}\phi e^{iS[\phi] + iK[\phi] + i \int_x \phi(x) J(x)}, \end{aligned} \quad (3.1.13)$$

which shows that it is nothing but the functional Fourier transform of $e^{iS[\phi] + iK[\phi]}$. Interpreting the exponential without source as a probability distribution, the partition function would be the corresponding moment generating functional and the n -point Green functions are the corresponding moments.⁴ Note that the functional integral over the initial-time fields ϕ_{\pm} , together with the correlation functional closes the trace for the time evolution amplitude. As a result, the boundary conditions present in the field integral (3.1.12) are removed. We furthermore elevated the field dependence of the correlation functional to be formally dependent on the field $\phi(x)$, whose time argument is defined on the entire Schwinger-Keldysh contour. This is nothing but a reformulation of the previous result and adds nothing new to the theory. When expanding the correlation functional in a Taylor series with respect to this field, there are, indeed, contour time integrations present and the kernels formally depend on contour time. Yet, each kernel

⁴Obviously, this is an abuse of language, since a probability distribution has to be non-negative and real-valued, but, once more, we just want to point out mathematically similar structures.

vanishes identically if any contour time argument does not equal the initial time, such that we recover the expansion (3.1.11) [13, 22].

To put it in a nutshell, the transition from the operator formalism to the functional integral formalism is given by the following substitution

$$\mathrm{Tr}(\rho(t_0)\cdots) \longrightarrow \int \mathcal{D}\phi \cdots \exp(iS[\phi] + iK[\phi]) . \quad (3.1.14)$$

Furthermore, the to-be-averaged operator-valued fields are replaced by complex number-valued fields⁵ and contour-time ordering is implicitly taken care of by the functional integral itself. The latter fact should be clear from its derivation from the operator formalism. In the following we will slightly abuse the notation by omitting the correlation functional. Since the precise form of the action $S[\phi]$ is of no interest to us in this chapter, we take the viewpoint that all the contributions of the correlation functional, however complicated they may be, are absorbed into the action. In addition, we will write $Z[J, \rho] = Z[J]$ for brevity, but we have to keep in mind, that the partition function and the other functionals we will introduce in the remainder of this chapter depend on the details of the density matrix.

Apart from a few exceptions it is impossible to calculate the partition function for interacting theories exactly, such that one is forced to make approximations. For the moment we want to sidestep this issue and consider the exactly solvable noninteracting limit of our field theory to get an intuition of the internal structures of correlation functions. To this end, we assume that the action is a quadratic functional of the bosonic field

$$S[\phi] = S_0[\phi] = \frac{1}{2} \int_{x,y} \phi(x) \Delta_0^{-1}(x,y) \phi(y) , \quad (3.1.15)$$

where $\Delta_0^{-1}(x,y)$ is an operator, specific to the theory in question. (Think of the Klein-Gordon operator to have an explicit example in mind.) Note that this assumption restricts the density matrices to be Gaussian as well, since we absorbed $K[\phi]$ into $S[\phi]$. The latter fact is not an approximation, but a mere restriction to a certain subclass of initial correlations and by extension a restriction to the experimental setup [13, 20]. In that case, the functional integral that defines the partition function (3.1.13) reduces to a Gaussian integral, which can be calculated exactly

$$\begin{aligned} Z[J] &= \int \mathcal{D}\phi \exp i \left(\frac{1}{2} \int_{x,y} \phi(x) \Delta_0^{-1}(x,y) \phi(y) + \int_x \phi(x) J(x) \right) \\ &= \exp \left(-i \frac{1}{2} \int_{x,y} J(x) \Delta_0(x,y) J(y) \right) . \end{aligned} \quad (3.1.16)$$

Here, both Δ_0^{-1} and Δ_0 are interpreted as matrices with continuous matrix indices x and y , fulfilling the inversion relation

$$\int_z \Delta_0^{-1}(x,z) \Delta_0(z,y) = \delta(x-y) . \quad (3.1.17)$$

On a more formal level Δ_0^{-1} and Δ_0 are not mere functions but distributions. As such, the above interpretation as matrices has to be taken with care, especially when it comes to actually solving Eq. (3.1.17). We note that the solution to this equation, Δ_0 , is not uniquely defined by the equation alone, but depends on boundary conditions that are encoded in the kernels of the

⁵For Hermitean field operators, as is the case here, the operator is replaced by a real-valued field. In order to deal with fermionic field theories, whose field operators obey anti-commutation relations instead of commutation relations, the appropriate replacement would be given in terms of Grassmann-valued fields [1–4, 9].

3.1. The partition function as a generator of correlation functions

correlation functional and that have to be chosen appropriately to describe a certain physical scenario. Moreover, it may also be the case that Eq. (3.1.17) is not well-defined at all, for example when dealing with gauge theories [4, 9], requiring further considerations. This obstacle occurs in the abelian Chern-Simons theory we present in chapter 4.3. For the purpose of this chapter, however, we assume that the solution to Eq. (3.1.17) is well-defined and boundary conditions are already taken care of.

Expanding the exponential function in Eq. (3.1.16) in a Taylor series, we see that the partition function only contains even powers of the source field

$$Z[J] = \sum_{n=0}^{\infty} \frac{1}{n!} \left(-i \frac{1}{2} \int_{x,y} J(x) \Delta_0(x,y) J(y) \right)^n . \quad (3.1.18)$$

In other words, only those correlation functions exist that possess an even number of external points. Furthermore, when comparing the above expansion with the general Volterra expansion (3.1.5), we observe that the individual summands factorize in powers of n , such that all correlation functions decompose into simple algebraic products of Δ_0 . In particular, the first three nontrivial correlation functions read

$$G(1, 2) = \Delta_0(1, 2), \quad (3.1.19a)$$

$$G(1, 2, 3, 4) = -i \Delta_0(1, 2) \Delta_0(3, 4) - i \Delta_0(1, 3) \Delta_0(2, 4) - i \Delta_0(1, 4) \Delta_0(2, 3), \quad (3.1.19b)$$

$$\begin{aligned} G(1, \dots, 6) = & -\Delta_0(1, 2) \Delta_0(3, 4) \Delta_0(5, 6) - \Delta_0(1, 4) \Delta_0(2, 5) \Delta_0(3, 6) - \Delta_0(1, 6) \Delta_0(2, 3) \Delta_0(4, 5) \\ & - \Delta_0(1, 2) \Delta_0(3, 6) \Delta_0(4, 5) - \Delta_0(1, 4) \Delta_0(2, 3) \Delta_0(5, 6) - \Delta_0(1, 6) \Delta_0(2, 5) \Delta_0(3, 4) \\ & - \Delta_0(1, 3) \Delta_0(2, 5) \Delta_0(4, 6) - \Delta_0(1, 4) \Delta_0(2, 6) \Delta_0(3, 5) - \Delta_0(1, 5) \Delta_0(2, 4) \Delta_0(3, 6) \\ & - \Delta_0(1, 2) \Delta_0(3, 5) \Delta_0(4, 6) - \Delta_0(1, 5) \Delta_0(2, 3) \Delta_0(4, 6) - \Delta_0(1, 5) \Delta_0(2, 6) \Delta_0(3, 4) \\ & - \Delta_0(1, 3) \Delta_0(2, 6) \Delta_0(4, 5) - \Delta_0(1, 3) \Delta_0(2, 4) \Delta_0(5, 6) - \Delta_0(1, 6) \Delta_0(2, 4) \Delta_0(3, 5). \end{aligned} \quad (3.1.19c)$$

Here, the numerical labels $1, 2, \dots$ are just a short notation for the space-time labels x_1, x_2, \dots . In the remainder of this chapter we will regularly switch between these two notations. The first equation tells us that the two-point correlator coincides with Δ_0 . Hence, the operator Δ_0^{-1} may be interpreted as the inverse two-point Green function. Based on the above progression, it should be clear that higher level correlation functions contain a rapidly increasing number of terms, leading to the question: what are the underlying rules, determining which terms are allowed and which are not? To put it differently, how do the indices within the factors Δ_0 in the product terms have to be arranged for a particular correlation function? To answer this question it is beneficial to translate the above analytic expressions into a diagrammatic language. By representing the term $\Delta_0(1, 2)$ as a solid line, connecting the external points 1 and 2

$$G(1, 2) = G_0(1, 2) = 1 \text{ --- } 2, \quad (3.1.20)$$

we can depict the four- and six-point function as follows

$$G(1, 2, 3, 4) = -i \begin{array}{c} 2 \text{ --- } 3 \\ \text{---} \\ 1 \text{ --- } 4 \end{array} - i \begin{array}{c} 2 \\ | \\ 1 \end{array} \begin{array}{c} 3 \\ | \\ 4 \end{array} - i \begin{array}{c} 3 \\ | \\ 4 \end{array} \begin{array}{c} 2 \\ | \\ 1 \end{array} - i \begin{array}{c} 3 \\ | \\ 4 \end{array} \begin{array}{c} 2 \\ \diagdown \\ 1 \end{array} \begin{array}{c} 3 \\ \diagup \\ 4 \end{array}, \quad (3.1.21)$$

$$\begin{aligned}
 G(1, \dots, 6) = & -2 \begin{array}{c} 3 \quad 4 \\ \text{---} \\ \diagdown \quad \diagup \\ 1 \quad 6 \end{array} 5 - 2 \begin{array}{c} 3 \quad 4 \\ \diagup \quad \diagdown \\ \text{---} \\ 1 \quad 6 \end{array} 5 - 2 \begin{array}{c} 3 \quad 4 \\ \diagdown \quad \diagup \\ \diagup \quad \diagdown \\ \text{---} \\ 1 \quad 6 \end{array} 5 \\
 & - 2 \begin{array}{c} 3 \quad 4 \\ \diagdown \quad \diagdown \\ \diagup \quad \diagup \\ \text{---} \\ 1 \quad 6 \end{array} 5 - 2 \begin{array}{c} 3 \quad 4 \\ \diagup \quad \diagup \\ \diagdown \quad \diagdown \\ \text{---} \\ 1 \quad 6 \end{array} 5 - 2 \begin{array}{c} 3 \quad 4 \\ \text{---} \\ \text{---} \\ \text{---} \\ 1 \quad 6 \end{array} 5 \\
 & - 2 \begin{array}{c} 3 \quad 4 \\ | \quad | \\ \text{---} \\ | \quad | \\ 1 \quad 6 \end{array} 5 - 2 \begin{array}{c} 3 \quad 4 \\ \diagdown \quad \diagup \\ \diagup \quad \diagdown \\ \text{---} \\ 1 \quad 6 \end{array} 5 - 2 \begin{array}{c} 3 \quad 4 \\ \diagdown \quad \diagup \\ \diagup \quad \diagdown \\ \text{---} \\ 1 \quad 6 \end{array} 5 \\
 & - 2 \begin{array}{c} 3 \quad 4 \\ \diagdown \quad | \\ \diagup \quad | \\ \text{---} \\ 1 \quad 6 \end{array} 5 - 2 \begin{array}{c} 3 \quad 4 \\ \diagup \quad | \\ \diagdown \quad | \\ \text{---} \\ 1 \quad 6 \end{array} 5 - 2 \begin{array}{c} 3 \quad 4 \\ \text{---} \\ \diagdown \quad \diagup \\ \text{---} \\ 1 \quad 6 \end{array} 5 \\
 & - 2 \begin{array}{c} 3 \quad 4 \\ | \quad \diagdown \\ | \quad \diagup \\ \text{---} \\ 1 \quad 6 \end{array} 5 - 2 \begin{array}{c} 3 \quad 4 \\ | \quad \diagup \\ | \quad \diagdown \\ \text{---} \\ 1 \quad 6 \end{array} 5 - 2 \begin{array}{c} 3 \quad 4 \\ \diagdown \quad \diagup \\ \text{---} \\ \diagdown \quad \diagup \\ 1 \quad 6 \end{array} 5. \tag{3.1.22}
 \end{aligned}$$

Each summand consists of two, respectively three, disconnected lines, which is understood as an algebraic multiplication of the corresponding analytical term. In this form the combinatorial structure of the above correlation functions, Eqs.(3.1.19), becomes transparent. The four- and six-point functions contain all those terms, where any distinct pair of two nonidentical external points is connected via a single solid line. Moreover, each combinatorially possible term contributes with the same statistical weight to the respective correlation function. This observation naturally leads us to the conclusion that a general $2n$ -point correlation function can be expressed as a sum of products [9],

$$G(1, \dots, 2n) = (-i)^n \sum_{\text{Pair Perm.}} \Delta_0(\sigma(1), \sigma(2)) \Delta_0(\sigma(3), \sigma(4)) \cdots \Delta_0(\sigma(2n-1), \sigma(2n)), \tag{3.1.23}$$

where each product term contains n two-point correlation functions. The latter represent an unordered pair of external points, and the sum accounts for all possible permutations of those pairs. Combining $2n$ external points into n unordered pairs, with each point being paired up only once, is a simple combinatorial problem that leads to $(2n-1)!! = (2n)!/n!2^n$ distinct contributions to the sum. So the 8-point function would already contain $(2 \cdot 4 - 1)!! = 105$ distinct summands.

The above example clearly shows that the only quantity we actually need to calculate (in the noninteracting theory) is the two-point correlator Δ_0 . All the other correlation functions

are then obtained as sums of products of this fundamental correlator invoking combinatorial considerations. These findings beg the question: is there a more efficient approach, which incorporates these insights outright and, if so, to what extent does it generalize to theories with interactions?

3.2 Connected correlation functions and their generating functional

In the remainder of this chapter we mostly present standard textbook material, which is covered in a similar form in the Refs. [1, 2, 4, 9]. Although these references either employ the real-time groundstate formalism based on the Gellman-Low theorem or the imaginary-time Matsubara formalism to treat thermal equilibrium, the fact that the time arguments of the fields and n -point correlation functions are defined on the Schwinger-Keldysh contour does not interfere with the upcoming constructions. A genuine nonequilibrium treatment using the Schwinger-Keldysh contour may be found in Ref. [11]. Nevertheless, it is still instructive to show a detailed derivation as a proper motivation for the nonperturbative formalisms constructed and employed in the following chapters.

Without further ado we introduce a new functional $W[J]$ as the natural logarithm of the partition function $W[J] = -i \ln Z[J]$. It is called “generating functional of connected correlation functions”, or connected functional for short. Again, we assume that the connected functional is an analytic functional of the source field J , such that we can write

$$\begin{aligned} W[J] &= \sum_{n=0}^{\infty} \frac{1}{n!} \int_{x_1, \dots, x_n} \frac{\delta^n W[J]}{\delta J(x_1) \cdots \delta J(x_n)} \Bigg|_{J=0} J(x_1) \cdots J(x_n) \\ &= \sum_{n=1}^{\infty} \frac{(-1)^n}{n!} \int_{x_1, \dots, x_n} G_c(x_1, \dots, x_n) J(x_1) \cdots J(x_n). \end{aligned} \quad (3.2.1)$$

Here, the second line defines the connected n -point correlation functions $G_c(x_1, \dots, x_n)$ as the n -fold derivative of the connected functional with respect to the source field J evaluated at vanishing source

$$G_c(x_1, \dots, x_n) = (-1)^{n-1} \frac{\delta^n W[J]}{\delta J(x_1) \cdots \delta J(x_n)} \Bigg|_{J=0}. \quad (3.2.2)$$

In statistical physics the connected functional is also called “cumulant generating functional”. According to that nomenclature the connected Green functions are the cumulants of the probability distribution $e^{iS[\phi]}$.

With the example of the free field theory fresh in mind, it should be convincing that this functional is indeed a useful quantity to work with. Since the partition function of a free field is a Gaussian functional of the source J , the Volterra expansion of the connected functional terminates at the second order

$$W[J] = -\frac{1}{2} \int_{x,y} J(x) \Delta_0(x,y) J(x), \quad (3.2.3)$$

reflecting the fact that the only quantity to calculate is the connected two-point correlator. Exponentiation of the connected functional then accounts for the correct combinatorics of the disconnected $2n$ -point correlators as was shown above.

As stated previously, in a general theory with interactions the partition function cannot be calculated exactly anymore. In particular, it cannot be written as a simple Gaussian functional,

which means that the Volterra expansion of the connected functional, Eq. (3.2.1), does not terminate at a finite order. In other words, all connected n -point correlators will be nontrivial. This fact, however, does not interfere with the statement that the exponentiation of the connected functional accounts for the correct combinatorics of the correlation functions. We will demonstrate this feature explicitly below. To this end, we write the partition function as $Z[J] = e^{iW[J]}$, expand the exponential, and insert the Volterra expansion for $W[J]$ on the right-hand side

$$\begin{aligned} Z[J] &= \sum_{n=0}^{\infty} \frac{1}{n!} \left(i \sum_{m=0}^{\infty} \frac{1}{m!} \int_{1,\dots,m} \frac{\delta^m W[J]}{\delta J(1) \cdots \delta J(m)} \Big|_{J=0} J(1) \cdots J(m) \right)^n \\ &= \sum_{n=0}^{\infty} \frac{i^n}{n!} \sum_{m_1, \dots, m_n=0}^{\infty} \frac{1}{m_1! \cdots m_n!} \int_{1_1, \dots, m_n} \frac{\delta^{m_1} W[J]}{\delta J(1_1) \cdots \delta J(m_1)} \cdots \frac{\delta^{m_n} W[J]}{\delta J(1_n) \cdots \delta J(m_n)} \Big|_{J=0} \\ &\quad \times J(1_1) \cdots J(m_1) \cdots J(1_n) \cdots J(m_n). \end{aligned} \quad (3.2.4)$$

Substituting the definitions of the connected correlators, Eq. (3.2.2), we obtain

$$\begin{aligned} Z[J] &= \sum_{n=0}^{\infty} \frac{i^n}{n!} \sum_{m_1, \dots, m_n=0}^{\infty} \frac{(-1)^{m_1-1} \cdots (-1)^{m_n-1}}{m_1! \cdots m_n!} \int_{1_1, \dots, m_n} G_c(1_1, \dots, m_1) \cdots G_c(1_n, \dots, m_n) \\ &\quad \times J(1_1) \cdots J(m_1) \cdots J(1_n) \cdots J(m_n). \end{aligned} \quad (3.2.5)$$

Here, we already see that the partition function contains products of connected correlators, similar to what we found previously. To obtain the desired representation of a general n -point correlation function in terms of connected correlation functions, we need to make use of the Volterra expansion for $Z[J]$, Eq. (3.1.5), and compare coefficients of equal powers of J . For the first four correlation functions we find

$$iG(1) = iG_c(1) = i\langle \phi(1) \rangle, \quad (3.2.6a)$$

$$iG(1, 2) = iG_c(1, 2) - iG_c(1)iG_c(2), \quad (3.2.6b)$$

$$\begin{aligned} iG(1, 2, 3) &= iG_c(1, 2, 3) - iG_c(1)iG_c(2, 3) - iG_c(2)iG_c(3, 1) - iG_c(3)iG_c(2, 1) \\ &\quad + iG_c(1)iG_c(2)iG_c(3), \end{aligned} \quad (3.2.6c)$$

$$\begin{aligned} iG(1, 2, 3, 4) &= iG_c(1, 2, 3, 4) - iG_c(12)iG_c(34) - iG_c(13)iG_c(24) - iG_c(14)iG_c(23) \\ &\quad - iG_c(1)iG_c(234) - iG_c(2)iG_c(341) - iG_c(3)iG_c(412) - iG_c(4)iG_c(123) \\ &\quad + iG_c(1)iG_c(2)iG_c(34) + iG_c(3)iG_c(4)iG_c(12) + iG_c(1)iG_c(3)iG_c(24) \\ &\quad + iG_c(2)iG_c(4)iG_c(13) + iG_c(1)iG_c(4)iG_c(23) + iG_c(2)iG_c(3)iG_c(14) \\ &\quad - iG_c(1)iG_c(2)iG_c(3)iG_c(4). \end{aligned} \quad (3.2.6d)$$

We emphasize that the correlation functions, be it the connected or disconnected ones, with an odd number of external points do not vanish in general. Such a feature is not necessarily reserved for an interacting theory. We remind the reader that we assumed the action of the noninteracting theory to be purely quadratic in the fields. It would have still been possible to calculate the partition function exactly had we assumed the action to contain a term linear in the field. In that case the Gaussian probability distribution $e^{iS[\phi]}$ would not be centered at $\phi = 0$, but at the nonvanishing field expectation value that is proportional to the linear term.

3.2. Connected correlation functions and their generating functional

As was the case for the noninteracting theory presented in the previous section, it is beneficial to visualize these relations with the help of diagrams, revealing the structure of the n -point correlation function more clearly. Since each connected n -point function is a unique mathematical object, that is independent of the other m -point functions ($n \neq m$), one should assign a unique diagrammatic representation to each one of them. For the one-point function we choose a blob with one external leg, for the two-point function we use a solid line as we did before in the noninteracting theory,⁶ and for the connected n -point correlators with $n > 2$ probably the most obvious choice is an n -sided polygon, where each corner represents one external point

$$\begin{aligned}
 G_c(1) &= \text{blob}(G_c) \text{ with leg } 1, & G_c(1,2) &= 1 \text{ --- } 2, & G_c(1,2,3) &= 1 \text{ --- } \triangle(G_c) \text{ --- } 2, 3, \\
 G_c(1,2,3,4) &= \text{square}(G_c) \text{ with legs } 1, 2, 3, 4, & G_c(1,2,3,4,5) &= 2 \text{ --- } \text{pentagon}(G_c) \text{ --- } 1, 3, 4, 5, & \dots
 \end{aligned} \tag{3.2.7}$$

With this notation the above correlation functions assume the form

$$iG(1,2) = i \text{ --- } 1 \text{ --- } 2 - i^2 \text{ --- } 1 \text{ --- } \text{blob} \text{ --- } 2, \tag{3.2.8}$$

$$\begin{aligned}
 iG(1,2,3) &= i \text{ --- } 1 \text{ --- } \triangle(G_c) \text{ --- } 2, 3 - i^2 \text{ --- } 1 \text{ --- } \text{blob} \text{ --- } \text{blob} \text{ --- } 2, 3 \\
 &\quad - i^2 \text{ --- } 1 \text{ --- } \text{blob} \text{ --- } \text{blob} \text{ --- } 2, 3 - i^2 \text{ --- } 1 \text{ --- } \text{blob} \text{ --- } \text{blob} \text{ --- } 2, 3 + i^3 \text{ --- } 1 \text{ --- } \text{blob} \text{ --- } \text{blob} \text{ --- } \text{blob} \text{ --- } 2, 3, \\
 &\hspace{15em} \tag{3.2.9}
 \end{aligned}$$

⁶To avoid confusion with the diagrammatic representation of the noninteracting theory one may represent the interacting connected two-point correlator with a blob as well, as done in Ref. [9]

$$G_c(1,2) = 1 \text{ --- } \text{blob}(G_c) \text{ --- } 2,$$

but in order to keep the upcoming expressions as clean as possible we decided not to do so.

$$\begin{aligned}
 iG(1, 2, 3, 4) = & +i \begin{array}{c} 2 \quad 3 \\ \square \\ 1 \quad 4 \end{array} G_c - i^2 \begin{array}{c} 2 \quad 3 \\ \text{---} \\ 1 \quad 4 \end{array} - i^2 \begin{array}{c} 2 \quad 3 \\ | \quad | \\ 1 \quad 4 \end{array} - i^2 \begin{array}{c} 2 \quad 3 \\ \diagdown \quad \diagup \\ 1 \quad 4 \end{array} \\
 & - i^2 \begin{array}{c} 2 \quad 3 \\ \circ \quad \diagdown \\ 1 \quad 4 \end{array} G_c - i^2 \begin{array}{c} 2 \quad 3 \\ \diagup \quad \circ \\ 1 \quad 4 \end{array} G_c - i^2 \begin{array}{c} 2 \quad 3 \\ \diagdown \quad \circ \\ 1 \quad 4 \end{array} G_c - i^2 \begin{array}{c} 2 \quad 3 \\ \circ \quad \diagup \\ 1 \quad 4 \end{array} G_c \\
 & + i^3 \begin{array}{c} 2 \quad 3 \\ \circ \quad \circ \\ \text{---} \\ 1 \quad 4 \end{array} + i^3 \begin{array}{c} 2 \quad 3 \\ \circ \quad \circ \\ \text{---} \\ 1 \quad 4 \end{array} + i^3 \begin{array}{c} 2 \quad 3 \\ | \quad \circ \\ | \quad \circ \\ 1 \quad 4 \end{array} + i^3 \begin{array}{c} 2 \quad 3 \\ \circ \quad \circ \\ | \quad \circ \\ | \quad \circ \\ 1 \quad 4 \end{array} \\
 & + i^3 \begin{array}{c} 2 \quad 3 \\ \diagdown \quad \circ \\ \circ \quad \diagup \\ 1 \quad 4 \end{array} + i^3 \begin{array}{c} 2 \quad 3 \\ \circ \quad \diagdown \\ \diagup \quad \circ \\ 1 \quad 4 \end{array} - i^4 \begin{array}{c} 2 \quad 3 \\ \circ \quad \circ \\ \circ \quad \circ \\ 1 \quad 4 \end{array} . \tag{3.2.10}
 \end{aligned}$$

The structures we find are certainly more complex than in the noninteracting theory, but from the purely combinatorial viewpoint they are no different. The n -point correlation functions of an interacting theory, that are generated by the partition function $Z[J]$, contain all possible diagrams and products of diagrams – the connected correlators and their algebraic products – whose number of external points add up to n , accounting for all distinct arrangements of those diagrams. In that sense the only difference between an interacting and a noninteracting theory is the number of mathematical objects that need to be arranged. So, if we are interested in a particular correlation function $G(1, \dots, n)$, all we need to calculate are all the connected correlation functions $G_c(1), G_c(1, 2), \dots$, up to $G_c(1, \dots, n)$, and the rest is combinatorics.

This insight drastically reduces the calculational effort, yet it leads to a new problem. How do we actually calculate these connected correlators in the presence of interactions? As of right now we have not encountered an actual equation, whose solution determines the connected two-point Green function, let alone a set of equations for all the other nontrivial n -point Green functions. In the noninteracting theory the only quantity needed to calculate was the connected two-point Green function. It was given by the solution to the equation (3.1.17), but this equation certainly cannot hold if interactions are present, since it was obtained by an exact solution of a Gaussian functional integral. In order to proceed we have to find such equations, which are valid for interacting quantum field theories. Otherwise the results of this section would have little to no practical value.

3.3 Effective action, vertex functions and the tree expansion of connected correlators

In order to answer the question that arose at the end of the previous section, it turns out that it is useful to introduce a new functional $\Gamma[\phi]$, which is defined as the functional Legendre transform of the connected functional

$$\Gamma[\phi] = W[J[\phi]] - \int_x \phi(x) J(x|\phi) . \tag{3.3.1}$$

Here, $J(x|\phi)$ is the source that is both, a bosonic field of x and a functional of the field expectation value $\phi(x) \equiv \phi(x|J) = \langle \hat{\phi}(x) \rangle_J$. Recall that the latter is defined as the first derivative of

the connected functional, Eq. (3.2.6a),

$$\langle \hat{\phi}(x) \rangle_J = \frac{\delta W[J]}{\delta J(x)} = \sum_{n=0}^{\infty} \frac{1}{n!} \int_{1, \dots, n} \frac{\delta^{n+1} W[J]}{\delta J(x) \delta J(1) \cdots \delta J(n)} \Big|_{J=0} J(1) \cdots J(n), \quad (3.3.2)$$

which has to be inverted in order to express J as a functional of ϕ . At this point we remind the reader of the connection between Lagrange mechanics and Hamilton mechanics, where the former employs positions and velocities as degrees of freedom, while the latter makes use of positions and canonical momenta to describe a physical system. The velocities are eliminated in favour of canonical momenta, which are defined as first derivatives of the Lagrange function with respect to the velocities. The Lagrange function itself is transformed to the Hamilton function by a Legendre transformation similar to the one above. For the functional $\Gamma[\phi]$ the field ϕ acts as a source, which we may use to generate a new type of correlation functions, see below. This new functional is known as the effective action and its first derivative with respect to the field ϕ is the equation of motion

$$\frac{\delta \Gamma[\phi]}{\delta \phi(x)} = -J(x). \quad (3.3.3)$$

In light of classical field theory this terminology is somewhat suspicious, but it becomes clear when we consider the free theory once more. In that case the connected functional could be calculated exactly, Eq. (3.2.3), which, when inserted into (3.3.1), leads to

$$\Gamma[\phi] = -\frac{1}{2} \int_{x,y} J(x|\phi) \Delta_0(x,y) J(y|\phi) - \int_x \phi(x) J(x|\phi). \quad (3.3.4)$$

Performing the first derivative of $W[J]$ with respect to the source field yields a linear functional of the source

$$\phi(x|J) = - \int_y \Delta_0(x,y) J(y). \quad (3.3.5)$$

By using Eq. (3.1.17) we can trivially invert this relation and express the source J as a functional of ϕ , which may be inserted back into Eq. (3.3.4). What we find is identical to the bare action of the free theory

$$\Gamma[\phi] = \frac{1}{2} \int_{x,y} \phi(x) \Delta_0^{-1}(x,y) \phi(y), \quad (3.3.6)$$

with the corresponding equation of motion

$$\int_y \Delta_0^{-1}(x,y) \phi(y) = -J(x). \quad (3.3.7)$$

At vanishing source J , the equation of motion may have a nontrivial solution, which defines a “classical” field $\langle \hat{\phi}(x) \rangle_{J=0} = \phi_c(x) \neq 0$. If Δ_0^{-1} is the Klein-Gordon operator, then the classical field $\phi_c(x)$ may be a plane wave or a wave packet.⁷ In this context recall Hamilton’s least action principle of the classical Lagrange formalism, where the first variation of the classical action yields the equations of motion of the system. It is precisely this resemblance to the classical formalism, which justifies the nomenclature “effective action” and “equation of motion”.

The mindful reader may have already spotted a seeming inconsistency in our treatment. Upon setting the source to zero, Eq. (3.3.5) implies that $\phi_c(x)$ has to vanish identically, in contradiction to the possibility of nontrivial homogeneous solutions of Eq. (3.3.7). In the present

⁷Often the onset of a finite field expectation value is accompanied by spontaneous symmetry breaking, so much so that some use these terms synonymously, but it obviously need not be the case as this example shows.

form Eq. (3.3.5) only accounts for the inhomogeneous solution of the differential operator Δ_0^{-1} , that arises in response to the external source J , but the homogeneous solutions are missing. To resolve this puzzle, recall that the field ϕ is the expectation value of a field operator $\hat{\phi}$ with respect to a density matrix $\rho(t_0)$, cf. Eqs. (3.1.1), (3.1.2) and (3.2.6a). In fact, the very existence of a homogeneous solution is tied to the details of the density matrix, dictating whether or not such a solution of the field equations is actually allowed. For example, if the density matrix is chosen to describe the vacuum state of Fock space – a pure state, where there are no particles present – then the vacuum expectation value indeed has to be trivial, if the theory does not feature spontaneous symmetry breaking that is [4, 9]. But if the density matrix would describe, say, a single-mode coherent state – think of laser light for that matter – then there has to be a nontrivial expectation value, describing a freely propagating plane wave. In a nutshell, the absence of the homogeneous solutions in Eq. (3.3.5) derives from our ignorance about the details of the operator Δ_0^{-1} and the initial density matrix. That being said, the cause of the above discrepancy can be traced back to Eq. (3.1.15), where we assumed the action to be purely quadratic in the fields. Since we absorbed the correlation functional $K[\phi_+, \phi_-]$ into the action, we thus made the implicit assumption that its Volterra expansion, Eq. (3.1.11), does not contain a linear term. It is straightforward to verify that this term contains the information about the initial field configuration $\phi(t_0, \vec{x})$ and, in the case of Δ_0^{-1} being the Klein-Gordon operator, the first time derivative of the initial field configuration $\dot{\phi}(t_0, \vec{x})$ [13]. By (implicitly) restricting $K[\phi_+, \phi_-]$ to be of such a quadratic form, we set both of these initial values to be identically zero. Since there is no way to generate a finite field expectation value in a noninteracting theory if it was not present initially, it is no surprise that the homogeneous solutions are missing in Eq. (3.3.5). It should be clear by now that the formally correct way to incorporate such nontrivial homogeneous solutions would be to properly take care of the correlation functional and solve the two-point Green function with the appropriate boundary and initial conditions. We may bypass the details of such a discussion simply by assuming the action to be of the form

$$S[\phi] = \frac{1}{2} \int_{xy} (\phi - \phi_c^0)(x) \Delta_0^{-1}(x, y) (\phi - \phi_c^0)(y), \quad (3.3.8)$$

where ϕ_c^0 is a homogeneous solution of the operator Δ_0^{-1} . At first glance this action seems to be identical to Eq. (3.1.15), by virtue of $\int_y \Delta_0^{-1}(x, y) \phi_c^0(y) = 0$, but there is a subtle difference. The action above contains a boundary term, incorporating the details of a finite initial field configuration and its initial time derivative, whereas the action of Eq. (3.1.15) does not. Upon shifting the field $\phi(x) \rightarrow \phi(x) + \phi_c^0(x)$ in the partition function, the connected functional then becomes

$$W[J] = -\frac{1}{2} \int_{x,y} J(x) \Delta_0(x, y) J(y) + \int_x \phi_c^0(x) J(x), \quad (3.3.9)$$

leading to the desired field expectation value

$$\phi(x|J) = \phi_c^0(x) - \int_y \Delta_0(x, y) J(y). \quad (3.3.10)$$

Upon setting the source to zero, we see that the classical field ϕ_c coincides with the homogeneous solution ϕ_c^0 as it should be. Inserting this alternative form of the connected functional into the Legendre transform, Eq. (3.3.1), and expressing everything in terms of ϕ we obtain

$$\Gamma[\phi] = S[\phi] = \frac{1}{2} \int_{xy} (\phi - \phi_c^0)(x) \Delta_0^{-1}(x, y) (\phi - \phi_c^0)(y). \quad (3.3.11)$$

This representation of $\Gamma[\phi]$ is, up to boundary terms, identical to Eq. (3.3.6). As a consequence, the equation of motion (3.3.7) remains unchanged, but now its solution is consistent with the field expectation value (3.3.10) we obtain from the connected functional.

Despite the simplicity of the above result we have to emphasize that it is far from trivial, since, in contrast to the classical action, the effective action contains all the information about statistical and quantum fluctuations of the system. Significant differences between these two functionals only occur if interactions are taken into account. As we have stated in the previous sections, for a general interacting theory the partition function and the connected functional cannot be calculated exactly. As a result, the Volterra expansion of the partition function does not factorize anymore, as was the case in Eq. (3.1.18), causing the Volterra expansion of the connected functional to contain infinitely many terms. Hence, we cannot expect the Volterra expansion of the effective action to terminate at a finite order, although the classical action typically does. In the presence of a finite classical field, irrespective of how it is generated, whether by spontaneous symmetry breaking or nontrivial initial correlations, it is advisable to expand the effective action around it⁸

$$\Gamma[\phi] = \sum_{n=0}^{\infty} \frac{1}{n!} \int_{x_1, \dots, x_n} \frac{\delta^n \Gamma[\phi]}{\delta \phi(x_1) \cdots \delta \phi(x_n)} \Bigg|_{\phi=\phi_c} (\phi - \phi_c)(x_1) \cdots (\phi - \phi_c)(x_n) \quad (3.3.12)$$

$$= \sum_{n=1}^{\infty} \frac{1}{n!} \int_{x_1, \dots, x_n} \Gamma^{(n)}(x_1, \dots, x_n) (\phi - \phi_c)(x_1) \cdots (\phi - \phi_c)(x_n). \quad (3.3.13)$$

The expansion coefficients

$$\Gamma^{(n)}(x_1, \dots, x_n) = \frac{\delta^n \Gamma[\phi]}{\delta \phi(x_1) \cdots \delta \phi(x_n)} \Bigg|_{\phi=\phi_c}, \quad (3.3.14)$$

are the new type of correlation functions, known as one-particle irreducible vertex functions, mentioned earlier. As we will see below, the effective action functional and the vertex functions bring us one step closer to calculate the connected correlation functions.

To find the relation between the two functionals $W[J]$ and $\Gamma[\phi]$ and the corresponding type of correlation functions they generate, we start with the simple relation

$$\frac{\delta \phi(y)}{\delta \phi(x)} = \delta(x - y). \quad (3.3.15)$$

According to Eq. (3.3.2) the field $\phi(y)$ is a functional of the source field J , such that we can make use of the functional chain rule

$$\frac{\delta}{\delta \phi(x)} = \int_z \frac{\delta J(z)}{\delta \phi(x)} \frac{\delta}{\delta J(z)}, \quad (3.3.16)$$

to arrive at

$$\frac{\delta \phi(y)}{\delta \phi(x)} = \int_z \frac{\delta J(z)}{\delta \phi(x)} \frac{\delta \phi(y)}{\delta J(z)} = \delta(x - y). \quad (3.3.17)$$

Now we may substitute the equation of motion (3.3.3) for $J(z)$, as well as the definition of the field expectation value $\phi(y)$ in terms of the first derivative of $W[J]$, which yields

$$- \int_z \frac{\delta^2 \Gamma[\phi]}{\delta \phi(x) \delta \phi(z)} \frac{\delta^2 W[J]}{\delta J(z) \delta J(y)} = \delta(x - y). \quad (3.3.18)$$

⁸In principle one could expand the effective action around $\phi = 0$, even if there is a nontrivial field expectation value, but the theory assumes its simplest form, if $\phi = \phi_c$ is chosen as the expansion point [24–28].

Evaluating this equation at vanishing sources reproduces the familiar Dyson equation that is known from early work on nonperturbative resummation of interaction corrections to the bare propagator [29, 30]

$$\int_z \left(G_0^{-1} - \Sigma \right) (x, z) G_c(z, y) = \delta(x - y). \quad (3.3.19)$$

Here, Σ is the bosonic self-energy, defined by

$$\left. \frac{\delta^2 \Gamma[\phi]}{\delta \phi(x) \delta \phi(y)} \right|_{\phi=\phi_c} = \left(G_0^{-1} - \Sigma \right) (x, y), \quad (3.3.20)$$

which collects all the one-particle irreducible interaction corrections into a single object.⁹

We emphasize that Eq. (3.3.18) is far more useful than what meets the eye, since we do not have to evaluate it at vanishing sources right away. As it stands Eq. (3.3.18) generalizes the Dyson equation to operators and propagators that are functionals of their respective source fields. Thus, it serves as a master equation, which generates the so-called tree expansion of connected correlation functions. This expansion allows us to understand the substructure of the connected correlators and expresses them in terms of connected single-particle propagators and vertex functions. To obtain the desired expansion for the connected three-point correlator we have to apply the functional derivative with respect to J to the generalized Dyson equation (3.3.18)

$$\frac{\delta^3 W[J]}{\delta J(1) \delta J(2) \delta J(3)} = - \frac{\delta}{\delta J(1)} \left(\frac{\delta^2 \Gamma[\phi]}{\delta \phi(1) \delta \phi(2)} \right)^{-1}. \quad (3.3.21)$$

To replace the source derivative on the right-hand side with a field derivative we make use of the functional chain rule once more

$$\frac{\delta}{\delta J(x)} = \int_y \frac{\delta \phi(y)}{\delta J(x)} \frac{\delta}{\delta \phi(y)} = \int_y \frac{\delta^2 W[J]}{\delta J(x) \delta J(y)} \frac{\delta}{\delta \phi(y)}. \quad (3.3.22)$$

Substituting this expression into Eq. (3.3.21) we find

$$\begin{aligned} \frac{\delta^3 W[J]}{\delta J(1) \delta J(2) \delta J(3)} &= - \int' \frac{\delta^2 W[J]}{\delta J(1) \delta J(1')} \frac{\delta}{\delta \phi(1')} \left(\frac{\delta^2 \Gamma[\phi]}{\delta \phi(1) \delta \phi(2)} \right)^{-1} \\ &= \int' \frac{\delta^2 W[J]}{\delta J(1) \delta J(1')} \left(\frac{\delta^2 \Gamma[\phi]}{\delta \phi(2) \delta \phi(2')} \right)^{-1} \frac{\delta^3 \Gamma[\phi]}{\delta \phi(1') \delta \phi(2') \delta \phi(3')} \left(\frac{\delta^2 \Gamma[\phi]}{\delta \phi(3) \delta \phi(3')} \right)^{-1} \\ &= \int' \frac{\delta^2 W[J]}{\delta J(1) \delta J(1')} \frac{\delta^2 W[J]}{\delta J(2) \delta J(2')} \frac{\delta^2 W[J]}{\delta J(3) \delta J(3')} \frac{\delta^3 \Gamma[\phi]}{\delta \phi(1') \delta \phi(2') \delta \phi(3')}, \end{aligned} \quad (3.3.23)$$

where the prime at the integral symbol indicates that all primed space-time arguments have to be integrated over their respective domain. In the second line we used the matrix relation $\delta M^{-1} =$

⁹The formal solution of Eq. (3.3.19) – the connected two-point function of the interacting theory – could be represented as the geometric series

$$G_c(x, y) = G_0(x, y) + \left(G_0 \Sigma G_0 \right) (x, y) + \left(G_0 \Sigma G_0 \Sigma G_0 \right) (x, y) + \left(G_0 \Sigma G_0 \Sigma G_0 \Sigma G_0 \right) (x, y) + \dots,$$

where $G_0(x, y)$ is the bare propagator and the terms in brackets, such as $(G_0 \Sigma G_0)$, should be understood as a distributional matrix product. Coming from perturbation theory, this is the standard way to introduce the concept of the single-particle self-energy [1–4, 9].

$-M^{-1}(\delta M)M^{-1}$,¹⁰ and in the third line we employed the generalized Dyson equation (3.3.18) to express the inverse second derivative of $\Gamma[\phi]$ in terms of the second derivative of $W[J]$. Upon setting the source field to zero we obtain an expression for the connected three-point correlator in terms of connected two-point correlators and the three-vertex function

$$G_c(1, 2, 3) = - \int' G_c(1, 1')G_c(2, 2')G_c(3, 3')\Gamma^{(3)}(1', 2', 3'). \quad (3.3.24)$$

To obtain the tree expansion for higher level connected correlation functions we just need to continue applying the functional derivative with respect to J , using the product rule and, as soon as the derivative acts on a term involving $\Gamma[\phi]$, the functional chain rule (3.3.22). For the fourth derivative of $W[J]$ we find

$$\begin{aligned} \frac{\delta^4 W[J]}{\delta J(1)\delta J(2)\delta J(3)\delta J(4)} &= \int' \left[\frac{\delta^2 W[J]}{\delta J(1)\delta J(6')} \frac{\delta^2 W[J]}{\delta J(2)\delta J(1')} \frac{\delta^2 W[J]}{\delta J(3)\delta J(2')} \frac{\delta^2 W[J]}{\delta J(4)\delta J(5')} \right. \\ &\quad + \frac{\delta^2 W[J]}{\delta J(1)\delta J(6')} \frac{\delta^2 W[J]}{\delta J(2)\delta J(1')} \frac{\delta^2 W[J]}{\delta J(3)\delta J(5')} \frac{\delta^2 W[J]}{\delta J(4)\delta J(2')} \\ &\quad \left. + \frac{\delta^2 W[J]}{\delta J(1)\delta J(1')} \frac{\delta^2 W[J]}{\delta J(2)\delta J(2')} \frac{\delta^2 W[J]}{\delta J(3)\delta J(5')} \frac{\delta^2 W[J]}{\delta J(4)\delta J(6')} \right] \\ &\quad \times \frac{\delta^3 \Gamma[\phi]}{\delta \phi(1')\delta \phi(2')\delta \phi(3')} \frac{\delta^2 W}{\delta J(3')\delta J(4')} \frac{\delta^3 \Gamma[\phi]}{\delta \phi(4')\delta \phi(5')\delta \phi(6')} \\ &\quad + \int' \frac{\delta^2 W}{\delta J(1)\delta J(1')} \frac{\delta^2 W}{\delta J(2)\delta J(2')} \frac{\delta^2 W}{\delta J(3)\delta J(3')} \frac{\delta^2 W}{\delta J(4)\delta J(4')} \\ &\quad \times \frac{\delta^4 \Gamma}{\delta \phi(1')\delta \phi(2')\delta \phi(3')\delta \phi(4')}, \end{aligned} \quad (3.3.25)$$

which, after setting the source field to zero, becomes

$$\begin{aligned} G_c(1, 2, 3, 4) &= \int' \left[G_c(1, 6')G_c(2, 1')G_c(3, 2')G_c(4, 5') + G_c(1, 6')G_c(2, 1')G_c(3, 5')G_c(4, 2') \right. \\ &\quad \left. + G_c(1, 1')G_c(2, 2')G_c(3, 5')G_c(4, 6') \right] \Gamma^{(3)}(1', 2', 3')G_c(3', 4')\Gamma^{(3)}(4', 5', 6') \\ &\quad (3.3.26) \end{aligned}$$

$$- \int' G_c(1, 1')G_c(2, 2')G_c(3, 3')G_c(4, 4')\Gamma^{(4)}(1', 2', 3', 4'). \quad (3.3.27)$$

The notion “tree expansion” derives from the fact that the connected n -point correlator can be expressed in terms of two-point functions and m -point vertex functions, with $m \leq n$, such that no loop structures occur. That means, if we start from any vertex, there is no closed “path” which would lead back to the same vertex upon traversing the tree through the two-point correlators and other vertices. In other words, removing any internal correlator – one where both of its space-time arguments are integrated – and its associated integrations would result in a factorized expression. On a purely analytical level this feature is difficult to appreciate, but a diagrammatic representation, where the two-point functions are the branches and the n -point vertices are the branching points to which the two-point correlators are attached to, may help

¹⁰To prove this relation we just need to apply a derivative to the equation $M^{-1}M = 1$. We immediately find

$$(\delta M^{-1})M + M^{-1}(\delta M) = 0 \iff \delta M^{-1} = -M^{-1}(\delta M)M^{-1},$$

where the matrix products are understood in the distributional sense.

us out once more. Representing the n -point vertices as grey-shaded n -sided polygons, the above equations (3.3.24) and (3.3.27) become¹¹

$$G_c(1,2,3) = - \text{Diagram} \quad (3.3.28)$$

$$G_c(1,2,3,4) = + \text{Diagram 1} + \text{Diagram 2} + \text{Diagram 3} - \text{Diagram 4} \quad (3.3.29)$$

In this form it should be obvious why the expansion of a connected n -point correlator in terms of two-point correlators and vertices is called tree expansion. In Fig. 3.2 we show two examples of diagrams that contain an internal loop to illustrate their topological difference. Such structures will only appear in the actual calculation of the vertex functions, which will be discussed in the next chapter. The operation of removing an internal Green function can be understood as “cutting” through an internal line, which obviously leads to disconnected diagrams corresponding to a factorized analytical expression.

Now that we have resolved the internal structure of the connected correlators it is the perfect time to summarize what we have achieved in this chapter. We started out by defining the n -point correlation functions as the primary objects of a quantum field theory and found an efficient way to generate them by introducing the partition function. It turned out that those correlation functions consist of more fundamental structures, the connected correlation functions, which can be generated by the connected functional, reducing the calculational effort to a large extent. By introducing the effective action – a functional that generalizes the classical action known from classical mechanics and classical field theory to the quantum regime – we could show that the connected correlators have an internal structure, being expressible as trees consisting of connected two-point correlators and vertex functions. This observation condenses the calculational effort even further, down to the truly fundamental quantities that need to be calculated, in order to obtain those correlation functions we actually want to calculate.

¹¹We note that the diagrammatic representation of the Coulomb interaction in Sec. 2.2.3 is related to the bare four-point vertex of the theory. Also recall that there an external line represents an in- or outgoing fermionic operator, while here and in the remainder of this thesis a line always represents a Green function.

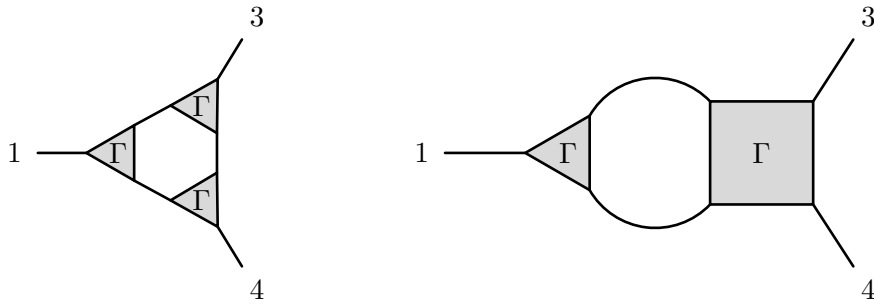


Figure 3.2: Two examples for diagrams that contain an internal loop. Such structures arise in the nonperturbative calculation of the vertex functions, see for instance Refs. [2, 31], but they cannot appear in the tree expansion of any connected correlator.

We emphasize that up to now no approximations have been made, all the relations between the various correlation functions are exact. However, we have not yet succeeded in deriving the connected correlation functions of the theory, since the final step of the calculation is missing – a consistent framework which provides the vertices. Formally exact, nonperturbative frameworks to calculate those vertex functions in general lead to a hierarchical structure, where an equation for the n -point vertex requires knowledge of the vertex itself, an $(n + 1)$ -point vertex or even higher level vertices. It is precisely at this point where approximations enter the theory. To practically solve such a system of equations it is inevitable to truncate it at a certain level, resulting in a finite set of self-consistency equations for the vertices that are kept. Nevertheless, even such a truncated set of equations for the vertex functions is genuinely nonperturbative, containing contributions to all orders in perturbation theory, but also instantons/solitons and other related structures that are inaccessible through perturbation theory. If one wishes to, the truncated hierarchy may be simplified to the point where it leads back to standard perturbation theory, but in light of the asymptotic divergence of such weak-coupling power series, the value of the latter simplification is at least questionable. In any case, the particular level of the truncation, and whether or not subsequent approximations can be justified, depend on the problem at hand. A great extent of this thesis is devoted to the development of such a formalism, diving even deeper into the intricacies of quantum field theory, but the considerations of this chapter should be enough motivation for such an attempt, since it brings us as close as we can get to actually solving the many-body Schrödinger equation.

3.A Appendix: Diagrammatic derivation of the tree expansion

Before we close this chapter we want to illustrate how the tree structure of the connected correlators arises on a purely diagrammatic level. Such an alternative approach will help the reader to get an intuition for the rather abstract concepts of quantum field theory and allows for an easier understanding of the derivations of the mathematical formulas to come.

To translate the latest results into a diagrammatic language, recall that the (negative) second functional derivative of $W[J]$ evaluated at vanishing sources defines the connected two-point correlator. Previously we represented this object as a simple solid line. We can generalize its diagrammatic representation for the case of a functional, containing non-vanishing source fields, simply by defining

$$G_c(x, y|J) \equiv -\frac{\delta^2 W[J]}{\delta J(x)\delta J(y)} = -\sum_{n=0}^{\infty} \frac{1}{n!} \int_{1, \dots, n} \frac{\delta^{n+2} W[J]}{\delta J(x)\delta J(y)\delta J(1) \cdots \delta J(n)} \Big|_{J=0} J(1) \cdots J(n)$$

$$= x \text{ --- } \textcircled{\text{shaded}} \text{ --- } y, \tag{3.A.1}$$

where the shaded blob indicates that the sources have not yet been set to zero. For vanishing source fields the shading would just vanish and we end up with the ordinary connected two point function as introduced before, see Eq. (3.2.7) and the footnote on that page. Figuratively speaking, performing a functional derivative with respect to J means to “pull” at the blob until a new branch with a new blob appears. In the process the original blob is split into two and a vertex, which holds everything together

$$\frac{\delta}{\delta J(3)} \text{ --- } \textcircled{\text{shaded}} \text{ --- } 2 = \text{ --- } \textcircled{\text{shaded}} \text{ --- } \text{shaded triangle} \begin{cases} \text{--- } \textcircled{\text{shaded}} \text{ --- } 2 \\ \text{--- } \textcircled{\text{shaded}} \text{ --- } 3 \end{cases} . \tag{3.A.2}$$

Here, the vertex is shaded as well, indicating that it is also a functional, which still depends on its sources. Applying the source derivative once more, there are now four possibilities at which one could pull out a new branch. Pulling at each one of the three blobs iterates the above structure, while pulling at the vertex itself produces a new vertex, being one order larger, with another branch attached to it

$$\frac{\delta}{\delta J(4)} \text{shaded triangle} \begin{cases} \text{--- } 2 \\ \text{--- } 3 \end{cases} = - \text{shaded square} \begin{cases} \text{--- } 2 \\ \text{--- } 3 \end{cases} \text{ --- } \textcircled{\text{shaded}} \text{ --- } 4 . \tag{3.A.3}$$

The latter rule remains valid for higher order vertices, taking care that the diagrammatic representation for the n -point and $(n + 1)$ -point vertices is substituted appropriately. To be clear,

3.A. Appendix: Diagrammatic derivation of the tree expansion

pulling at a four-vertex yields a five-vertex, pulling at a five-vertex yields a six-vertex and so on. Hence, the connected four-point function prior to setting J to zero reads

$$\begin{aligned}
 \frac{\delta}{\delta J(4)} & \begin{array}{c} 2 \\ \diagdown \\ \text{---} \text{---} \text{---} \\ \diagup \\ 1 \end{array} \begin{array}{c} \text{---} \text{---} \text{---} \\ \diagdown \\ \text{---} \text{---} \text{---} \\ \diagup \\ 3 \end{array} = + \begin{array}{c} 2 \\ \diagdown \\ \text{---} \text{---} \text{---} \\ \diagup \\ 1 \end{array} \begin{array}{c} \text{---} \text{---} \text{---} \\ \diagdown \\ \text{---} \text{---} \text{---} \\ \diagup \\ 3 \end{array} + \begin{array}{c} 2 \\ \diagdown \\ \text{---} \text{---} \text{---} \\ \diagup \\ 1 \end{array} \begin{array}{c} \text{---} \text{---} \text{---} \\ \diagdown \\ \text{---} \text{---} \text{---} \\ \diagup \\ 3 \end{array} \\
 & + \begin{array}{c} 2 \\ \diagdown \\ \text{---} \text{---} \text{---} \\ \diagup \\ 1 \end{array} \begin{array}{c} \text{---} \text{---} \text{---} \\ \diagdown \\ \text{---} \text{---} \text{---} \\ \diagup \\ 4 \end{array} - \begin{array}{c} 2 \\ \diagdown \\ \text{---} \text{---} \text{---} \\ \diagup \\ 1 \end{array} \begin{array}{c} \text{---} \text{---} \text{---} \\ \diagdown \\ \text{---} \text{---} \text{---} \\ \diagup \\ 4 \end{array} .
 \end{aligned}
 \tag{3.A.4}$$

We could continue to apply derivatives as much as needed to obtain the tree expansion for any connected correlator we are interested in. Based on the above diagrammatic rules it should be evident that no loop structures can occur, irrespective of the order of the connected correlator. Setting the source field in Eqs. (3.A.2) and (3.A.4) to zero, then yields the diagrammatic representation of the three- and four-point correlators (3.3.28) and (3.3.29).

Bibliography

- [1] Negele, J. W. and Orland, H., *Quantum Many-Particle Systems*. Westview Press, 1998.
- [2] Kopietz, P. and Bartosch, L. and Schütz, F., *Introduction to the Functional Renormalization Group*. Springer, 2010.
- [3] Altland, A. and Simons, B., *Condensed Matter Field Theory*. Cambridge University Press, 2010.
- [4] Peskin, M. E. and Schroeder, D. V., *An Introduction to Quantum Field Theory*. Westview Press, 1995.
- [5] C. Bauer, A. Rückriegel, A. Sharma, and P. Kopietz, “Nonperturbative renormalization group calculation of quasiparticle velocity and dielectric function of graphene,” *Phys. Rev. B*, vol. 92, p. 121409, Sept. 2015.
- [6] A. Sharma and P. Kopietz, “Multilogarithmic velocity renormalization in graphene,” *Phys. Rev. B*, vol. 93, p. 235425, June 2016.
- [7] A. Kamenev, *Field Theory of Non-Equilibrium Systems*. Cambridge University Press, 2011.
- [8] J. Rammer, *Quantum Field Theory of Non-equilibrium States*. Cambridge University Press, 2007.
- [9] Greiner, W. and Reinhardt, J., *Field Quantization*. Springer, 1996.
- [10] P. Danielewicz, “Quantum theory of nonequilibrium processes, I,” *Annals of Physics*, vol. 152, no. 2, pp. 239 – 304, 1984.
- [11] K.-c. Chou, Z.-b. Su, B.-l. Hao, and L. Yu, “Equilibrium and Nonequilibrium Formalisms Made Unified,” *Phys. Rept.*, vol. 118, p. 1, 1985.
- [12] N. P. Landsman and C. G. van Weert, “Real- and imaginary-time field theory at finite temperature and density,” *Physics Reports*, vol. 145, pp. 141–249, Jan. 1987.
- [13] J. Berges, “Introduction to Nonequilibrium Quantum Field Theory,” *AIP Conference Proceedings*, vol. 739, no. 1, pp. 3–62, 2004.
- [14] M. Wagner, “Expansions of nonequilibrium Green’s functions,” *Phys. Rev. B*, vol. 44, pp. 6104–6117, Sep 1991.
- [15] R. van Leeuwen, N. E. Dahlen, G. Stefanucci, C.-O. Almbladh, and U. von Barth, “Introduction to the Keldysh formalism and applications to time-dependent density-functional theory,” *eprint arXiv:cond-mat/0506130*, June 2005.

- [16] Balzer, K. and Bonitz, M., *Nonequilibrium Green's Function Approach to Inhomogeneous Systems*. Springer, 2013.
- [17] J. Schwinger, "Brownian Motion of a Quantum Oscillator," *Journal of Mathematical Physics*, vol. 2, no. 3, pp. 407–432, 1961.
- [18] L. V. Keldysh, "Diagram technique for nonequilibrium processes," *Zh. Eksp. Teor. Fiz.*, vol. 47, pp. 1515–1527, 1964. [Sov. Phys. JETP20,1018(1965)].
- [19] Billingsley, P., *Probability and Measure*. John Wiley & Sons, Inc., 2012.
- [20] J. Berges and J. Cox, "Thermalization of quantum fields from time-reversal invariant evolution equations," *Physics Letters B*, vol. 517, pp. 369–374, Oct. 2001.
- [21] R. E. Pugh, "Feynman path integral and the interaction picture," *Phys. Rev. D*, vol. 33, pp. 1027–1032, Feb 1986.
- [22] E. Calzetta and B. L. Hu, "Nonequilibrium quantum fields: Closed-time-path effective action, Wigner function, and Boltzmann equation," *Phys. Rev. D*, vol. 37, pp. 2878–2900, May 1988.
- [23] Kleinert, H., *Path Integrals in Quantum Mechanics, Statistics, Polymer Physics, and Financial Markets*. World Scientific, 2009.
- [24] C. Wetterich, "Average action and the renormalization group equations," *Nuclear Physics B*, vol. 352, no. 3, pp. 529 – 584, 1991.
- [25] T. R. Morris, "On truncations of the exact renormalization group," *Physics Letters B*, vol. 334, no. 3, pp. 355 – 362, 1994.
- [26] J. Berges, N. Tetradis, and C. Wetterich, "Non-perturbative renormalization flow in quantum field theory and statistical physics," *Physics Reports*, vol. 363, pp. 223–386, June 2002.
- [27] K.-I. Aoki, K. Morikawa, W. Souma, J.-I. Sumi, and H. Terao, "The Effectiveness of the Local Potential Approximation in the Wegner-Houghton Renormalization Group," *Progress of Theoretical Physics*, vol. 95, no. 2, pp. 409–420, 1996.
- [28] K.-I. Aoki, K. Morikawa, W. Souma, J.-I. Sumi, and H. Terao, "Rapidly Converging Truncation Scheme of the Exact Renormalization Group," *Progress of Theoretical Physics*, vol. 99, no. 3, pp. 451–466, 1998.
- [29] F. J. Dyson, "The S Matrix in Quantum Electrodynamics," *Phys. Rev.*, vol. 75, pp. 1736–1755, Jun 1949.
- [30] J. Schwinger, "On the Green's functions of quantized fields. I," *Proceedings of the National Academy of Sciences*, vol. 37, no. 7, pp. 452–455, 1951.
- [31] W. Metzner, M. Salmhofer, C. Honerkamp, V. Meden, and K. Schönhammer, "Functional renormalization group approach to correlated fermion systems," *Rev. Mod. Phys.*, vol. 84, pp. 299–352, Mar 2012.

Chapter 4

Coulomb interactions in graphene

This chapter collects the three papers, which revolve around Coulomb interactions in graphene. In the first paper we develop a nonperturbative framework to calculate the vertex functions in and out of thermal equilibrium, which combines the functional renormalization group method with the Keldysh formalism. To test the formalism we calculate the renormalized finite-temperature Fermi velocity and static dielectric function at charge neutrality. The second paper builds upon those ideas and represents a variation of the Keldysh fRG, where the chemical potential is interpreted as a flow parameter to calculate the density dependence of the vertex functions, generalizing the results of the Fermi velocity and dielectric function found in the first paper. In the third paper we extend the interacting field theory by incorporating a set of abelian Chern-Simons gauge fields to gain access to the fractional quantum Hall regime. After performing a stationary phase approximation with Gaussian fluctuations for the gauge fields we calculate the electromagnetic response tensor from which we extract the possible filling fractions of the multicomponent fractional quantum Hall system.

Included papers

Pages 85-108	“Keldysh functional renormalization group for electronic properties of graphene”
Pages 109-119	“Chemical-potential flow equations for graphene with Coulomb interactions”
Pages 121-142	“Abelian Chern-Simons theory for the fractional quantum Hall effect in graphene”



4.1. Paper: “*Keldysh functional renormalization group for electronic properties of graphene*”

4.1 Paper: “*Keldysh functional renormalization group for electronic properties of graphene*”

4.1. Paper: *“Keldysh functional renormalization group for electronic properties of graphene”*

Keldysh functional renormalization group for electronic properties of graphene

Christian Fräßdorf

Dahlem Center for Complex Quantum Systems and, Institut für Theoretische Physik, Freie Universität Berlin, Arnimallee 14, 14195 Berlin, Germany

Johannes E. M. Mosig

Department of Mathematics and Statistics, University of Otago, PO Box 56, Dunedin 9054, New Zealand

(Received 19 September 2016; revised manuscript received 14 December 2016; published 9 March 2017)

We construct a nonperturbative nonequilibrium theory for graphene electrons interacting via the instantaneous Coulomb interaction by combining the functional renormalization group method with the nonequilibrium Keldysh formalism. The Coulomb interaction is partially bosonized in the forward scattering channel resulting in a coupled Fermi-Bose theory. Quantum kinetic equations for the Dirac fermions and the Hubbard-Stratonovich boson are derived in Keldysh basis, together with the exact flow equation for the effective action and the hierarchy of one-particle irreducible vertex functions, taking into account a possible nonzero expectation value of the bosonic field. Eventually, the system of equations is solved approximately under thermal equilibrium conditions at finite temperature, providing results for the renormalized Fermi velocity and the static dielectric function, which extends the zero-temperature results of Bauer *et al.*, *Phys. Rev. B* **92**, 121409 (2015).

DOI: [10.1103/PhysRevB.95.125412](https://doi.org/10.1103/PhysRevB.95.125412)**I. INTRODUCTION**

The band structure of graphene features two isolated points where valence and conduction bands touch [1–3]. At these touching points the electrons have a linear energy-momentum dispersion, similar to massless relativistic Dirac particles [4]. This pseudorelativistic band structure is responsible for the appearance of phenomena usually related to the relativistic domain, such as Klein tunneling through potential barriers [5–8], the Zitterbewegung [9], or an anomalous quantized Hall effect [10–13].

For a description of realistic graphene samples, effects of disorder and electron-electron interactions have to be added to this idealized band structure. Disorder smears out the singularity at the nodal point, but preserves many of graphene’s remarkable electronic properties [1,2], and even leads to fundamentally new phenomena by itself, such as the absence of Anderson localization if disorder does not couple the nodal points [14–16]. The effect of interactions is most pronounced if the singularity in the density of states of the noninteracting theory is not smeared by disorder and the chemical potential is close to the nodal point [17]. The vanishing carrier density at the nodal point at zero temperature [18] implies the absence of screening, which leads to strongly enhanced interaction corrections. In particular, interactions are found to effectively renormalize the Fermi velocity at the nodal point, and the corrections to the velocity diverge logarithmically in the low-temperature limit [19,20]. These logarithmic corrections have recently been verified experimentally, and good agreement with theoretical calculations was reported [21].

Although there is consensus about the way in which interactions affect the electronic structure of graphene [17], a quantitative evaluation of the corrections proved to be problematic. The dimensionless interaction strength for the electrons in graphene is $\alpha = e^2/\epsilon_0\hbar v_F$, which approximately equals 2.2 in the freestanding case in vacuum ($\epsilon_0 = 1$). For such a large interaction strength a perturbative calculation of the renormalization effect cannot be reliable, and at first

sight, the reported agreement of one-loop perturbation theory with the experimentally observed increase of the Fermi velocity appears surprising. Indeed, a two-loop calculation leads to a completely different result, a decrease of the Fermi velocity for small momenta [22–24]. An alternative approach is to make use of the largeness of the number of fermion species (which is $N_f = 4$ in graphene), and a perturbation theory in $1/N_f$ gives results largely consistent with the approach based on a perturbative treatment of the interaction strength [25,26].

To address such a situation in which no small parameter, to organize a perturbative expansion, is available, nonperturbative methods have been applied to the problem of interacting Dirac fermions in two dimensions. One of those nonperturbative methods is given by the set of exact Schwinger-Dyson equations, which, in a sensible truncation, may resum whole classes of diagrams, thus giving access to the strong coupling regime mentioned above. In fact, the authors of Ref. [27] studied the Fermi velocity renormalization, considering the possibility of a dynamically generated gap, by solving the fermionic Schwinger-Dyson equation, where the electron propagator is calculated self-consistently with a (dynamically) screened Coulomb interaction in the random phase approximation (RPA). Although this approach is a major improvement to a simple perturbative calculation, a fully self-consistent treatment, going well beyond the RPA, has to be employed in order to obtain quantitatively reliable results. This extension is necessary, since a strong renormalization of the Fermi velocity also implies a strong renormalization of the polarization function, which, in turn, leads to a non-negligible “backreaction” in the fermion propagator that is not accounted for in the RPA. For related studies using the exact Schwinger-Dyson equations see also Refs. [28,29].

An alternative nonperturbative approach is the functional renormalization group (fRG), which shares some features with the celebrated Wilsonian renormalization group [30,31], but rigorously extends the concept of flowing coupling constants to (one-particle irreducible vertex) functions. Initiated by Wetterich [32,33], this method has found widespread applications

in high energy and in condensed matter physics [34–39]. Of particular relevance to the present problem is the work of Bauer *et al.* [40], who studied the Fermi velocity renormalization and the static dielectric function in graphene at zero temperature using the fRG framework and found excellent agreement with the experiment, surpassing the results of the conventional perturbative methods.

As powerful as the fRG is, it clearly has its limitations when used within its most commonly employed formulation in imaginary time. First and foremost, true nonequilibrium phenomena (beyond linear response) are out of reach of the Matsubara formalism. Second, even for linear response calculations the imaginary time formalism requires an analytical continuation from imaginary to real time at the end of a calculation, which may pose technical difficulties. The appropriate framework to describe true nonequilibrium dynamics is the Keldysh formalism [41–43], which has the additional advantage that it erases the necessity of analytical continuations, making it also a useful tool for equilibrium applications [44–47]. Gezzi *et al.* implemented a Keldysh formulation of fRG for applications to impurity problems [48]. Jakobs *et al.* further developed the theory, constructing a “Keldysh-compatible” cutoff scheme that respects causality, with applications to quantum dots and nanowires coupled to external baths [49,50]. Keldysh formulations of fRG were also developed for various systems involving bosons [51–55].

In the present paper, we construct a Keldysh fRG theory for interacting Dirac fermions, as they occur at the nodal points in the graphene band structure. As a test of the formalism, we recalculate the Fermi velocity renormalization and the static dielectric function in graphene, finding full agreement with the zero-temperature Matsubara-formalism calculation of Bauer *et al.* [40]. We also extend the calculation to finite temperatures, an extension that in principle is possible within the Matsubara formalism, too, but that comes at no additional calculational cost when done in the Keldysh formalism. We leave applications to true nonequilibrium properties of graphene for future work, but already notice that there is a vast body of perturbative (or in other ways approximate) true nonequilibrium theoretical results for graphene that such a theory can be compared with, see, e.g., Refs. [56–59]. Although our theory focuses on graphene, a major part of the formalism we develop here is also applicable to conventional nonrelativistic fermions.

The extension of an imaginary-time fRG formulation to a Keldysh-based formulation involves quite a number of subtle steps and manipulations. One issue is the choice of a cutoff scheme, which preferentially is compatible with the causality structure of the Keldysh formalism and, for equilibrium applications, with the fluctuation-dissipation theorem [49,50]. Another issue is the possibility of an arbitrary nonequilibrium initial condition and the truncation of the (in principle) infinite hierarchy of flow equations in the fRG approach. To do justice to these issues, we have chosen to make this article self-contained, although we tried to keep the discussion of standard issues as brief as possible.

The outline of the paper is as follows. In Sec. II, we introduce the formal aspects of nonequilibrium quantum field theory, using the Keldysh technique applied to graphene. The originally purely fermionic problem is formulated as a coupled

fermion-boson problem by means of a Hubbard-Stratonovich transformation, singling out the dominant interaction channel. The ideas of the functional renormalization group are reviewed in Sec. III, where we combine them with the nonequilibrium Keldysh formalism. We implement an infrared regularization and derive the exact spectral Dyson equations and quantum kinetic equations, as well as an exact flow equation, which incorporates all of the nonperturbative aspects of the theory. Finally, we perform a vertex expansion leading to an exact, infinite hierarchy of coupled integro-differential equations for the one-particle irreducible vertex functions. Section IV deals with a solution of our theory in thermal equilibrium. We discuss the necessary limitations for the construction of suitable regulator functions, which preserve causality and, at the same time, the fluctuation-dissipation theorem, allowing a solution of the quantum kinetic equations at all scales. We further present a simple truncation scheme for the calculation of the Fermi velocity and static dielectric function at finite temperature, extending the results of Bauer *et al.* [40].

II. NONEQUILIBRIUM QUANTUM FIELD THEORY

This section mainly serves as an introduction to the Fermi-Bose quantum field theory of interacting electrons in graphene in the nonequilibrium Keldysh formulation. The reader who is familiar with this formulation may skim through our notational conventions and continue reading in Sec. III.

We consider interacting Dirac fermions in two dimensions, which are described by a grand canonical Hamiltonian in the Heisenberg picture:

$$H(t) = H_f(t) + H_{\text{int}}(t). \quad (1)$$

Here, H_f describes the low-energy approximation of free electrons hopping on the honeycomb lattice, and H_{int} contains the interaction effects. The first term reads [57] (setting $\hbar = c = 1$)

$$H_f(t) = \int_{\vec{r}} \Psi^\dagger(\vec{r}, t) (-\mu + e\varphi(\vec{r}, t)) \Psi(\vec{r}, t) - i v_F \int_{\vec{r}} \Psi^\dagger(\vec{r}, t) \sigma_0^s \otimes \vec{\Sigma} \cdot (\vec{\nabla} + i e \vec{A}(\vec{r}, t)) \Psi(\vec{r}, t), \quad (2)$$

with the chemical potential μ and the external electromagnetic potentials φ and \vec{A} . The Dirac electrons are described by eight-dimensional spinors, where we choose the basis as $\Psi \equiv (\Psi_\uparrow \quad \Psi_\downarrow)^\top$, with

$$\Psi_\sigma \equiv (\psi_{AK_+} \quad \psi_{BK_+} \quad \psi_{BK_-} \quad \psi_{AK_-})_\sigma^\top. \quad (3)$$

The indices $\sigma = \uparrow, \downarrow$ denote the spin, K_\pm the valley and A/B the sublattice degree of freedom. Further, σ_0^s is the two-dimensional unit matrix acting in spin space and $\Sigma_{x,y} = \tau_3 \otimes \sigma_{x,y}$, with the Pauli matrices τ_3 and $\sigma_{x,y}$ acting in valley and sublattice space, respectively. The interaction part is given by the instantaneous Coulomb interaction

$$H_{\text{int}}(t) = \frac{1}{2} \int_{\vec{r}, \vec{r}'} \delta n(\vec{r}, t) V(\vec{r} - \vec{r}') \delta n(\vec{r}', t), \quad (4)$$

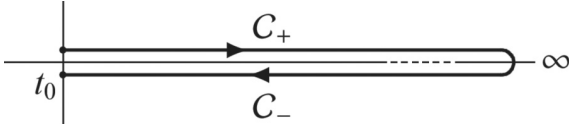


FIG. 1. Schwinger-Keldysh time contour in the complex time plane with reference time t_0 as starting and end point. C_+ and C_- are the forward and backward branches, respectively.

where

$$V(\vec{r} - \vec{r}') = \frac{e^2}{\epsilon_0 |\vec{r} - \vec{r}'|}, \quad (5)$$

$$\delta n(\vec{r}, t) = \Psi^\dagger(\vec{r}, t) \Psi(\vec{r}, t) - \bar{n}(\vec{r}, t), \quad (6)$$

and ϵ_0 is the dielectric constant of the medium, being unity for freestanding graphene in vacuum. Although the interparticle Coulomb potential $V(\vec{r} - \vec{r}')$ is actually logarithmic in exactly two dimensions, here it remains in its three-dimensional form, due to the quasi two-dimensional nature of the physical system. That means only the fermions are constrained to propagate in two spatial dimensions, whereas their interaction extends into the third dimension in which the graphene layer is embedded. The term $\bar{n}(\vec{r}, t)$ in Eq. (6) is a background charge density, representing the charge accumulated on a nearby metal gate. Away from the charge neutrality point it essentially acts as a counterterm, which removes the zero wave-number singularity of the Coulomb interaction at finite charge carrier density.

A. Single-particle Green functions

Relevant physical observables can be expressed as correlation functions of the field operators, and the purpose of a field-theoretic treatment is to provide a formalism in which such correlation functions can be calculated efficiently. For an explicitly time-dependent Hamiltonian, such as the one above, one considers the evolution of the field operators along the ‘‘Schwinger-Keldysh contour’’ [41–43], a closed time contour starting at a reference time t_0 , extending to $+\infty$, and eventually returning from $+\infty$ to t_0 , see Fig. 1. Consequently, the time arguments t of the field operators are elevated to the ‘‘contour time,’’ and the building blocks of the theory are formed by the expectation values of ‘‘path ordered’’ products of the field operators. The concept of path ordering generalizes the concept of (imaginary) time ordering, such that field operators with a higher contour time appear to the right of operators with a lower contour time. In particular, the single-particle propagator reads

$$G_{ij}^{\mathcal{T}_C}(\vec{r}, t; \vec{r}', t') = -i \langle \mathcal{T}_C \psi_i(\vec{r}, t) \psi_j^\dagger(\vec{r}', t') \rangle, \quad (7)$$

where the indices i, j represent collectively the sublattice, valley and spin degrees of freedom. Below, we also display the matrix structure implied by these two indices with a hat symbol. \mathcal{T}_C is the contour-time ordering operator and the expectation value is performed with respect to some initial density matrix specified at a reference time t_0 ,

$$\langle \dots \rangle = \text{Tr}[\rho(t_0) \dots]. \quad (8)$$

Since there are four possibilities where the two time variables can be located to each other with respect to the two time branches C_+ and C_- , one can map the contour-ordered Green

function to a 2×2 matrix representation with time-arguments defined on the real axis:

$$\begin{aligned} \mathbf{G}_{ij}(\vec{r}, t; \vec{r}', t') &= \begin{pmatrix} G_{ij}^{++}(\vec{r}, t; \vec{r}', t') & G_{ij}^{+-}(\vec{r}, t; \vec{r}', t') \\ G_{ij}^{-+}(\vec{r}, t; \vec{r}', t') & G_{ij}^{--}(\vec{r}, t; \vec{r}', t') \end{pmatrix} \\ &= \begin{pmatrix} G_{ij}^{\mathcal{T}}(\vec{r}, t; \vec{r}', t') & G_{ij}^<(\vec{r}, t; \vec{r}', t') \\ G_{ij}^>(\vec{r}, t; \vec{r}', t') & G_{ij}^{\bar{\mathcal{T}}}(\vec{r}, t; \vec{r}', t') \end{pmatrix}. \end{aligned} \quad (9)$$

The constituents of this matrix are the time ordered, antitime ordered, greater and lesser Green function, respectively,

$$G_{ij}^{\mathcal{T}}(\vec{r}, t; \vec{r}', t') = -i \langle \mathcal{T} \psi_i(\vec{r}, t) \psi_j^\dagger(\vec{r}', t') \rangle, \quad (10a)$$

$$G_{ij}^{\bar{\mathcal{T}}}(\vec{r}, t; \vec{r}', t') = -i \langle \bar{\mathcal{T}} \psi_i(\vec{r}, t) \psi_j^\dagger(\vec{r}', t') \rangle, \quad (10b)$$

$$G_{ij}^>(\vec{r}, t; \vec{r}', t') = -i \langle \psi_i(\vec{r}, t) \psi_j^\dagger(\vec{r}', t') \rangle, \quad (10c)$$

$$G_{ij}^<(\vec{r}, t; \vec{r}', t') = +i \langle \psi_j^\dagger(\vec{r}', t') \psi_i(\vec{r}, t) \rangle. \quad (10d)$$

By definition, these functions are linearly dependent and subject to the following constraint [41–43]:

$$\hat{G}^{\mathcal{T}} - \hat{G}^< - \hat{G}^> + \hat{G}^{\bar{\mathcal{T}}} = 0, \quad (11)$$

which allows a basis transformation to three linearly independent propagators. This transformation is given by the involutorial matrix $\tau_1 L$, where τ_1 is a Pauli matrix and L is the orthogonal matrix

$$L = \frac{1}{\sqrt{2}} \begin{pmatrix} 1 & -1 \\ 1 & 1 \end{pmatrix}, \quad (12)$$

originally introduced by Keldysh [60]. Its application to Eq. (9) yields

$$\tau_1 L \hat{\mathbf{G}} (\tau_1 L)^{-1} = \begin{pmatrix} \hat{G}^K & \hat{G}^R \\ \hat{G}^A & 0 \end{pmatrix}, \quad (13)$$

with

$$\hat{G}^R = \frac{1}{2} (\hat{G}^{\mathcal{T}} - \hat{G}^< + \hat{G}^> - \hat{G}^{\bar{\mathcal{T}}}), \quad (14a)$$

$$\hat{G}^A = \frac{1}{2} (\hat{G}^{\mathcal{T}} + \hat{G}^< - \hat{G}^> - \hat{G}^{\bar{\mathcal{T}}}), \quad (14b)$$

$$\hat{G}^K = \frac{1}{2} (\hat{G}^{\mathcal{T}} + \hat{G}^< + \hat{G}^> + \hat{G}^{\bar{\mathcal{T}}}). \quad (14c)$$

The functions $\hat{G}^{R/A/K}$ are the retarded, advanced, and Keldysh propagators, respectively. The latter one is also known as the statistical propagator. They obey the symmetry relations

$$(\hat{G}^R)^\dagger = \hat{G}^A, \quad (\hat{G}^K)^\dagger = -\hat{G}^K, \quad (15)$$

as well as the causality relations [41–43]

$$\hat{G}^R(\vec{r}, t; \vec{r}', t') = 0, \quad \text{if } t < t', \quad (16a)$$

$$\hat{G}^A(\vec{r}, t; \vec{r}', t') = 0, \quad \text{if } t > t'. \quad (16b)$$

Explicit expressions for the free propagators may easily be obtained in thermal equilibrium and in the absence of the electromagnetic potentials. To this end, we send the reference time $t_0 \rightarrow -\infty$ and Fourier transform the field operators following the conventions

$$\psi_i(\vec{r}, t) = \int_{\vec{k}, \epsilon} e^{+i\vec{k}\cdot\vec{r} - i\epsilon t} \psi_i(\vec{k}, \epsilon), \quad (17)$$

with $\int_{\vec{k}, \varepsilon} \equiv \int \frac{d^2k}{(2\pi)^2} \frac{d\varepsilon}{2\pi}$. After a short calculation, one finds

$$\hat{G}_0^{R/A}(\vec{k}, \varepsilon) = \frac{1}{\sigma_0^s \otimes (\Sigma_0(\varepsilon + \mu \pm i0) - v_F \vec{\Sigma} \cdot \vec{k})}, \quad (18a)$$

$$\hat{G}_0^K(\vec{k}, \varepsilon) = \tanh\left(\frac{\varepsilon}{2T}\right) (\hat{G}_0^R(\vec{k}, \varepsilon) - \hat{G}_0^A(\vec{k}, \varepsilon)), \quad (18b)$$

where $\Sigma_0 = \tau_0 \otimes \sigma_0$ is the 4×4 unit matrix in valley-sublattice space and T is the temperature ($k_B = 1$). Note that the entire statistical information of the system is contained in the Keldysh propagator. These expressions may be further simplified by expanding the propagators in the chiral basis,

$$\hat{G}_0^{R/A}(\vec{k}, \varepsilon) = \sum_{\pm} \hat{\mathcal{P}}_{\pm}(\hat{k}) G_{\pm,0}^{R/A}(k, \varepsilon), \quad (19)$$

in which $\hat{\mathcal{P}}_{\pm}(\hat{k})$ are the chiral projection operators

$$\hat{\mathcal{P}}_{\pm}(\hat{k}) = \sigma_0^s \otimes \left(\frac{\Sigma_0 \pm \vec{\Sigma} \cdot \hat{k}}{2} \right), \quad (20)$$

with $\hat{k} = \vec{k}/k$. In the chiral basis, the propagators then take the simple form

$$G_{\pm,0}^R(k, \varepsilon) = \frac{1}{(\varepsilon + \mu + i0) \mp v_F k}, \quad (21a)$$

$$G_{\pm,0}^A(k, \varepsilon) = \frac{1}{(\varepsilon + \mu - i0) \mp v_F k}, \quad (21b)$$

$$G_{\pm,0}^K(k, \varepsilon) = -2\pi i \tanh\left(\frac{\varepsilon}{2T}\right) \delta(\varepsilon + \mu \mp v_F k). \quad (21c)$$

The density of electrons in the system is given by

$$\begin{aligned} n(\vec{r}, t) &= -i \operatorname{tr} \hat{G}^<(\vec{r}, t, \vec{r}, t) \\ &= -\frac{i}{2} \operatorname{tr} (\hat{G}^K - (\hat{G}^R - \hat{G}^A))(\vec{r}, t, \vec{r}, t), \end{aligned} \quad (22)$$

which is formally divergent. The charge carrier density, however, which is defined as [57]

$$\bar{n}(\vec{r}, t) = -\frac{i}{2} \operatorname{tr} \hat{G}^K(\vec{r}, t, \vec{r}, t), \quad (23)$$

is finite. It is a function of the external doping μ and of the gauge invariant external electromagnetic fields. In the absence of such external fields, it vanishes at the charge neutrality point ($\mu = 0$).

B. Contour-time generating functional

The entire physical content of the theory can be conveniently expressed by the partition function [41,42,51,61,62]

$$Z[\eta; \rho] = \langle \mathcal{T}_{\mathcal{C}} e^{i\eta^\dagger \Psi + i\Psi^\dagger \eta} \rangle, \quad (24)$$

which is a generating functional for all n -point correlation functions, including the single-particle propagators described above. Its arguments η and η^\dagger , where only the former is shown on the left-hand side for brevity, are eight component spinorial external source terms. Here and in the remainder of this paper, we employed a condensed vector notation

$$\eta^\dagger \Psi \equiv \int_{\mathcal{C}, x} \eta^\dagger(x) \Psi(x), \quad \Psi^\dagger \eta \equiv \int_{\mathcal{C}, x} \Psi^\dagger(x) \eta(x), \quad (25)$$

where $x = (\vec{r}, t)$ labels space and (contour-) time coordinates, such that

$$\int_{\mathcal{C}, x} \equiv \int_{\mathcal{C}} dt \int d^2r. \quad (26)$$

The symbol \mathcal{C} indicates that the time integration has to be performed along the Schwinger-Keldysh closed time contour. An important property of the partition function is that it is normalized to unity when the sources are set equal to zero [63]:

$$Z[0; \rho] = \operatorname{Tr} \rho(t_0) = 1. \quad (27)$$

In fact, this normalization is the very reason for the algebraic identity (11) and it leads to similar constraints for higher-order correlation functions, see Ref. [41]. It further ensures that any correlation function computed from the partition function (24) does not contain disconnected bubble diagrams.

The partition function (24) can be represented in terms of a fermionic coherent state functional integral as [41,42,61,62]

$$Z[\eta; \rho] = \int \mathcal{D}\psi \mathcal{D}\psi^\dagger e^{iS[\psi] + iK_\rho[\psi] + i\eta^\dagger \Psi + i\Psi^\dagger \eta}. \quad (28)$$

Here, $S[\psi]$ is the contour-time action of the system and $K_\rho[\psi]$ is the correlation functional, which incorporates the statistical information of the initial density matrix [41,62,64]. Their dependence on the Grassmann-valued spinor fields Ψ and Ψ^\dagger has been abbreviated by ψ , as we did for the source field dependence of the partition function.

The action can be written as a contour-time integral over the Lagrangian $L(t)$,

$$S[\psi] = \int_{\mathcal{C}, t} L(t), \quad (29)$$

with

$$L(t) = \int_{\vec{r}} \Psi^\dagger(x) i \partial_t \Psi(x) - H(t). \quad (30)$$

Similarly to the Hamiltonian (1), the action decomposes into free contribution and an interaction term,

$$S[\psi] = S_f[\psi] + S_{\text{int}}[\psi], \quad (31)$$

expressions for which can be obtained immediately by substitution of Eqs. (2) and (4).

The functional $K_\rho[\psi]$ describes the initial correlations of the system, corresponding to the density matrix $\rho(t_0)$. It may be expanded in powers of fields as

$$\begin{aligned} K_\rho[\psi] &= \sum_{m=0}^{\infty} \frac{(-1)^m}{(m!)^2} \int_{\mathcal{C}, x_m x'_m} \sum_{i_m i'_m} \\ &\times K_\rho^{(2m)}(x_1 i_1, \dots, x_m i_m; x'_1 i'_1, \dots, x'_m i'_m) \\ &\times \psi_{i_1}^\dagger(x_1) \dots \psi_{i_m}^\dagger(x_m) \psi_{i'_m}(x'_m) \dots \psi_{i'_1}(x'_1), \end{aligned} \quad (32)$$

where the kernels $K_\rho^{(2m)}$ are nonvanishing only, if all their respective contour-time arguments equal the initial time t_0 . The statistical information contained in the kernels $K_\rho^{(2m)}$, specifying the correlations present in the initial state, is in a one-to-one correspondence to the statistical information contained in the density matrix [55,62,64]. In practice, only a limited set of initial correlations is taken into account, either because of an implicit assumption that the initial state is

a thermal equilibrium state for an effectively noninteracting system [42,43] or as an expression of the finite knowledge that is available about an experimental setup [64]. In the remainder of this work, we mainly focus on Gaussian density matrices, i.e., we truncate the series (32) after the first term, absorbing the statistical information of $K_\rho^{(2)}$ into the boundary conditions of the two-point function and simply write $Z[\eta, \rho] \equiv Z[\eta]$. Yet most of our results are not affected by this simplification and valid even in the general case. We come back to this issue in Sec. III E, where we comment on some questions regarding the possible implementation of correlated initial states.

Although it is possible to treat the theory presented so far within the formalism of the (fermionic) functional renormalization group [34,65], we here choose a formulation in which a bosonic field is introduced by means of a Hubbard-Stratonovich transformation, that decouples the Coulomb interaction [39,42,61]. It is well known that bosonic degrees of freedom, such as Cooper pairs in the celebrated BCS-theory of superconductivity [61], naturally emerge as collective, low-energy degrees of freedom of composite fermions. Therefore it is reasonable to introduce a collective bosonic field right from the beginning, which captures the dominant contributions of the interaction. For the Coulomb interaction, the dominant scattering processes involve small momentum transfers. Hence we choose to decouple the interaction term in the density-density channel, which emphasizes forward scattering and gives rise to collective plasmon modes if the system is doped away from charge neutrality [17].

The Hubbard-Stratonovich transformation is an exact integral identity replacing the four-fermion interaction $S_{\text{int}}[\psi]$ by a quadratic form of a real bosonic field and a Fermi-Bose interaction

$$e^{iS_{\text{int}}[\psi]} = \int \mathcal{D}\phi e^{iS_b[\phi] + iS_{\text{int}}[\psi, \phi]}. \quad (33)$$

The free bosonic part is given by

$$S_b[\phi] = \frac{1}{2} \int_{\mathcal{C}, xy} \phi(x) V^{-1}(x-y) \phi(y), \quad (34)$$

where V^{-1} is the inverse Coulomb interaction, understood in the distributional sense. The interaction term contains a trilinear Yukawa-type interaction and a linear term, describing the coupling of the Hubbard-Stratonovich boson to the background charge density $\tilde{n}(x)$:

$$S_{\text{int}}[\psi, \phi] = - \int_{\mathcal{C}, x} \phi(x) (\Psi^\dagger(x) \Psi(x) - \tilde{n}(x)). \quad (35)$$

Note that the fluctuating Bose field ϕ appears on the same footing as the external scalar potential φ , see Eq. (2).

We generalize the Hubbard-Stratonovich transformed partition function by introducing an additional source term

$$\phi^\top J \equiv \int_{\mathcal{C}, x} \phi(x) J(x), \quad (36)$$

so that it gives access to bosonic as well as mixed Fermi-Bose correlators. The generalized Fermi-Bose partition function reads

$$Z[\eta, J] = \int \mathcal{D}\psi \mathcal{D}\psi^\dagger \mathcal{D}\phi e^{iS[\psi, \phi] + i\eta^\dagger \Psi + i\Psi^\dagger \eta + i\phi^\top J}, \quad (37)$$

with $S[\psi, \phi] = S_f[\psi] + S_b[\phi] + S_{\text{int}}[\psi, \phi]$. It fulfills the same normalization condition, when the sources are set to zero, as the purely fermionic partition function

$$Z[0, 0] = 1. \quad (38)$$

C. Real-time representation

Although the contour-time representation allows for a compact and concise notation during any step of a calculation, it is desirable to formulate the theory in a single-valued “physical” time, which appeals to physical intuition and transparency. Hereto one splits the contour \mathcal{C} into forward (\mathcal{C}_+) and backward (\mathcal{C}_-) branch, thereby defining a doubled set of fields, Ψ_\pm and ϕ_\pm , allocated to the respective branch

$$\begin{aligned} S[\psi, \phi] &= \int_{\mathcal{C}, t} L[\psi, \phi] \\ &= \int_{\mathcal{C}_+, t} L[\psi_+, \phi_+] + \int_{\mathcal{C}_-, t} L[\psi_-, \phi_-]. \end{aligned} \quad (39)$$

In a next step, one performs a rotation from \pm -field space to Keldysh space, using the involutorial matrix $\tau_1 L$, see Eq. (12), which was already employed for the rotation of the Green functions in Sec. II A. Further, one defines the symmetric and antisymmetric linear combinations of the \pm -fields as “classical” (c) and “quantum” (q) components, respectively, and combines these into vectors Ψ, Ψ^\dagger and ϕ as

$$\Psi \equiv \begin{pmatrix} \Psi_c \\ \Psi_q \end{pmatrix} \equiv \tau_1 L \begin{pmatrix} \Psi_+ \\ \Psi_- \end{pmatrix}, \quad \Psi^\dagger = (\Psi)^\dagger, \quad (40)$$

$$\phi \equiv \begin{pmatrix} \phi_c \\ \phi_q \end{pmatrix} \equiv \frac{1}{\sqrt{2}} \tau_1 L \begin{pmatrix} \phi_+ \\ \phi_- \end{pmatrix}. \quad (41)$$

The source fields are rotated and combined into vectors η, η^\dagger and J likewise. Two remarks are in order. First, the mapping of the bosonic source term yields an additional factor of two, due to our choice of normalization in Eq. (41), which we choose to absorb into a redefinition of J . The second remark is concerned about our definition of the Keldysh rotation for the fermionic field Ψ^\dagger . Some authors prefer a different convention, which was originally proposed by Larkin and Ovchinnikov [66]. In a purely fermionic theory, this is reasonable, since it leads to a certain technical simplification. However, this modified rotation is not possible for bosons. In the context of the coupled Fermi-Bose theory, we are dealing with, the implementation of the Larkin-Ovchinnikov rotation would lead to an asymmetry in the arising Keldysh structures, which we want to avoid. Therefore we define the Keldysh rotation as proposed in Eq. (40). Further, one has to keep in mind that the naming “classical” for the fermions is just terminology. For the bosons on the other hand, this naming has a physical meaning.

We here summarize the main results of the real-time mapping and explain the structure of the theory obtained after the above Keldysh rotation. For the partition function $Z[\eta, J]$, we find

$$Z[\eta, J] = \int \mathcal{D}\Psi \mathcal{D}\Psi^\dagger \mathcal{D}\phi e^{iS[\Psi, \phi] + i\eta^\dagger \tau_1 \Psi + i\Psi^\dagger \tau_1 \eta + i\phi^\top \tau_1 J}. \quad (42)$$

We have used here the short-hand notation

$$\eta^\dagger \tau_1 \Psi \equiv \int_x (\eta_c^\dagger(x) \eta_q^\dagger(x)) \tau_1 \begin{pmatrix} \Psi_c(x) \\ \Psi_q(x) \end{pmatrix}, \quad (43)$$

in which the Pauli matrix τ_1 acts in Keldysh space, coupling a “classical” source to a “quantum” field and vice versa. Further, all the time integrations are defined from now on along the forward time branch \mathcal{C}_+ only

$$\int_x \equiv \int_{\mathcal{C}_+,x} = \int_0^\infty dt \int d^2r. \quad (44)$$

The action $S[\boldsymbol{\psi}, \boldsymbol{\phi}]$ is the sum of three contributions,

$$S[\boldsymbol{\psi}, \boldsymbol{\phi}] = S_f[\boldsymbol{\psi}] + S_b[\boldsymbol{\phi}] + S_{\text{int}}[\boldsymbol{\psi}, \boldsymbol{\phi}]. \quad (45)$$

Its quadratic part in the fermionic sector is given by

$$S_f[\boldsymbol{\psi}] = \int_{xy} (\Psi_c^\dagger(x) \Psi_q^\dagger(x)) \hat{G}_0^{-1}(x,y) \begin{pmatrix} \Psi_c(y) \\ \Psi_q(y) \end{pmatrix}. \quad (46)$$

The inverse free propagator \hat{G}_0^{-1} has a trigonal matrix structure

$$\hat{G}_0^{-1} = \begin{pmatrix} 0 & (\hat{G}_0^A)^{-1} \\ (\hat{G}_0^R)^{-1} & (\hat{G}_0^{-1})^K \end{pmatrix}, \quad (47)$$

with retarded/advanced $(\hat{G}_0^{R/A})^{-1}$ and Keldysh blocks $(\hat{G}_0^{-1})^K$, which obey the symmetries [42,43]

$$((\hat{G}_0^R)^{-1})^\dagger = (\hat{G}_0^A)^{-1}, \quad ((\hat{G}_0^{-1})^K)^\dagger = -(\hat{G}_0^{-1})^K. \quad (48)$$

The retarded/advanced blocks are the inverse free retarded/advanced propagators

$$(\hat{G}_0^{R/A})^{-1}(x,y) = \delta(x-y) \sigma_0^s \otimes (\Sigma_0 i \mathcal{D}_{y_0} + i v_F \vec{\Sigma} \cdot \mathcal{D}_{\vec{y}}), \quad (49)$$

where the gauge covariant derivative is given by

$$i \mathcal{D}_{x_0} = i \partial_{x_0} \pm i0 + \mu - e\varphi(x), \quad \mathcal{D}_{\vec{x}} = \partial_{\vec{x}} + i e \vec{A}(x). \quad (50)$$

Note that the regularization term $\pm i0$, which we have written here explicitly, enforces the retarded, respectively advanced, boundary condition. It has to be emphasized that the external gauge fields therein are understood as entirely classical:

$$\varphi(x) \equiv \varphi_c(x) = \frac{1}{2}(\varphi_+(x) + \varphi_-(x)), \quad (51a)$$

$$\vec{A}(x) \equiv \vec{A}_c(x) = \frac{1}{2}(\vec{A}_+(x) + \vec{A}_-(x)). \quad (51b)$$

Since these fields are not quantized, their quantum components in Keldysh space vanish identically. Yet it is formally possible to keep them as source fields, which could be used to generate density-density or current-current correlation functions [42]. On the other hand, this is not necessary, since we have the single-particle sources $\boldsymbol{\eta}$ at our disposal. In contrast to the retarded and advanced blocks of Eq. (47), the Keldysh block $(\hat{G}_0^{-1})^K$ does not take the form of a simple inverse propagator. It carries the statistical information of the theory and can be written as

$$(\hat{G}_0^{-1})^K = -(\hat{G}_0^R)^{-1} \hat{G}_0^K (\hat{G}_0^A)^{-1}, \quad (52)$$

with the noninteracting Keldysh Green function \hat{G}_0^K . Since the latter is an antiHermitian matrix, see Eq. (15), it can be parametrized in terms of a Hermitian matrix $\hat{\mathcal{F}}_0$ and the spectral functions $\hat{G}_0^{R/A}$ as [42]

$$\hat{G}_0^K = \hat{G}_0^R \hat{\mathcal{F}}_0 - \hat{\mathcal{F}}_0 \hat{G}_0^A. \quad (53)$$

Substitution into Eq. (52) then yields that for noninteracting fermions the Keldysh block of the inverse matrix propagator is a pure regularization term [67]:

$$(\hat{G}_0^{-1})^K = 2i0\hat{\mathcal{F}}_0. \quad (54)$$

Only when interactions are considered the Keldysh block will acquire a finite value. We will come back to this issue in Sec. III C. The free propagator \hat{G}_0 is obtained by inverting Eq. (47), where the Keldysh structure is given by Eq. (13).

The quadratic part of the action in the bosonic sector reads

$$S_b[\boldsymbol{\phi}] = \frac{1}{2} \int_{xy} \boldsymbol{\phi}^\top(x) \mathbf{D}_0^{-1}(x,y) \boldsymbol{\phi}(y). \quad (55)$$

The bosonic matrix \mathbf{D}_0^{-1} has the same trigonal structure as the fermionic one

$$\mathbf{D}_0^{-1} = \begin{pmatrix} 0 & (\mathbf{D}_0^A)^{-1} \\ (\mathbf{D}_0^R)^{-1} & (\mathbf{D}_0^{-1})^K \end{pmatrix}, \quad (56)$$

with the same symmetry relations as Eq. (48). Owing to the fact that the bosons are real, the above quantities fulfill the additional symmetries [42,43]:

$$((\mathbf{D}_0^R)^{-1})^\top = (\mathbf{D}_0^A)^{-1}, \quad ((\mathbf{D}_0^{-1})^K)^\top = (\mathbf{D}_0^{-1})^K. \quad (57)$$

The retarded and advanced blocks are twice the inverse bare Coulomb interaction:

$$(\mathbf{D}_0^{R/A})^{-1}(x,y) = 2V^{-1}(x-y). \quad (58)$$

The Keldysh component for bosons has the same structure as the fermionic one

$$(\mathbf{D}_0^{-1})^K = -(\mathbf{D}_0^R)^{-1} \mathbf{D}_0^K (\mathbf{D}_0^A)^{-1}. \quad (59)$$

Similarly to the fermionic case we can parametrize the bosonic Keldysh Green function in terms of a Hermitian function \mathcal{B}_0 [42]:

$$\mathbf{D}_0^K = \mathbf{D}_0^R \mathcal{B}_0 - \mathcal{B}_0 \mathbf{D}_0^A. \quad (60)$$

Since the bare Coulomb interaction is instantaneous, the above Keldysh propagator together with the Keldysh block (59) vanish identically. For that reason, we may write

$$\mathbf{D}_0^{-1} = 2V^{-1} \equiv 2V^{-1} \tau_1. \quad (61)$$

Again, the interaction with the fermions will eventually lead to a finite bosonic Keldysh self-energy and, hence, a nonvanishing Keldysh propagator as in the fermionic case.

Finally, we discuss the Fermi-Bose interaction term. Its linear counterterm maps in the same way as the sources do, but with the important difference that the quantum component $\tilde{n}_q(x)$ is identically zero. Nevertheless, we may still use the Keldysh vector notation for this term as well. The trilinear term maps to four interaction terms in real time, which can be arranged in a matrix form similar to Eq. (46),

$$S_{\text{int}}[\boldsymbol{\psi}, \boldsymbol{\phi}] = - \int_x \boldsymbol{\Psi}^\dagger(x) \begin{pmatrix} \phi_q(x) & \phi_c(x) \\ \phi_c(x) & \phi_q(x) \end{pmatrix} \boldsymbol{\Psi}(x) + 2 \int_x \boldsymbol{\phi}^\top(x) \tau_1 \tilde{\mathbf{n}}(x). \quad (62)$$

Note the factor of two in front of the linear term in comparison to the linear source term, which could not be absorbed into a redefinition of any of those fields as was the case for \mathbf{J} . Further observe that the classical components of the fluctuating Bose field appear in the same off-diagonal position as the external gauge field φ does in Eq. (46). The quantum components on the other hand are located in the diagonal. Now that all of our notational conventions have been established we can move on to the central part of this work.

III. NONEQUILIBRIUM FUNCTIONAL RENORMALIZATION GROUP

The idea of the functional renormalization group is to modify the bare action of the theory by introducing a dependence on a parameter Λ , in such a way that the partition function can be easily (and exactly) calculated if Λ is set equal to an initial value Λ_0 , whereas the true physical system corresponds to $\Lambda = 0$. Using the solution of the modified partition function at $\Lambda = \Lambda_0$, one obtains the “physical” partition function at $\Lambda = 0$ by tracking its changes upon lowering Λ from Λ_0 to 0. In practice, the parameter Λ is chosen as an infrared regularization which effectively removes low-energy (or low-momentum) modes, determined by the cutoff Λ , from the functional integration. In this case, the initial value Λ_0 is the ultraviolet cutoff of the action $S[\boldsymbol{\psi}, \boldsymbol{\phi}]$. For graphene, this ultraviolet cutoff is the momentum or energy at which the linear dispersion in Eq. (2) breaks down.

A. Infrared regularization

We implement the idea of an infrared regularization by modifying the quadratic terms in the Fermi and Bose sectors of the contour-time action via additive regulator functions $\hat{R}_{f,\Lambda}, R_{b,\Lambda}$ [32,35]:

$$S_f[\boldsymbol{\psi}] \rightarrow S_{f,\Lambda}[\boldsymbol{\psi}] = S_f[\boldsymbol{\psi}] + \boldsymbol{\Psi}^\dagger \hat{R}_{f,\Lambda} \boldsymbol{\Psi}, \quad (63a)$$

$$S_b[\boldsymbol{\phi}] \rightarrow S_{b,\Lambda}[\boldsymbol{\phi}] = S_b[\boldsymbol{\phi}] + \frac{1}{2} \boldsymbol{\phi}^\top \mathbf{R}_{b,\Lambda} \boldsymbol{\phi}. \quad (63b)$$

It is also possible to regularize only one of the two sectors, by setting either $\hat{R}_{f,\Lambda}$ or $R_{b,\Lambda}$ to zero. The regulators have to be analytic functions of Λ . For $\Lambda \rightarrow \Lambda_0$, they have to diverge, such that all infrared modes occurring in the functional integral are effectively frozen out, while for $\Lambda \rightarrow 0$ they have to vanish [34,35,39]. In this way, the partition function (37) becomes a cutoff dependent quantity, $Z[\boldsymbol{\eta}, \mathbf{J}] \rightarrow Z_\Lambda[\boldsymbol{\eta}, \mathbf{J}]$, where only the modes above Λ contribute to the functional integral. In the limit $\Lambda \rightarrow 0$, it reduces to the original partition function of the previous section, see Eq. (42).

After mapping the contour-time regulator terms to a real-time representation and performing the Keldysh rotation as explained in Sec. II C, the cutoff dependent quadratic parts of the action become

$$S_{f,\Lambda}[\boldsymbol{\psi}] = S_f[\boldsymbol{\psi}] + \boldsymbol{\Psi}^\dagger \hat{R}_{f,\Lambda} \boldsymbol{\Psi}, \quad (64a)$$

$$S_{b,\Lambda}[\boldsymbol{\phi}] = S_b[\boldsymbol{\phi}] + \boldsymbol{\phi}^\top \mathbf{R}_{b,\Lambda} \boldsymbol{\phi}. \quad (64b)$$

Note the absence of the factor 1/2 in front of the bosonic regulator term, which is due to our choice of normalization for the bosonic rotation (41). In principle, the most general choice

for the contour-time regulators results in the following 2×2 matrix structure for the real-time regulators:

$$\hat{\mathbf{R}}_{f,\Lambda}(x, y) = \begin{pmatrix} \hat{R}_{f,\Lambda}^Z(x, y) & \hat{R}_{f,\Lambda}^A(x, y) \\ \hat{R}_{f,\Lambda}^R(x, y) & \hat{R}_{f,\Lambda}^K(x, y) \end{pmatrix}, \quad (65a)$$

$$\mathbf{R}_{b,\Lambda}(x, y) = \begin{pmatrix} R_{b,\Lambda}^Z(x, y) & R_{b,\Lambda}^A(x, y) \\ R_{b,\Lambda}^R(x, y) & R_{b,\Lambda}^K(x, y) \end{pmatrix}. \quad (65b)$$

Although it is not strictly necessary if the evolution from $\Lambda = \Lambda_0$ to $\Lambda = 0$ could be tracked exactly, for the correct implementation of approximate evolution schemes, it is important that the regulators are chosen in such a way that they respect the symmetries and the causality structure of the theory. In particular, in order to ensure that the partition function is normalized to unity at any scale, and hence retain the algebraic identities among the correlation functions, *cf.* Eq. (11), we choose the regulators such that the “anomalous” components $\hat{R}_{f,\Lambda}^Z, R_{b,\Lambda}^Z$ vanish. The remaining components are constructed in such a way that they are compatible with the symmetry and causality structure of the bare inverse propagators, see Eqs. (48) and (57). This choice of the regulator functions ensures that the partition function has the correct causality structure at any value of the cutoff Λ , independent of eventual approximations made when solving the evolution equations.

In addition to the Λ dependence of the action introduced via Eqs. (64), we allow the counterterm to be explicitly cutoff dependent, setting

$$\tilde{n} \rightarrow \tilde{n}_\Lambda. \quad (66)$$

The counterterm \tilde{n}_Λ describes a flowing background charge density, which has to be tuned to remove potentially divergent contributions from the Coulomb interaction at finite charge carrier density.

B. Connected functional and effective action

The evolution equation will not be derived for the partition function $Z_\Lambda[\boldsymbol{\eta}, \mathbf{J}]$, but rather for the effective action $\Gamma_\Lambda[\boldsymbol{\psi}, \boldsymbol{\phi}]$, which is essentially the Legendre transformation of the cutoff dependent connected functional [41,61]

$$W_\Lambda[\boldsymbol{\eta}, \mathbf{J}] = -i \ln Z_\Lambda[\boldsymbol{\eta}, \mathbf{J}], \quad (67)$$

being a generating functional for connected correlation functions. Differentiation with respect to the sources yield the expectation values of the fields $\boldsymbol{\Psi}(x)$ and $\boldsymbol{\phi}(x)$,

$$\frac{\delta W_\Lambda}{\delta \boldsymbol{\eta}^\dagger(x)} = +\tau_1 \langle \boldsymbol{\Psi}(x) \rangle, \quad \frac{\delta W_\Lambda}{\delta \boldsymbol{\eta}(x)} = -\langle \boldsymbol{\Psi}^\dagger(x) \rangle \tau_1, \quad (68)$$

$$\frac{\delta W_\Lambda}{\delta \mathbf{J}(x)} = \langle \boldsymbol{\phi}^\top(x) \rangle \tau_1. \quad (69)$$

These expectation values, being complicated nonlinear functionals of the sources $\boldsymbol{\eta}$ and \mathbf{J} , define “macroscopic” fields which inherit a Λ -dependence from the regulators (and the counterterm). A macroscopic Fermi field can only exist when the sources are finite, otherwise it is strictly zero. The classical component of the macroscopic bosonic field $\langle \phi_c(x) \rangle$, on the other hand, can very well acquire a finite value in the absence of source terms [41,51–53]. Such a macroscopic field expectation

value may signal a spontaneous symmetry breaking, but in the theory we consider here this is not the case. The bosonic field $\phi(x)$ is conjugate to the particle density $n(x)$ and as such it reflects, e.g., a local deviation away from charge neutrality driven by an external potential $\varphi(x)$. In the following we omit the brackets to denote the average of a single field, for brevity. Since we are always working with averages of fields, there can be no confusion.

The second derivatives of W_Λ define the connected two-point correlators

$$\frac{\delta^2 W_\Lambda}{\delta \eta^\dagger(x) \delta \eta(y)} = -i \tau_1 \langle \Psi(x) \Psi^\dagger(y) \rangle_c \tau_1, \quad (70)$$

$$\frac{\delta^2 W_\Lambda}{\delta \mathbf{J}^\top(x) \delta \mathbf{J}(y)} = +i \tau_1 \langle \phi(x) \phi^\top(y) \rangle_c \tau_1, \quad (71)$$

where we introduced the connected average $\langle AB \rangle_c \equiv \langle AB \rangle - \langle A \rangle \langle B \rangle$. Explicitly displaying the 2×2 Keldysh structure, we have

$$\begin{aligned} \langle \Psi(x) \Psi^\dagger(y) \rangle_c &\equiv i \hat{G}_\Lambda(x, y | \eta, \mathbf{J}) \\ &= i \begin{pmatrix} \hat{G}_\Lambda^K(x, y | \eta, \mathbf{J}) & \hat{G}_\Lambda^R(x, y | \eta, \mathbf{J}) \\ \hat{G}_\Lambda^A(x, y | \eta, \mathbf{J}) & \hat{G}_\Lambda^Z(x, y | \eta, \mathbf{J}) \end{pmatrix}, \end{aligned} \quad (72)$$

$$\begin{aligned} \langle \phi(x) \phi^\top(y) \rangle_c &\equiv i D_\Lambda(x, y | \eta, \mathbf{J}) \\ &= i \begin{pmatrix} D_\Lambda^K(x, y | \eta, \mathbf{J}) & D_\Lambda^R(x, y | \eta, \mathbf{J}) \\ D_\Lambda^A(x, y | \eta, \mathbf{J}) & D_\Lambda^Z(x, y | \eta, \mathbf{J}) \end{pmatrix}. \end{aligned} \quad (73)$$

The above propagators are source- and cutoff-dependent functionals, which do not obey the usual triangular structure. In particular, the anomalous statistical propagators \hat{G}_Λ^Z and D_Λ^Z are nonvanishing as long as the source terms are finite. By construction of the regulators, the familiar triangular structure together with the symmetry and causality relations arise once the single-particle sources are set to zero. All the other higher-order connected correlation functions can be obtained by further differentiation as in the equilibrium Matsubara theory [61].

The central object in the functional renormalization group is the effective action $\Gamma_\Lambda[\psi, \phi]$. It is the generating functional for one-particle irreducible vertex functions, and defined as the Legendre transform of the connected functional W_Λ :

$$\begin{aligned} \Gamma_\Lambda[\psi, \phi] &= W_\Lambda[\eta_\Lambda, \mathbf{J}_\Lambda] - \eta^\dagger_\Lambda \tau_1 \Psi - \Psi^\dagger \tau_1 \eta_\Lambda - \phi^\top \tau_1 \mathbf{J}_\Lambda \\ &\quad - \Psi^\dagger \hat{\mathcal{R}}_{f,\Lambda} \Psi - \phi^\top \mathbf{R}_{b,\Lambda} \phi. \end{aligned} \quad (74)$$

In the Legendre transform, the single-particle sources must be understood as Λ -dependent functionals of the field expectation values, obtained by inversion of the defining relations Eqs. (68) and (69). The Legendre transform is modified in such a way that the cutoff terms are subtracted on the right-hand side. This ensures that the flowing action does not contain the cutoff terms at any scale, but spoils the convexity of an ordinary Legendre transform.

The properties and physical interpretation of this functional, mainly in the context of its equilibrium counterpart, have been discussed at length in the literature [34,35,39]. Most importantly the flowing action has the nice property that it interpolates smoothly between the microscopic laws of physics, parametrized by an action Γ_{Λ_0} , and the full effective

action $\Gamma_{\Lambda=0}$, where all thermal and quantum fluctuations are taken into account. In many cases, the microscopic laws are simply governed by the bare action of the system $\Gamma_{\Lambda_0} = S$. This latter statement, however, depends on the actual cutoff scheme. In certain situations, it is preferable to devise a cutoff scheme where the initial effective action does not coincide with the bare action, and hence the initial conditions of the flow are nontrivial [39,49,50,68,69]. We will come back to this issue at the end of the next subsection.

Taking the first functional derivative of Eq. (74) with respect to the fields, one finds that the effective action satisfies the “equations of motion:”

$$\frac{\delta \Gamma_\Lambda}{\delta \Psi^\dagger(x)} = -\tau_1 \eta_\Lambda(x) - \int_y \hat{\mathcal{R}}_{f,\Lambda}(x, y) \Psi(y), \quad (75)$$

$$\frac{\delta \Gamma_\Lambda}{\delta \Psi(x)} = +\eta^\dagger_\Lambda(x) \tau_1 + \int_y \Psi^\dagger(y) \hat{\mathcal{R}}_{f,\Lambda}(y, x), \quad (76)$$

$$\frac{\delta \Gamma_\Lambda}{\delta \phi^\top(x)} = -\tau_1 \mathbf{J}_\Lambda(x) - 2 \int_y \mathbf{R}_{b,\Lambda}(x, y) \phi(y). \quad (77)$$

The second functional derivatives of the connected functional $W_\Lambda[\eta, \mathbf{J}]$ and the second functional derivatives of the effective action $\Gamma_\Lambda[\psi, \phi]$ are subject to an inversion relation [34,39,61], which can be written in the compact form

$$-(\hat{\mathbf{f}}_\Lambda^{(2)} + \hat{\mathcal{R}}_\Lambda) \tau_1 \hat{\mathbf{W}}_\Lambda^{(2)} \tau_1 = \hat{\mathbb{1}}. \quad (78)$$

Here we have defined the matrices

$$\hat{\mathcal{R}}_\Lambda \equiv \text{diag}(-\hat{\mathcal{R}}_{f,\Lambda}, \hat{\mathcal{R}}_{f,\Lambda}^\top, 2\mathbf{R}_{b,\Lambda}), \quad (79)$$

$$\tau_1 \equiv \text{diag}(\tau_1, \tau_1, \tau_1), \quad (80)$$

and the Hesse matrices $\hat{\mathbf{W}}_\Lambda^{(2)}$ and $\hat{\mathbf{f}}_\Lambda^{(2)}$ of second functional derivatives:

$$\hat{\mathbf{W}}_\Lambda^{(2)} = \begin{pmatrix} \delta_{\eta^\dagger} \delta_\eta & -\delta_{\eta^\dagger} \delta_{\eta^\dagger}^\top & -\delta_{\eta^\dagger} \delta_{\mathbf{J}} \\ -\delta_\eta^\top \delta_\eta & \delta_\eta^\top \delta_{\eta^\dagger}^\top & \delta_\eta^\top \delta_{\mathbf{J}} \\ -\delta_{\mathbf{J}}^\top \delta_\eta & \delta_{\mathbf{J}}^\top \delta_{\eta^\dagger}^\top & \delta_{\mathbf{J}}^\top \delta_{\mathbf{J}} \end{pmatrix} W_\Lambda, \quad (81)$$

$$\hat{\mathbf{f}}_\Lambda^{(2)} = \begin{pmatrix} \delta_{\Psi^\dagger} \delta_\Psi & \delta_{\Psi^\dagger} \delta_{\Psi^\dagger}^\top & \delta_{\Psi^\dagger} \delta_\phi \\ \delta_\Psi^\top \delta_\Psi & \delta_\Psi^\top \delta_{\Psi^\dagger}^\top & \delta_\Psi^\top \delta_\phi \\ \delta_\phi^\top \delta_\Psi & \delta_\phi^\top \delta_{\Psi^\dagger}^\top & \delta_\phi^\top \delta_\phi \end{pmatrix} \Gamma_\Lambda. \quad (82)$$

The inversion relation (78) generalizes the standard Dyson equations for single-particle propagators to the case of source-dependent functional propagators, Eqs. (72) and (73). If the sources are finite, Eq. (78) also includes mixed Fermi-Bose correlators, which disappear upon setting the sources to zero. Applying further functional derivatives to this equation yields a tree expansion of a connected n -particle correlation function in terms of m -particle vertex functions ($m \leq n$) and full propagators; see Refs. [34,39,61].

C. Dyson and quantum kinetic equations in the functional renormalization group

Evaluating the generalized Dyson equation at vanishing sources, we obtain the scale dependent nonequilibrium Dyson

equations for fermions and bosons:

$$(\hat{G}_0^{-1} - \hat{\Sigma}_\Lambda + \hat{R}_{f,\Lambda})\hat{G}_\Lambda = \hat{1}, \quad (83)$$

$$2(V^{-1} + \Pi_\Lambda + R_{b,\Lambda})D_\Lambda = \mathbb{1}, \quad (84)$$

where we employed the definition of the unregularized inverse full propagators

$$\left. \frac{\delta^2 \Gamma_\Lambda}{\delta \Psi^\dagger(x) \delta \Psi(y)} \right|_{\phi_c = \bar{\phi}_c} = -(\hat{G}_0^{-1} - \hat{\Sigma}_\Lambda)(x, y), \quad (85)$$

$$\left. \frac{\delta^2 \Gamma_\Lambda}{\delta \phi^\top(x) \delta \phi(y)} \right|_{\phi_c = \bar{\phi}_c} = 2(V^{-1} + \Pi_\Lambda)(x, y). \quad (86)$$

Here, Eqs. (85) and (86) define the (fermionic) self-energy $\hat{\Sigma}_\Lambda$ and the (bosonic) polarization function Π_Λ , respectively. The latter is also known as bosonic self-energy, which will be used synonymously in the remainder of this work [70]. By construction of the regulators, the fermionic and bosonic self-energies have the same trigonal structure in Keldysh space as the inverse free propagators and the regulators

$$\hat{\Sigma}_\Lambda = \begin{pmatrix} 0 & \hat{\Sigma}_\Lambda^A \\ \hat{\Sigma}_\Lambda^R & \hat{\Sigma}_\Lambda^K \end{pmatrix}, \quad \Pi_\Lambda = \begin{pmatrix} 0 & \Pi_\Lambda^A \\ \Pi_\Lambda^R & \Pi_\Lambda^K \end{pmatrix}. \quad (87)$$

Besides, they inherit their causality and symmetry relations, see Eqs. (48) and (57).

The diagonal components of Eqs. (83) and (84) contain the respective retarded and advanced Dyson equations,

$$((\hat{G}_0^{R/A})^{-1} - \hat{\Sigma}_\Lambda^{R/A} + \hat{R}_{f,\Lambda}^{R/A})\hat{G}_\Lambda^{R/A} = \hat{1}, \quad (88)$$

$$2(V^{-1} + \Pi_\Lambda^{R/A} + R_{b,\Lambda}^{R/A})D_\Lambda^{R/A} = \mathbb{1}, \quad (89)$$

whereas their off-diagonal yield the Keldysh Green functions:

$$\hat{G}_\Lambda^K = -\hat{G}_\Lambda^R(-\hat{\Sigma}_\Lambda^K + \hat{R}_{f,\Lambda}^K)\hat{G}_\Lambda^A, \quad (90)$$

$$D_\Lambda^K = -2D_\Lambda^R(\Pi_\Lambda^K + R_{b,\Lambda}^K)D_\Lambda^A. \quad (91)$$

These relations are a straightforward generalization of Eqs. (52) and (59) to the interacting case and the presence of infrared regulators.

Continuing the parallels with the noninteracting case, the flowing full Keldysh propagators \hat{G}_Λ^K and D_Λ^K can be parameterized in terms of cutoff dependent Hermitian matrices $\hat{\mathcal{F}}_\Lambda$ and \mathcal{B}_Λ , respectively,

$$\hat{G}_\Lambda^K = \hat{G}_\Lambda^R \hat{\mathcal{F}}_\Lambda - \hat{\mathcal{F}}_\Lambda \hat{G}_\Lambda^A, \quad (92)$$

$$D_\Lambda^K = D_\Lambda^R \mathcal{B}_\Lambda - \mathcal{B}_\Lambda D_\Lambda^A. \quad (93)$$

This parametrization can be used to derive an equation of motion for each of the distribution functions $\hat{\mathcal{F}}_\Lambda$ and \mathcal{B}_Λ . Such equations of motion are known as the quantum kinetic equations [42]. To this end we insert the above parametrization into Eq. (90), respectively Eq. (91). Applying the retarded inverse full propagator from the left and the advanced one from the right, we obtain the two kinetic

equations:

$$[\hat{\mathcal{F}}_\Lambda, \hat{G}_0^{-1}] + \hat{R}_{f,\Lambda}^K - (\hat{R}_{f,\Lambda}^R \hat{\mathcal{F}}_\Lambda - \hat{\mathcal{F}}_\Lambda \hat{R}_{f,\Lambda}^A) = \hat{\Sigma}_\Lambda^K - (\hat{\Sigma}_\Lambda^R \hat{\mathcal{F}}_\Lambda - \hat{\mathcal{F}}_\Lambda \hat{\Sigma}_\Lambda^A), \quad (94)$$

$$[\mathcal{B}_\Lambda, V^{-1}] + R_{b,\Lambda}^K - (R_{b,\Lambda}^R \mathcal{B}_\Lambda - \mathcal{B}_\Lambda R_{b,\Lambda}^A) = -\Pi_\Lambda^K + (\Pi_\Lambda^R \mathcal{B}_\Lambda - \mathcal{B}_\Lambda \Pi_\Lambda^A), \quad (95)$$

where $[\cdot, \cdot]$ denotes the commutator. The left-hand side of these equations is the kinetic term, while their right-hand side is known as the collision integral. Note that the commutator for the bosonic distribution function \mathcal{B}_Λ does not involve any time derivatives; the dynamics of \mathcal{B}_Λ is entirely driven by the bosonic collision integral, and thus induced by the dynamics of the fermions. In a general nonequilibrium situation, the kinetic terms do not vanish and, hence, the Keldysh self-energies do not admit the same decomposition as the Keldysh propagators, leading to a finite collision integral.

We want to stress that the Λ dependence of the distribution functions, since it is a parametric one, poses a serious complication. The kinetic equations have to be solved at each scale, together with the flow equations for the various self-energies and higher-order vertex functions, self-consistently. The latter set of flow equations will be derived in the next subsections. Therefore further approximations are inevitable, if one hopes to obtain numerical solutions for a specific nonequilibrium problem. For example, if the external fields are taken to be slowly varying functions of time and/or space, one could use a Wigner transformation and perform a gradient expansion to some low order [42, 71]. Often this approximation is combined with the so-called quasiparticle approximation, which reduces the phase space of the distribution functions and eventually leads to the Boltzmann transport equation. An important technical simplification is achieved by the class of cutoff schemes where the Keldysh regulators are parameterized in the same way as the Keldysh propagators:

$$\hat{R}_{f,\Lambda}^K = \hat{R}_{f,\Lambda}^R \hat{\mathcal{F}}_\Lambda - \hat{\mathcal{F}}_\Lambda \hat{R}_{f,\Lambda}^A, \quad (96)$$

$$R_{b,\Lambda}^K = R_{b,\Lambda}^R \mathcal{B}_\Lambda - \mathcal{B}_\Lambda R_{b,\Lambda}^A. \quad (97)$$

As a consequence, the regulators on the left-hand side of the above kinetic equations drop out and we are left with the kinetic equations in their standard form, as if no regulators were present, see Ref. [42]. Especially in the treatment of equilibrium problems this fact has a great advantage. Namely, it is possible to solve the kinetic equations at all scales simultaneously with the well-known equilibrium distribution functions. In this way, the results of the Matsubara formalism are reproduced directly in real time, avoiding the necessity of cumbersome analytic continuations. We will come back to the equilibrium problem in the final section of this article, Sec. IV. The drawback of these schemes, however, is that the initial conditions of the flow equations, become nontrivial as pointed out in the Refs. [49–52], meaning that Γ_Λ in the limit $\Lambda \rightarrow \Lambda_0$ does not coincide with the bare action S . On the other hand, this is a rather small price to pay.

D. Exact flow equation

The implementation of the infrared regulators described above enables us to derive an exact evolution equation for the effective action Γ_Λ , which describes its flow in the infinite dimensional space of all possible actions as a function of the flowing cutoff Λ . The flow equation for Γ_Λ follows upon taking the Λ derivative of the defining relation, Eq. (74), at a fixed field configuration. To this end, recall that the connected functional $W_\Lambda[\eta_\Lambda, \mathbf{J}_\Lambda]$ therein has an explicit and an implicit Λ dependence. The flow of the sources η_Λ and \mathbf{J}_Λ , viewed as functionals of the fields Ψ and ϕ , does not contribute to the flow of Γ_Λ as the respective terms cancel each other [34,35]. We thus find

$$\partial_\Lambda \Gamma_\Lambda = \partial_\Lambda W_\Lambda - \Psi^\dagger \partial_\Lambda \hat{\mathcal{R}}_{f,\Lambda} \Psi - \phi^\top \partial_\Lambda \mathbf{R}_{b,\Lambda} \phi, \quad (98)$$

where the scale derivative of the first term on the right-hand side, $\partial_\Lambda W_\Lambda$, has to be performed for fixed source fields η and \mathbf{J} . It obeys an exact flow equation as well, which is readily derived from the definition (67):

$$\begin{aligned} \partial_\Lambda W_\Lambda &= \langle \Psi^\dagger \partial_\Lambda \hat{\mathcal{R}}_{f,\Lambda} \Psi \rangle + \langle \phi^\top \partial_\Lambda \mathbf{R}_{b,\Lambda} \phi \rangle + 2\phi^\top \tau_1 \partial_\Lambda \tilde{n}_\Lambda \\ &= -\text{Tr}((\partial_\Lambda \hat{\mathcal{R}}_{f,\Lambda})(\langle \Psi \Psi^\dagger \rangle_c + \Psi \Psi^\dagger)) \\ &\quad + \text{Tr}((\partial_\Lambda \mathbf{R}_{b,\Lambda})(\langle \phi \phi^\top \rangle_c + \phi \phi^\top)) + 2\phi^\top \tau_1 \partial_\Lambda \tilde{n}_\Lambda. \end{aligned} \quad (99)$$

Here, the trace Tr encompasses an integration over position and time, as well as a summation over the Keldysh components c and q and, for fermions, a summation over the spin, valley, and sublattice indices. Note the occurrence of the flowing counterterm \tilde{n}_Λ on the right-hand side, and recall that it possesses a classical component only. Upon insertion of Eq. (99) into Eq. (98) the additional regulator terms cancel, such that the flow equation contains connected functional propagators and the counterterm only. Making use of Eqs. (70), (71), and (81), we can write our intermediate result in the compact form:

$$\partial_\Lambda \Gamma_\Lambda = -\frac{i}{2} \text{STr}((\partial_\Lambda \hat{\mathcal{R}}_\Lambda) \tau_1 \hat{\mathcal{W}}_\Lambda^{(2)} \tau_1) + 2\phi^\top \tau_1 \partial_\Lambda \tilde{n}_\Lambda. \quad (100)$$

We recognize here the well-known one-loop structure of the flow equation with the cutoff insertion $\partial_\Lambda \hat{\mathcal{R}}_\Lambda$. The usual minus sign for a closed fermion loop has been absorbed into the definition:

$$\text{STr}(\dots) \equiv \text{Tr} \left(\begin{pmatrix} -1 & 0 & 0 \\ 0 & -1 & 0 \\ 0 & 0 & 1 \end{pmatrix} \dots \right). \quad (101)$$

In order to close Eq. (100), we make use of the generalized Dyson equation (78) and write

$$\begin{aligned} \partial_\Lambda \Gamma_\Lambda &= \frac{i}{2} \text{STr}((\partial_\Lambda \hat{\mathcal{R}}_\Lambda)(\hat{\mathcal{F}}_\Lambda^{(2)} + \hat{\mathcal{R}}_\Lambda)^{-1}) + 2\phi^\top \tau_1 \partial_\Lambda \tilde{n}_\Lambda \\ &= \frac{i}{2} \partial_\Lambda \text{STr} \ln(\hat{\mathcal{F}}_\Lambda^{(2)} + \hat{\mathcal{R}}_\Lambda) + 2\phi^\top \tau_1 \partial_\Lambda \tilde{n}_\Lambda, \end{aligned} \quad (102)$$

where we have defined the ‘‘single-scale derivative’’ ∂_Λ in the third line, which acts on the regulator only. This equation is the desired exact flow equation for the effective action of a Fermi-Bose theory in the nonequilibrium Keldysh formalism. Despite its apparent simplicity it is a highly complicated nonlinear functional integro-differential equation, which captures all of the nonperturbative features of the theory.

E. Vertex expansion

In practice, the exact flow equation (102) is too complex to be solved directly. Instead, one has to resort to approximation schemes.

A particularly crude approximation scheme is to neglect the Λ dependence of $\hat{\mathcal{F}}_\Lambda^{(2)}$ on the right-hand side of the flow equation (102) and replace it by its initial value at the scale $\Lambda = \Lambda_0$. In this approximation, the single-scale derivative ∂_Λ turns into an ordinary one and the flow equation can be integrated exactly. For certain cutoff schemes (see Ref. [35]), this approximation then immediately yields the effective action to one-loop order in perturbation theory:

$$\Gamma_{1\text{-loop}}[\psi, \phi] = S[\psi, \phi] + \frac{i}{2} \text{STr} \ln(\hat{\mathcal{S}}^{(2)}[\psi, \phi]). \quad (103)$$

Other approximations, such as the RPA or (a differential form of) the self-consistent Hartree-Fock approximation, can be obtained by similar considerations.

In recent years, there have been many proposals for systematic approximations of the effective action, which are capable of describing truly nonperturbative phenomena [35]. We here pursue an expansion into powers of fields Ψ and ϕ , following Refs. [34,39,68]. Assuming the effective action to be an analytic functional of the fields, we can perform a formally exact Taylor expansion, known as ‘‘vertex expansion.’’ It can be employed to replace the single functional integrodifferential equation by an equivalent infinite hierarchy of coupled ordinary integrodifferential equations for the one-particle irreducible vertex functions. Clearly, to solve the complete hierarchy exactly is still an impossible task. However, a truncation of the infinite hierarchy at a certain finite order is still nonperturbative in essence and does not necessarily rely on the presence of a smallness parameter in the interaction S_{int} .

Taking into account that the bosonic field may develop a finite expectation value $\bar{\phi}_c(x)$, e.g., due to a finite external scalar potential, we should expand the bosonic field around this macroscopic field, rather than around zero,

$$\phi_c(x) = \bar{\phi}_c(x) + \Delta\phi_c(x), \quad \phi_q(x) = \Delta\phi_q(x). \quad (104)$$

The general vertex expansion in the presence of bosonic field expectation values has been worked out for ‘‘superfields,’’ a condensed notation collecting fermionic and bosonic degrees of freedom into a single field, in thermal equilibrium by Schütz and Kopietz [39,68]. In our case, the vertex expansion reads

$$\begin{aligned} \Gamma_\Lambda[\psi, \phi] &= \sum_{m=0}^{\infty} \sum_{n=0}^{\infty} \frac{(-1)^m}{(m!)^2} \frac{1}{n!} \int_{x_m, x'_m} \sum_{i_m, i'_m} \sum_{\alpha_m, \alpha'_m} \int_{y_n} \sum_{\beta_n} \Gamma_\Lambda^{(2m,n)}(x_1 i_1 \alpha_1, \dots, x_m i_m \alpha_m; x'_1 i'_1 \alpha'_1, \dots, x'_m i'_m \alpha'_m; y_1 \beta_1, \dots, y_n \beta_n) \\ &\quad \times \psi_{i_1 \alpha_1}^\dagger(x_1) \cdots \psi_{i_m \alpha_m}^\dagger(x_m) \psi_{i'_m \alpha'_m}(x'_m) \cdots \psi_{i'_1 \alpha'_1}(x'_1) \Delta\phi_{\beta_1}(y_1) \cdots \Delta\phi_{\beta_n}(y_n). \end{aligned} \quad (105)$$

Here, latin indices i_n collectively denote the discrete fermionic degrees of freedom, sublattice, valley and spin, whereas greek indices α_n, β_n are reserved for the degrees of freedom in Keldysh space, the classical and quantum components. The coefficient functions $\Gamma_\Lambda^{(2m,n)}$ in this expansion define the one-particle irreducible vertex functions

$$\Gamma_\Lambda^{(2m,n)}(x_1 i_1 \alpha_1, \dots, x_m i_m \alpha_m; x'_1 i'_1 \alpha'_1, \dots, x'_m i'_m \alpha'_m; y_1 \beta_1, \dots, y_n \beta_n) = \frac{\delta^{(2m+n)} \Gamma_\Lambda}{\delta \psi_{i_1 \alpha_1}^\dagger(x_1) \cdots \delta \psi_{i_m \alpha_m}^\dagger(x_m) \delta \psi_{i'_1 \alpha'_1}(x'_1) \cdots \delta \psi_{i'_m \alpha'_m}(x'_m) \delta \phi_{\beta_1}(y_1) \cdots \delta \phi_{\beta_n}(y_n)} \Big|_{\phi_c = \bar{\phi}_c}. \quad (106)$$

In the above definition, it is understood that after performing the $(2m+n)$ -fold derivative, all fields have to be set to zero except the classical component of the bosonic field, which is set to its possibly nonzero expectation value $\bar{\phi}_c(x)$. This notation has already been employed in Eqs. (85) and (86). Further, the normalization of the partition function implies that vertex functions, which possess classical indices, only vanish identically [41].

We note at this point that, although the bosonic field ϕ has originally been introduced to eliminate the quartic fermion interaction term, the general vertex expansion (105) contains such a term (among all other higher-order vertex functions), which will inevitably be elevated to a finite value by the flow as the cutoff Λ is decreased. Thus, in hindsight, it may seem that the introduction of the bosonic field in the first place was unnecessary. Yet if the bosonic field indeed describes the dominant interaction contribution, which is expected in our case, then these newly generated terms merely represent corrections thereof and a truncation of the hierarchy of flow equations at a low order still captures the essential physics.

Besides, instead of bosonizing the interaction only once at the ultraviolet scale, one could implement a scale dependent bosonization or “flowing bosonization” scheme, which, at least partially, eliminates the four vertex also at lower scales. Such a construction, however, would alter the exact flow equation (102) and, in turn, lead to an alternative set of vertex flow equations as the one we present below, where accordingly part of the four vertex flow is shifted to the flow of other vertex functions. The flowing bosonization method could be employed to devise new truncation schemes, which may also improve the results obtained for “conventional” truncations with a fixed bosonization scale. We refer to Ref. [72] for a thorough discussion of this issue.

To obtain the hierarchy of flow equations for the vertex functions, we have to insert the expansion (105) into the exact flow equation (102) and compare coefficients. It is important to emphasize that both the vertex functions, as well as the bosonic expectation value are functions of the flowing cutoff Λ . Thus we obtain two contributions on the left-hand side of (102)

$$\begin{aligned} \partial_\Lambda \Gamma_\Lambda &= \sum_{m=0}^{\infty} \sum_{n=0}^{\infty} \frac{(-1)^m}{(m!)^2} \frac{1}{n!} \int_{x_m, x'_m} \sum_{i_m, i'_m} \sum_{\alpha_m, \alpha'_m} \int_{y_n} \sum_{\beta_n} \\ &\times \left[\partial_\Lambda \Gamma_\Lambda^{(2m,n)}(\dots; y_1 \beta_1, \dots, y_n \beta_n) - \int_y \Gamma_\Lambda^{(2m,n+1)}(\dots; y_1 \beta_1, \dots, y_n \beta_n, y_c) \partial_\Lambda \bar{\phi}_c(y) \right] \\ &\times \psi_{i_1 \alpha_1}^\dagger(x_1) \cdots \psi_{i_m \alpha_m}^\dagger(x_m) \psi_{i'_m \alpha'_m}(x'_m) \cdots \psi_{i'_1 \alpha'_1}(x'_1) \Delta \phi_{\beta_1}(y_1) \cdots \Delta \phi_{\beta_n}(y_n). \end{aligned} \quad (107)$$

In the second line, we suppressed the fermionic arguments of the vertex functions $\Gamma_\Lambda^{(2m,n)}$ and $\Gamma_\Lambda^{(2m,n+1)}$ for clarity. For the right-hand side, it is beneficial to separate the field-independent part from the field-dependent part of $\hat{\Gamma}_\Lambda^{(2)}$. Recalling the generalized Dyson equation (78), we write [34]

$$\hat{\Gamma}_\Lambda^{(2)}[\psi, \phi] = \hat{\mathcal{G}}_\Lambda^{-1} - \hat{\Sigma}_\Lambda[\psi, \phi], \quad (108)$$

with

$$\hat{\mathcal{G}}_\Lambda^{-1} = \hat{\Gamma}_\Lambda^{(2)}|_{\phi_c = \bar{\phi}_c}, \quad \hat{\Sigma}_\Lambda[\psi, \phi] = \hat{\Gamma}_\Lambda^{(2)}|_{\phi_c = \bar{\phi}_c} - \hat{\Gamma}_\Lambda^{(2)}. \quad (109)$$

Here, $\hat{\mathcal{G}}_\Lambda^{-1}$ is a 3×3 matrix in field space, which contains the unregularized inverse full propagators, see Eqs. (85) and (86), whereas $\hat{\Sigma}_\Lambda[\psi, \phi]$ is the field-dependent self-energy, which must not be confused with the (field independent) self-energy in the inverse full propagators. Now we can expand the logarithm on the right-hand side of Eq. (102) in terms of

(regularized) full propagators $(\hat{\mathcal{G}}_\Lambda^{-1} + \hat{\mathcal{R}}_\Lambda)^{-1}$ as follows:

$$\begin{aligned} \ln(\hat{\Gamma}_\Lambda^{(2)} + \hat{\mathcal{R}}_\Lambda) &= \ln(1 - (\hat{\mathcal{G}}_\Lambda^{-1} + \hat{\mathcal{R}}_\Lambda)^{-1} \hat{\Sigma}_\Lambda[\psi, \phi]) \\ &= - \sum_{n=1}^{\infty} \frac{1}{n} ((\hat{\mathcal{G}}_\Lambda^{-1} + \hat{\mathcal{R}}_\Lambda)^{-1} \hat{\Sigma}_\Lambda[\psi, \phi])^n. \end{aligned} \quad (110)$$

The desired hierarchy of flow equations is given by comparing coefficients in the expansions of (107) and (110). This can be done in a systematic way, because, by construction, the field dependent self-energy $\hat{\Sigma}_\Lambda[\psi, \phi]$ only contains terms which are at least linear in one field variable.

In the following, we present a truncated set of equations, with the further approximation that only vertices with one bosonic and two fermionic legs have been kept. The motivation for this approximation is that these structures are already present in the bare action. Accounting for the purely


bosonic three-vertex and other higher-order vertices, which are inevitably generated by the flow, is possible by using the strategy explained above. The equation for the bosonic field expectation value reads


$$\begin{aligned} & \int_{x'_1} ((V^{-1} + \Pi_\Lambda^R + R_{b,\Lambda}^R)(x_1, x'_1) \partial_\Lambda \bar{\phi}_c(x'_1) \\ & + \partial_\Lambda R_{b,\Lambda}^R(x_1, x'_1) \bar{\phi}_c(x'_1)) \\ & = -\frac{i}{2} \partial_\Lambda \sum_{\alpha, \beta} \sum_{k, l} \int_{x'_1, x'_2} G_{\Lambda, kl}^{\alpha\beta}(x'_1, x'_2) \Gamma_{\Lambda, lk}^{(2,1)}(x'_2 \beta, x'_1 \alpha; x_1 q) \\ & - \partial_\Lambda \bar{n}_\Lambda(x_1), \end{aligned} \quad (111)$$

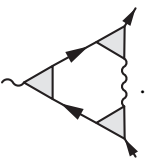
The derivation of this equation makes use of the equation of motion (77) at its extremal value $\Psi = 0, \Delta\phi = 0$, replacing the flow of the one-point function.

In the presence of a bosonic regulator, a graphical representation of the above equation is rather exceptional and not very helpful. However, for purely fermionic cutoff schemes, we recognize the typical tadpole structure, also known as Hartree diagrams, by applying $(V^{-1} + \Pi_\Lambda^R)^{-1}$ on both sides of the equation. Further note the counterterm flow on the right-hand side. It is the only location where the background charge density $\bar{n}(x)$ enters the flow equations explicitly. We can understand its presence here by considering exemplarily the space-time translation invariant system at finite density. In that case, the first term on the right-hand side is finite and closely related to the charge carrier density. (In fact, in the simple truncation scheme where the three-vertex flow is neglected it is identical to the charge carrier density.) In turn, this would imply that the expectation value $\bar{\phi}_c$ has to be finite. The counterterm, however, cancels the finite contribution on the right-hand side at any scale, such that the expectation value is consistently removed from the theory and all tadpole diagrams with it. In other physical situations, depending on the experimental setup, the counterterm flow has to be constructed by further physical considerations.

We here show the flow equations for the fermionic self-energy, bosonic polarization and the three-vertex in their graphical form only. Their explicit analytical form is given in Appendix,

$$\partial_\Lambda \hat{\Sigma}_\Lambda = i \partial_\Lambda \left(\text{Diagram 1} + \text{Diagram 2} \right), \quad (112)$$


$$\partial_\Lambda \Pi_\Lambda = \frac{i}{2} \partial_\Lambda \left(\text{Diagram 3} \right), \quad (113)$$


$$\partial_\Lambda \Gamma_\Lambda^{(2,1)} = i \partial_\Lambda \left(\text{Diagram 4} \right). \quad (114)$$


In these diagrams, the straight line corresponds to a fermionic full propagator, the wiggly line to a bosonic full propagator, the triangle to a vertex and the crossed circle to the bosonic field expectation value. The dot above the crossed circle denotes the scale derivative acting on the expectation value. Sum-

mation over discrete degrees of freedom (including Keldysh space) and integration over continuous ones is implied. The above flow equations closely resemble one-loop perturbation theory, a fact which is not surprising, since the exact flow equation (102) has a one-loop structure.

As mentioned earlier, in a genuine nonequilibrium setting one has to solve the system of flow equations, truncated at the desired level, self-consistently together with the quantum kinetic equations. In order to devise a sensible and consistent truncation, one has to supplement these equations by an analysis of (modified) Ward identities [73]. The latter connect various correlation functions to one another as a consequence of underlying continuous symmetries (e.g., charge conservation), which should be respected by the truncated flow. This issue is not special to the nonequilibrium fRG in particular, but applies to all nonperturbative methods irrespective of the initial state. We will comment further on the importance of Ward identities in Sec. IV C.

By construction, the single-scale derivative ∂_Λ appearing in the above expressions does not act on the vertex functions, but only on the regulator occurring in the expressions for the internal full propagators [such as the factor $G_{\Lambda, kl}^{\alpha\beta}$ in Eq. (111)]. In other words, ∂_Λ is a scale-derivative at constant self-energy, which yield what is known in the literature as single-scale propagators [34,39]:

$$\partial_\Lambda \hat{G}_\Lambda = -\hat{G}_\Lambda \partial_\Lambda \hat{R}_{f,\Lambda} \hat{G}_\Lambda \equiv \hat{S}_{f,\Lambda}, \quad (115)$$

$$\partial_\Lambda \mathbf{D}_\Lambda = -\mathbf{D}_\Lambda \partial_\Lambda 2\mathbf{R}_{b,\Lambda} \mathbf{D}_\Lambda \equiv \mathbf{S}_{b,\Lambda}. \quad (116)$$

Graphically, the single-scale propagators are often depicted as a (straight or wiggly) line with a slash. They have the same trigonal structure as the flowing propagators:

$$\hat{S}_{f,\Lambda} = \begin{pmatrix} \hat{S}_{f,\Lambda}^K & \hat{S}_{f,\Lambda}^R \\ \hat{S}_{f,\Lambda}^A & 0 \end{pmatrix}, \quad \mathbf{S}_{b,\Lambda} = \begin{pmatrix} \mathbf{S}_{b,\Lambda}^K & \mathbf{S}_{b,\Lambda}^R \\ \mathbf{S}_{b,\Lambda}^A & 0 \end{pmatrix}. \quad (117)$$

The advantage of using the single-scale derivative is that the computational effort to arrive at the vertex flow equations as well as their analysis is greatly reduced. The reason being, in particular, that ∂_Λ obeys the product rule for differentiation, according to which, at the graphical level, for each internal line on the right-hand side of Eqs. (112)–(114) the single-scale derivative produces an additional equivalent term, where the corresponding line has been substituted by a single-scale propagator. Therefore one may perform all analytical manipulations within the integrals first and apply the scale derivative afterwards.

We close this section by discussing the role of correlated initial states in the above set of exact flow equations. Recall from Sec. II B that correlated initial states manifest themselves as higher-order terms in the expansion of the correlation functional $K_\rho[\psi]$, see Eq. (32). The kernels of this expansion would appear within the effective action Γ_Λ as a contribution to the respective higher-order vertex function in the expansion (105) already at the initial scale Λ_0 [64]. Since a common truncation strategy of the infinite hierarchy of flow equations is to keep only those vertices that are already present in the bare action, the number of flow equations, which should be considered for correlated initial states, grows rapidly. Even for the simplest

possible non-Gaussian extension, which is a quartic term in the fermionic correlation functional, the analysis is considerably impeded. First, one would have to keep the four-vertex contribution to the fermionic self-energy flow, and second it should be revised, if it is justifiable to neglect the four-vertex flow entirely or if at least the flow of some dominant interaction channel has to be taken into account. Owing to the complicated structure of the flow equations, it becomes clear that the study of non-Gaussian initial correlations is practically limited to a low order [74]. On the other hand, the field is vastly unexplored and may lead to interesting new physical effects. In any case, the nonequilibrium functional renormalization group as we presented above is an excellent framework for such an undertaking.

IV. THERMAL EQUILIBRIUM

As a first application and a test of the methods developed in the previous section, we now apply the general nonequilibrium formalism to the equilibrium case and show how the results of the Matsubara imaginary-time formalism are recovered. In thermal equilibrium, physical observables do not depend on time. In particular, the reference time t_0 drops out in any calculation, so that the limit $t_0 \rightarrow -\infty$ may be taken at the beginning of the calculation and a Fourier transform to frequency space can be performed. In contrast to the Matsubara formalism, the frequencies in the Keldysh formulation are real and continuous, which removes the need for an analytical continuation at the end of a calculation. The temperature dependence enters through the solution of the kinetic equations and the fluctuation-dissipation theorem, which will be discussed below.

In the following, we further restrict ourselves to spatially translation invariant systems, setting the external electromagnetic potentials to zero. Since the propagators and each vertex now conserve energy and momentum, the flow equations simplify considerably. We also limit ourselves to intrinsic, freestanding graphene, setting the chemical potential μ and the background charge density \tilde{n} to zero, and the dielectric constant of the medium ϵ_0 to unity. As a consequence the bosonic field expectation value and the counterterm vanish. After discussing some general aspects, we present a simple truncation scheme for the flow equations, and solve the resulting system of equations numerically for finite temperatures.

A. Fluctuation-dissipation theorem and cutoff schemes

The equilibrium state is uniquely specified by the Boltzmann statistical operator $\hat{\rho} = \exp(-\beta\hat{H})$. This particular density matrix leads to a periodicity of the fermionic and bosonic field operators along the imaginary time axis, which can be expressed by the KMS boundary conditions [61]. Eventually, these boundary conditions manifest themselves as constraining relations between the various n -point correlation functions, which is known as the fluctuation-dissipation theorem. Demanding its validity at any scale greatly reduces the numerical effort, since the flow equations themselves have to preserve these constraints. Thus the number of independent flow equations is diminished. We here concentrate on the fluctuation-dissipation relation for the connected two-point

correlators and self-energies. We refer to Refs. [75] and [76] for a more elaborate discussion.

In the Keldysh formalism, the fluctuation-dissipation theorem can be very elegantly formulated. The necessary condition for thermal equilibrium is the vanishing of the kinetic term in the quantum kinetic equations (94) and (95). Assuming that the Hermitian matrix $\hat{\mathcal{F}}_\Lambda(\vec{k}, \varepsilon)$ is proportional to the unit matrix, we thus have

$$\hat{\Sigma}_\Lambda^K(\vec{k}, \varepsilon) = \mathcal{F}_\Lambda(\vec{k}, \varepsilon)(\hat{\Sigma}_\Lambda^R(\vec{k}, \varepsilon) - \hat{\Sigma}_\Lambda^A(\vec{k}, \varepsilon)), \quad (118)$$

$$\Pi_\Lambda^K(\vec{q}, \omega) = \mathcal{B}_\Lambda(\vec{q}, \omega)(\Pi_\Lambda^R(\vec{q}, \omega) - \Pi_\Lambda^A(\vec{q}, \omega)). \quad (119)$$

The fluctuation-dissipation theorem states that the distribution functions \mathcal{F}_Λ and \mathcal{B}_Λ take the simple, scale independent form

$$\mathcal{F}_\Lambda(\vec{k}, \varepsilon) = \tanh\left(\frac{\varepsilon}{2T}\right), \quad (120)$$

$$\mathcal{B}_\Lambda(\vec{q}, \omega) = \coth\left(\frac{\omega}{2T}\right). \quad (121)$$

Since the equilibrium solution is unique, their independence of the scale Λ is crucial. Using the above solution, we can immediately write down the corresponding Keldysh propagators:

$$\hat{G}_\Lambda^K(\vec{k}, \varepsilon) = \tanh\left(\frac{\varepsilon}{2T}\right)(\hat{G}_\Lambda^R(\vec{k}, \varepsilon) - \hat{G}_\Lambda^A(\vec{k}, \varepsilon)), \quad (122)$$

$$D_\Lambda^K(\vec{q}, \omega) = \coth\left(\frac{\omega}{2T}\right)(D_\Lambda^R(\vec{q}, \omega) - D_\Lambda^A(\vec{q}, \omega)). \quad (123)$$

Whereas the fluctuation-dissipation theorem is generally valid in thermal equilibrium for the physical limit $\Lambda \rightarrow 0$, its validity at all scales Λ is not automatic. Requiring Eqs. (121) for arbitrary cutoff Λ puts strong constraints on the choice of the infrared regulators. As discussed in the previous section, these constraints have to be implemented together with the restrictions that ensure that the cutoff scheme preserves causality and respects all the symmetries of the model.

Following Ref. [40], we now describe a regularization scheme that meets these conditions. We have adopted this regularization scheme for our numerical calculations, in order to facilitate the comparison of our results and those of Ref. [40]. In this scheme, regularization is applied in the fermionic sector only,

$$R_{b,\Lambda}^{R/A/K} = 0. \quad (124)$$

As a consequence, the bosonic single-scale propagators vanish identically. For the fermionic degrees of freedom, we consider a regulator with momentum dependence only,

$$\begin{aligned} \hat{R}_{f,\Lambda}^R(\vec{k}, \varepsilon) &= \hat{R}_{f,\Lambda}^A(\vec{k}, \varepsilon) = \hat{G}_{0,\Lambda}^{-1}(\vec{k}, \varepsilon) - \hat{G}_0^{-1}(\vec{k}, \varepsilon), \\ \hat{R}_{b,\Lambda}^K(\vec{k}, \varepsilon) &= 0 \end{aligned} \quad (125)$$

with

$$\hat{G}_{0,\Lambda}^{-1}(\vec{k}, \varepsilon) = \hat{G}_0^{-1}(\vec{k}, \varepsilon)(\Theta(k - \Lambda))^{-1}. \quad (126)$$

The absence of a frequency dependence of the regulator function implies that the frequency structure of the propagators is untouched by the regularization procedure and causality is manifestly preserved. The sharp Θ -function cutoff in momentum space simplifies the flow equations even further by eliminating one of the integrations involved on their right-hand side.

Several aspects of this choice of the regulator function are worthwhile discussing. The first issue is the role of the Fermi surface. At charge neutrality, the Fermi surface consists of the points located at the K_+ and K_- points, a fact that is not altered by the interaction. This is a major simplification, because there is no need to adapt the regulators to a continuously changing Fermi surface. Since this simplification is special to the charge neutrality point, other regularization schemes may be preferable away from it, see our discussion below.

Second, the above choice of regularization function transforms the additive regularization into a multiplicative one. Such multiplicative regularizations are also common in the literature, see, e.g., Refs. [34,39]. The Keldysh regulator has been set to zero in order to guarantee the trivial initial conditions $\Gamma_{\Lambda_0} = S$. Although now the kinetic terms in the kinetic equations contain explicitly the regulators, it is still possible to obtain the scale independent equilibrium solutions of the previous section. This fact is a simple consequence of the scalar multiplicative cutoff.

At the end of Sec. III C, we discussed that a parametrization of the Keldysh regulators $\hat{R}_{f,\Lambda}^K$ and $R_{b,\Lambda}^K$ in terms of the distribution functions $\hat{\mathcal{F}}_\Lambda$ and \mathcal{B}_Λ , respectively, in principle leads to a simplification of the kinetic terms in the kinetic equations, see Eqs. (94)–(97). In this parametrization, the kinetic terms no longer explicitly contain the regularization functions. As a result the kinetic equations can be solved immediately by the above scale independent distribution functions. This fact applies to regulator functions that act in the momentum and/or frequency domain. The possibility to use cutoffs in the frequency domain that manifestly preserve causality is a major technical advantage of the Keldysh formulation and does not exist for frequency cutoffs in the imaginary-time formulation, where the causality structure is usually destroyed. Of course, in frequency-independent regularization schemes, such as the one of Eqs. (125), causality issues are avoided for both approaches. An additional advantage of a frequency cutoff in the fermionic sector is that no explicit reference to a Fermi surface needs to be made.

An example for a cutoff scheme, which incorporates all of the above mentioned properties, is the “hybridization cutoff” of Jakobs *et al.* [49,50]. In this scheme the infinitesimal regulators $\pm i0$ in the inverse bare propagators and the Keldysh blocks are elevated to cutoff dependent quantities $\pm i\Lambda$. Being essentially a frequency cutoff, the hybridization scheme is particularly useful in those cases where a momentum cutoff is not appropriate, such as graphene away from the charge neutrality point or the presence of a finite magnetic field. In both cases, the Fermi surface (if it can be defined at all) will be subject to change during the renormalization group flow, requiring a continuous adjustment of the momentum cutoff. The frequency cutoff of Refs. [49,50], on the other hand, is insensitive to a changing Fermi surface and compatible with spatially varying external fields. Another example of a frequency cutoff is the “outscattering rate cutoff” employed by Kloss and Kopietz [53]. It is similar to the hybridization cutoff, but has the important difference that the Keldysh blocks of the inverse free propagators are not regularized. In this case, the distribution functions become explicitly scale dependent and the fluctuation dissipation theorem is

manifestly violated, making the outscattering rate cutoff not suitable for an equilibrium setting.

B. Dressed flowing propagators

After having discussed the regularization scheme, we can now give explicit expressions for the dressed flowing propagators, which are central to the flow equations of the functional renormalization group. The temperature arguments of the fermionic and bosonic self-energies are suppressed in the following.

As discussed in Sec. II A, the expressions for the fermionic propagators take their simplest form in the chiral basis. Since by construction of the regulators the exact flow equation preserves chirality at all scales, the same holds true for the fermionic self-energy and the flowing propagators

$$\hat{\Sigma}_\Lambda^{R/A}(\vec{k}, \varepsilon) = \sum_{\pm} \hat{\mathcal{P}}_{\pm}(\hat{k}) \Sigma_{\pm, \Lambda}^{R/A}(k, \varepsilon), \quad (127)$$

$$\hat{G}_\Lambda^{R/A}(\vec{k}, \varepsilon) = \sum_{\pm} \hat{\mathcal{P}}_{\pm}(\hat{k}) G_{\pm, \Lambda}^{R/A}(k, \varepsilon), \quad (128)$$

where the $\hat{\mathcal{P}}_{\pm}(\hat{k})$ are the chiral projection operators, see Eq. (20). Thus the retarded and advanced chiral flowing propagators can be written in the compact form

$$\begin{aligned} G_{\pm, \Lambda}^{R/A}(k, \varepsilon) &= \frac{\Theta(k - \Lambda)}{\varepsilon \mp v_F k - \Sigma_{\pm, \Lambda}^{R/A}(k, \varepsilon)}, \\ &= \frac{\Theta(k - \Lambda)}{(\varepsilon - \Sigma_{\varepsilon, \Lambda}^{R/A}(k, \varepsilon)) \mp (v_F + \Sigma_{v, \Lambda}^{R/A}(k, \varepsilon))k}, \end{aligned} \quad (129)$$

where we have defined

$$\Sigma_{\varepsilon, \Lambda}^{R/A}(k, \varepsilon) = \frac{1}{2} (\Sigma_{+, \Lambda}^{R/A} + \Sigma_{-, \Lambda}^{R/A})(k, \varepsilon), \quad (130a)$$

$$\Sigma_{v, \Lambda}^{R/A}(k, \varepsilon) = \frac{1}{2k} (\Sigma_{+, \Lambda}^{R/A} - \Sigma_{-, \Lambda}^{R/A})(k, \varepsilon). \quad (130b)$$

Recall that the single-scale derivative only acts on the Θ function, such that the sharp momentum cutoff yields a particularly simple single-scale propagator.

The retarded and advanced propagators in the bosonic sector are given by

$$D_\Lambda^{R/A}(q, \omega) = \frac{1}{2} \frac{1}{V^{-1}(q) + \Pi_\Lambda^{R/A}(q, \omega)}, \quad (131)$$

where $V(q)$ is the two-dimensional Fourier transform of the Coulomb interaction,

$$V(q) = \frac{2\pi e^2}{q}. \quad (132)$$

The Λ dependence of the bosonic propagators is entirely determined by the flowing polarization function. By introducing the dielectric function

$$\epsilon_\Lambda^{R/A}(q, \omega) \equiv 1 + V(q) \Pi_\Lambda^{R/A}(q, \omega), \quad (133)$$

the propagators can be written in the convenient form

$$D_\Lambda^{R/A}(q, \omega) = \frac{1}{2} \frac{V(q)}{\epsilon_\Lambda^{R/A}(q, \omega)}. \quad (134)$$

C. Fermi velocity and static dielectric function at finite temperature

We now proceed to solve the truncated flow equations using a finite-temperature real-time analog of the truncation scheme employed by Bauer *et al.* [40]. We consider intrinsic graphene, so that the bosonic field expectation value ϕ_c and the counterterm are absent. The system of equations (112)–(114), see also Appendix, is further simplified by neglecting the flow of the three-vertex functions entirely, keeping these at their initial values at $\Lambda = \Lambda_0$. We also neglect the Λ dependence of the scalar self energy $\Sigma_{\varepsilon,\Lambda}^{R/A}$ of Eq. (130a), as well as

the frequency dependence of the scalar self energy $\Sigma_{v,\Lambda}^{R/A}$ of Eq. (130b). These approximations lead to well-defined Λ -dependent poles of the single-particle propagators (129) at

$$\xi_\Lambda(k) = v_\Lambda(k)k, \quad (135)$$

where the renormalized Fermi velocity is given by

$$v_\Lambda(k) = v_F + \Sigma_{v,\Lambda}(k). \quad (136)$$

Finally, we neglect the frequency dependence of the dielectric function $\epsilon_\Lambda^{R/A}(q, \omega) = \epsilon_\Lambda(q)$. As a consequence the bosonic Keldysh propagator remains identically zero during the flow.

The complete truncation scheme can be conveniently expressed if we parametrize the effective action as

$$\begin{aligned} \Gamma_\Lambda[\Psi, \phi] = & \int_{\vec{k}, \varepsilon} \Psi^\dagger(\vec{k}, \varepsilon) \sigma_0^s \otimes \begin{pmatrix} 0 & \Sigma_0(\varepsilon - i0) + v_\Lambda(k) \vec{\Sigma} \cdot \vec{k} \\ \Sigma_0(\varepsilon + i0) + v_\Lambda(k) \vec{\Sigma} \cdot \vec{k} & 2i0 \tanh\left(\frac{\varepsilon}{2T}\right) \Sigma_0 \end{pmatrix} \Psi(\vec{k}, \varepsilon) \\ & + \int_{\vec{q}, \omega} \phi^\top(-\vec{q}, -\omega) \begin{pmatrix} 0 & (V(q)/\epsilon_\Lambda(q))^{-1} \\ (V(q)/\epsilon_\Lambda(q))^{-1} & 0 \end{pmatrix} \phi(\vec{q}, \omega) \\ & - \int_{\vec{k}, \varepsilon, \vec{q}, \omega} \Psi^\dagger(\vec{k} + \vec{q}, \varepsilon + \omega) \begin{pmatrix} \phi_q(\vec{q}, \omega) & \phi_c(\vec{q}, \omega) \\ \phi_c(\vec{q}, \omega) & \phi_q(\vec{q}, \omega) \end{pmatrix} \Psi(\vec{k}, \varepsilon). \end{aligned} \quad (137)$$

We note that if one wishes to go beyond the static approximation of Eq. (137), and include the dynamical effects of plasmons and quasiparticle wave-function renormalization, one should not neglect the three-vertex flow entirely. A naive extension, where only the renormalization of $\Sigma_{\varepsilon,\Lambda}^{R/A}$ and the frequency dependencies of $\Sigma_{v,\Lambda}^{R/A}$ and $\epsilon_\Lambda^{R/A}$ are taken into account, is not sufficient. As Bauer *et al.* have shown [40], one should at least include the marginal part of the three-vertex in the analysis. In that case, the vertex flow reduces to a differential form of a Ward identity, leading to a partial cancellation of fermionic self-energy- and vertex-corrections. Neglecting the vertex flow would violate the Ward identity and lead to an inconsistency in the flow of the quasiparticle wave-function renormalization.

The sequence of approximations described above results in two coupled flow equations, one for the Fermi velocity $v_\Lambda(k)$ and one for the static dielectric function $\epsilon_\Lambda(q)$. The approximations are self-consistent in the sense that neither a quasiparticle wave-function renormalization nor a frequency dependence of the dielectric function are generated during the flow. Within the truncation of the effective action given above, we obtain the flow equation for the Fermi velocity

$$\Lambda \partial_\Lambda v_\Lambda(k) = -\frac{e^2}{2\pi} \frac{\Lambda}{k} \int_0^\pi d\varphi \tanh\left(\frac{\xi_\Lambda(\Lambda)}{2T}\right) \frac{\cos\varphi}{\sqrt{1 + \left(\frac{k}{\Lambda}\right)^2 - 2\frac{k}{\Lambda}\cos\varphi}} \frac{1}{\epsilon_\Lambda(\Lambda\sqrt{1 + \left(\frac{k}{\Lambda}\right)^2 - 2\frac{k}{\Lambda}\cos\varphi})}, \quad (138)$$

whereas the flow equation for the static dielectric function takes the form

$$\begin{aligned} \Lambda \partial_\Lambda \epsilon_\Lambda(q) = & -\frac{2e^2}{\pi} q \int_0^{\pi/2} d\varphi \Theta\left(\cos\varphi + \frac{2\Lambda}{q} - 1\right) \frac{1}{\sqrt{\left(1 + \frac{q}{2\Lambda}\cos\varphi\right)^2 - \left(\frac{q}{2\Lambda}\right)^2}} \\ & \times \left[\left(\tanh\left(\frac{\xi_\Lambda(\Lambda)}{2T}\right) + \tanh\left(\frac{\xi_\Lambda(\Lambda + q\cos\varphi)}{2T}\right) \right) \frac{\sin^2\varphi}{\xi_\Lambda(\Lambda) + \xi_\Lambda(\Lambda + q\cos\varphi)} \right. \\ & \left. + \left(\tanh\left(\frac{\xi_\Lambda(\Lambda)}{2T}\right) - \tanh\left(\frac{\xi_\Lambda(\Lambda + q\cos\varphi)}{2T}\right) \right) \frac{(2\Lambda/q + \cos\varphi)^2 - 1}{\xi_\Lambda(\Lambda) - \xi_\Lambda(\Lambda + q\cos\varphi)} \right]. \end{aligned} \quad (139)$$

The derivation of Eq. (139) requires the use of elliptic coordinates. At the initial scale $\Lambda = \Lambda_0$ the fermionic and bosonic self-energies vanish, which translates to the initial conditions $v_{\Lambda_0}(k) = v_F, \epsilon_{\Lambda_0}(k) = 1$. In the limit $T \rightarrow 0$, our equations reduce to the expressions given in Ref. [40]. The temperature dependence enters the Fermi velocity flow equation only as a simple factor in the integrand, due to the absence of plasmonic effects. The temperature dependence of the dielectric function flow equation, on the other hand, is more complicated. The two contributions in the second and third lines of Eq. (139) can be

traced back to inter- and intraband transitions, respectively. At $T = 0$, the valence band is fully occupied, while the conduction band is empty. Thus the fermionic phase space for intraband transitions is Pauli blocked and only interband transitions contribute to the polarization function. A finite temperature, however, lifts this Pauli blockade by opening the intraband phase space for momenta of the order T , leading to the additional term in the third line.

The above equations have been solved numerically for different temperatures with the dimensionless coupling

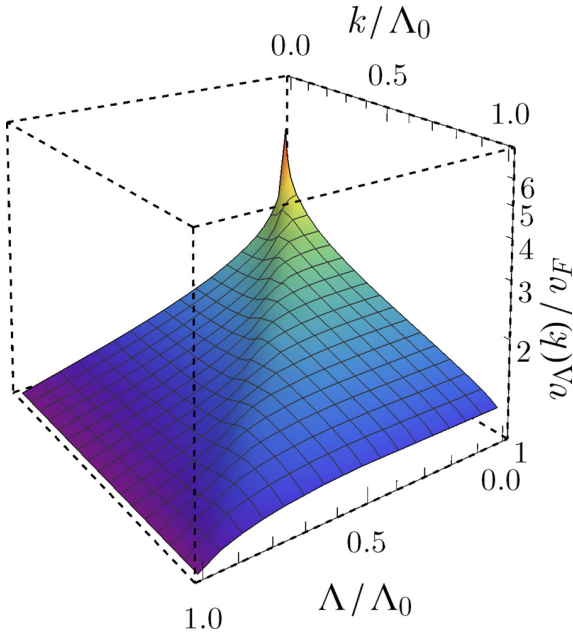


FIG. 2. Cutoff dependent Fermi velocity $v_\Lambda(k)$ at temperature $T/v_F\Lambda_0 = 10^{-3}$. The physical limit corresponds to $\Lambda = 0$. Note that the renormalized Fermi velocity is finite at $\Lambda = k = 0$. Further observe that the figure is almost symmetric around $k = \Lambda$, suggesting that the momentum k acts as an infrared cutoff for the Fermi velocity viewed as a function of Λ in the same way as Λ acts as a cutoff for the Fermi velocity as a function of k .

constant $\alpha = e^2/v_F = 2.2$. Specifically, they have been rewritten as pure Volterra integral equations of the second kind by integration over the scale variable Λ , see Ref. [77], and using the initial conditions. We discretized the parameter spaces by nonuniform, adaptive grids, which were interpolated linearly when intermediate values were required. The case $k = 0$ could not be included in the grids due to divergent terms. Therefore we built the grids down to $k/\Lambda_0 = 10^{-5}$ and extrapolated for lower momenta if necessary. The coupled system of integral equations has been solved iteratively, starting from the initial values $v_\Lambda(k) = v_F$ and $\epsilon_\Lambda(q) = 1$ for the zero-temperature calculation and continuing the iteration until a self-consistent solution was obtained. During the iterative procedure, the grids were occasionally refined according to a gradient criterion. For finite temperature we used previously computed and converged results at a nearby temperature as an initial value in order to minimize the computation time.

The results of the numerical integration for the Fermi velocity $v_\Lambda(k)$ in its full parameter space is shown exemplarily for the reduced temperature $T/v_F\Lambda_0 = 10^{-3}$ in Fig. 2, whereas Fig. 3 summarizes our result in the physical limit $\Lambda = 0$ for all temperatures we considered. The corresponding results for the dielectric function $\epsilon_\Lambda(q)$ are shown in Figs. 4 and 5, respectively.

At zero temperature, the Fermi velocity shows the well-known logarithmic renormalization, which has been reported previously by many authors within one-loop perturbation theory [1,17,20]. Our numerical result could be fitted by

$$v(k) = A + B \ln(\Lambda_0/k), \quad (140)$$

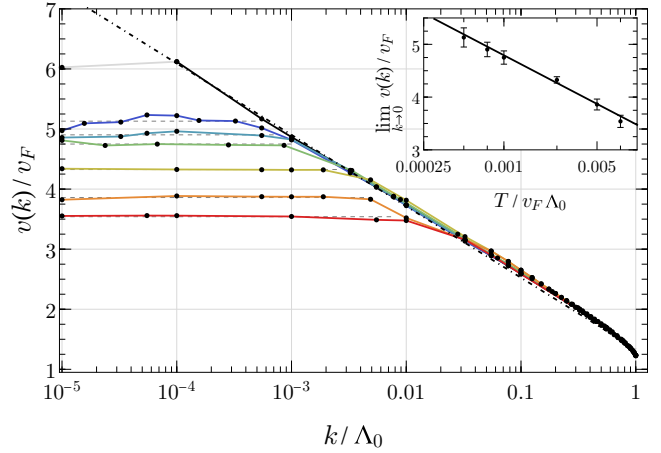


FIG. 3. Fermi velocity versus momentum k , for temperatures $T/v_F\Lambda_0 = 0, 5.0 \times 10^{-4}, 7.5 \times 10^{-4}, 1.0 \times 10^{-3}, 2.5 \times 10^{-3}, 5.0 \times 10^{-3}$, and 7.5×10^{-3} (top to bottom data sets). The inset shows the logarithmic temperature dependence of the Fermi velocity at $k = 0$. The single data point at $v(10^{-5})/v_F = 6$ shows a nonphysical deviation from the logarithmic divergence at zero temperature, indicating that our numerical algorithm breaks down there. This behavior could be expected, since the grids have only been built down to $k/\Lambda_0 = 10^{-5}$. At finite temperatures, similar convergence problems occur upon approaching the lower grid cutoff $T/v_F\Lambda_0 \approx 10^{-5}$.

with $A = 1.34(4)$ and $B = 0.52(1)$, which coincides with the result of Bauer *et al.* [40] within numerical accuracy. At nonzero temperature, we find that v is finite for $k \rightarrow 0$, while for large momenta the Fermi velocity merges into the logarithmic behavior found at zero temperature. This fact can be readily explained by the presence of thermally excited charge

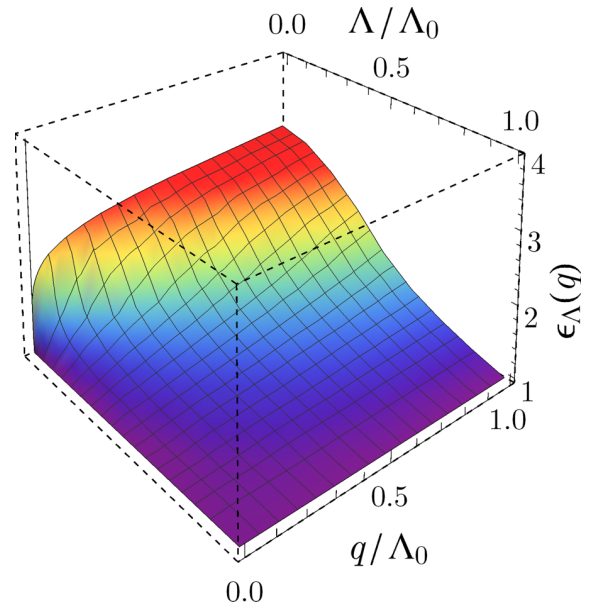


FIG. 4. Cutoff dependent dielectric function $\epsilon_\Lambda(q)$ at temperature $T/v_F\Lambda_0 = 10^{-3}$. Note the sharp feature at $\Lambda = 0$ for momenta $q \lesssim T/v_F$.

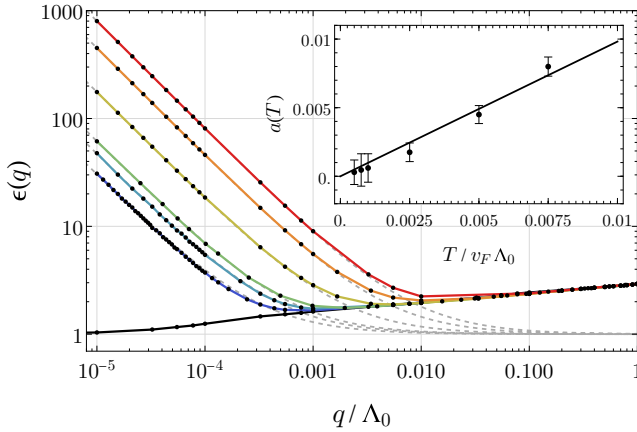


FIG. 5. Dielectric function as a function of momentum q for temperatures $T/v_F\Lambda_0 = 0, 5.0 \times 10^{-4}, 7.5 \times 10^{-4}, 1.0 \times 10^{-3}, 2.5 \times 10^{-3}, 5.0 \times 10^{-3},$ and 7.5×10^{-3} (bottom to top data sets). For momenta q/Λ_0 below the reduced temperature $\tilde{T} = T/v_F\Lambda_0$ our data are consistent with the $1/q$ dependence predicted by perturbation theory. The temperature dependence of the prefactor could be fitted by $\epsilon(q) = 1 + a(\tilde{T})\Lambda_0/q$, indicated by dashed lines, where $a(\tilde{T})$ is a linear function as shown in the inset.

carriers, which can screen the bare Coulomb interaction at long wavelengths. Thus the effective Coulomb interaction becomes short ranged, cutting off the divergence at small momenta. The larger the temperature the more charge carriers are excited, leading to an enhancement in the suppression of the divergence. Indeed, our numerics show that this suppression is a logarithmic function of the temperature, which could be fitted by

$$\lim_{k \rightarrow 0} v(k) = C + D \ln(v_F\Lambda_0/T), \quad (141)$$

with $C = 0.84(33)$ and $D = 0.57(6)$. For momenta $k \gg T/v_F$, the long-wavelength screening of the Coulomb interaction becomes irrelevant and the Fermi velocity asymptotically approaches the zero-temperature value.

A well known issue in the comparison with experimental data is the value of the ultraviolet cutoff Λ_0 . Since we already fixed the numerical value of the bare Fermi velocity by setting $\alpha = 2.2$, the cutoff Λ_0 can be used as a fit parameter. Alternatively, one could take the ultraviolet cutoff to be fixed (given by the inverse lattice spacing), and instead use α , i.e., v_F , as a fit parameter. The drawback of the latter method, however, is that the dimension of the free parameter space would be enlarged. One would have to solve the flow equations for different temperatures *and* couplings α , which would increase the numerical effort even further.

The zero-temperature result for the dielectric function $\epsilon(q)$ is only very weakly momentum dependent for large momenta, while for $q \rightarrow 0$ it logarithmically approaches unity, in contrast to the momentum independence of the one-loop prediction. This behavior is in accord with the result of Bauer *et al.* [40], although we observe a systematic deviation to slightly larger values at momenta of order unity. This fact may be explained by differences in the numerical implementation of the flow equations. At finite temperature, however, a strong temperature dependence, proportional to $1/q$, sets in for momenta $q \lesssim T/v_F$. The emergence of the power-law

divergence for small momenta can be easily understood from perturbation theory, already at the one-loop level [58,78,79]. In the regime $q \ll T/v_F$, the static polarization function becomes momentum independent, scaling linearly with temperature, which results in the one-loop dielectric function

$$\epsilon_{1\text{-loop}}(q) = 1 + a(T)\frac{\Lambda_0}{q}, \quad v_F q \ll T, \quad (142)$$

with

$$a(T) = 8 \ln 2 \alpha \frac{T}{v_F \Lambda_0}. \quad (143)$$

The divergence at zero momentum is a consequence of the presence of thermally excited charge carriers, screening the bare Coulomb interaction. Our numerical calculations qualitatively confirm this one-loop picture as they reproduce the $1/q$ dependence as well as the linear temperature dependence of the prefactor $a(T)$. On the quantitative level, however, we find a considerable deviation in the numerical value of the proportionality constant, the numerics could be fitted by $a(T) = 0.98(5)T/v_F\Lambda_0$, which is about one order of magnitude lower than the one-loop prediction. This discrepancy can be understood by considering the fact that a one-loop calculation employs only noninteracting propagators, while the fRG result is obtained by a self-consistent calculation, using fully interacting propagators, such that a strong renormalization of the former result is to be expected.

In the high-temperature limit, we expect a strong screening of the Coulomb interaction, implying the absence of velocity renormalization, due to its logarithmic suppression with increasing temperatures, and hence the emergence of a free field fix point. However, such an asymptotically free fix point has little practical relevance, since in that regime the electron-phonon interaction should be taken into account in a realistic model, which would drive the system into a crumpled phase [80] and eventually lead to an instability of the underlying honeycomb lattice. In other words, graphene would have melted long before the free field fix point would have been reached.

V. CONCLUSIONS

In this paper, we formulated a nonperturbative nonequilibrium theory for Dirac electrons interacting via the Coulomb interaction, which is based on the Keldysh functional renormalization group. Our theory should be a good description of the low-energy properties of graphene.

The essential parts of the theoretical description are the exact Dyson equations for the real-time Fermi-Bose theory, from which the quantum kinetic equations follow, as well as an exact flow equation for the effective action. The functional flow equation has been transformed into a hierarchy of ordinary coupled integrodifferential equations, describing the flow of the one-particle irreducible vertex functions, by means of a vertex expansion. This hierarchy has to be solved approximately using a self-consistent truncation scheme. As a test of our formalism, we reproduced the results for the Fermi velocity renormalization and the dielectric function at zero temperature that were previously obtained by Bauer

et al. [40] using the imaginary-time Matsubara formalism, and we extended these results to finite temperature.

The research provided in this paper can be extended into several different ways. For equilibrium problems, one may take into account dynamical effects, yielding the dynamical polarization function and quasiparticle wave function renormalization. This extension would go hand in hand with a nonperturbative study of collective plasmon modes. A purely bosonic cutoff combined with exact Schwinger-Dyson equations, as recently proposed by Sharma and Kopietz in Ref. [69], would be highly advantageous for such an undertaking.

Another interesting extension is to investigate modifications of the isotropic Dirac spectrum, such as trigonal warping [1], or anisotropies in strained graphene [81]. Both phenomena would require the modification of the noninteracting Hamiltonian H_f , see Eq. (2), but the general structure of the calculation is not modified. Furthermore, it would be interesting to study the fate of gaps, or masses, in the spectrum under the renormalization group flow. A particularly exciting scenario is the possibility of a *spontaneous* mass generation [17], for which one starts from an infinitesimal mass term at the initial scale $\Lambda = \Lambda_0$, which may be elevated to a finite value at the end of the flow. This extension, too, requires no modifications of the general formalism, as the vertex expansion in Sec. III E is sufficiently general enough to cope with such situations.

The application of our formalism to extrinsic graphene requires a different cutoff scheme than the one we used here, since the presence of a finite Fermi surface is incompatible with the use of a simple “static” momentum cutoff in the fermionic sector. One possibility would be to modify the momentum cutoff to “dynamically” adapt to a continuously changing Fermi surface at each scale Λ . However, this modification would complicate the flow equations considerably and is therefore not convenient [34]. An alternative cutoff scheme, circumventing this difficulty, is the causality preserving frequency cutoff of Jakobs *et al.* [49,50], which may be used either within the simple rotation invariant conical Dirac spectrum considered in this work or within one of the modifications of the bare spectrum mentioned above. Moreover, as explained at the end of Sec. IV A, frequency cutoffs are advantageous for the study of external magnetic fields in the (integer) quantum Hall regime, since then momentum is not a well-defined quantum number, and hence cannot be employed as a flow parameter.

Whereas the use of the Keldysh formulation is technically convenient (but not essential) for equilibrium problems, because it avoids the necessity of an analytical continuation, for nonequilibrium problems the Keldysh formalism is essential. Possible applications of the formalism developed here are non-thermal fixed points, thermalization, and quantum transport in linear or even beyond linear response. Another issue of interest is the topic of non-Gaussian initial correlations, for which we outlined their implementation within our theoretical framework, although an actual application is beyond the scope of the present article.

For applications to realistic graphene samples, not only interactions, but also disorder has to be taken into account. This applies to quantum transport problems in particular, see Refs. [42,82,83]. The Keldysh formulation we presented here is perfectly suited for such a research programme. As is

well-known the normalization of the partition function can be exploited to perform the impurity average directly on the level of the partition function. There is no need for supersymmetry or the replica trick in the Matsubara formalism. For Gaussian correlated disorder the averaging procedure leads to a quartic fermionic pseudo-interaction term. Especially at the charge neutrality point the deviations from the usual Fermi-liquid behavior should be strongly pronounced. Similarly to the Coulomb interaction treated here, the theory at this point lacks a small parameter and conventional approximation strategies, such as the self-consistent Born approximation (SCBA), break down. An immediate consequence of the breakdown of the SCBA is that a rigorous derivation of a (diffusive) nonlinear sigma model along the standard lines [42] can no longer be justified, as both approaches rely on the existence of the same expansion parameter, $1/E_F\tau$. (E_F is the Fermi energy, being identically zero at the charge neutrality point, and τ is the elastic scattering time.) Since the common truncation strategies of the infinite hierarchy of flow equations do not rely on the existence of a smallness parameter, the Keldysh fRG offers the necessary tools to go beyond these approximations in a consistent manner [84].

As a closing remark, we want to point out that the good agreement between the functional forms of the momentum and temperature dependencies of the one-loop perturbation theory and the functional renormalization group results presented here may come as a surprise, since there is no small parameter justifying a perturbative approach. Indeed, a two-loop calculation for the Fermi velocity already shows the lack of convergence of the perturbative approach, as it predicts a logarithmic decrease for small momenta [23]. Nevertheless, the exact flow equation (102) has a one-loop structure, so it becomes clear that some features of one-loop perturbation theory are qualitatively reproduced. For the future applications discussed above it is, therefore, reasonable to expect that the results derived from a perturbative one-loop calculation at least hint into the right direction, although not all features of the exact theory are reproduced quantitatively correctly. In the end, quantitatively accurate results can be expected only by more sophisticated nonperturbative approaches, such as the functional renormalization group developed here.

ACKNOWLEDGMENTS

We want to thank Piet Brouwer for support in the preparation of the manuscript and for discussions, as well as Severin Jakobs, Peter Kopietz, Johannes Reuter, and Georg Schwieter for helpful discussions. This work is supported by the German Research Foundation (DFG) in the framework of the Priority Program 1459 “Graphene.”

APPENDIX: ANALYTICAL FORM OF THE VERTEX FLOW EQUATIONS

In this Appendix, we give the explicit analytical form of the flow equations for the fermionic self-energy, bosonic polarization, and the three-legged Fermi-Bose vertex. For completeness sake we also state the flow equation for the bosonic expectation value here again. We emphasize once

more that the purely bosonic three-vertex, as well as all higher-order vertices have already been neglected.

We employ here a condensed notation, where the numerical indices such as 1 and 1' represent space-time coordinates $x_1 = (\vec{r}_1, t_1)$ and $x'_1 = (\vec{r}'_1, t'_1)$, respectively, and the integration sign with a prime denotes integration over all primed space-time coordinates. Besides, the three-vertices are written in the compact form $\Gamma_{\Lambda}^{(2,1)}(1i\alpha, 2j\beta; 3\gamma) =$

$\Gamma_{\Lambda, ij}^{\alpha\beta\gamma}(1, 2; 3)$. As explained in Sec. III E, latin indices denote the internal degrees of freedom of the fermions (sublattice, valley, spin), and greek letters denote the Keldysh degrees of freedom (classical and quantum). In the following, we also omit the Λ indices for brevity, since all quantities appearing here are scale dependent (except for the bare Coulomb interaction V), and thus there can be no confusion.

1. Field expectation value

$$\int' ((V^{-1} + \Pi^R + R_b^R)(1, 1')\partial_{\Lambda}\bar{\phi}_c(1') + \partial_{\Lambda}R_b^R(1, 1')\bar{\phi}_c(1')) = -\frac{i}{2}\vartheta_{\Lambda} \sum_{\alpha, \beta} \sum_{k, l} \int' G_{kl}^{\alpha\beta}(1', 2')\Gamma_{lk}^{\beta\alpha q}(2', 1'; 1) - \partial_{\Lambda}\bar{n}(1), \quad (\text{A1})$$

2. Self-energy

$$\partial_{\Lambda}\Sigma_{ij}^{\alpha\beta}(1, 2) = \int' \Gamma_{ij}^{\alpha\beta c}(1, 2; 1')\partial_{\Lambda}\bar{\phi}_c(1') + i\vartheta_{\Lambda} \sum_{\gamma_1, \gamma_2, \gamma_3, \gamma_4} \sum_{k, l} \int' \Gamma_{ik}^{\alpha\gamma_1\gamma_4}(1, 1'; 4')G_{kl}^{\gamma_1\gamma_2}(1', 2')\Gamma_{lj}^{\gamma_2\beta\gamma_3}(2', 2; 3')D^{\gamma_3\gamma_4}(3', 4'), \quad (\text{A2})$$

3. Polarization

$$\partial_{\Lambda}\Pi^{\alpha\beta}(1, 2) = \frac{i}{2}\vartheta_{\Lambda} \sum_{\gamma_1, \gamma_2, \gamma_3, \gamma_4} \sum_{k, l, m, n} \int' G_{kl}^{\gamma_1, \gamma_2}(1', 2')\Gamma_{lm}^{\gamma_2\gamma_3\alpha}(2', 3'; 1)G_{mn}^{\gamma_3, \gamma_4}(3', 4')\Gamma_{nk}^{\gamma_4, \gamma_2\beta}(4', 1'; 2), \quad (\text{A3})$$

4. 3-vertex

$$\partial_{\Lambda}\Gamma_{ij}^{\alpha\beta\gamma}(1, 2; 3) = i\vartheta_{\Lambda} \sum_{\gamma_i} \sum_{k, l, m, n} \int' \Gamma_{ik}^{\alpha\gamma_1\gamma_6}(1, 1'; 6')\Gamma_{nj}^{\gamma_4\gamma_2\gamma_5}(4', 2; 5')\Gamma_{lm}^{\gamma_2\gamma_3\gamma_3}(2', 3'; 3)G_{kl}^{\gamma_1\gamma_2}(1', 2')G_{mn}^{\gamma_3\gamma_4}(3', 4')D^{\gamma_5\gamma_6}(5', 6'). \quad (\text{A4})$$

Recall that in the bare action only four of the above 3-vertices are present, namely the ones with the Keldysh indices qcc, qcc, ccq, qqg being all equal to unity. The remaining three ones, with the Keldysh indices qqc, ccq, qcc , are generated during the flow, while the ccc vertex is constrained to vanish at all scales. Therefore we state in the following a further truncated set of the above equations, where only the four 3-vertices present in the bare action have been kept. These equations were the starting point for our analysis of thermal equilibrium in Sec. IV.

5. Field expectation value

$$\int' ((V^{-1} + \Pi^R + R_b^R)(1, 1')\partial_{\Lambda}\bar{\phi}_c(1') + \partial_{\Lambda}R_b^R(1, 1')\bar{\phi}_c(1')) = -\frac{i}{2}\vartheta_{\Lambda} \sum_{k, l} \int' G_{kl}^K(1', 2')\Gamma_{lk}^{ccq}(2', 1'; 1) - \partial_{\Lambda}\bar{n}(1), \quad (\text{A5})$$

6. Self-energy

$$\begin{aligned} \partial_{\Lambda}\Sigma_{ij}^R(1, 2) = & \int' \Gamma_{ij}^{qcc}(1, 2; 1')\partial_{\Lambda}\bar{\phi}_c(1') + i\vartheta_{\Lambda} \sum_{k, l} \int' (\Gamma_{ik}^{qcc}(1, 1'; 4')G_{kl}^K(1', 2')\Gamma_{lj}^{ccq}(2', 2; 3')D^A(3', 4') \\ & + \Gamma_{ik}^{qcc}(1, 1'; 4')G_{kl}^R(1', 2')\Gamma_{lj}^{qcc}(2', 2; 3')D^K(3', 4')), \end{aligned} \quad (\text{A6})$$

$$\begin{aligned} \partial_{\Lambda}\Sigma_{ij}^A(1, 2) = & \int' \Gamma_{ij}^{ccq}(1, 2; 1')\partial_{\Lambda}\bar{\phi}_c(1') + i\vartheta_{\Lambda} \sum_{k, l} \int' (\Gamma_{ik}^{ccq}(1, 1'; 4')G_{kl}^K(1', 2')\Gamma_{lj}^{ccq}(2', 2; 3')D^R(3', 4') \\ & + \Gamma_{ik}^{ccq}(1, 1'; 4')G_{kl}^A(1', 2')\Gamma_{lj}^{ccq}(2', 2; 3')D^K(3', 4')), \end{aligned} \quad (\text{A7})$$

$$\begin{aligned} \partial_{\Lambda}\Sigma_{ij}^K(1, 2) = & i\vartheta_{\Lambda} \sum_{k, l} \int' (\Gamma_{ik}^{qcc}(1, 1'; 4')G_{kl}^K(1', 2')\Gamma_{lj}^{ccq}(2', 2; 3')D^K(3', 4') + \Gamma_{ik}^{qcc}(1, 1'; 4')G_{kl}^R(1', 2')\Gamma_{lj}^{qqg}(2', 2; 3')D^A(3', 4') \\ & + \Gamma_{ik}^{qqg}(1, 1'; 4')G_{kl}^A(1', 2')\Gamma_{lj}^{ccq}(2', 2; 3')D^R(3', 4')), \end{aligned} \quad (\text{A8})$$

$$\begin{aligned} 0 \stackrel{!}{=} \partial_{\Lambda}\Sigma_{ij}^Z(1, 2) = & i\vartheta_{\Lambda} \sum_{k, l} \int' (\Gamma_{ik}^{ccq}(1, 1'; 4')G_{kl}^R(1', 2')\Gamma_{lj}^{qcc}(2', 2; 3')D^R(3', 4') \\ & + \Gamma_{ik}^{ccq}(1, 1'; 4')G_{kl}^A(1', 2')\Gamma_{lj}^{ccq}(2', 2; 3')D^A(3', 4')). \end{aligned} \quad (\text{A9})$$

7. Polarization

$$\begin{aligned} \partial_\Lambda \Pi^R(1,2) = \frac{i}{2} \partial_\Lambda \sum_{k,l,m,n} \int' & (G_{kl}^K(1',2') \Gamma_{lm}^{ccq}(2',3';1) G_{mn}^R(3',4') \Gamma_{nk}^{qcc}(4',1';2) \\ & + G_{kl}^A(1',2') \Gamma_{lm}^{ccq}(2',3';1) G_{mn}^K(3',4') \Gamma_{nk}^{ccq}(4',1';2)), \end{aligned} \quad (\text{A10})$$

$$\begin{aligned} \partial_\Lambda \Pi^A(1,2) = \frac{i}{2} \partial_\Lambda \sum_{k,l,m,n} \int' & (G_{kl}^K(1',2') \Gamma_{lm}^{ccq}(2',3';1) G_{mn}^A(3',4') \Gamma_{nk}^{ccq}(4',1';2) \\ & + G_{kl}^R(1',2') \Gamma_{lm}^{qcc}(2',3';1) G_{mn}^K(3',4') \Gamma_{nk}^{ccq}(4',1';2)), \end{aligned} \quad (\text{A11})$$

$$\begin{aligned} \partial_\Lambda \Pi^K(1,2) = \frac{i}{2} \partial_\Lambda \sum_{k,l,m,n} \int' & (G_{kl}^K(1',2') \Gamma_{lm}^{ccq}(2',3';1) G_{mn}^K(3',4') \Gamma_{nk}^{ccq}(4',1';2) \\ & + G_{kl}^R(1',2') \Gamma_{lm}^{qqq}(2',3';1) G_{mn}^A(3',4') \Gamma_{nk}^{ccq}(4',1';2) \\ & + G_{kl}^A(1',2') \Gamma_{lm}^{ccq}(2',3';1) G_{mn}^R(3',4') \Gamma_{nk}^{qqq}(4',1';2)), \end{aligned} \quad (\text{A12})$$

$$\begin{aligned} 0 \stackrel{!}{=} \partial_\Lambda \Pi^Z(1,2) = \frac{i}{2} \partial_\Lambda \sum_{k,l,m,n} \int' & (G_{kl}^R(1',2') \Gamma_{lm}^{qcc}(2',3';1) G_{mn}^R(3',4') \Gamma_{nk}^{qcc}(4',1';2) \\ & + G_{kl}^A(1',2') \Gamma_{lm}^{ccq}(2',3';1) G_{mn}^A(3',4') \Gamma_{nk}^{qcc}(4',1';2)). \end{aligned} \quad (\text{A13})$$

8. 3-vertex

$$\begin{aligned} \partial_\Lambda \Gamma_{ij}^{ccq}(1,2;3) = i \partial_\Lambda \sum_{k,l,m,n} \int' & (D^K(5',6') \Gamma_{ik}^{ccq}(1,1';6') G_{kl}^A(1',2') \Gamma_{lm}^{ccq}(2',3';3) G_{mn}^R(3',4') \Gamma_{nj}^{qcc}(4',2;5') \\ & + D^R(5',6') \Gamma_{ik}^{ccq}(1,1';6') G_{kl}^K(1',2') \Gamma_{lm}^{ccq}(2',3';3) G_{mn}^R(3',4') \Gamma_{nj}^{qcc}(4',2;5') \\ & + D^A(5',6') \Gamma_{ik}^{ccq}(1,1';6') G_{kl}^A(1',2') \Gamma_{lm}^{ccq}(2',3';3) G_{mn}^K(3',4') \Gamma_{nj}^{ccq}(4',2;5')), \end{aligned} \quad (\text{A14})$$

$$\begin{aligned} \partial_\Lambda \Gamma_{ij}^{qcc}(1,2;3) = i \partial_\Lambda \sum_{k,l,m,n} \int' & (D^K(5',6') \Gamma_{ik}^{qcc}(1,1';6') G_{kl}^A(1',2') \Gamma_{lm}^{qcc}(2',3';3) G_{mn}^A(3',4') \Gamma_{nj}^{qcc}(4',2;5') \\ & + D^R(5',6') \Gamma_{ik}^{qcc}(1,1';6') G_{kl}^K(1',2') \Gamma_{lm}^{qcc}(2',3';3) G_{mn}^A(3',4') \Gamma_{nj}^{qcc}(4',2;5') \\ & + D^R(5',6') \Gamma_{ik}^{qcc}(1,1';6') G_{kl}^R(1',2') \Gamma_{lm}^{qcc}(2',3';3) G_{mn}^K(3',4') \Gamma_{nj}^{qcc}(4',2;5')), \end{aligned} \quad (\text{A15})$$

$$\begin{aligned} \partial_\Lambda \Gamma_{ij}^{qcc}(1,2;3) = i \partial_\Lambda \sum_{k,l,m,n} \int' & (D^K(5',6') \Gamma_{ik}^{qcc}(1,1';6') G_{kl}^R(1',2') \Gamma_{lm}^{qcc}(2',3';3) G_{mn}^R(3',4') \Gamma_{nj}^{qcc}(4',2;5') \\ & + D^A(5',6') \Gamma_{ik}^{qcc}(1,1';6') G_{kl}^R(1',2') \Gamma_{lm}^{qcc}(2',3';3) G_{mn}^K(3',4') \Gamma_{nj}^{ccq}(4',2;5') \\ & + D^A(5',6') \Gamma_{ik}^{qcc}(1,1';6') G_{kl}^K(1',2') \Gamma_{lm}^{qcc}(2',3';3) G_{mn}^A(3',4') \Gamma_{nj}^{ccq}(4',2;5')), \end{aligned} \quad (\text{A16})$$

$$\begin{aligned} \partial_\Lambda \Gamma_{ij}^{qqq}(1,2;3) = i \partial_\Lambda \sum_{k,l,m,n} \int' & (D^K(5',6') \Gamma_{ik}^{qcc}(1,1';6') G_{kl}^K(1',2') \Gamma_{lm}^{ccq}(2',3';3) G_{mn}^K(3',4') \Gamma_{nj}^{ccq}(4',2;5') \\ & + D^K(5',6') \Gamma_{ik}^{qcc}(1,1';6') G_{kl}^R(1',2') \Gamma_{lm}^{qqq}(2',3';3) G_{mn}^A(3',4') \Gamma_{nj}^{ccq}(4',2;5') \\ & + D^R(5',6') \Gamma_{ik}^{qqq}(1,1';6') G_{kl}^A(1',2') \Gamma_{lm}^{ccq}(2',3';3) G_{mn}^K(3',4') \Gamma_{nj}^{qcc}(4',2;5') \\ & + D^A(5',6') \Gamma_{ik}^{qcc}(1,1';6') G_{kl}^K(1',2') \Gamma_{lm}^{ccq}(2',3';3) G_{mn}^R(3',4') \Gamma_{nj}^{qqq}(4',2;5')). \end{aligned} \quad (\text{A17})$$

[1] A. H. Castro Neto, F. Guinea, N. M. R. Peres, K. S. Novoselov, and A. K. Geim, *Rev. Mod. Phys.* **81**, 109 (2009).

[2] S. Das Sarma, S. Adam, E. H. Hwang, and E. Rossi, *Rev. Mod. Phys.* **83**, 407 (2011).

[3] N. M. R. Peres, *Rev. Mod. Phys.* **82**, 2673 (2010).

[4] P. R. Wallace, *Phys. Rev.* **71**, 622 (1947).

[5] O. Klein, *Z. Phys.* **53**, 157 (1929).

[6] V. V. Cheianov and V. I. Falko, *Phys. Rev. B* **74**, 041403(R) (2006).

- [7] M. I. Katsnelson, K. S. Novoselov, and A. K. Geim, *Nat. Phys.* **2**, 620 (2006).
- [8] C. W. J. Beenakker, *Rev. Mod. Phys.* **80**, 1337 (2008).
- [9] M. I. Katsnelson, *Eur. Phys. J. B* **51**, 1434 (2006).
- [10] V. P. Gusynin and S. G. Sharapov, *Phys. Rev. Lett.* **95**, 146801 (2005).
- [11] K. S. Novoselov, A. K. Geim, S. V. Morozov, D. Jiang, M. I. Katsnelson, I. V. Grigorieva, S. V. Dubonos, and A. A. Firsov, *Nature (London)* **438**, 197 (2005).
- [12] Y. Zhang, Y.-W. Tan, H. L. Stormer, and P. Kim, *Nature (London)* **438**, 201 (2005).
- [13] K. S. Novoselov, Z. Jiang, Y. Zhang, S. V. Morozov, H. L. Stormer, U. Zeitler, J. C. Maan, and G. S. Boebinger, *Science* **315**, 1379 (2007).
- [14] J. H. Bardarson, J. Tworzydło, P. W. Brouwer, and C. W. J. Beenakker, *Phys. Rev. Lett.* **99**, 106801 (2007).
- [15] K. Nomura, M. Koshino, and S. Ryu, *Phys. Rev. Lett.* **99**, 146806 (2007).
- [16] P. San-Jose, E. Prada, and D. S. Golubev, *Phys. Rev. B* **76**, 195445 (2007).
- [17] V. N. Kotov, B. Uchoa, V. M. Pereira, F. Guinea, and A. H. Castro Neto, *Rev. Mod. Phys.* **84**, 1067 (2012).
- [18] J. P. Hobson and W. A. Nierenberg, *Phys. Rev.* **89**, 662 (1953).
- [19] J. González, F. Guinea, and M. A. H. Vozmediano, *Nucl. Phys. B* **424**, 595 (1994).
- [20] M. A. H. Vozmediano, *Philos. Trans. R. Soc., A* **369**, 2625 (2011).
- [21] D. C. Elias, R. V. Gorbachev, A. S. Mayorov, S. V. Morozov, A. A. Zhukov, P. Blake, L. A. Ponomarenko, I. V. Grigorieva, K. S. Novoselov, F. Guinea, and A. K. Geim, *Nat. Phys.* **7**, 701 (2011).
- [22] E. G. Mishchenko, *Phys. Rev. Lett.* **98**, 216801 (2007).
- [23] O. Vafek and M. J. Case, *Phys. Rev. B* **77**, 033410 (2008).
- [24] E. Barnes, E. H. Hwang, R. E. Throckmorton, and S. Das Sarma, *Phys. Rev. B* **89**, 235431 (2014).
- [25] M. S. Foster and I. L. Aleiner, *Phys. Rev. B* **77**, 195413 (2008).
- [26] J. González, F. Guinea, and M. A. H. Vozmediano, *Phys. Rev. B* **59**, R2474 (1999).
- [27] C. Popovici, C. S. Fischer, and L. von Smekal, *Phys. Rev. B* **88**, 205429 (2013).
- [28] J.-R. Wang and G.-Z. Liu, *New J. Phys.* **14**, 043036 (2012).
- [29] O. V. Gamayun, E. V. Gorbar, and V. P. Gusynin, *Phys. Rev. B* **81**, 075429 (2010).
- [30] A. Altland and B. Simons, *Condensed Matter Field Theory* (Cambridge University Press, Cambridge, UK, 2010).
- [31] C. Bagnuls and C. Bervillier, *Phys. Rep.* **348**, 91 (2001).
- [32] C. Wetterich, *Nucl. Phys. B* **352**, 529 (1991).
- [33] A research programme called the “exact renormalization group” has already been initiated in the 1970’s by F. Wegner, see Refs. [31,85,86].
- [34] W. Metzner, M. Salmhofer, C. Honerkamp, V. Meden, and K. Schönhammer, *Rev. Mod. Phys.* **84**, 299 (2012).
- [35] J. Berges, N. Tetradis, and C. Wetterich, *Phys. Rep.* **363**, 223 (2002).
- [36] C. Wetterich, *Int. J. Mod. Phys. A* **16**, 1951 (2001).
- [37] H. Gies and C. Wetterich, *Acta Phys. Slov.* **52**, 215 (2002).
- [38] H. Gies, Introduction to the Functional RG and Applications to Gauge Theories, in *Renormalization Group and Effective Field Theory Approaches to Many-Body Systems*, edited by A. Schwenk and J. Polonyi (Springer Berlin Heidelberg, Berlin, Heidelberg, 2012), pp. 287.
- [39] P. Kopietz, I. Bartosch, and F. Schütz, *Introduction to the Functional Renormalization Group* (Springer, Heidelberg, 2010).
- [40] C. Bauer, A. Rückriegel, A. Sharma, and P. Kopietz, *Phys. Rev. B* **92**, 121409 (2015).
- [41] K.-c. Chou, Z.-b. Su, B.-I. Hao, and L. Yu, *Phys. Rept.* **118**, 1 (1985).
- [42] A. Kamenev, *Field Theory of Non-Equilibrium Systems* (Cambridge University Press, Cambridge, UK, 2011).
- [43] J. Rammer, *Quantum Field Theory of Non-equilibrium States* (Cambridge University Press, Cambridge, UK, 2007).
- [44] A. A. Kovalev, K. Výborný, and J. Sinova, *Phys. Rev. B* **78**, 041305 (2008).
- [45] H. T. Ueda, A. Takeuchi, G. Tatara, and T. Yokoyama, *Phys. Rev. B* **85**, 115110 (2012).
- [46] S. Smirnov, *Phys. Rev. B* **92**, 195312 (2015).
- [47] A. Altland, Y. Gefen, and B. Rosenow, *Phys. Rev. Lett.* **108**, 136401 (2012).
- [48] R. Gezzi, T. Pruschke, and V. Meden, *Phys. Rev. B* **75**, 045324 (2007).
- [49] S. G. Jakobs, V. Meden, and H. Schoeller, *Phys. Rev. Lett.* **99**, 150603 (2007).
- [50] S. G. Jakobs, M. Pletyukhov, and H. Schoeller, *Phys. Rev. B* **81**, 195109 (2010).
- [51] J. Berges and D. Mesterházy, *Nucl. Phys. B, Proc. Suppl.* **228**, 37 (2012).
- [52] J. Berges and G. Hoffmeister, *Nucl. Phys. B* **813**, 383 (2009).
- [53] T. Kloss and P. Kopietz, *Phys. Rev. B* **83**, 205118 (2011).
- [54] T. Gasenzer and J. M. Pawłowski, *Phys. Lett. B* **670**, 135 (2008).
- [55] T. Gasenzer, S. Keßler, and J. M. Pawłowski, *Eur. Phys. J. C* **70**, 423 (2010).
- [56] E. V. Gorbar, V. P. Gusynin, V. A. Miransky, and I. A. Shovkovy, *Phys. Rev. B* **66**, 045108 (2002).
- [57] V. P. Gusynin, S. G. Sharapov, and J. P. Carbotte, *Int. J. Mod. Phys. B* **21**, 4611 (2007).
- [58] M. Schütt, P. M. Ostrovsky, I. V. Gornyi, and A. D. Mirlin, *Phys. Rev. B* **83**, 155441 (2011).
- [59] B. N. Narozhny, I. V. Gornyi, M. Titov, M. Schütt, and A. D. Mirlin, *Phys. Rev. B* **91**, 035414 (2015).
- [60] L. V. Keldysh, *Zh. Eksp. Teor. Fiz.* **47**, 1515 (1964) [*Sov. Phys. JETP* **20**, 1018 (1965)].
- [61] J. W. Negele and H. Orland, *Quantum Many-Particle Systems* (Westview Press, USA, 1998).
- [62] E. Calzetta and B. L. Hu, *Phys. Rev. D* **37**, 2878 (1988).
- [63] Actually, this holds true even for nonzero source terms provided that they are identical on both time branches as shown in Ref. [41].
- [64] J. Berges and J. Cox, *Phys. Lett. B* **517**, 369 (2001).
- [65] Y. Tanizaki, G. Fejős, and T. Hatsuda, *Prog. Theor. Exp. Phys.* (2014) 043101.
- [66] A. I. Larkin and Yu. N. Ovchinnikov, *Zh. Eksp. Teor. Fiz.* **68**, 1915 (1975) [*Sov. Phys. JETP* **41**, 960 (1975)].
- [67] We implicitly assumed here that the bare distribution function commutes with the Hermitian part of the inverse bare propagator.
- [68] F. Schütz and P. Kopietz, *J. Phys. A: Math. Gen.* **39**, 8205 (2006).
- [69] A. Sharma and P. Kopietz, *Phys. Rev. B* **93**, 235425 (2016).
- [70] To be accurate, the bosonic self-energy is twice the negative polarization function. This becomes clear by writing the bosonic

Dyson equation in a form resembling the fermionic one,

$$(\mathbf{D}_0^{-1} - \boldsymbol{\Sigma}_{b,\Lambda} + \tilde{\mathbf{R}}_{b,\Lambda})\mathbf{D}_\Lambda = \mathbb{1},$$

where \mathbf{D}_0^{-1} is defined in Eqs. (55)–(59), and $\tilde{\mathbf{R}}_{b,\Lambda} = 2\mathbf{R}_{b,\Lambda}$. We may still use the terms polarization function and bosonic self-energy synonymously.

- [71] J. Berges and S. Borsányi, *Phys. Rev. D* **74**, 045022 (2006).
- [72] S. Floerchinger and C. Wetterich, *Phys. Lett. B* **680**, 371 (2009).
- [73] Ward identities encode the invariance of the functional integral measure under a continuous symmetry transformation and thus represent quantum conservation laws at the level of correlation functions. These identities are generically modified by the presence of the additional regulator terms in the action, and reduce to their conventional form only at the end of the flow [38].
- [74] A yet another method, which is especially suited for the description of equilibrium density matrices at a finite initial time t_0 , is to modify the original Schwinger-Keldysh contour. At the end of the backward branch one allows the contour to extend into the complex time plane by a finite amount, which corresponds to the imaginary-time Matsubara contour. In this way the Keldysh formalism is modified into a 3×3 matrix structure, where the correlators carry real and imaginary time arguments in general. See Ref. [87] for further reading.
- [75] M. E. Carrington, T. Fugleberg, D. S. Irvine, and D. Pickering, *Eur. Phys. J. C* **50**, 711 (2007).
- [76] L. M. Sieberer, A. Chiocchetta, A. Gambassi, U. C. Täuber, and S. Diehl, *Phys. Rev. B* **92**, 134307 (2015).
- [77] A.-M. Wazwaz, *Linear and Nonlinear Integral Equations* (Springer, Heidelberg, Germany, 2011).
- [78] E. H. Hwang and S. Das Sarma, *Phys. Rev. B* **75**, 205418 (2007).
- [79] B. Wunsch, T. Stauber, F. Sols, and F. Guinea, *New J. Phys.* **8**, 318 (2006).
- [80] E. Mariani and F. von Oppen, *Phys. Rev. Lett.* **100**, 076801 (2008).
- [81] B. Amorim, A. Cortijo, F. de Juan, A. G. Grushin, F. Guinea, A. Gutiérrez-Rubio, H. Ochoa, V. Parente, R. Roldán, P. San-José, J. Schiefele, M. Sturla, and M. A. H. Vozmediano, *Phys. Rep.* **617**, 1 (2016).
- [82] G. Schwiete and A. M. Finkel'stein, *Phys. Rev. B* **89**, 075437 (2014).
- [83] G. Schwiete and A. M. Finkel'stein, *Phys. Rev. B* **90**, 155441 (2014).
- [84] We should mention here that it is still possible to construct a nonlinear sigma model in the low-doping/strong disorder regime where $E_F\tau < 1$, see Refs. [88–91]. Such a model could of course serve as a starting point for an analysis by means of the Wilsonian or even functional renormalization group. Nevertheless, the fRG applied to the fermionic pseudointeraction term obtained after disorder averaging represents an alternative approach to the problem of disordered fermions which could yield valuable insights.
- [85] T. R. Morris, *Int. J. Mod. Phys. A* **9**, 2411 (1994).
- [86] T. R. Morris, *Prog. Theor. Phys. Suppl.* **131**, 395 (1998).
- [87] P. Danielewicz, *Ann. Phys.* **152**, 239 (1984).
- [88] I. L. Aleiner and K. B. Efetov, *Phys. Rev. Lett.* **97**, 236801 (2006).
- [89] A. Altland, *Phys. Rev. Lett.* **97**, 236802 (2006).
- [90] P. M. Ostrovsky, I. V. Gornyi, and A. D. Mirlin, *Phys. Rev. Lett.* **98**, 256801 (2007).
- [91] S. Ryu, C. Mudry, H. Obuse, and A. Furusaki, *Phys. Rev. Lett.* **99**, 116601 (2007).

4.2 Paper: *“Chemical-potential flow equations for graphene with Coulomb interactions”*

Chemical-potential flow equations for graphene with Coulomb interactionsChristian Fräßdorf¹ and Johannes E. M. Mosig²¹*Dahlem Center for Complex Quantum Systems and, Institut für Theoretische Physik, Freie Universität Berlin, Arnimallee 14, 14195 Berlin, Germany*²*Department of Mathematics and Statistics, University of Otago, PO Box 56, Dunedin 9054, New Zealand*

(Received 13 July 2017; revised manuscript received 22 March 2018; published 11 June 2018)

We calculate the chemical potential dependence of the renormalized Fermi velocity and static dielectric function for Dirac quasiparticles in graphene nonperturbatively at finite temperature. By reinterpreting the chemical potential as a flow parameter in the spirit of the functional renormalization group (fRG) we obtain a set of flow equations, which describe the change of these functions upon varying the chemical potential. In contrast to the fRG the initial condition of the flow is nontrivial and has to be calculated separately. Our results are consistent with a charge carrier-independent Fermi velocity $v(k)$ for small densities $n \lesssim k^2/\pi$, supporting the comparison of the zero-density fRG calculation of Bauer *et al.* [*Phys. Rev. B* **92**, 121409 (2015)], with the experiment of Elias *et al.* [*Nat. Phys.* **7**, 701 (2011)].

DOI: [10.1103/PhysRevB.97.235415](https://doi.org/10.1103/PhysRevB.97.235415)**I. INTRODUCTION**

The spectrum of free electrons in graphene is characterized by two Dirac points around which the energy disperses linearly as a function of momentum [1–3]. One important peculiarity of the linear band structure is that it leads to a vanishing density of states at these nodal points. The vanishing charge carrier density implies the absence of screening, leading to strongly enhanced corrections of the system's single-particle properties by the long-range tail of the Coulomb interaction. One-loop calculations have shown that the Fermi velocity acquires logarithmic corrections upon approaching the nodal points [4–7]. These corrections diverge precisely at the nodal points at zero temperature, which corresponds to a strongly increasing Fermi velocity.

This effect becomes most pronounced in the strong coupling regime, which is experimentally realized by freestanding graphene, where there is no screening dielectric surrounding the graphene sheet. Such an experiment has been performed recently by Elias *et al.* [8], with the goal to experimentally verify the predicted logarithmic divergence of the velocity near the nodal points. Since perturbative calculations are not reliable in such a situation—the dimensionless interaction strength in freestanding graphene is about 2.2—nonperturbative methods have been employed for a quantitative theory of this effect. Bauer *et al.* [9] used the functional renormalization group (fRG) formalism to access the strong coupling regime [10–13], finding excellent agreement with the experiment of Elias *et al.* Upon closer inspection, however, the calculation of Ref. [9] addresses a slightly different quantity than what is measured in the experiment of Ref. [8]. The theoretical calculation has been performed at zero density and equates the momentum dependent quasiparticle velocity $v(k)$ with the Fermi velocity in a system with finite carrier density at Fermi momentum $k = k_F$. The experiment, in contrast, observed the logarithmic increase of the Fermi velocity as a function of the charge carrier density $n = k_F^2/\pi$. Strictly speaking these two veloci-

ties are different aspects of a more general velocity function, $v(k, \mu, T)$, which depends on momentum k , chemical potential μ (or the carrier density n , respectively), and temperature T . Equating the velocities of Refs. [8] and [9] requires that the carrier density dependence of the full velocity function is negligible for $n \lesssim k^2/\pi$. This identification allows one to map the momentum dependence to a density dependence, which could then be compared to the experiment. It is the goal of this paper to provide a theoretical framework for a nonperturbative calculation of the velocity function $v(k, \mu, T)$ and to calculate the density dependence of the static dielectric function.

Within a standard application of the fRG to calculate the renormalization of the Fermi velocity at finite density one faces the challenge that a renormalization of the Fermi surface under the RG flow has to be accounted for. The feature of a flowing Fermi surface is typically accompanied by significant technical complications regarding its implementation in certain cutoff and truncation schemes used in the literature [12,13]. Furthermore, studying an actual functional chemical potential dependence of correlation functions is numerically very expensive, since it requires a repeated solution of the truncated vertex flow equations for every value of the chemical potential. To circumvent both complications, we here explore a variant of the fRG, where the chemical potential μ is interpreted as a flow parameter [14,15], in combination with nontrivial input from a prior nonperturbative calculation at charge neutrality [9,16]. In contrast to conventional fRG where one is only interested in the one-particle irreducible vertex functions at the end of the flow, the chemical-potential flow bears physical information for all values of the flow parameter. The solution to the chemical-potential flow equations directly gives access to the full μ dependence of the vertex functions. Of particular importance in the chemical-potential flow is the initial condition. Among others it contains the information about the renormalization of the spectrum—and hence the interacting Fermi surface—at the initial chemical potential μ_0 (the latter being zero

at the charge neutrality point). A further renormalization of the spectrum and Fermi surface at different values for the chemical potential, $\mu \neq \mu_0$, is then taken care of by the flow itself.

In the ideal case—that is if the fRG equations could be solved exactly—the chemical-potential flow and the conventional fRG, where the flow equations are solved for each μ separately, yield the same answer. However, since there are always approximations involved by truncating the flow equations at a finite order, the solutions one obtains in the two approaches need not be equal. Hence the chemical-potential flow should be regarded as a complementary approach to the conventional finite density fRG to study density dependences. Since the chemical-potential flow has attracted much less attention in comparison to its standard fRG counterpart, there are no extensive studies whether the typical low-level truncation schemes, that are employed in the standard finite density fRG framework, are sufficient for a chemical potential-based flow, and to what extent their respective outcomes are quantitatively comparable. Due to the lack of finite-density fRG calculations for graphene, which could serve as a benchmark for the method we want to employ here, we may resort to the existing perturbative calculations for the self-energy and polarization function, which—among others—have been carried out in Refs. [17] and [18], respectively. Although such calculations should be a good approximation in the weak coupling regime only, but certainly not for strong coupling we study here, their predictions at least yield a qualitative reference point for a comparison. Nevertheless, graphene is an ideal testing ground for our method, due to the available experimental data for the strong coupling regime.

In the present paper we use a minimal truncation that only takes into account the flow of the renormalized Fermi velocity and dielectric function. As we will explain in the main part of this work, this represents a rather crude approximation. While the resulting μ -dependent dielectric function appears to be consistent with the expectations from one-loop perturbation theory, the results for the renormalized Fermi velocity are not satisfactory for large densities $n \gtrsim k^2/\pi$. For the low and intermediate density regime, $n \lesssim k^2/\pi$, we find a negligible density dependence of $v(k, \mu, T)$, consistent with the approximations made in Ref. [9]. In spite of the deficiencies of the simple truncation scheme studied here, the chemical-potential flow method is open to systematic improvements through higher order truncations, which we leave for future work.

The outline of the paper is as follows. In Sec. II we introduce the microscopic continuum model of interacting graphene electrons, we briefly discuss the general idea behind the chemical-potential flow and its difference to the standard fRG, followed by the truncation that is employed in this paper. In Sec. III we present the numerical solution and discuss the results. We conclude in the final section. Details about the derivation of the chemical-potential flow equation for the effective action, the vertex flow equations for the one-particle irreducible vertex functions, and their corresponding one-loop approximations are shown in two appendixes. The one-loop flow equations allow for a direct derivation of the results obtained in Refs. [17] and [18] within the chemical-potential flow framework.

II. MODEL AND FLOW EQUATIONS

Interacting Dirac fermions in graphene are described by the Hamiltonian ($\hbar = 1$) [19]

$$H_\mu = - \int_{\vec{r}} \Psi^\dagger(\vec{r}) (\mu + i v_F \sigma_0^s \otimes \vec{\Sigma} \cdot \vec{\nabla}) \Psi(\vec{r}) + \frac{1}{2} \int_{\vec{r}, \vec{r}'} \delta n_\mu(\vec{r}) \frac{e^2}{\epsilon_0 |\vec{r} - \vec{r}'|} \delta n_\mu(\vec{r}'), \quad (1)$$

with $\delta n_\mu(\vec{r}) = \Psi^\dagger(\vec{r}) \Psi(\vec{r}) - \tilde{n}_\mu(\vec{r})$. The Dirac electrons are described by eight-component spinors $\Psi \equiv (\Psi_\uparrow \quad \Psi_\downarrow)^\top$, with $\Psi_\sigma \equiv (\psi_{AK_+} \quad \psi_{BK_+} \quad \psi_{BK_-} \quad \psi_{AK_-})_\sigma^\top$. The indices $\sigma = \uparrow, \downarrow$ denote the spin, K_\pm the valley, and A/B the sublattice degree of freedom. Furthermore, σ_0^s is the two-dimensional unit matrix acting in spin space and $\Sigma_{1,2} = \tau_3 \otimes \sigma_{1,2}$ are four-dimensional matrices, with the Pauli matrices τ_3 and $\sigma_{1,2}$ acting in valley and sublattice space, respectively. The term $\tilde{n}_\mu(\vec{r})$ is a background charge density, which depends implicitly on the chemical potential. It represents the charge accumulated on a nearby metal gate and removes the zero wave number singularity of the bare Coulomb interaction. Furthermore, the constant ϵ_0 in the denominator of the Coulomb interaction amplitude is the dielectric constant of the medium, which accounts for the screening effects of a substrate or a surrounding dielectric on the bare Coulomb interaction. For freestanding graphene it is equal to one.

The key insight of our method is that the chemical potential in Eq. (1) couples to a fermion bilinear in exactly the same way as an additive infrared regulator in the fRG. Since the Hamiltonian is a continuous and differentiable function of μ , the chemical potential may formally be reinterpreted as a flow parameter [14,15]. This interpretation enables us to derive an exact flow equation for the chemical potential-dependent effective action Γ_μ and to apply the by now well-established methods of the fRG. Since the essential steps to arrive at an exact flow equation are identical to the fRG, we can immediately transfer the general (finite temperature and density) fRG equations from Ref. [16], taking care that the regularization prescription is substituted appropriately. In Fig. 1 we show a graphical representation of the truncated flow equations for the one-particle irreducible vertex functions of the theory in its Fermi-Bose form. The bosonic field was introduced by a Hubbard-Stratonovich transformation of the Coulomb interaction in the density-density channel [9,13,16,20–22].

In contrast to the standard fRG the main issue of concern in the chemical-potential flow theory is the initial condition of the flow. Since the chemical potential is different from an infrared regulator by its analytical structures, the effective action at some—arbitrarily chosen—initial chemical potential μ_0 is nontrivial in general. In particular, it typically does not coincide with the bare action, but already contains the full information about thermal and quantum fluctuations. Formally, the exact initial condition Γ_{μ_0} requires the knowledge of an infinite set of vertex functions, which—for obvious reasons—is impossible to obtain, but instead has to be approximated reasonably well by a separate calculation, using an appropriate nonperturbative method such as the fRG or Schwinger-Dyson equations [23], for example [24]. Such a preceding calculation is essential for the chemical-potential flow as the differential

FIG. 1. Graphical representation of the chemical potential flow equations for the self-energy $\hat{\Sigma}_\mu$ and the polarization function Π_μ . Contributions from higher order vertices $\Gamma_\mu^{(m,n)}$, with $m > 2, n > 1$ are already neglected. Straight and wiggly lines represent the flowing fermionic and bosonic propagators, respectively, and the shaded triangle represents the Fermi-Bose three-vertex $\Gamma_\mu^{(2,1)}$. The derivative ∂_μ on the right hand side only acts on the flowing fermionic propagators, substituting the latter by the so-called single scale propagator [16]. An analytical representation of these flow equations is given in Appendix B.

flow equations gain quantitative predictive power through the correct initial condition only. Apart from the truncation of the chemical-potential flow equations, the necessity to truncate the infinite dimensional theory space of the initial effective action to a finite dimensional subspace represents another level of approximation that is absent in the standard fRG and has to be dealt with with care.

One such issue we want to discuss briefly are Ward identities. In the standard fRG formalism Ward identities are modified due to the introduction of an artificial infrared regulator. Only at the end of the flow—that is at $\Lambda = 0$, where the infrared cutoff is removed—the modified Ward identities assume their original form. In a particular truncation of the standard fRG equations one has to make sure that those modified Ward identities are fulfilled at each value of the flowing cutoff, in particular at the end of the flow. Within the chemical-potential flow formalism, on the other hand, the Ward identities themselves are not modified at all, because the bare action requires no modification. Since the calculation of the initial condition relies on certain approximations, one has to make sure that those approximations are compatible with the Ward identities. Otherwise the initial condition would introduce an error that would simply be propagated by the chemical-potential flow, leading to results that are not reliable.

To calculate the initial condition for the present work we have chosen to use the Keldysh-fRG framework [25–32] we implemented in Ref. [16]. In that work, we calculated the Fermi velocity and the static dielectric function as functions of momentum and temperature at zero carrier density, finding

full agreement with the previously established zero temperature results of Ref. [9]. The charge neutrality point was chosen, because it allows for a rather simplistic truncation, which is based on the dominance of a single interaction channel: the density-density channel, pronouncing forward scattering. Furthermore, technical complications arising from a renormalization group flow of the Fermi surface are avoided, since at $\mu_0 = 0$ the Fermi surface collapses to a point that is invariant under renormalization [33]. The truncation scheme in Refs. [9] and [16] neglects any dynamical effects, such as plasmons and the quasiparticle wave function renormalization, the three-vertex renormalization, and higher-order vertices entirely. We note that this truncation is compatible with an approximate Ward identity, which connects the marginal three-vertex renormalization with the quasiparticle wave function renormalization as shown in Ref. [9]. We use these results as the starting point of the chemical-potential flow.

Drawing inspiration from the initial fRG calculation, we employ the same level of truncation and the same approximations for the chemical potential-based flow. (For a more elaborate discussion regarding the justification of this truncation, see the end of this section.) That means, in particular, we limit ourselves to the flow of the isotropic quasiparticle pole (temperature arguments are suppressed throughout, if not stated otherwise),

$$\xi_\mu(k) \equiv v_\mu(k)k, \quad (2)$$

and the flow of the static dielectric function,

$$\epsilon_\mu(\vec{q}) \equiv \epsilon_0(1 + V(\vec{q})\Pi_\mu^{R/A}(\omega = 0, \vec{q})). \quad (3)$$

Here, we put the functional μ dependence as an index to resemble standard fRG notation. The renormalized and μ -dependent Fermi velocity $v_\mu(k)$ has been defined as $v_\mu(k) = v_F + \Sigma_{v,\mu}(k)$ [9,16] and $V(\vec{q}) = 2\pi e^2/\epsilon_0 q$ is the Fourier transform of the bare Coulomb interaction. Assuming the absence of spontaneous chiral symmetry breaking, we obtain two coupled flow equations from the general vertex flow equations shown in Fig. 1: one for the Fermi velocity $v_\mu(k)$ and one for the static dielectric function $\epsilon_\mu(q)$; see Appendix B for details. For convenience we introduce the function $\chi_\mu(q) \equiv \epsilon_\mu(q)q$, which is—up to constants—the algebraic inverse of the renormalized Coulomb interaction, and we state the two flow equations in terms of $\xi_\mu(k)$ and $\chi_\mu(q)$ ($k_B = 1$),

$$\partial_\mu \xi_\mu(k) = \frac{e^2}{4\pi} \int_0^\infty dq \int_0^\pi d\varphi \frac{1}{2T} \left(\cosh^{-2} \left(\frac{\xi_\mu(q) + \mu}{2T} \right) - \cosh^{-2} \left(\frac{\xi_\mu(q) - \mu}{2T} \right) \right) \frac{q \cos \varphi}{\chi_\mu(\sqrt{q^2 + k^2 - 2qk \cos \varphi})}, \quad (4)$$

$$\partial_\mu \chi_\mu(q) = -\frac{e^2 q^2}{4\pi T} \int_0^\infty d\rho \int_0^\pi d\phi \left[\sum_{v=\pm 1} v \left(\cosh^{-2} \left(\frac{\xi_\mu(Q_-) - v\mu}{2T} \right) + \cosh^{-2} \left(\frac{\xi_\mu(Q_+) - v\mu}{2T} \right) \right) \frac{\sin^2 \phi}{\xi_\mu(Q_-) + \xi_\mu(Q_+)} \right. \\ \left. + \sum_{v=\pm 1} v \left(\cosh^{-2} \left(\frac{\xi_\mu(Q_-) - v\mu}{2T} \right) - \cosh^{-2} \left(\frac{\xi_\mu(Q_+) - v\mu}{2T} \right) \right) \frac{\sinh^2 \rho}{\xi_\mu(Q_-) - \xi_\mu(Q_+)} \right]. \quad (5)$$

These equations are supplemented by the nonperturbative initial conditions [16]

$$\xi_{\mu_0=0}^{\text{fRG}}(k) = v_{\mu_0=0}^{\text{fRG}}(k)k, \quad \chi_{\mu_0=0}^{\text{fRG}}(q) = \epsilon_{\mu_0=0}^{\text{fRG}}(q)q. \quad (6)$$

We emphasize once more that they are essential to obtain quantitatively reliable results. For example, the function $v_{\mu_0=0}^{\text{fRG}}(k)$ contains logarithmic momentum corrections to the bare Fermi velocity v_F at charge neutrality, that cannot be generated by the

above flow equations. Naively using the bare Fermi velocity as initial condition would yield meaningless results.

In Eq. (5) the quantity \mathcal{Q}_{\pm} is a short hand notation for the function $\mathcal{Q}_{\pm}(\rho, \phi, q) = \frac{1}{2}q (\cosh \rho \pm \cos \phi)$, where ρ and ϕ are elliptic coordinates, and the summation over $\nu = \pm 1$ covers the valence and conduction band. The derivation of the flow equations makes use of the particle-hole and chiral symmetries of the low energy Dirac model. As a result, the flow equations are fully symmetric with respect to the sign of μ , and the spectrum remains gapless and isotropic, leading to a circularly shaped Fermi surface defined by the equation $\xi_{\mu}(k_F) \pm \mu = 0$ [34]. Deviations from isotropy, most importantly trigonal warping, are expected to occur only for very large values of μ , which are of the order of the upper band cutoff Λ_0 of the Hamiltonian (1). For a systematic study of those nonisotropic corrections one would need to modify the quadratic part of the Hamiltonian (1) by including terms that are of second order in the spatial derivatives, which derive from a second order $k \cdot p$ approximation [3]. Within the minimal truncation employed here such contributions would modify the flow equation of the dielectric function and, additionally, lead to a more complex flow equation for the then nonisotropic quasiparticle pole or, alternatively, another flow equation, associated to the deviation from isotropy. In addition, it would be necessary to calculate the proper initial condition for such a deviation by nonperturbative means. The hyperbolic cosines appearing in the flow equations are a consequence of the single-scale derivative $\not{\partial}_{\mu}$ acting on the fermionic distribution functions, the latter being part of the fermionic Keldysh propagator; see Appendixes A and B. In the limit of vanishing temperature the inverse hyperbolic cosine is proportional to a delta function, centered at the interacting Fermi surface. For finite, not too large temperatures the delta-function singularity is smeared out, but remains strongly peaked at the Fermi surface $\xi_{\mu}(k_F) \pm \mu = 0$, whereas those modes for which $\xi_{\mu}(k) \pm \mu \gg 2T$ are exponentially suppressed. Hence the momentum integrals of the two flow equations are finite, both in the ultraviolet and infrared regime [14]. Due to the particle-hole symmetry we may restrict the analysis to positive μ , i.e., n doping.

Before discussing the numerical solution of the flow equations we want to elaborate on the level of truncation. While the single channel truncation of the conventional fRG calculation at charge neutrality is justified by the dominance of the density-density channel, no such simplification can be made at finite density. It is expected that with increasing carrier density the other interaction channels gain in significance leading to the significantly more complex scenario of multiple competing interaction channels, see, e.g., Refs. [12,13,15], even before nonisotropic corrections become relevant [35]. The information about those additional interaction channels is encoded in the higher order vertices (most importantly the three- and four-vertices), whose contribution to the flow has already been neglected. We remind the reader that the above truncation is minimal in the sense that it only takes into account the flow of those quantities, which have been obtained by the initial fRG calculation. To be clear, there is no rigorous justification for such a low level truncation, such that a critical reflection of our results is necessary. Yet, it was deliberately chosen, since it allows for a clear identification of the effects of this single interaction channel, which makes it easy to understand

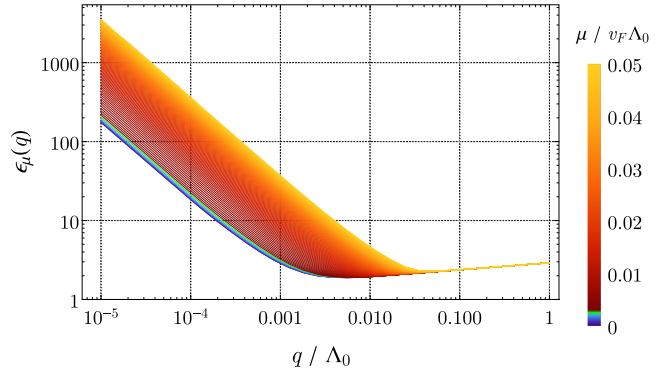


FIG. 2. Dielectric function $\epsilon_{\mu}(q)$ as a function of momentum and chemical potential at the reduced temperature $T/v_F\Lambda_0 = 2.5 \times 10^{-3}$. The colors blue to green and red to orange separate the two regimes $\mu \leq T$ and $\mu > T$, respectively. At the charge neutrality point the long range tail of the bare Coulomb interaction is cut off, due to thermal screening.

the conceptual similarities and differences to the conventional fRG approach. Furthermore, as we show in Appendix B, after certain approximations are made our flow equations for the self-energy and the polarization function can be reduced to a differential form of the corresponding equations that are found within diagrammatic one-loop perturbation theory, the latter of which have been calculated in Refs. [17,18] for the fermionic self-energy and bosonic polarization in graphene, respectively. Hence the solution of the flow equations (4) and (5) represents a direct generalization of those perturbative results, which incorporates the mutual effects of Fermi velocity renormalization and charge carrier induced screening in a selfconsistent manner.

III. NUMERICAL RESULTS AND DISCUSSION

The flow equations (4) and (5) together with their initial conditions, Eq. (6), have been solved numerically for different temperatures with the dimensionless coupling constant $\alpha = e^2/\epsilon_0 v_F = 2.2$ appropriate for freestanding graphene [3,7,9].

The numerical results for the dielectric function are shown in Fig. 2 for the reduced temperature $T/v_F\Lambda_0 = 2.5 \times 10^{-3}$. Recall that Λ_0 is the upper band cutoff of the low-energy Hamiltonian (1). At the charge neutrality point the dielectric function shows a distinctively different behavior in the two momentum regimes $q > T/v_F$ and $q < T/v_F$. While the dielectric function is only weakly dependent on the momentum in the regime $q \gg T/v_F$, a strong $1/q$ divergence can be observed for $q \ll T/v_F$. As explained in Ref. [16], this divergence could be attributed to thermally induced charge carriers. In the presence of a finite chemical potential, that is excess charge carriers, the large momentum components of the dielectric function remain unaffected, whereas the initial $1/q$ divergence found in the low momentum regime becomes strongly enhanced, leading to an increasingly short ranged renormalized Coulomb interaction. This picture is consistent with the results obtained in one-loop perturbation theory. For comparison, in the regime $q \ll T/v_F$ perturbation theory predicts a polarization function, that—in the static limit—is

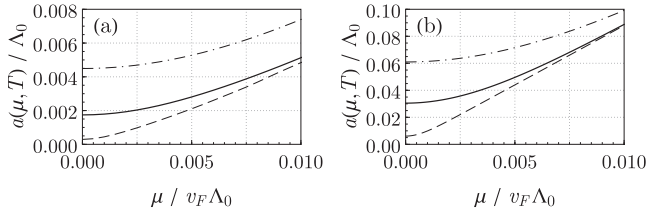


FIG. 3. Quantitative comparison between the (a) fully self-consistent solution and (b) one loop approximation of the coefficient function $a(\mu, T)$ for the reduced temperatures $T/v_F \Lambda_0 = 5 \times 10^{-4}, 2.5 \times 10^{-3}, 5 \times 10^{-3}$ (bottom to top data sets). In the small momentum regime, $q \ll T/v_F, \mu/v_F$, the static dielectric function shows a $1/q$ divergence according to $\epsilon_\mu(q \ll T/v_F) = 1 + a(\mu, T)\Lambda_0/q$. Observe that the self-consistent solution is about an order of magnitude smaller than the one-loop prediction.

independent of momentum and a function of temperature and chemical potential only [18],

$$\epsilon_\mu^{1\text{-loop}}(q \ll T/v_F) = 1 + a(\mu, T) \frac{\Lambda_0}{q}, \quad (7)$$

with

$$a(\mu, T) = 8\alpha \frac{T}{v_F \Lambda_0} \ln\left(2 \cosh \frac{\mu}{2T}\right). \quad (8)$$

Here, the coefficient function $a(\mu, T)$ is directly proportional to the static limit of the polarization function. At the charge neutrality point $a(\mu, T)$ scales linearly with temperature, whereas for $\mu \gg T$ it becomes independent of temperature, scaling linearly with the chemical potential. The former feature has been shown to remain valid in a nonperturbative fRG calculation [16], showing a strong renormalization of the slope. To verify whether the latter feature remains valid beyond perturbation theory, we solved the self-consistency Eqs. (4) and (5) for the two additional temperatures $T/v_F \Lambda_0 = 5 \times 10^{-4}, 5 \times 10^{-3}$ and extracted the coefficient functions $a(\mu, T)$; see Fig. 3. For large chemical potentials we observed a transition into a linear regime, which is consistent with the result obtained by perturbation theory. However, the precise slope could not be determined sufficiently accurately due to convergence issues of the numerical integration: at very small momenta and increasingly large chemical potentials the integrand of Eq. (5) becomes very strongly peaked, such that limited machine precision becomes problematic. Nevertheless, our results indicate that the scaling behavior predicted by perturbation theory is indeed correct, albeit with a strongly renormalized slope. A precise estimation of the slope would require a recalculation of the temperature dependence of the renormalized Fermi velocity and dielectric function at the charge neutrality point with a better resolution and accuracy than what was achieved previously in Ref. [16].

The numerical results for the chemical potential dependence of the renormalized Fermi velocity are shown in Fig. 4. At the initial chemical potential $\mu_0 = 0$ the infrared divergence of the renormalized Fermi velocity is regularized due to the temperature-induced screening of the renormalized Coulomb interaction [16], while in the large momentum regime, $k \gg T/v_F$, the renormalized Fermi velocity shows the logarithmic

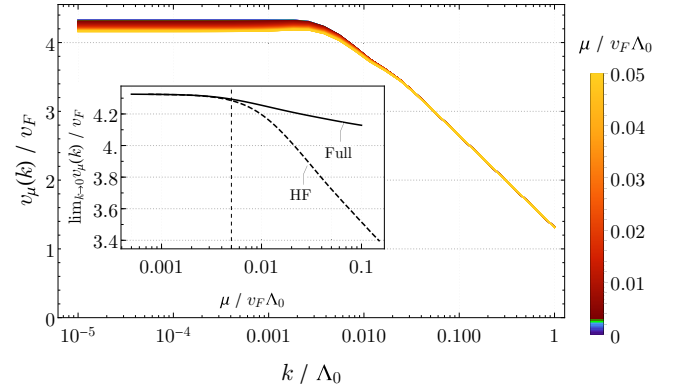


FIG. 4. Renormalized Fermi velocity $v_\mu(k)$ as a function of momentum and chemical potential at temperature $T/v_F \Lambda_0 = 2.5 \times 10^{-3}$ in the fully self-consistent calculation. The renormalized Fermi velocity is finite at $k = 0$ at the initial chemical potential $\mu_0 = 0$ due to temperature induced screening of the renormalized Coulomb interaction. Increasing the chemical potential away from the charge neutrality point shows a weak suppression of the Fermi velocity for small momenta. The inset shows a comparison between the $k \rightarrow 0$ limits of the Fermi velocity in the self-consistent treatment and in Hartree-Fock approximation as functions of the chemical potential. The dashed vertical line marks $\mu = 2T$. For $\mu > 2T$ both calculations show a logarithmic suppression of $v_\mu(k \rightarrow 0)$. This suppression is significantly weakened in the full computation when compared to the result of the Hartree-Fock approximation.

behavior [9,16]

$$v_{\mu=0}(k \gg T/v_F)/v_F = A + B \ln(\Lambda_0/k), \quad (9)$$

with $A = 1.34(4)$ and $B = 0.52(1)$. Upon increasing the chemical potential the solution shows a further, but only very weak suppression of the Fermi velocity at low momenta in accord with the assumption of Bauer *et al.* [9]. The other temperatures we investigated also show a negligible μ dependence (data not shown). Our full calculation allows us to understand this behavior by considering the combined effect of strong screening and the formation of a nontrivial Fermi surface. By increasing the chemical potential the additional charge carriers fill up the renormalized spectrum and introduce a circularly shaped Fermi surface, which is driven further and further away from the nodal point, while the renormalized Coulomb interaction becomes increasingly short ranged. As a result, the screened Coulomb interaction only operates near the Fermi surface and, loosely speaking, does not reach far enough down the spectrum to have a significant impact on the small momentum regime of the renormalized Fermi velocity. Neglecting the charge carrier-induced screening would cause a much stronger suppression of the Fermi velocity, since then the Coulomb interaction could reach down to the nodal point. In order to validate this picture we also performed a Hartree-Fock-like calculation of the velocity, see the inset of Fig. 4, where only Eq. (4) has been solved self-consistently for $\xi_\mu(k)$. The μ flow of the dielectric function therein was neglected and the function $\chi_\mu(q) = \epsilon_\mu(q)q$ was kept at its initial value $\chi_\mu(q) = \chi_{\mu_0=0}(q)$, where only temperature induced screening is present. The Hartree-Fock solution shows the same features as the fully self-consistent solution. However, the low momentum

regime of the Hartree-Fock Fermi velocity is much stronger suppressed, supporting the above reasoning. Our observations are also consistent with the findings from one-loop perturbation theory. As was shown in Ref. [17], at zero temperature a finite chemical potential regularizes the logarithmic divergence according to

$$v_{\mu}^{1\text{-loop}}(k=0)/v_F = 1 + \frac{\alpha}{4} \ln(\Lambda_0/k_F), \quad (10)$$

with the Fermi momentum $k_F = \mu/v_F$. Here, the suppression of the infrared divergence is much stronger than what we find in our self-consistent approach, since it is the bare, unscreened Coulomb interaction that enters their calculations. Although the intrinsic ($\mu = 0$) part of the self-energy leads to an infrared divergence as a function of momentum, it is immediately cut off by the extrinsic ($\mu \neq 0$) part of the self-energy, even for large μ , far away from the nodal point, due to the infinite range of the unscreened Coulomb interaction.

Since our data show that the Fermi velocity is virtually independent from the chemical potential in its entire momentum regime, the μ -flow fRG together with the truncation scheme used here is consistent with the approximation of Ref. [9]. However, the high μ independence of the velocity function we find is actually problematic and cannot hold for all values of the chemical potential, as the following line of arguments shows.

In the critical evaluation of our results for the chemical potential dependence of the Fermi velocity the main focus lies on the low momentum regime, in particular the zero momentum singularity found at zero temperature. In contrast to Ref. [17] we are working at finite temperature, which already provides a proper regularization of the logarithmic infrared divergence, making it necessary to distinguish the two regimes $\mu \ll T$ and $\mu \gg T$. In the regime $\mu \ll T$ the chemical potential should be irrelevant for the suppression of the logarithmic divergence, since there temperature induced screening dominates. Our numerical data fully support this intuition as can be seen in the inset of Fig. 4. This result may have already been anticipated from the analytical form of Eq. (4) prior to the numerical solution, since in this limit the inverse hyperbolic cosines in the integrand cancel each other, leading to a constant velocity as a function of the chemical potential. In the regime $\mu \gg T$, on the other hand, one should expect the suppression of the logarithmic divergence to be driven solely by the chemical potential—independent of temperature—in much the same way as the $1/q$ divergence of the dielectric function becomes temperature independent for large enough μ ; cf. Fig. 3. It is unphysical that temperature controls the regularization of the infrared divergence far away from the charge neutrality point. Hence its influence should vanish in that regime. Although our data show a certain logarithmic suppression of $v_{\mu}(k=0)$ as a function of μ for all the temperatures investigated, the suppression itself is far too weak to be compatible with the expectation presented above.

As it stands our results show a certain “asymmetry” in how the small momentum regime of the Fermi velocity is affected by a finite temperature in comparison to a finite chemical potential, which contradicts physical intuition and should not be present. Based on the physics that is contained within our flow equations, as well as taking into account the arguments of the discussion at the end of the previous section, we, thus,

conclude that the minimal truncation employed here is not capable of describing the proper chemical potential dependence of the Fermi velocity in the small momentum regime. Since both the chemical-potential flow theory and more standard fRG approaches are based on the same exact flow equation, whose approximative solutions converge to the same result in the exact theory, we are convinced that a higher order truncation of the chemical-potential flow equations will resolve these issues and lead to the expected behavior. To this end one should systematically improve our truncation by including the effects of the quasiparticle wave function renormalization and three-vertex renormalization (recall that those quantities are connected via a Ward identity), and possibly also the flow of the four-vertex. As an alternative to the Fermi-Bose framework employed here, one could also consider a purely fermionic formulation, which removes the bias introduced by the choice of a particular interaction channel via partial bosonization. In such a framework one would have to implement the initially nontrivial dielectric function as part of the initial fermionic four-vertex. Only if a truncation is able to produce a strong enough suppression of the small momentum components of the renormalized Fermi velocity, that becomes temperature independent upon increasing μ into the regime $\mu \gg T$, could it be claimed with confidence that the particularly chosen truncation is justified.

IV. CONCLUSIONS

The idea to use the chemical potential as a flow parameter in a functional renormalization group calculation was first put forward by Berges *et al.* [14] in the context of a particle-physics problem and since then has rarely been adopted by other authors; see, e.g., Ref. [15] for an application in condensed matter theory. We here have presented another application of the fRG with the chemical potential as the flow parameter in a condensed matter system. In contrast to the physical system investigated in Ref. [15] a separate nonperturbative calculation is required to establish the initial condition for the flow. This initial “investment” pays off, because for a chemical-potential based flow each point in the solution of the flow equation is of physical relevance, in contrast to more standard fRG approaches, where only the end point of the flow matters. The alternative would be to run a conventional fRG calculation for each value of the chemical potential separately. The two approaches should converge to the same result if the respective truncations are of sufficiently high order, but the standard fRG approach involves much greater effort to study a functional μ dependence. Nevertheless, it would be an important research topic to investigate this convergence issue systematically—be it for graphene or nonrelativistic Fermi liquids—by comparing the predictions of the two approaches for several truncations against each other. While the standard finite density fRG has already proven to be a reliable framework for a plethora of materials, the chemical-potential flow has—in our opinion—great potential, but lacks those numerous tests, which are necessary for this method to become a viable alternative.

We have applied the technique for the calculation of the carrier density dependence of the Fermi velocity and the static dielectric function in graphene, using a conventional fRG calculation at zero chemical potential as initial condition. Graphene is a very suitable context for an application of the

chemical-potential flow technique. In this material physical quantities in principle have a strong dependence of the carrier density, providing a need for such a calculation, while the high-symmetry point of zero carrier density brings significant simplifications, allowing for an efficient “conventional” non-perturbative calculation at that point. Our numerical results are consistent with the earlier work of Bauer *et al.* [9], which took the momentum-dependent Fermi velocity to be independent of the chemical potential for $n \lesssim k^2/\pi$, yielding practically identical fits to the experimental data of Elias *et al.* [8]. However, our approximations yield a suppression of the infrared divergence that is too weak to be compatible with the expected symmetry $\max(\mu, T)$, that is the divergence should be cut off by either the chemical potential or temperature, depending on which of these two quantities is larger, which we believe to be not physical. Although a stronger suppression of the small momentum regime should have little impact on the actual fit to the experimental data, most certainly not being able to invalidate it, further work is necessary to settle the issue satisfyingly. The dielectric function is, however, strongly dependent on the chemical potential, reflecting the strong carrier dependence of the screening length in graphene. For this observable we expect a higher order truncation to yield only minor modifications, since the main features that should occur at finite density—in particular the transition into a temperature independent regime for $\mu \gg T$ —could already be observed. Even though the current truncation is not sufficient for the Fermi velocity, it appears to be a reasonable approximation to the static dielectric function. Once the issues for the Fermi velocity at small momenta are resolved, it would be interesting to apply our method to the three dimensional analog of graphene, the so-called Weyl semimetals. Such materials feature a conical spectrum as well and a chemical-potential based flow could be implemented equally efficiently.

ACKNOWLEDGMENTS

We thank Piet Brouwer and Björn Sbierski for support in the preparation of the manuscript. This work is supported by the German Research Foundation (DFG) in the framework of the Priority Program 1459 “Graphene.”

APPENDIX A: DERIVATION OF THE CHEMICAL-POTENTIAL FLOW EQUATION

In this appendix, we explain some details about the general chemical potential flow theory, which is the basis for the flow equations (4) and (5). Since the theory relies on a reinterpretation of the chemical potential as a flow parameter, the main results can be transferred directly from Ref. [16].

The starting point for the derivation of an exact flow equation is the μ -dependent partition function $Z_\mu[\eta, \mathbf{J}]$. It is defined as the functional Fourier transform of the exponentiated bare action $S_\mu[\psi, \phi]$ [13,20,22,32],

$$Z_\mu[\eta, \mathbf{J}] = \int \mathcal{D}\psi \mathcal{D}\psi^\dagger \mathcal{D}\phi e^{iS_\mu[\psi, \phi] + i\eta^\dagger \tau_1 \Psi + i\Psi^\dagger \tau_1 \eta + i\phi^\top \tau_1 \mathbf{J}}. \quad (\text{A1})$$

The bare action is a functional of fermionic and bosonic fields, which can be derived from the purely fermionic Hamiltonian

(1) by a standard procedure [16,20–22]. The bosonic field is introduced by a Hubbard-Stratonovich transformation of the Coulomb interaction term in the density-density channel. The index μ indicates that both the partition function and the bare action depend on the chemical potential. The chemical potential dependence of the bare action enters explicitly via the quadratic μ term in the Hamiltonian and implicitly via the background density \tilde{n}_μ . In contrast to the conventional fRG there is no additional infrared regulator [14]. Furthermore, we work in the real-time Keldysh formalism [25–32], which involves a doubling of degrees of freedom, with classical (c) and quantum (q) component for each field [16,21,22,32]

$$\Psi \equiv (\Psi_c \quad \Psi_q)^\top, \quad \Psi^\dagger = (\Psi^\dagger)^\dagger, \quad \phi \equiv (\phi_c \quad \phi_q)^\top. \quad (\text{A2})$$

Lastly, η and \mathbf{J} are fermionic and bosonic source fields, respectively. In Eq. (A1) we employed a condensed vector notation for the source terms, containing integration and summation of continuous and discrete field degrees of freedom implicitly, e.g.,

$$\eta^\dagger \tau_1 \Psi \equiv \int_x \eta^\dagger(x) \tau_1 \Psi(x), \quad (\text{A3})$$

where τ_1 is a Pauli matrix acting in Keldysh space.

The effective action may now be introduced as the modified Legendre transform of the connected functional $W_\mu[\eta, \mathbf{J}] = -i \ln Z_\mu[\eta, \mathbf{J}]$ [10–14],

$$\Gamma_\mu[\psi, \phi] = W_\mu[\eta_\mu, \mathbf{J}_\mu] - \eta_\mu^\dagger \tau_1 \Psi - \Psi^\dagger \tau_1 \eta_\mu - \phi^\top \tau_1 \mathbf{J}_\mu - \Psi^\dagger \hat{R}_\mu \Psi, \quad (\text{A4})$$

with

$$\hat{R}_\mu(x, y) = \begin{pmatrix} 0 & \mu \delta(x - y) \hat{1} \\ \mu \delta(x - y) \hat{1} & 0 \end{pmatrix}. \quad (\text{A5})$$

The term $\Psi^\dagger \hat{R}_\mu \Psi$ is the explicit chemical-potential term one obtains in the bare action $S_\mu[\psi, \phi]$. Its resemblance with an additive infrared regulator in the conventional fRG is the foundation of the chemical-potential flow theory [14,15]. According to the usual definition of the effective flowing action, the “chemical-potential regulator term” has been subtracted on the right hand side [10–14]. Consequently, the effective action Γ_μ involves flowing vertex functions only, and the explicit chemical-potential term—in comparison to the bare action—is absent. Note that some authors prefer to include a finite chemical potential in the fermionic distribution function, rather than in the spectral part of the inverse propagators as we do here [22]. Such an alternative choice would affect the structure of the regulator (A5) and the vertex expansion of the effective action, but it cannot lead to any observable consequences, since these two choices are connected by a (time dependent) gauge transformation.

The exact chemical-potential flow equation follows immediately upon taking the μ derivative of Eq. (A4), keeping the

fields ψ and ϕ fixed,

$$\partial_\mu \Gamma_\mu[\psi, \phi] = \frac{i}{2} \delta_\mu \text{STr} \ln(\hat{\Gamma}_\mu^{(2)}[\psi, \phi] + \hat{\mathcal{R}}_\mu) + 2\phi_q \partial_\mu \tilde{n}_\mu, \quad (\text{A6})$$

where $\hat{\Gamma}_\mu^{(2)}$ is a Hesse matrix of second derivatives, and

$$\hat{\mathcal{R}}_\mu \equiv \text{diag}(-\hat{R}_\mu, \hat{R}_\mu^\dagger, 0). \quad (\text{A7})$$

The “single-scale derivative” δ_μ in Eq. (A6) only acts on the regulator $\hat{\mathcal{R}}_\mu$. The above flow equation is the Keldysh analog of the original, imaginary-time flow equation proposed by Berges *et al.* [14]. We note here that the initial condition for this exact flow equation is given by the exact effective action (A4) at some arbitrarily chosen initial chemical potential μ_0 . As already stressed in the main text, this initial condition has to be calculated separately by other nonperturbative techniques,

since the “chemical potential regulator” does not provide an infrared regularization in the standard fRG sense.

APPENDIX B: VERTEX FLOW EQUATIONS AND ONE-LOOP APPROXIMATION

The flow equations for the one-particle irreducible vertex functions are obtained by expanding the effective action in powers of fields, which needs to be inserted into the above equation, and comparing coefficients [12,13,16]. Since we are only interested in thermal equilibrium, where the fluctuation-dissipation theorem holds [22], we only need to consider the resulting flow equations for the retarded components of the self-energy and polarization function. In a condensed notation, where numerical arguments denote space and time coordinates, $1 \equiv (\vec{r}_1, t_1)$, and latin indices encompass the discrete fermionic degrees of freedom, sublattice, valley, and spin, these flow equations read

$$\begin{aligned} \partial_\mu \Sigma_{\mu,ij}^R(1,2) &= i \delta_\mu \sum_{k,l} \int' (\Gamma_{\mu,ik}^{qcc}(1,1';4') G_{\mu,kl}^K(1',2') \Gamma_{\mu,lj}^{ccq}(2',2;3') D_\mu^A(3',4') \\ &\quad + \Gamma_{\mu,ik}^{qcc}(1,1';4') G_{\mu,kl}^R(1',2') \Gamma_{\mu,lj}^{qcc}(2',2;3') D_\mu^K(3',4')), \end{aligned} \quad (\text{B1})$$

$$\begin{aligned} \partial_\mu \Pi_\mu^R(1,2) &= \frac{i}{2} \delta_\mu \sum_{k,l,m,n} \int' (G_{\mu,kl}^K(1',2') \Gamma_{\mu,lm}^{ccq}(2',3';1) G_{\mu,mn}^R(3',4') \Gamma_{\mu,nk}^{qcc}(4',1';2) \\ &\quad + G_{\mu,kl}^A(1',2') \Gamma_{\mu,lm}^{ccq}(2',3';1) G_{\mu,mn}^K(3',4') \Gamma_{\mu,nk}^{qcc}(4',1';2)). \end{aligned} \quad (\text{B2})$$

The functions $\Gamma_{\mu,ij}^{\alpha\beta\gamma}(1,2;3)$, with $\alpha, \beta, \gamma = c, q$, are the Fermi-Bose three-vertices of the theory in the real-time Keldysh formulation. The primed integration sign indicates that all primed arguments have to be integrated. Here, the contributions to the flow from four-vertices has already been neglected. A transformation to Fourier space is beneficial, due to energy and momentum conservation. The flowing frequency-momentum space propagators that enter the transformed flow equations read

$$\hat{G}_\mu^{R/A}(\vec{k}, \varepsilon) = \frac{1}{\sigma_0^s \otimes (\varepsilon + \mu - v_F \vec{\Sigma} \cdot \vec{k} - \hat{\Sigma}_\mu^{R/A}(\vec{k}, \varepsilon))}, \quad (\text{B3a})$$

$$\hat{G}_\mu^K(\vec{k}, \varepsilon) = \tanh \frac{\varepsilon}{2T} (\hat{G}_\mu^R(\vec{k}, \varepsilon) - \hat{G}_\mu^A(\vec{k}, \varepsilon)), \quad (\text{B3b})$$

$$D_\mu^{R/A}(\vec{q}, \omega) = \frac{1}{2 V^{-1}(\vec{q}) + \Pi_\mu^{R/A}(\vec{q}, \omega)}, \quad (\text{B4a})$$

$$D_\mu^K(\vec{q}, \omega) = \coth \frac{\omega}{2T} (D_\mu^R(\vec{q}, \omega) - D_\mu^A(\vec{q}, \omega)). \quad (\text{B4b})$$

The single-scale derivative in Eqs. (B1) and (B2) only acts on the flowing fermionic propagators, substituting the latter by a single-scale propagator

$$\delta_\mu \hat{G}_\mu^{R/A}(\vec{k}, \varepsilon) = -(\hat{G}_\mu^{R/A}(\vec{k}, \varepsilon))^2. \quad (\text{B5})$$

Here, the μ dependence of the flowing self-energy is held constant upon taking the single-scale derivative δ_μ . By using the approximations mentioned in the main text—that is, setting all the three-vertices to unity as well as neglecting any

dynamical effects—and employing all the symmetries, after a straightforward calculation we arrive at the flow equations (4) and (5).

As an important crosscheck of the formalism, it is desirable to reproduce the results of the one-loop approximation of diagrammatic perturbation theory directly within the chemical-potential flow framework. To this end one should neglect the chemical potential dependence of the three-vertices, setting them to their (noninteracting) initial value at $\mu = 0$, and one should replace the interacting flowing propagators in the flow equations (B1) and (B2) by their noninteracting counterparts, Eqs. (B3a)–(B4b) with $\hat{\Sigma}_\mu^{R/A}$ and $\Pi_\mu^{R/A}$ set to zero. It is then possible to perform the summations and integrations on the right hand side of the flow equations analytically exactly, such that—in real-space representation—one is left with simple algebraic products of noninteracting propagators. Furthermore, with these approximations the single-scale derivative δ_μ turns into an ordinary partial derivative ∂_μ , since the remaining terms do not contain any nontrivial μ dependences apart from the one given by the chemical potential regulator within the noninteracting flowing propagators. Thus the above flow equations reduce to the simple form

$$\partial_\mu \hat{\Sigma}_\mu^R(1,2) = i \partial_\mu (\hat{G}_{0,\mu}^R(1,2) D_{0,\mu}^K(2,1) + \hat{G}_{0,\mu}^K(1,2) D_{0,\mu}^A(2,1)), \quad (\text{B6})$$

$$\begin{aligned} \partial_\mu \Pi_\mu^R(1,2) &= \frac{i}{2} \partial_\mu \text{tr} (\hat{G}_{0,\mu}^R(1,2) \hat{G}_{0,\mu}^K(2,1) \\ &\quad + \hat{G}_{0,\mu}^K(1,2) \hat{G}_{0,\mu}^A(2,1)), \end{aligned} \quad (\text{B7})$$

which is nothing but a differential form of the well-known one-loop result for the fermionic self-energy and bosonic polarization function [22]. Here, the subscript “0” at the propagators indicates that they are the noninteracting ones, and the trace in Eq. (B7) covers the discrete fermionic degrees of freedom: sublattice, valley, and spin. The one-loop flow equations may be integrated trivially to obtain the results of diagrammatic perturbation theory. To be consistent with the one-loop approximation one should employ the perturbative results for the initial

condition at $\mu = 0$ on the left hand side of the integrated flow equations: $\hat{\Sigma}_{\mu=0}^R = (\hat{\Sigma}_{\mu=0}^R)_{1\text{-loop}}$ and $\Pi_{\mu=0}^R = (\Pi_{\mu=0}^R)_{1\text{-loop}}$. The above one-loop self-energy has been obtained in Ref. [17], albeit in the imaginary time Matsubara formalism at zero temperature, showing that the logarithmic zero momentum divergence found at charge neutrality is regularized by a finite chemical potential; cf. Eq. (10). The one-loop polarization function at finite temperature and density has been calculated in Ref. [18] also within the Keldysh formalism.

-
- [1] P. R. Wallace, *Phys. Rev.* **71**, 622 (1947).
- [2] G. W. Semenoff, *Phys. Rev. Lett.* **53**, 2449 (1984).
- [3] A. H. Castro Neto, F. Guinea, N. M. R. Peres, K. S. Novoselov, and A. K. Geim, *Rev. Mod. Phys.* **81**, 109 (2009).
- [4] J. González, F. Guinea, and M. A. H. Vozmediano, *Nucl. Phys. B* **424**, 595 (1994).
- [5] J. González, F. Guinea, and M. A. H. Vozmediano, *Phys. Rev. B* **59**, R2474(R) (1999).
- [6] M. A. H. Vozmediano, *Philos. Trans. R. Soc. London A* **369**, 2625 (2011).
- [7] V. N. Kotov, B. Uchoa, V. M. Pereira, F. Guinea, and A. H. Castro Neto, *Rev. Mod. Phys.* **84**, 1067 (2012).
- [8] D. C. Elias, R. V. Gorbachev, A. S. Mayorov, S. V. Morozov, A. A. Zhukov, P. Blake, L. A. Ponomarenko, I. V. Grigorieva, K. S. Novoselov, F. Guinea, and A. K. Geim, *Nat. Phys.* **7**, 701 (2011).
- [9] C. Bauer, A. Rückriegel, A. Sharma, and P. Kopietz, *Phys. Rev. B* **92**, 121409(R) (2015).
- [10] C. Wetterich, *Int. J. Mod. Phys. A* **16**, 1951 (2001).
- [11] J. Berges, N. Tetradis, and C. Wetterich, *Phys. Rep.* **363**, 223 (2002).
- [12] W. Metzner, M. Salmhofer, C. Honerkamp, V. Meden, and K. Schönhammer, *Rev. Mod. Phys.* **84**, 299 (2012).
- [13] P. Kopietz, L. Bartosch, and F. Schütz, *Introduction to the Functional Renormalization Group* (Springer, New York, 2010).
- [14] J. Berges, D.-U. Jungnickel, and C. Wetterich, *Int. J. Mod. Phys. A* **18**, 3189 (2003).
- [15] F. Sauli and P. Kopietz, *Phys. Rev. B* **74**, 193106 (2006).
- [16] C. Fräßdorf and J. E. M. Mosig, *Phys. Rev. B* **95**, 125412 (2017).
- [17] E. H. Hwang, B. Y.-K. Hu, and S. Das Sarma, *Phys. Rev. Lett.* **99**, 226801 (2007).
- [18] M. Schütt, P. M. Ostrovsky, I. V. Gornyi, and A. D. Mirlin, *Phys. Rev. B* **83**, 155441 (2011).
- [19] V. P. Gusynin, S. G. Sharapov, and J. P. Carbotte, *Int. J. Mod. Phys. B* **21**, 4611 (2007).
- [20] J. W. Negele and H. Orland, *Quantum Many-Particle Systems* (Westview Press, Boulder, CO, 1998).
- [21] G. Schwiete and A. M. Finkel’stein, *Phys. Rev. B* **89**, 075437 (2014).
- [22] A. Kamenev, *Field Theory of Non-Equilibrium Systems* (Cambridge University Press, Cambridge, UK, 2011).
- [23] C. Popovici, C. S. Fischer, and L. von Smekal, *Phys. Rev. B* **88**, 205429 (2013).
- [24] There are cases, however, where a certain initial reference point can lead to significant simplifications. For example, in the study of the low density regime of the two-dimensional electron gas performed in Ref. [15], the initial chemical potential $\mu_0 = 0$ corresponds to the case of vanishing particle density, implying that the self-energy vanishes identically and the effective interaction is obtained via a resummation of particle-particle ladder diagrams.
- [25] R. Gezzi, T. Pruschke, and V. Meden, *Phys. Rev. B* **75**, 045324 (2007).
- [26] S. G. Jakobs, V. Meden, and H. Schoeller, *Phys. Rev. Lett.* **99**, 150603 (2007).
- [27] T. Gasenzer and J. M. Pawłowski, *Phys. Lett. B* **670**, 135 (2008).
- [28] J. Berges and G. Hoffmeister, *Nucl. Phys. B* **813**, 383 (2009).
- [29] C. Karrasch, M. Pletyukhov, L. Borda, and V. Meden, *Phys. Rev. B* **81**, 125122 (2010).
- [30] T. Kloss and P. Kopietz, *Phys. Rev. B* **83**, 205118 (2011).
- [31] D. M. Kennes, S. G. Jakobs, C. Karrasch, and V. Meden, *Phys. Rev. B* **85**, 085113 (2012).
- [32] J. Berges and D. Mesterházy, *Nucl. Phys. B Proc. Suppl.* **228**, 37 (2012).
- [33] Although for $\mu_0 = 0$ the renormalization of the Fermi surface is trivial, the spectrum around charge neutrality is still renormalized nontrivially, which yields a significant contribution to the renormalization of the Fermi surface at μ found after flowing from $\mu_0 = 0$ to μ . If one would want to initialize the flow at some finite μ_0 instead, then the calculation of the initial condition has to incorporate a—now nontrivial—renormalization towards the interacting Fermi surface at μ_0 .
- [34] Depending on the sign of μ , the interacting Fermi surface, being a circle of radius k_F , is located either within the conduction or valence band.
- [35] Within the standard finite-density fRG approach one typically employs a purely fermionic formulation, taking into account the flow of the full four-vertex, in combination with so-called patching techniques. Such a formulation has the advantage that it does not favor a particular interaction channel, in contrast to a theory containing a Hubbard-Stratonovich boson. Although the Hubbard-Stratonovich transformation is an exact integral identity, it introduces a certain bias towards a particular interaction channel once the hierarchy of flow equations is truncated (especially if truncated at a low level).

4.3. Paper: “*Abelian Chern-Simons theory for the fractional quantum Hall effect in graphene*”

4.3 Paper: “*Abelian Chern-Simons theory for the fractional quantum Hall effect in graphene*”

4.3. Paper: “Abelian Chern-Simons theory for the fractional quantum Hall effect in graphene”

Abelian Chern-Simons theory for the fractional quantum Hall effect in graphene

Christian Fräßdorf

Dahlem Center for Complex Quantum Systems and, Institut für Theoretische Physik, Freie Universität Berlin, Arnimallee 14, 14195 Berlin, Germany

(Received 10 December 2017; published 12 March 2018)

We develop a theory for the pseudorelativistic fractional quantum Hall effect in graphene, which is based on a multicomponent Abelian Chern-Simons theory in the fermionic functional integral approach. Calculations are performed in the Keldysh formalism, directly giving access to real-time correlation functions at finite temperature. We obtain an exact effective action for the Chern-Simons gauge fields, which is expanded to second order in the gauge field fluctuations around the mean-field solution. The one-loop fermionic polarization tensor as well as the electromagnetic response tensor in random phase approximation are derived, from which we obtain the Hall conductivities for various FQH states, lying symmetrically around charge neutrality.

DOI: [10.1103/PhysRevB.97.115123](https://doi.org/10.1103/PhysRevB.97.115123)**I. INTRODUCTION**

The integer quantum Hall effect (IQHE) is a remarkable experimental discovery of the early 1980s, since it proves quantum mechanics at work on macroscopic scales [1]. In a nonrelativistic two-dimensional electron gas (2DEG) at low temperatures and in high external magnetic fields, the Hall conductivity shows a plateau structure as a function of the magnetic field or chemical potential occurring at integer multiples of the “conductance quantum” e^2/h . Remarkably, the existence of these plateaus can already be understood in simple noninteracting models by the formation of discrete, equidistant energy levels, the Landau levels (LLs) [2].

In sharp contrast to an ordinary 2DEG with its parabolic band structure, in the vicinity of the charge neutrality point, the band structure of graphene mimics the energy-momentum dispersion of massless, relativistic Dirac particles [3–7]. When subjected to strong magnetic fields such a pseudorelativistic dispersion relation has profound consequences on the LLs, which, in turn, influences the measurable Hall conductivity [6,8]. In theoretical studies one finds an anomalous quantization, where each of the four fermionic flavors in graphene contributes a half-integer, $n + 1/2$, to the total Hall conductivity [8–10]

$$\sigma_{0,xy} = \pm 4 \left(n + \frac{1}{2} \right) \frac{e^2}{h}, \quad n = 0, 1, 2, \dots \quad (1)$$

The additional fraction of $1/2$ can be traced back to the existence of a half-filled Landau level located directly at the charge neutrality point, which has only half the degeneracy of the other levels (the spectral anomaly), while the factor of four is a direct consequence of the four independent SU(4) symmetric flavors of charge carriers in the low-energy Dirac model. With the recent success of graphene’s experimental isolation, these theoretical predictions became experimentally accessible and could indeed be verified [11,12].

Shortly after the IQHE was discovered in nonrelativistic semiconducting devices, measurements on high quality samples revealed the occurrence of additional plateaus at certain

fractional fillings [13,14], and more recently this effect has also been observed in graphene [15–17]. For this fractional quantum Hall effect (FQHE), electron-electron interactions are an essential ingredient in the theoretical treatment to gain further understanding of the underlying physics. The main difficulty here is that the noninteracting Landau levels, forming the basis of the analysis, are macroscopically degenerate. As a consequence, conventional perturbative approaches inevitably fail, making the FQH system a prime example for strongly correlated matter, which has to be analyzed by truly nonperturbative methods.

Based on the seminal work of Laughlin [18], Jain introduced the idea that physical electrons/holes and magnetic flux quanta, or vortices, form bound states, so-called “composite fermions” [19]. Due to the process of flux nucleation, the magnetic field is reduced, leading to a new set of effective Landau levels that are occupied by the composite fermions. The integer fillings of those effective LLs map to the fractional fillings observed in the experiments. Thus, the fractional QHE of ordinary fermions can be understood as an integer QHE of composite fermions [2,20]. This intuitive, albeit rather unconventional picture led to a vast body of theoretical predictions, which could be verified experimentally to a large extent [21–36]. Applying these ideas to the Dirac electrons in graphene leads to the notion of “composite Dirac fermions.” Accordingly, one might expect that their pseudorelativistic spectrum, which leads to the anomalous quantization of the Hall conductivity in the noninteracting case, leaves its marks in the FQHE.

In the theoretical treatment of the FQHE, there are several slightly different approaches to realize Jain’s idea of flux-binding. Within the trial wave function approach, vortices are attached in the form of Jastrow factors multiplying the many-body wave function of noninteracting fermions in an IQH state [2,20]. To make use of this strategy in graphene, one considers a completely empty or completely filled lowest LL—usually the one at the charge neutrality point—as the vacuum state and attaches flux quanta to the physical electrons/holes that partially fill/deplete this energy level. Thereby it is assumed that the effective LLs and their associated single-particle wave

functions, which make up the IQH state, are *not* of the Dirac type, but coincide with the nonrelativistic Schrödinger type ones [8,37,38]. This assumption is justified by the fact that the quenched Hamiltonian of graphene projected to the lowest LL is identical to the Hamiltonian encountered in systems with a nonrelativistic parabolic dispersion [8,37–39]. Loosely speaking, graphene electrons confined to the lowest LL lose their identity as Dirac fermions upon projection, such that the only impact of graphene’s unconventional band structure is the SU(4) symmetry of the ansatz wave function, which derives from the SU(4) symmetry of the individual fermionic flavors. This construction leads to the conventional Jain sequence and wave functions. Straightforward generalizations of this approach are given by Halperin wave functions [8,40–44], which potentially break the SU(4) symmetry down to SU(2)^{⊗2} or even U(1)^{⊗4}.

Despite its indisputable successes, the trial wave function approach has several drawbacks, two of which we want to comment on further. First, it crucially depends on projected Hamiltonians, which typically neglect LL mixing. While for nonrelativistic systems for the most part this is only a minor issue, since at large magnetic fields LL mixing is suppressed as $1/\sqrt{B}$ [45], in graphene, it is a substantially more severe problem. Here, LL mixing is controlled by the fine structure constant α , which is independent of the magnetic field and—more importantly—genuinely large ($\alpha \approx 2.2$ in suspended graphene), making LL mixing a nonperturbative problem already on the level of the Hamiltonian [46,47]. Hence, although the kinetic energy may be quenched within a partially filled LL, the electrons in graphene still feel their Dirac heritage. Yet, if LL mixing is taken into account, at least perturbatively, Refs. [46,47] reported—quite surprisingly—that it has practically no effect on the wave functions in the zeroth LL. Not entirely decoupled from the above, the second main problem is concerned with particle-hole symmetry, or rather its strong breaking inherent in the construction of trial wave functions. The origin of particle-hole symmetry is different for nonrelativistic and relativistic systems. For the former, it is only an emergent symmetry of the lowest LL projected Hamiltonian, but for the latter, it is an exact symmetry of the unprojected Hamiltonian (and, hence, is a good symmetry even if LL mixing is taken into account). The construction of particle-hole conjugated wave functions is still possible, but the explicit symmetry breaking is not only unsatisfying but also comes with its own complications, see, for example, Refs. [48,49] for a more elaborate discussion.

A complementary approach to the construction of explicit wave functions is the Chern-Simons field theory, which does not rely on a projection to the lowest LL. Here, magnetic flux tubes—which should be distinguished from the vortices of the wave-function approach—are attached to the fermionic degrees of freedom either via a singular gauge transformation [20,50], or equivalently via a minimal coupling of a Chern-Simons gauge field to the kinetic action in addition to a kinetic Chern-Simons term [51–55]. (See also Ref. [56] for a similar treatment involving bosons.) In the process, ordinary fermions are transformed into composite fermions, whose nature—Schrödinger or Dirac—is determined by the structure of the kinetic action. Hence, as opposed to the picture drawn in

Ref. [37], the Chern-Simons composite fermions in graphene are actual Dirac-type particles. Accordingly, one might expect that the spectral anomaly of the composite Dirac fermions (the half-integer quantization of the filling fractions) enters the analytical formulas for the total filling fraction/Hall conductivity of the electronic system. However, the graphene Chern-Simons theories proposed in Refs. [57,58] attach flux to the physical electrons/holes with respect to the bottom/top of the lowest LL, which eliminates the spectral anomaly and yields predictions for the total filling fraction that are in accordance with the wave-function approach. Concerning LL mixing, the Chern-Simons approaches reside on the other side of the spectrum, meaning there is a large amount of LL mixing [59], which is a result of the Chern-Simons transformation and the absence of projection. Regarding the nonperturbative nature of LL mixing in graphene, this feature should not necessarily be considered a flaw, but the question, if the Chern-Simons induced LL mixing describes the physical reality accurately, remains.

Although the non-Dirac nature of the composite fermions in graphene’s lowest LL appears to be fully established by the results of Ref. [47], the conclusion that theoretical frameworks that employ Dirac-type composite fermions, such as the aforementioned pseudorelativistic Chern-Simons theories of Refs. [57,58], lose their viability would be too hasty as Son’s work, Ref. [49], impressively shows. Focussing on the conventional nonrelativistic FQH system, Son proposed a manifestly particle-hole symmetric, pseudorelativistic effective model, which declares Jain’s composite fermion to be a Dirac particle by nature. Specifically, the $\nu = 1/2$ state is described by a charge neutral Dirac particle interacting with an emergent gauge field (*not* of the Chern-Simons type) that forms a Fermi liquid, while Jain’s principal sequence around half-filling can be explained as the IQHE of those Dirac quasiparticles, fully incorporating the particle-hole symmetry of the lowest Landau level.

In contrast to Son’s effective model, in the present paper, we employ a rather standard microscopic Chern-Simons theory, similar to Refs. [57,58]. The crucial difference to those works is the reference point at which we implement Chern-Simons flux-attachment, namely the particle-hole symmetric Dirac point at charge neutrality. This shift in the reference point should not be underestimated as a mere shift in the total filling fraction, since it allows for a flux-attachment scheme that is distinctively different from the aforementioned approaches. Instead of attaching flux to the physical electrons/holes, it is possible to attach flux to the charge carrier density, that is, electron- or hole-like quasiparticles measured from the charge neutrality point. In particular, we obtain a mean-field equation which involves the charge carrier density, instead of the electron/hole density, and within the calculation of Gaussian fluctuations, we naturally encounter pseudorelativistic propagators experiencing an effective magnetic field, which incorporates the spectral anomaly. Our central result is the electromagnetic polarization tensor in linear response to an external perturbation, which—among others—gives access to the Hall conductivity of the multicomponent fractional quantum Hall system:

$$\sigma_{xy} = \sum_{\alpha} \sigma_{0,xy}^{\alpha} - \sum_{\alpha,\beta} \sigma_{0,xy}^{\alpha} (\hat{\sigma}_{0,xy} + \hat{K}^{-1})_{\alpha\beta}^{-1} \sigma_{0,xy}^{\beta}. \quad (2)$$

Here, $\sigma_{0,xy}^\alpha$ is the Hall conductivity of a noninteracting, single flavour α , which is half-integer quantized at low temperatures, due to the Dirac nature of the composite fermions, $\hat{\sigma}_{0,xy}$ is a diagonal matrix containing these single flavour conductivities, and $\hat{\mathcal{K}}$ is an integer-valued symmetric matrix accounting for the flux-attachment [60].

We show that Eq. (2) leads to particle-hole symmetric Hall plateaus around charge neutrality, if positive flux-attachment to electronlike and negative flux-attachment to hole-like quasiparticles is considered. This observation enables us to construct manifestly particle-hole symmetric filling fractions as functions of the chemical potential. This result seems surprising, since the Chern-Simons term explicitly breaks particle-hole symmetry—which is why Son discarded such a term in his effective theory [49]—irrespective of the reference point where the Chern-Simons flux is attached. Since this symmetry cannot be generated dynamically, particle-hole symmetric Hall plateaus are not expected to occur in such a symmetry broken theory. The puzzle is resolved as follows. The standard definition of the particle-hole transformation involves fermionic and bosonic fields only, but leaves the Chern-Simons coupling untouched. By allowing the coupling to depend on the sign of the carrier density, we have altered the flux-attachment prescription in such a way to make it consistent with the standard particle-hole symmetry transformation. One may also interpret it the other way around: we use the standard flux-attachment but change the symmetry transformation to involve a sign flip of the Chern-Simons coupling. Thus, one may argue that the Chern-Simons term only breaks particle-hole symmetry in a weak sense, since it can be circumvented altogether by sufficiently modifying the symmetry transformation or the flux-attachment prescription, alleviating the seeming incompatibility of particle-hole symmetry and Chern-Simons theory. Furthermore, we show that the above formula reproduces the Hall conductivities proposed in Refs. [61,62] as special cases, as well as several other filling fractions that have been obtained in the wave-function approach.

In this paper, we employ the real-time Keldysh formalism, which offers several technical advantages in comparison to the conventional real-time ground-state formalism. This formulation will allow for a natural regularization of the otherwise ill-defined mean-field equations, upon which the flux-attachment interpretation is based, and it additionally yields results that are valid at finite temperature, which come without further calculational costs. Our exposition is inspired by the original work of Refs. [51,53], where the fermion Chern-Simons theory for the FQHE of nonrelativistic matter has been introduced. Since there are several subtle differences due to the Dirac nature of the quasiparticles and the Keldysh formulation, we will present the theory in a self-contained manner. The outline of the article is as follows. In Sec. II, we describe the field theory of interacting Dirac fermions coupled to statistical Chern-Simons fields with the Abelian gauge group $U(1)^{\otimes 4}$. In the subsequent section, we derive an exact effective action for the statistical gauge fields and discuss its Gaussian approximation around the mean-field solution of the quantum Hall liquid. Section IV contains our main results. We address the topic of gauge fixing and calculate the full electromagnetic response tensor together with Hall conductivities for a selected set of states. We conclude in the final section.

Further technical details of the computation are given in two appendices.

II. ABELIAN CHERN-SIMONS THEORY

The starting point of our considerations is the second quantized low-energy Hamiltonian for interacting Dirac electrons in monolayer graphene ($\hbar = 1$),

$$H = \int_{\vec{x}} \Psi^\dagger(\vec{x}) \hat{\mathcal{H}}_D \Psi(\vec{x}) + \frac{1}{2} \int_{\vec{x}, \vec{y}} \delta n(\vec{x}) V(\vec{x} - \vec{y}) \delta n(\vec{y}), \quad (3)$$

with $\delta n(\vec{x}) = \Psi^\dagger(\vec{x}) \Psi(\vec{x}) - \bar{n}(x)$. The fermionic field operators Ψ and Ψ^\dagger are, in fact, eight-component spinors $\Psi \equiv (\Psi_\uparrow \ \Psi_\downarrow)^\top$, with $\Psi_\sigma \equiv (\psi_{AK_+} \ \psi_{BK_+} \ \psi_{BK_-} \ \psi_{AK_-})_\sigma^\top$. The indices A/B , K_\pm , and \uparrow, \downarrow represent sublattice, valley, and spin degrees of freedom, respectively.

The first term—the Dirac part of the Hamiltonian—describes the dynamics of the four flavors of Dirac electrons $\alpha = (K_+\uparrow, K_-\uparrow, K_+\downarrow, K_-\downarrow)$. Within the basis chosen above, the single-particle Hamiltonian $\hat{\mathcal{H}}_D$ assumes a diagonal form in flavor space,

$$\hat{\mathcal{H}}_D = \text{diag}(\mathcal{H}_{D,K_+\uparrow}, \mathcal{H}_{D,K_-\uparrow}, \mathcal{H}_{D,K_+\downarrow}, \mathcal{H}_{D,K_-\downarrow}), \quad (4)$$

where the Hamiltonian for each individual flavor reads

$$\mathcal{H}_{D,\alpha} = -\kappa_\alpha i v_F \vec{\sigma} \cdot \vec{\nabla}. \quad (5)$$

Here, $\kappa_\alpha = \pm 1$ distinguishes between the two valleys K_\pm , and v_F is the Fermi velocity with the numerical value $v_F \approx c/300$. Note that we indicated the 4×4 matrix structure of the flavor space in Eq. (4) with a hat symbol explicitly, while the 2×2 matrix structure of the sublattice space is implicit.

The second term of Eq. (3) describes two-particle interactions between the Dirac fermions. The interaction amplitude is given by the instantaneous, $U(4)$ symmetric Coulomb interaction

$$V(\vec{x} - \vec{y}) = \frac{e^2}{\epsilon |\vec{x} - \vec{y}|}. \quad (6)$$

The term $\bar{n}(\vec{x}) = \sum_\alpha \bar{n}_\alpha(\vec{x})$ in the definition of the bosonic operator $\delta n(\vec{x})$ is a background density. In general, it is space- and possibly even time-dependent, but for our purposes, however, will be constant. It acts as a counterterm, that cancels the zero momentum singularity of the bare Coulomb interaction. Furthermore, ϵ is the dielectric constant of the medium (being unity in vacuum), which describes the influence of a substrate on the bare Coulomb interaction.

In this paper, we employ the Keldysh formalism to formulate a real-time theory at finite temperature and density for the four interacting flavors of Dirac particles in graphene, that are subject to an external magnetic field and coupled to four statistical $U(1)$ gauge fields. Within the Keldysh formulation, the dynamical degrees of freedom of the theory are defined on the Schwinger-Keldysh contour, which is a closed contour in the complex time plane [63,64]. The time arguments of the field operators are elevated to contour-time and correlation functions are derived as the expectation value of their “path ordered” products. As shown in Fig. 1, the time contour starts at a reference time t_0 —at which the initial density matrix is specified—extends into the infinite future along the real axis and returns to the reference time eventually. Here, we are mainly interested in

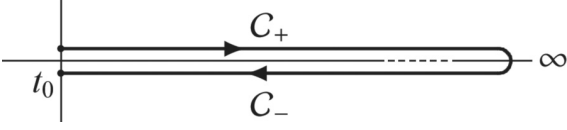


FIG. 1. Schwinger-Keldysh closed time contour in the complex time plane with forward (C_+) and backward time branch (C_-). Here, t_0 is a reference time, where an initial density matrix enters the theory. Since we are only interested in the system's linear response properties close to thermal equilibrium, we send the reference time to the remote past ($t_0 = -\infty$) outright.

the thermal equilibrium state in linear response to an external electromagnetic perturbation. Therefore we send the reference time t_0 to the infinite past, which erases all the information about possible nontrivial initial correlations and transient regimes [65,66]. As a consequence, the quantum kinetic equations are of no further concern, since they can be trivially solved by the well-known thermal distribution functions [64].

Before we discuss the field theoretic model in its action formulation, a few remarks concerning notational conventions are in order. First, to a large extent, we will work within the abstract contour-time representation, and only switch to a physical real-time representation at the end of Sec. III when we discuss Gaussian fluctuations of the bosonic effective action around the mean-field solution of the fractional quantum Hall liquid. The major advantage of the contour-time representation is that it allows for a compact and concise notation, resembling the zero temperature vacuum (or ground state) theory, yet encoding the full information of thermal fluctuations [63]. Furthermore, we employ a covariant notation, where upper and lower case greek letters μ , ν , and λ denote contra- and covariant components of a Minkowski three-vector, respectively. As usual, a repeated index implies summation according to the Einstein summation convention. This summation rule is lifted if a repeated index is bracketed. [This statement will only apply for repeated flavor space indices α and β , see Eq. (13) for instance.] The convention for the flat Minkowski metric is chosen to be $\eta_{\mu\nu} = \text{diag}(1, -1, -1)$, and natural units ($\hbar = c = 1$) are used throughout the article. Lastly, space-time integrations will be denoted by

$$\int_{\mathcal{C},x} \equiv \int_{\mathcal{C}} dt \int d^2r, \quad (7)$$

where \mathcal{C} indicates that the time integration is performed along the Schwinger-Keldysh contour, and $x = x^\mu = (t, \vec{r})$ labels (contour-)time and spatial variables. After introducing these general notational conventions, we proceed to describe the details of the model.

The entire physical content of the theory is summarized by the coherent state functional integral [63,64,67]

$$Z[eA_\mu + \mathcal{A}_\mu^\alpha] = \int \mathcal{D}\psi \mathcal{D}\psi^\dagger \mathcal{D}a e^{iS[\psi, eA_\mu + \mathcal{A}_\mu^\alpha, a]}, \quad (8)$$

which is a generating functional of correlation functions. The action S in the exponential can be written as a sum of three terms:

$$S[\psi, eA_\mu + \mathcal{A}_\mu^\alpha, a] = S_D[\psi, eA_\mu + \mathcal{A}_\mu^\alpha + a^\alpha] + S_{\text{Coul}}[\psi] + S_{\text{CS}}[a^\alpha], \quad (9)$$

where the first two terms, involving the fermionic fields, are readily obtained from the Heisenberg picture Hamiltonian $H(t)$ by the definition

$$S_D[\psi] + S_{\text{Coul}}[\psi] = \int_{\mathcal{C},t} \left(\int_{\mathcal{F}} \Psi^\dagger(x) i \partial_t \Psi(x) - H(t) \right). \quad (10)$$

The bosonic fields within the Dirac part of the action, A_μ , \mathcal{A}_μ^α , and a_μ^α , are introduced via the minimal coupling prescription. They represent an external electromagnetic potential, local two-particle source fields, and the statistical gauge fields, respectively. The source fields will later be used to generate the desired correlation functions. The Dirac action can be written compactly as a quadratic form of an eight-component Grassmann spinor Ψ [5,9]

$$S_D[\psi, eA_\mu + \mathcal{A}_\mu^\alpha + a_\mu^\alpha] = \int_{\mathcal{C},xy} \Psi^\dagger(x) \hat{G}_0^{-1}(x,y) \Psi(y). \quad (11)$$

The matrix \hat{G}_0^{-1} is the inverse contour-time propagator, which inherits the flavor diagonal structure from the single-particle Hamiltonian (4):

$$\hat{G}_0^{-1} = \text{diag}(G_{0,K+\uparrow}^{-1}, G_{0,K-\uparrow}^{-1}, G_{0,K+\downarrow}^{-1}, G_{0,K-\downarrow}^{-1}). \quad (12)$$

According to Eq. (5), the dynamics of each flavor is governed by the pseudorelativistic, massless Weyl operator

$$G_{0,\alpha}^{-1}(x,y) = \delta_{\mathcal{C}}(x-y) (i\sigma_{(\alpha)}^\mu \mathcal{D}_\mu^{(\alpha)} + \mu_\alpha). \quad (13)$$

Here, $\delta_{\mathcal{C}}(x-y) = \delta_{\mathcal{C}}(x_0 - y_0) \delta(\vec{x} - \vec{y})$ involves the contour-time delta function [63] and $\sigma_\alpha^\mu \equiv (\sigma_0, \kappa_\alpha v_F \sigma_1, \kappa_\alpha v_F \sigma_2)$ is a three-vector of Pauli matrices, acting in sublattice space. The gauge covariant derivative

$$\mathcal{D}_\mu^\alpha = \partial_\mu + ieA_\mu(x^\mu) + i\mathcal{A}_\mu^\alpha(x^\mu) + ia_\mu^\alpha(x^\mu) \quad (14)$$

contains the aforementioned covariant vector potentials A_μ , \mathcal{A}_μ^α , and a_μ^α . For the external potential A_μ , we choose the Landau gauge, $A_\mu(x^\mu) = (0, Bx^2, 0) = (0, By, 0)$, to describe a uniform and static magnetic field B perpendicular to the graphene plane. Note that it does not depend on the flavor index α , so that all flavors universally couple to the same field. The source fields \mathcal{A}_μ^α and the statistical gauge fields a_μ^α , on the other hand, do carry a flavor index and, thus, couple to each fermionic flavor individually. Such a coupling breaks the global $U(4)$ symmetry of the theory without Chern-Simons fields down to a local $U(1)^{\otimes 4}$ symmetry. Finally, we introduced a flavor dependent chemical potential μ_α , allowing for independent doping of the individual flavors. Physically, this flavor dependence may be thought of as originating from a generalized Zeeman term [8].

The Coulomb interaction part requires no further discussion as it is directly obtained from the interaction part of the Hamiltonian (3),

$$S_{\text{Coul}}[\psi] = -\frac{1}{2} \int_{\mathcal{C},xy} \delta n(x) V(x-y) \delta n(y), \quad (15)$$

with $V(x-y) = V(\vec{x} - \vec{y}) \delta_{\mathcal{C}}(x_0 - y_0)$.

The third term in the action (9) is the kinetic term for the four statistical gauge fields, which is given by a generalized

Chern-Simons action [51,53,54,59]

$$S_{\text{CS}}[a_\mu^\alpha] = \frac{1}{2} (\hat{\mathcal{K}}^{-1})_{\alpha\beta} \int_{\mathcal{C},x} \varepsilon^{\mu\nu\lambda} a_\mu^\alpha(x) \partial_\nu a_\lambda^\beta(x). \quad (16)$$

Herein $\varepsilon^{\mu\nu\lambda}$ is the total antisymmetric Levi-Civita tensor (we use the convention $\varepsilon^{012} = 1$), and $\hat{\mathcal{K}}$ is a regular, i.e., invertible, symmetric 4×4 matrix,

$$\hat{\mathcal{K}} = 2\pi \begin{pmatrix} 2k_1 & m_1 & n_1 & n_2 \\ m_1 & 2k_2 & n_3 & n_4 \\ n_1 & n_3 & 2k_3 & m_2 \\ n_2 & n_4 & m_2 & 2k_4 \end{pmatrix}, \quad (17)$$

with integers k_i, m_i, n_i . For those configurations of integers where $\hat{\mathcal{K}}$ happens to be singular, Eq. (16) needs to be regularized. This may be achieved by adding a diagonal matrix $\hat{\mathcal{R}} = 2\pi \text{diag}(+i\eta, -i\eta, +i\eta, -i\eta)$ to Eq. (17), where η is an infinitesimal (the signs therein are purely conventional). The physical meaning of the \mathcal{K} matrix is to attach statistical magnetic flux to the fermions. This feature will become more clear in the next section when we discuss the stationary phase approximation.

The theory we described above possesses a *local* $U(1)^{\otimes 4}$ symmetry, in comparison to the symmetry of the original model of interacting electrons in graphene, being a *global* $U(4)$ flavor symmetry ($U(2) \times U(2)$), respectively, if one takes into account a Zeeman term [5]. It has to be emphasized that the symmetry is broken explicitly by considering the flavor dependent chemical potential in addition to the $U(1)^{\otimes 4}$ symmetric gauge field coupling. As pointed out by the authors of Ref. [54], who studied the FQHE for nonrelativistic fermions in bilayers, as well as $SU(2)$ symmetric monolayers, the original $U(4)$ symmetry may only be generated dynamically (once the flavor dependence of the chemical potential is neglected [54]). Therefore it is expected that some of the fractional quantum Hall states we obtain in this work—after certain necessary approximations have been made—may not be realized in the exact theory, as they could be destabilized by higher-order fluctuations. A manifestly $U(4)$ [respectively, $U(2) \times U(2)$] symmetric theory, on the other hand, could be constructed in analogy to Refs. [52,54], by considering an appropriate non-Abelian generalization of Eq. (16), with a corresponding set of non-Abelian statistical gauge fields, coupling gauge covariantly to holon and spinon fields; see Sec. V for a brief discussion. Clearly, such a non-Abelian gauge theory is in many aspects significantly more complex than the Abelian theory of the present article and we leave its construction and analysis for future work.

As a final remark we want to stress that the partition function (8) as it stands is not well-defined. Since the Chern-Simons fields a_μ^α are gauge fields, the functional integral contains an infinite summation over all, physically equivalent orbits of pure gauge, leading to a strong divergence. In order to extract physically meaningful information from the partition function, the gauge equivalent orbits have to be removed, such that each gauge field configuration in the functional integral uniquely corresponds to a physical field configuration. To this end, we employ the well-known Fadeev-Popov procedure [68], but we postpone the details of the discussion to Sec. IV. For now

we work with Eqs. (8) and (9) as they are, but keep in mind that they need to be modified.

III. EFFECTIVE BOSONIC ACTION, MEAN-FIELD THEORY, AND GAUSSIAN FLUCTUATIONS

In this section, we derive an exact expression for the effective action of the gauge fields a_μ^α , following Ref. [51]. Subsequently, the nonpolynomial action we obtain will be expanded to second order in the fluctuations around its mean-field solution, resulting in an exactly solvable Gaussian model. The quadratic action will be stated in its real-time form in Keldysh basis.

Due to the Coulomb interaction being quartic in the fermionic fields, an integration of these microscopic degrees of freedom is not readily possible. For this reason, we rewrite the problematic interaction term by means of a Hubbard-Stratonovich transformation in the density-density channel [64], which introduces an auxiliary boson ϕ :

$$e^{iS_{\text{int}}[\psi]} = \int \mathcal{D}\phi e^{iS_{\text{HS}}[\phi] + iS_{\text{int}}[\psi, \phi]}. \quad (18)$$

The quadratic action of the Hubbard-Stratonovich boson is given by

$$S_{\text{HS}}[\phi] = \frac{1}{2} \int_{\mathcal{C},xy} \phi(x) V^{-1}(x-y) \phi(y), \quad (19)$$

with the inverse Coulomb interaction V^{-1} , which, of course, has to be understood in the distributional sense. The second term contains a trilinear Yukawa-type interaction and a linear term, describing the interaction of the auxiliary boson with the background density \bar{n} :

$$S_{\text{int}}[\psi, \phi] = - \int_{\mathcal{C},x} \phi(x) (\Psi^\dagger(x) \Psi(x) - \bar{n}(x)). \quad (20)$$

Note that the fluctuating Bose field ϕ in the Yukawa interaction appears on the same footing as the zero component of the external gauge potential A_μ , coupling to all flavors identically, see Eqs. (11)–(14). As a consequence of the above manipulation, the Grassmann fields ψ appear only quadratically, such that the fermionic integral can be performed exactly. Our intermediate result for the effective action now only contains bosonic degrees of freedom:

$$\begin{aligned} S'_{\text{eff}}[eA_\mu + \mathcal{A}_\mu^\alpha, a_\mu^\alpha, \phi] \\ = -i \text{tr} \ln \hat{G}_0^{-1} [eA_\mu + \mathcal{A}_\mu^\alpha + a_\mu^\alpha + \phi \delta_{0\mu}] \\ + S_{\text{HS}}[\phi] + \phi \bar{n} + S_{\text{CS}}[a_\mu^\alpha]. \end{aligned} \quad (21)$$

Remarkably, the Hubbard-Stratonovich boson ϕ can be integrated exactly after shifting the statistical gauge fields as follows: $a_\mu^\alpha \rightarrow a_\mu^\alpha - \phi \delta_{0\mu}$ [51,54]. The result is the desired effective action of the Chern-Simons gauge fields in the presence of the two-particle source fields \mathcal{A}_μ^α :

$$\begin{aligned} S_{\text{eff}}[eA_\mu + \mathcal{A}_\mu^\alpha, a_\mu^\alpha] = -i \text{tr} \ln \hat{G}_0^{-1} [eA_\mu + \mathcal{A}_\mu^\alpha + a_\mu^\alpha] \\ + S_V[a_\mu^\alpha] + S_{\text{CS}}[a_\mu^\alpha]. \end{aligned} \quad (22)$$

The term $S_V[a_\mu^\alpha]$ is a quadratic functional of the gauge fields that is generated by the ϕ integration:

$$S_V[a_\mu^\alpha] = -\frac{1}{2} \int_{\mathcal{C},xy} ((\hat{\mathcal{K}}^{-1})_{\alpha_1\beta_1} \varepsilon^{0\mu_1\nu_1} \partial_{\mu_1} a_{\nu_1}^{\beta_1} - \bar{n}_{\alpha_1})(x) \\ \times V^{\alpha_1\alpha_2}(x-y) ((\hat{\mathcal{K}}^{-1})_{\alpha_2\beta_2} \varepsilon^{0\mu_2\nu_2} \partial_{\mu_2} a_{\nu_2}^{\beta_2} - \bar{n}_{\alpha_2})(y). \quad (23)$$

Here we have defined $V^{\alpha\beta}(x-y) \equiv V(x-y)$, where the additional flavor-space indices keep track of the correct summation. Note that Eq. (23) is nothing but the Coulomb interaction term (15), in which the density of flavor α , $\Psi_{(\alpha)}^\dagger(x)\Psi_{(\alpha)}(x)$, is substituted by $(\hat{\mathcal{K}}^{-1})_{\alpha\beta} \varepsilon^{0\mu\nu} \partial_\mu a_\nu^\beta(x)$. In the above derivation, no approximations were involved. Yet, due to the nonpolynomial trace-log term, the residual functional integral over the gauge fields cannot be performed exactly. A common strategy to deal with this problem, which we adopt here as well, is to find the field configuration in which the effective action becomes stationary and, subsequently, expand in powers of fluctuations around the mean.

The variation of Eq. (22) in the absence of two-particle sources \mathcal{A}_μ^α yields

$$\frac{\delta S_{\text{eff}}}{\delta a_\mu^\alpha(z)} = -j_\alpha^\mu(z) + (\hat{\mathcal{K}}^{-1})_{\alpha\beta} \varepsilon^{\mu\nu\lambda} \partial_\nu a_\lambda^\beta(z) \\ - \int_{\mathcal{C},xy} ((\hat{\mathcal{K}}^{-1})_{\alpha_1\beta_1} \varepsilon^{0\mu_1\nu_1} \partial_{\mu_1} \delta_{\nu_1}^{\beta_1} \delta_{\mathcal{C}}(x-z)) \\ \times V^{\alpha_1\alpha_2}(x-y) ((\hat{\mathcal{K}}^{-1})_{\alpha_2\beta_2} \varepsilon^{0\mu_2\nu_2} \partial_{\mu_2} a_{\nu_2}^{\beta_2} - \bar{n}_{\alpha_2})(y). \quad (24)$$

Here, j_α^μ is the particle 3-current density per flavor α in the presence of an external gauge potential A_μ and the Chern-Simons fields a_μ^α :

$$j_\alpha^\mu(x) = -i \frac{\delta}{\delta a_\mu^\alpha(x)} \text{tr} \ln \hat{G}_0^{-1} [eA_\mu + a_\mu^\alpha]. \quad (25)$$

We have to stress at this point that Eqs. (24) and (25) have to be treated with special care as they demand a proper regularization. First, in the infinite system, the particle current is not well defined, since its $\mu = 0$ component—being the particle density—diverges. This fact is a direct consequence of the Dirac approximation of the tight-binding graphene spectrum. Another issue is related to the fact that the definition of the particle current involves the average of a (contour-)time ordered product of two fermionic fields evaluated at the same time. However, these problems are immediately resolved once the theory is mapped to the physical real-time representation in Keldysh basis. Hereto, one splits the Schwinger-Keldysh contour into a forward and backward branch and defines a doubled set of fields, Ψ_\pm and $(a_\pm)^\alpha$, which are associated to the respective branch [63,64]. In a next step, one performs a rotation from \pm basis to Keldysh basis by defining “classical” and “quantum” fields, indexed by c and q , respectively, as symmetric and antisymmetric linear combinations of the \pm fields [63,64]. The net result is that the derivative in Eq. (24) is performed with respect to the quantum components of the gauge fields, the particle 3-current densities are replaced by the well-defined charge carrier 3-current densities $\tilde{j}_\mu^\alpha(x)$, see

Eq. (A12), and the gauge fields on the right-hand side are replaced by their classical components [69].

The requirement of a vanishing first variation defines the mean-field equations for the Chern-Simons fields. As pointed out by the authors of Refs. [51,54], these mean-field equations allow for several physically different scenarios such as Wigner crystals and solitonic field configurations. Following Refs. [51,54], we here concentrate on those solutions, which lead to a vanishing charge carrier current and a uniform and time independent charge carrier density \bar{n}_α , describing a quantum Hall liquid. In that case, Eq. (24) reduces to the relation

$$\bar{n}_\alpha = (\hat{\mathcal{K}}^{-1})_{\alpha\beta} \varepsilon^{0\mu\nu} \partial_\mu \bar{a}_\nu^\beta = -e (\hat{\mathcal{K}}^{-1})_{\alpha\beta} b^\beta. \quad (26)$$

Here, the second equality defines the (uniform) Chern-Simons magnetic field b^α , experienced by the flavor α charge carriers, in terms of the expectation value of the Chern-Simons fields $\bar{a}_\mu^\alpha \equiv \langle (a_c)^\alpha \rangle$. Inverting the above relation yields the statistical magnetic fields b^α as functions of the densities \bar{n}_α :

$$b^\alpha = -\frac{1}{e} \mathcal{K}^{\alpha\beta} \bar{n}_\beta. \quad (27)$$

Writing the mean-field equation in this form reveals the physical meaning of the \mathcal{K} -matrix, as it defines the precise flux-attachment procedure of the multicomponent quantum Hall system. Each flavor β of charge carriers, contributes to the statistical magnetic field for the flavor α with a magnetic flux $\mathcal{K}^{\alpha(\beta)} \bar{n}_{(\beta)}$. Hence the component $\mathcal{K}^{\alpha\beta}$ represents the contribution to the statistical flux per flavor β as seen by flavor α . Thus Eq. (27) may be interpreted as a “flux-binding” relation, which transforms ordinary Dirac fermions into “composite Dirac fermions.” Furthermore, it is important to notice that Eq. (27) is well-defined even for singular \mathcal{K} matrices, in contrast to Eq. (26). Such singular configurations should not be discarded, however, as the following discussion shows. Consider, for example, the special case, where all components of $\hat{\mathcal{K}}$ equal the same constant $2k$. In that case, the four equations (27) reduce to a single one, yielding a unique statistical field b associated to the density of charge carriers $\bar{n} = \sum_\alpha \bar{n}_\alpha$. This scenario corresponds to a Chern-Simons theory, where only a single dynamical gauge field, $a_\mu = \sum_\alpha a_\mu^\alpha$, is present that couples to the different flavors identically [57]. The other three eigenvectors one obtains by diagonalizing Eq. (17) span a triply degenerate subspace with eigenvalue zero, and thus decouple. Likewise, for other singular \mathcal{K} -matrix configurations, one would obtain a theory with only two or three dynamical gauge fields and a correspondingly reduced parameter space. (In the extreme case where $\hat{\mathcal{K}}$ is identically zero, all gauge fields would decouple and no flux binding could occur, which leads back to the integer quantum Hall regime.) With this physical picture in mind we now continue our discussion.

By virtue of the gauge covariant derivative (14), each one of the statistical magnetic fields (27) adds to the external magnetic field B individually, resulting in a flavor-dependent effective magnetic field [70]

$$B_{\text{eff}}^\alpha = B + b^\alpha = B - \frac{1}{e} \mathcal{K}^{\alpha\beta} \bar{n}_\beta. \quad (28)$$

It is this effective magnetic field, rather than the external field B alone, which enters the fermionic propagators, such that

Eqs. (27) and (28), in fact, represent self-consistency equations. A straightforward calculation of the free propagator for Dirac fermions moving in the effective magnetic field B_{eff}^α yields the charge carrier density for the flavor α as a function of the chemical potential μ_α , the effective magnetic field B_{eff}^α , and temperature T (see Appendix A for details):

$$\bar{n}_\alpha(\mu_\alpha, B_{\text{eff}}^\alpha, T) = \frac{1}{2\pi\ell_{(\alpha)}^2} \nu_{(\alpha)}(\mu_\alpha, B_{\text{eff}}^\alpha, T). \quad (29)$$

Here, we have introduced the magnetic length $\ell_\alpha = 1/\sqrt{|eB_{\text{eff}}^\alpha|}$ and the filling fraction per flavor [9,10],

$$\nu_\alpha = \frac{1}{2} \left(\tanh \frac{\mu_\alpha}{2T} + \sum_{n=1}^{\infty} \sum_{\lambda=\pm 1} \tanh \frac{\lambda\sqrt{n}\omega_c^\alpha + \mu_\alpha}{2T} \right), \quad (30)$$

where $\omega_c^\alpha = \sqrt{2}v_F/\ell_\alpha$ denotes the pseudorelativistic cyclotron frequency. The charge carrier density as a function of an effective magnetic field B_{eff}^α at constant chemical potential μ_α and the filling fraction as a function of the chemical potential at constant field are shown in Fig. 2. At large magnetic fields and low temperatures, the filling fraction shows the typical plateau structure that is characteristic for the (anomalous) integer quantum Hall effect. This issue will be discussed in more detail at the end of this section, once we have obtained the Gaussian approximation to the exact action (22).

From the above mean-field equation, one may calculate the possible fractional fillings at which the spectrum is gapped, leading to a plateau structure for the “interacting Hall conductivity,” which is the hallmark of the fractional quantum Hall effect. However, we prefer to extract the filling fractions directly from the interacting Hall conductivity, which will be derived in the next section. To continue, we only need to know that the mean-field equation has a nontrivial solution, which depends on the \mathcal{K} matrix, the external magnetic field, temperature, and chemical potential. Furthermore, observe that the effective magnetic field is invariant upon changing the sign of $\mathcal{K}_{\alpha\beta}$ and \bar{n}_α simultaneously. This is a first hint, how to construct manifestly particle-hole symmetric filling fractions in the presence of a Chern-Simons term.

The stationary field configuration we found above serves as a reference point around which one should expand the effective action (22) in powers of field fluctuations. To this end, one writes $a_\mu^\alpha = \bar{a}_\mu^\alpha + \Delta a_\mu^\alpha$ and expands the effective action to the desired order in the fluctuation Δa_μ^α and the source \mathcal{A}_μ^α . As mentioned before, here we are only interested in an expansion up to second order. Terms linear in the fluctuation vanish since the effective action is evaluated at the saddle point, whereas linear source terms do not vanish. However, since the latter only couple to the above mean-field 3-currents, their contribution is not interesting for the further analysis and will be omitted. We state the result in the physical real-time representation in Keldysh basis:

$$\begin{aligned} S_{\text{eff}}[\mathcal{A}_\mu^\alpha, \Delta a_\mu^\alpha] &= \int_{xy} \left((\Delta a_c)_\mu^\alpha + (\mathcal{A}_c)_\mu^\alpha \quad (\Delta a_q)_\mu^\alpha + (\mathcal{A}_q)_\mu^\alpha \right)(x) \begin{pmatrix} 0 & (\Pi^A)_{\alpha\beta}^{\mu\nu} \\ (\Pi^R)_{\alpha\beta}^{\mu\nu} & (\Pi^K)_{\alpha\beta}^{\mu\nu} \end{pmatrix}(x, y) \begin{pmatrix} (\Delta a_c)_\nu^\beta + (\mathcal{A}_c)_\nu^\beta \\ (\Delta a_q)_\nu^\beta + (\mathcal{A}_q)_\nu^\beta \end{pmatrix}(y) \\ &+ \int_{xy} \left((\Delta a_c)_\mu^\alpha \quad (\Delta a_q)_\mu^\alpha \right)(x) \begin{pmatrix} 0 & (C^A)_{\alpha\beta}^{\mu\nu} \\ (C^R)_{\alpha\beta}^{\mu\nu} & (C^K)_{\alpha\beta}^{\mu\nu} \end{pmatrix}(x, y) \begin{pmatrix} (\Delta a_c)_\nu^\beta \\ (\Delta a_q)_\nu^\beta \end{pmatrix}(y) \\ &\equiv \int_{xy} [(\Delta a_\mu^\alpha + \mathcal{A}_\mu^\alpha)^\top(x) \Pi_{\alpha\beta}^{\mu\nu}(x, y) (\Delta a_\nu^\beta + \mathcal{A}_\nu^\beta)(y) + \Delta a_\mu^\alpha(x) C_{\alpha\beta}^{\mu\nu}(x, y) \Delta a_\nu^\beta(y)]. \end{aligned} \quad (31)$$

As discussed in the paragraph following Eq. (24), the additional degrees of freedom are a consequence of the mapping from abstract contour to physical real time. The second line defines a compact notation, where the Keldysh degrees of freedom are indicated by bold symbols. While Δa_μ^α and \mathcal{A}_μ^α are two-dimensional vectors in Keldysh space with “classical” and “quantum” components, $\Pi_{\alpha\beta}^{\mu\nu}$ and $C_{\alpha\beta}^{\mu\nu}$ are triangular 2×2 matrices with retarded, advanced, and Keldysh components. The latter contain the statistical information of the theory. Since in this article we are only interested in the linear response regime at finite temperatures, the Keldysh components $(\Pi^K)_{\alpha\beta}^{\mu\nu}$ and $(C^K)_{\alpha\beta}^{\mu\nu}$ both obey the bosonic fluctuation-dissipation theorem [64,71].

In Eq. (31), $\Pi_{\alpha\beta}^{\mu\nu}(x, y)$ is the one-loop fermionic polarization tensor

$$\Pi_{\alpha\beta}^{\mu\nu}(x, y) = -\frac{i}{2} \frac{\delta^2}{\delta a_\nu^\beta(y) \delta a_\mu^\alpha(x)} \text{tr} \ln \hat{G}_0^{-1} [eA_\mu + a_\mu^\alpha] \Big|_{a=\bar{a}}, \quad (32)$$

in which $\hat{G}_0^{-1} [eA_\mu + a_\mu^\alpha]$ is the inverse fermionic propagator (12) mapped to Keldysh space. Referring to Appendix B for details, we calculated this tensor at nonvanishing temperatures. Since the free propagators are diagonal in the flavor index, we find that the polarization tensor is diagonal in flavor space as well, $\Pi_{\alpha\beta}^{\mu\nu} = \Pi_{(\alpha)}^{\mu\nu} \delta_{(\alpha)\beta}$. However, this may need not be the case at higher orders, so for now we keep both indices. The tensor $C_{\alpha\beta}^{\mu\nu}(x, y)$, which we refer to as Chern-Simons–Coulomb tensor, is the integral kernel of $S_{\text{CS}}[\Delta a_\mu^\alpha] + S_V[\bar{a}_\mu^\alpha + \Delta a_\mu^\alpha]$. Its real space representation reads

$$\begin{aligned} (C^{R/A})_{\alpha\beta}^{\mu\nu}(x, y) &= (\hat{\mathcal{K}}^{-1})_{\alpha\beta} \varepsilon^{\mu\lambda\nu} \delta(x-y) \overrightarrow{\partial}_\lambda \\ &- \overleftarrow{\partial}_{\mu_1} \varepsilon^{0\mu_1\mu} (\hat{\mathcal{K}}^{-1})_{\alpha\alpha_1} V^{\alpha_1\beta_1}(x-y) (\hat{\mathcal{K}}^{-1})_{\beta_1\beta} \varepsilon^{0\nu_1\nu} \overrightarrow{\partial}_{\nu_1}, \end{aligned} \quad (33)$$

where the arrows above the partial derivatives indicate the direction in which they operate.

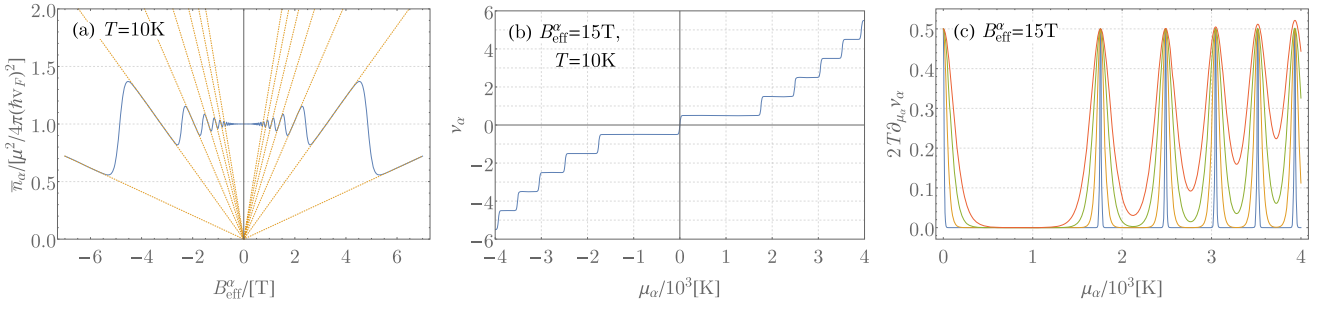


FIG. 2. (a) Charge carrier density at constant chemical potential as a function of the effective magnetic field B_{eff}^α at $T = 10 \text{ K}$ (blue). The straight dotted lines (orange) indicate the first few Landau levels. At vanishing magnetic field, the charge carrier density scales quadratically with the chemical potential [5, 10]. (Without loss of generality the sign of the chemical is assumed to be positive). Upon increasing (the absolute value of) the effective magnetic field B_{eff}^α —while keeping the chemical potential fixed—the carrier density shows oscillations in the regime $\omega_c^\alpha < \mu_\alpha$, whereas for $\omega_c^\alpha \gg \mu_\alpha$ it grows linearly as a function of the magnetic field. This behavior is readily explained by the formation of Landau levels, and the dependence of their degeneracy and relative energetic separation on the magnetic field. (b) Filling fraction per flavor ν_α at constant effective magnetic field $B_{\text{eff}}^\alpha = 15 \text{ T}$ and temperature $T = 10 \text{ K}$ as a function of the chemical potential. The plateaus occur at half-integer filling fractions $\nu_\alpha = \pm(n_\alpha + 1/2)$. The transitions between the plateaus are smeared out due to temperature. (c) Derivative of ν_α with respect to the chemical potential as a measure for temperature-induced Landau level broadening at $B_{\text{eff}}^\alpha = 15 \text{ T}$ for the temperatures $T = 5, 25, 50, 75 \text{ K}$. Increasing the temperature clearly leads to a broadening of the discrete energy levels. Since the relativistic Landau levels are not equidistant in energy space, the level broadening causes the Landau levels to overlap significantly away from the charge neutrality point. The Landau level located directly at the charge neutrality point, however, remains well-defined up to rather large temperatures.

Both the fermionic polarization tensor $\Pi_{\alpha\beta}^{\mu\nu}$, as well as the Chern-Simons–Coulomb tensor $C_{\alpha\beta}^{\mu\nu}$, are transverse, which may be expressed by the identities

$$\vec{\partial}_\mu \Pi_{\alpha\beta}^{\mu\nu} = 0, \quad \Pi_{\alpha\beta}^{\mu\nu} \overleftarrow{\partial}_\nu = 0, \quad (34a)$$

$$\vec{\partial}_\mu C_{\alpha\beta}^{\mu\nu} = 0, \quad C_{\alpha\beta}^{\mu\nu} \overleftarrow{\partial}_\nu = 0. \quad (34b)$$

As is well-known, this property is a consequence of gauge invariance [68]. Furthermore, for the polarization tensor, it is possible to factorize its tensorial structure and expand it into three distinct scalar kernels $\Pi_{\alpha\beta}^0$, $\Pi_{\alpha\beta}^1$, and $\Pi_{\alpha\beta}^2$ [51, 54]. Transforming to Fourier space, the $2 + 1$ -dimensional representation of this expansion, where timelike ($\mu, \nu = 0$) and spacelike ($\mu, \nu = i, j = 1, 2$) indices are separated, reads

$$\Pi_{\alpha\beta}^{00}(\omega, \vec{q}) = -\vec{q}^2 \Pi_{\alpha\beta}^0(\omega, \vec{q}), \quad (35a)$$

$$\Pi_{\alpha\beta}^{0i}(\omega, \vec{q}) = -\omega q^i \Pi_{\alpha\beta}^0(\omega, \vec{q}) + i \varepsilon^{0ij} q_j \Pi_{\alpha\beta}^1(\omega, \vec{q}), \quad (35b)$$

$$\Pi_{\alpha\beta}^{i0}(\omega, \vec{q}) = -\omega q^i \Pi_{\alpha\beta}^0(\omega, \vec{q}) - i \varepsilon^{0ij} q_j \Pi_{\alpha\beta}^1(\omega, \vec{q}), \quad (35c)$$

$$\Pi_{\alpha\beta}^{ij}(\omega, \vec{q}) = -\omega^2 \delta^{ij} \Pi_{\alpha\beta}^0(\omega, \vec{q}) + i \varepsilon^{0ij} \omega \Pi_{\alpha\beta}^1(\omega, \vec{q}) + (\delta^{ij} \vec{q}^2 - q^i q^j) \Pi_{\alpha\beta}^2(\omega, \vec{q}). \quad (35d)$$

One can readily check that the above expansion fulfills the transversality condition (34a).

We close this section by a short discussion about the (anomalous) integer quantum Hall effect in graphene. Although the electromagnetic response of the interacting system to an external perturbation is encoded in the electromagnetic response tensor to be derived in the next section, the response properties of the noninteracting system are already contained in the fermionic polarization tensor $\Pi_{\alpha\beta}^{\mu\nu}$. In fact, it is established that the essential physics of the integer quantum Hall effect can largely be understood within a noninteracting model and interactions only play a minor role [72]. We therefore only need

to consider $\Pi_{\alpha\beta}^{\mu\nu}$, in particular its retarded component. The dc conductivity tensor per fermionic flavor α can be obtained as the limit [9]

$$(\sigma_0^y)_\alpha^{ij} = \lim_{\omega \rightarrow 0} \lim_{\vec{q} \rightarrow 0} \frac{e^2}{i\omega} (\Pi^R)_\alpha^{ij}(\omega, \vec{q}), \quad (36)$$

where i, j are the aforementioned spacelike indices ($i, j = 1, 2$). Recall that to one-loop order the polarization tensor is diagonal in flavor space, hence we dropped the second flavor index. Furthermore, we here concentrate on the off-diagonal Hall conductivity, which reduces Eq. (36) to the kernel $(\Pi^R)_\alpha^1(0, 0)$,

$$(\sigma_0^{xy})_\alpha = e^2 (\Pi^R)_\alpha^1(0, 0) = \text{sign}(e B_{\text{eff}}^\alpha) \frac{e^2}{2\pi} \nu_\alpha. \quad (37)$$

The second equality follows after a lengthy, but straightforward calculation. As we mentioned earlier in this section, at large magnetic fields and zero temperatures, the filling fraction ν_α is quantized into plateaus located at $\pm(n_\alpha + \frac{1}{2})$, with $n_\alpha = 0, 1, 2, \dots$, see Eq. (30) and Fig. 2. Consequently, Eq. (37) describes the anomalous integer quantum Hall effect of the single fermionic flavor α . A summation of the remaining flavor index then yields the Hall conductivity of the entire system of Dirac particles. For simplicity, we may assume the absence of Zeeman terms and flux-binding for the moment by setting $\mu_\alpha = \mu$ and $B_{\text{eff}}^\alpha = B$. In that case, the contributions from the individual flavors are identical, giving rise to the well-known factor of four after summing over all flavors. Restoring \hbar we, thus, obtain the anomalous integer quantization of the Hall conductivity in graphene [9, 10]:

$$\sigma_0^{xy} = \pm \text{sign}(eB) \frac{e^2}{2\pi\hbar} 4 \left(n + \frac{1}{2} \right), \quad n = 0, 1, 2, \dots \quad (38)$$

A finite temperature leads to a smearing of these plateaus, due to the thermal broadening of the Landau levels. However, since the Landau levels are not equidistant in energy because of the

linear Dirac spectrum, even a small temperature eventually washes out the plateau structure at large fillings. Only the lowest levels are relatively robust against the thermal smearing. Taking into account the rather large value of the relativistic cyclotron frequency ω_c , it is possible to observe the quantum Hall effect experimentally at room temperature [12]. By now, this is a well-known fact, but still it is insofar astonishing, as the quantum Hall effect for ordinary, nonrelativistic fermions can only be observed at low temperatures, close to absolute zero.

IV. ELECTROMAGNETIC RESPONSE TENSOR AND HALL CONDUCTANCE

In order to obtain the electromagnetic polarization tensor, we need to perform the residual functional integration over the statistical gauge fields, which—according to the rules of Gaussian integration—involves the inverse of $(\mathbf{\Pi} + \mathbf{C})_{\alpha\beta}^{\mu\nu}$. However, since both $\mathbf{\Pi}_{\alpha\beta}^{\mu\nu}$ and $\mathbf{C}_{\alpha\beta}^{\mu\nu}$ are transverse, neither their individual inverse nor the inverse of their sum does exist. This problem is rooted in the gauge invariance of the partition function (8). As advertised at the end of Sec. II, we here discuss the issues of the gauge fixing procedure—resorting to the contour-time representation for the moment—and derive the electromagnetic response tensor, from which we obtain the dc Hall conductivity. We emphasize that the technique described below is not limited to the Gaussian approximation of the effective action (22).

The problematic gauge equivalent orbits, causing Eq. (8) to diverge, can be factorized from the nonequivalent physical field configurations by the well-known Fadeev-Popov gauge fixing procedure. Referring to Ref. [68] for details, we obtain the intermediate result

$$Z[\mathcal{A}_\mu^\alpha] = \mathcal{N} \int \mathcal{D}\Delta a \delta[G(\Delta a_\mu^\alpha)] e^{iS_{\text{eff}}[\mathcal{A}_\mu^\alpha, \Delta a_\mu^\alpha]}. \quad (39)$$

Here, the divergent integral over pure gauge fields as well as the so-called Fadeev-Popov determinant have been absorbed into the formally infinite normalization constant \mathcal{N} . Since it does not enter any correlation function, this constant may safely be omitted [77]. The functional delta distribution enforces the gauge constraint $G(\Delta a_\mu^\alpha) = 0$ within the functional integral, such that only physically inequivalent field configurations contribute to the amplitude. The gauge fixing function can be chosen at will, but for definiteness, we consider the generalized Lorentz gauge condition,

$$G(\Delta a_\mu^\alpha) = \partial_\mu \Delta a_\alpha^\mu(x) - \omega(x), \quad (40)$$

where $\omega(x)$ is an arbitrary function, in the remainder of this paper.

In its present form, Eq. (39) can in principle be employed to calculate the desired correlation functions, yet it is beneficial to make use of Feynman's trick of “averaging over gauges” [68]. Hereto one averages the partition function (39) over different field configurations $\omega(x)$ with a Gaussian “probability measure.” This procedure closely resembles a Gaussian disorder average of the partition function, albeit a disorder potential would couple in a different manner [63,64,78,79]. The net

result is the gauge fixed partition function

$$Z_{\text{GF}}[\mathcal{A}_\mu^\alpha] = \int \mathcal{D}\Delta a e^{iS_{\text{eff}}[\mathcal{A}_\mu^\alpha, \Delta a_\mu^\alpha] + iS_{\text{GF}}[\Delta a_\mu^\alpha]}, \quad (41)$$

where the additional contribution in the exponent is the gauge fixing action

$$\begin{aligned} S_{\text{GF}}[\Delta a_\mu^\alpha] &= \frac{1}{2\xi} \int_{\mathcal{C},x} (\partial_\mu \Delta a_\alpha^\mu(x))^2 \\ &\equiv \frac{1}{2} \int_{\mathcal{C},xy} \Delta a_\mu^\alpha(x) \mathcal{G}_{\alpha\beta}^{\mu\nu}(x,y) \Delta a_\nu^\beta(x). \end{aligned} \quad (42)$$

Here, ξ is a real-valued parameter, which may be chosen at will to simplify calculations. In the end, for any physical—that is gauge invariant—observable the dependence on ξ has to drop out. After mapping this contour-time action to the physical real-time representation and performing the Keldysh rotation, the additional gauge fixing term effectively leads to the substitution $\mathbf{C}_{\alpha\beta}^{\mu\nu} \rightarrow (\mathbf{C} + \mathcal{G})_{\alpha\beta}^{\mu\nu}$ in the effective action (31). Since $\mathcal{G}_{\alpha\beta}^{\mu\nu}$ is invertible so is the sum $(\mathbf{\Pi} + \mathbf{C} + \mathcal{G})_{\alpha\beta}^{\mu\nu}$, resulting in a well-defined functional integral over the statistical gauge fields.

For nonvanishing source fields, the residual Gaussian integration yields the generating functional of connected correlation functions [64,67]

$$W[\mathcal{A}_\mu^\alpha] = -i \ln Z_{\text{GF}}[\mathcal{A}_\mu^\alpha] = \int_{xy} \mathcal{A}_\mu^\alpha(x) \mathbf{K}_{\alpha\beta}^{\mu\nu}(x,y) \mathcal{A}_\nu^\beta(y). \quad (43)$$

In this expression, $\mathbf{K}_{\alpha\beta}^{\mu\nu}(x,y)$ defines the electromagnetic polarization tensor. Accordingly, it represents the linear electromagnetic response of the system to an external perturbation. We state its explicit form in terms of the fermionic polarization tensor and the Chern-Simons-Coulomb tensor of the preceding section by employing a condensed matrix notation. For the moment the hat symbol not only indicates the flavor-space matrix structure, but also covers the discrete Minkowski indices μ, ν and the continuous space-time variables x, y , if not stated otherwise,

$$\hat{\mathbf{K}} = \hat{\mathbf{\Pi}} - \hat{\mathbf{\Pi}}(\hat{\mathbf{\Pi}} + \hat{\mathbf{C}} + \hat{\mathcal{G}})^{-1} \hat{\mathbf{\Pi}}. \quad (44)$$

In this expression, matrix multiplication is defined naturally by implying summation over discrete and integration over continuous degrees of freedom. This tensor has the usual triangular Keldysh space structure, with retarded, advanced, and Keldysh components [64]

$$\mathbf{K}_{\alpha\beta}^{\mu\nu}(x,y) = \begin{pmatrix} 0 & (K^A)_{\alpha\beta}^{\mu\nu}(x,y) \\ (K^R)_{\alpha\beta}^{\mu\nu}(x,y) & (K^K)_{\alpha\beta}^{\mu\nu}(x,y) \end{pmatrix}. \quad (45)$$

Transforming to frequency-momentum space, these components read

$$\hat{\mathbf{K}}_{\omega,\vec{q}}^{R/A} = \hat{\mathbf{\Pi}}_{\omega,\vec{q}}^{R/A} - \hat{\mathbf{\Pi}}_{\omega,\vec{q}}^{R/A} ((\hat{\mathbf{\Pi}} + \hat{\mathbf{C}} + \hat{\mathcal{G}})_{\omega,\vec{q}}^{R/A})^{-1} \hat{\mathbf{\Pi}}_{\omega,\vec{q}}^{R/A}, \quad (46a)$$

$$\hat{\mathbf{K}}_{\omega,\vec{q}}^K = \coth\left(\frac{\omega}{2T}\right) (\hat{\mathbf{K}}_{\omega,\vec{q}}^R - \hat{\mathbf{K}}_{\omega,\vec{q}}^A). \quad (46b)$$

Here, the frequency and momentum dependence has been written as an index, flavor and Minkowski indices are still

covered by the hat symbol. The second equation is just a manifestation of the bosonic fluctuation-dissipation theorem.

Although the electromagnetic response tensor as given by Eq. (44) contains the gauge fixing kernel $\hat{\mathcal{G}}$ explicitly, any reference of it drops out in the final expression for $\hat{\mathbf{K}}$. In fact, the electromagnetic response tensor is a physical observable and, thus, has to be gauge-invariant. We have checked explicitly for a single flavor that other common choices, such as the Coulomb and axial gauge, indeed, lead to the same result. As a consequence of gauge invariance, the electromagnetic response tensor $\hat{\mathbf{K}}$ is transverse and, hence, admits the very

$$\hat{\mathbf{K}}_0^R = \hat{\mathcal{K}}^{-1}(\hat{\mathcal{D}}^R)^{-1}\hat{\mathcal{K}}^{-1}, \quad (47a)$$

$$\hat{\mathbf{K}}_1^R = \hat{\mathcal{K}}^{-1} + \frac{1}{2}\hat{\mathcal{K}}^{-1}[(\vec{q}^2\hat{\mathcal{V}}\hat{\mathcal{K}}^{-1} - (\hat{\Pi}_0^R)^{-1}(\hat{\Pi}_1^R + \hat{\mathcal{K}}^{-1}))(\hat{\mathcal{D}}^R)^{-1} + (\hat{\mathcal{D}}^R)^{-1}(\hat{\mathcal{K}}^{-1}\vec{q}^2\hat{\mathcal{V}} - (\hat{\Pi}_1^R + \hat{\mathcal{K}}^{-1})(\hat{\Pi}_0^R)^{-1})]\hat{\mathcal{K}}^{-1}, \quad (47b)$$

$$\begin{aligned} \hat{\mathbf{K}}_2^R = & -\frac{1}{\vec{q}^2}\hat{\mathcal{K}}^{-1}(\vec{q}^2\hat{\mathcal{V}}\hat{\mathcal{K}}^{-1} - (\hat{\Pi}_0^R)^{-1}(\hat{\Pi}_1^R + \hat{\mathcal{K}}^{-1}))(\hat{\mathcal{D}}^R)^{-1}(\hat{\mathcal{K}}^{-1}\vec{q}^2\hat{\mathcal{V}} - (\hat{\Pi}_1^R + \hat{\mathcal{K}}^{-1})(\hat{\Pi}_0^R)^{-1})\hat{\mathcal{K}}^{-1} \\ & + \frac{1}{\vec{q}^2}\hat{\mathcal{K}}^{-1}((\hat{\Pi}_0^R)^{-1} - \vec{q}^2\hat{\mathcal{V}} + \omega^2(\hat{\mathcal{D}}^R)^{-1})\hat{\mathcal{K}}^{-1}, \end{aligned} \quad (47c)$$

with

$$\begin{aligned} \hat{\mathcal{D}}^{R/A} = & -(\omega \pm i0)^2\hat{\Pi}_0^{R/A} + \vec{q}^2(\hat{\Pi}_2^{R/A} - \hat{\mathcal{K}}^{-1}\hat{\mathcal{V}}\hat{\mathcal{K}}^{-1}) \\ & + (\hat{\Pi}_1^{R/A} + \hat{\mathcal{K}}^{-1})(\hat{\Pi}_0^{R/A})^{-1}(\hat{\Pi}_1^{R/A} + \hat{\mathcal{K}}^{-1}). \end{aligned} \quad (48)$$

The advanced kernels are obtained by Hermitian conjugation just as usual. We have to emphasize at this point, that—in contrast to the one-loop fermionic polarization tensor $\hat{\Pi}$ —the electromagnetic polarization tensor $\hat{\mathbf{K}}$ is in general not diagonal in flavor space, but a symmetric matrix. This fact derives from the \mathcal{K} matrix, which is also not necessarily diagonal, but symmetric.

The above equations, together with the results for the fermionic polarization tensor $\hat{\Pi}$ given in Appendix B, represent the main result of this work. Given a particular \mathcal{K} -matrix configuration, the electromagnetic polarization tensor $\hat{\mathbf{K}}$ contains the full information about the system's response to a weak, external electromagnetic perturbation. The kernel $\hat{\mathbf{K}}_0^R$, when multiplied with $-\vec{q}^2$, equals the density response function, cf. Eq. (35a),

$$\mathbf{K}_{\alpha\beta}^{00}(\omega, \vec{q}) = -\vec{q}^2\mathbf{K}_{\alpha\beta}^0(\omega, \vec{q}), \quad (49)$$

and as such determines the dynamical screening properties, as well as the collective modes. The latter can be obtained by the roots of the denominator matrix $\hat{\mathcal{D}}^R$, Eq. (48). Furthermore, in the zero temperature and long wavelength limit, it is possible to calculate the absolute value square of the ground-state wave function and corrections thereof (as an expansion in q/B), which was shown in Ref. [80]. The current response tensor is given by the spatial components, $\mu, \nu = 1, 2$, of the polarization tensor, encoding the information about the (dynamical) conductivity tensor. In the remainder of this paper, we focus on the dc Hall conductivity. A further investigation of the above mentioned quantities will be left for future work.

In close analogy to the noninteracting case, we need to investigate the zero frequency and momentum limit of the

same decomposition as the fermionic polarization tensor $\hat{\Pi}$, see Eqs. (35a)–(35d). The only difference are the kernels $\hat{\mathbf{K}}_{0/1/2}$, which are now complicated functions of the kernels $\hat{\Pi}_{0/1/2}$, the \mathcal{K} -matrix and the (Fourier transformation of the) Coulomb interaction matrix $\hat{\mathcal{V}}(\vec{q})$. Recall that the latter is a 4×4 matrix in flavor space, with all its components being equal to the same Coulomb interaction amplitude (6); see also Eq. (23), the comments thereafter and Eq. (33). Suppressing frequency and momentum labels (the hat symbol only indicates flavor space here), we obtain for the retarded kernels

kernel $\hat{\mathbf{K}}_1^R$ to obtain the Hall conductivity. Using Eqs. (47b) and (48), as well as $\lim_{\vec{q} \rightarrow 0} \vec{q}^2\hat{\mathcal{V}}(\vec{q}) = 0$, we obtain

$$\begin{aligned} \hat{\mathbf{K}}_1^R(0,0) = & \lim_{\omega \rightarrow 0} \lim_{\vec{q} \rightarrow 0} \frac{1}{i\omega} (\hat{\mathbf{K}}^R)^{12}(\omega, \vec{q}) \\ = & [\hat{\mathcal{K}} + (\hat{\Pi}_1^R(0,0))^{-1}]^{-1}. \end{aligned} \quad (50)$$

Clearly, if $\hat{\mathcal{K}}$ is identically zero, the kernel $\hat{\mathbf{K}}_1^R$ reduces to the noninteracting kernel $\hat{\Pi}_1^R$, leading back to the integer quantum Hall regime, Eq. (37). For the most general \mathcal{K} matrix, Eq. (50) reads

$$\hat{\mathbf{K}}_1^R = \frac{1}{2\pi} \begin{pmatrix} 2k_1 + \frac{1}{\nu_1} & m_1 & n_1 & n_2 \\ m_1 & 2k_2 + \frac{1}{\nu_2} & n_3 & n_4 \\ n_1 & n_3 & 2k_3 + \frac{1}{\nu_3} & m_2 \\ n_2 & n_4 & m_2 & 2k_4 + \frac{1}{\nu_4} \end{pmatrix}^{-1}. \quad (51)$$

Observe that the temperature dependence only enters via the kernel $\hat{\Pi}_1^R$, i.e., via the filling fractions ν_α . A finite temperature does not modify the \mathcal{K} matrix in any way, as it should be. Only the composite Dirac fermions, filling the effective Landau levels, are subject to thermal fluctuations, the flux-binding itself, as described by Eq. (27), is not influenced. Furthermore, note that we absorbed the sign of the effective magnetic field into the filling fractions ν_α . As discussed above, the kernel $\hat{\mathbf{K}}_1^R$ is a nondiagonal but symmetric matrix. In order to obtain the Hall conductivity, one has to sum over all of its components:

$$\sigma_{xy} = e^2 \sum_{\alpha, \beta} (\hat{\mathbf{K}}_1^R)_{\alpha\beta}(0,0). \quad (52)$$

This fact becomes clear by taking into account that a physical electromagnetic fluctuation should couple identically to all flavors. Therefore one has to neglect the flavor index of the source fields $\mathcal{A}_\mu^\alpha(x)$ in Eq. (43), which, in turn, leads to

TABLE I. Filling fraction ν_G for three distinct \mathcal{K} -matrix configurations, leading to a Hall conductivity $\sigma_{xy} = \frac{e^2}{2\pi\hbar} \nu_G$ (\hbar restored). The examples (2a) and (2b), respectively, (3a) and (3b), correspond to states with the same analytical properties but interchanged spin and valley degrees of freedom. The temperature dependence, contained within the composite-fermion filling fractions ν_α , is suppressed. For the singular \mathcal{K} matrices (1), (2a), and 2(b), there exists an equivalent Abelian gauge theory with a reduced set of Chern-Simons fields. The associated gauge groups are shown in the last column.

	\mathcal{K} matrix	Total filling fraction ν_G	Gauge symmetry
1	$\begin{pmatrix} 2k & 2k & 2k & 2k \\ 2k & 2k & 2k & 2k \\ 2k & 2k & 2k & 2k \\ 2k & 2k & 2k & 2k \end{pmatrix}$	$\frac{\nu_1 + \nu_2 + \nu_3 + \nu_4}{2k(\nu_1 + \nu_2 + \nu_3 + \nu_4) + 1}$	U(1)
2a	$\begin{pmatrix} 2k_1 & 2k_1 & n & n \\ 2k_1 & 2k_1 & n & n \\ n & n & 2k_2 & 2k_2 \\ n & n & 2k_2 & 2k_2 \end{pmatrix}$	$\frac{(2k_1 + \frac{1}{\nu_1 + \nu_2}) - n}{(2k_1 + \frac{1}{\nu_1 + \nu_2})(2k_2 + \frac{1}{\nu_3 + \nu_4}) - n^2} + \frac{(2k_2 + \frac{1}{\nu_3 + \nu_4}) - n}{(2k_1 + \frac{1}{\nu_1 + \nu_2})(2k_2 + \frac{1}{\nu_3 + \nu_4}) - n^2}$	U(1) _↑ ⊗ U(1) _↓
2b	$\begin{pmatrix} 2k_1 & n & 2k_1 & n \\ n & 2k_2 & n & 2k_2 \\ 2k_1 & n & 2k_1 & n \\ n & 2k_2 & n & 2k_2 \end{pmatrix}$	$\frac{(2k_1 + \frac{1}{\nu_1 + \nu_3}) - n}{(2k_1 + \frac{1}{\nu_1 + \nu_3})(2k_2 + \frac{1}{\nu_2 + \nu_4}) - n^2} + \frac{(2k_2 + \frac{1}{\nu_2 + \nu_4}) - n}{(2k_1 + \frac{1}{\nu_1 + \nu_3})(2k_2 + \frac{1}{\nu_2 + \nu_4}) - n^2}$	U(1) _{K+} ⊗ U(1) _{K-}
3a	$\begin{pmatrix} 2k_1 & m_1 & 0 & 0 \\ m_1 & 2k_2 & 0 & 0 \\ 0 & 0 & 2k_3 & m_2 \\ 0 & 0 & m_2 & 2k_4 \end{pmatrix}$	$\sum_{i=1,2} \frac{(2k_i + \frac{1}{\nu_i}) - m_1}{(2k_1 + \frac{1}{\nu_1})(2k_2 + \frac{1}{\nu_2}) - m_1^2} + \sum_{i=3,4} \frac{(2k_i + \frac{1}{\nu_i}) - m_2}{(2k_3 + \frac{1}{\nu_3})(2k_4 + \frac{1}{\nu_4}) - m_2^2}$	U(1) ^{⊗4}
3b	$\begin{pmatrix} 2k_1 & 0 & m_1 & 0 \\ 0 & 2k_2 & 0 & m_2 \\ m_1 & 0 & 2k_3 & 0 \\ 0 & m_2 & 0 & 2k_4 \end{pmatrix}$	$\sum_{i=1,3} \frac{(2k_i + \frac{1}{\nu_i}) - m_1}{(2k_1 + \frac{1}{\nu_1})(2k_3 + \frac{1}{\nu_3}) - m_1^2} + \sum_{i=2,4} \frac{(2k_i + \frac{1}{\nu_i}) - m_2}{(2k_2 + \frac{1}{\nu_2})(2k_4 + \frac{1}{\nu_4}) - m_2^2}$	U(1) ^{⊗4}

a summation over all matrix components rather than, e.g., taking a trace. Equation (52) is the simplest form of the Hall conductivity. Alternatively, our result could be written in terms of the (anomalous) integer quantum Hall conductivities of the noninteracting system, which may be slightly more complicated but possibly more appealing in physical terms. As advertised in the introduction, we get Eq. (2),

$$\sigma_{xy} = \sum_{\alpha} \sigma_{0,xy}^{\alpha} - \sum_{\alpha,\beta} \sigma_{0,xy}^{\alpha} (\hat{\sigma}_{0,xy} + \hat{\mathcal{K}}^{-1})_{\alpha\beta}^{-1} \sigma_{0,xy}^{\beta}.$$

Continuing the parallels with the noninteracting case, the Hall conductivity should be proportional to some filling factor ν_G (adopting here the notation of Ref. [8]). This filling factor can easily be extracted from Eq. (52), using the equality $\sigma_{xy} = \frac{e^2}{2\pi} \nu_G$. It is a complicated rational function of all the components of the \mathcal{K} matrix and the filling factors of the individual composite fermions ν_α . Clearly, for such a large parameter space some of its input will be mapped to the exact same filling fraction ν_G . In other words, several different FQH states produce the same filling fraction, respectively, the same Hall conductivity. Hence the measurement of a Hall plateau at a particular filling fraction alone does not identify a single FQH state. In order to distinguish from the theoretical side which state realizes a certain filling fraction in an actual experiment, one should estimate the energy associated to all of the states in question. In principle, this should lead to a unique lowest energy state, which realizes that particular FQH plateau. In addition, one could investigate—theoretically and experimentally—the screening properties and/or collective

modes of the respective states to gain a deeper understanding and potentially exclude a certain subset of states.

Considering the complexity of the matrix inverse in Eq. (51) for the most general \mathcal{K} -matrix configuration, it becomes clear that a complete analysis of the full parameter space is highly involved. For its systematic study, it is advisable to partially restrict the parameter space and collect the corresponding \mathcal{K} -matrix configurations into several distinct classes, which should have some overlap in their restricted parameter space. In this context, recall our discussion of singular \mathcal{K} matrices in the preceding section. Employing this strategy it is not only possible to explore the full parameter space eventually, but it also simplifies the identification of the underlying physics that is described by a particular class of \mathcal{K} -matrix configurations considerably. In the remainder of this paper we outline this strategy, concentrating on a few special cases. Those \mathcal{K} -matrix configurations we decided to investigate further, together with their resulting Hall conductivities are listed in Table I.

We encountered the first of these examples already in our discussion of singular \mathcal{K} matrices. The states described by this particular \mathcal{K} matrix belong to the simplest possible class of FQH states, which can be described by a simpler Chern-Simons gauge theory, where only a single local U(1) gauge field is present. The structure of the \mathcal{K} matrix indicates a residual global SU(4) flavor symmetry, which is weakly broken by the Zeeman terms. Once the symmetry breaking terms are neglected—that is, equating all composite-fermion filling fractions $\nu_\alpha = \nu$ —we obtain a hierarchy of states described by the filling fractions $\nu_G = \frac{4\nu}{2k \cdot 4\nu + 1}$, which have also been

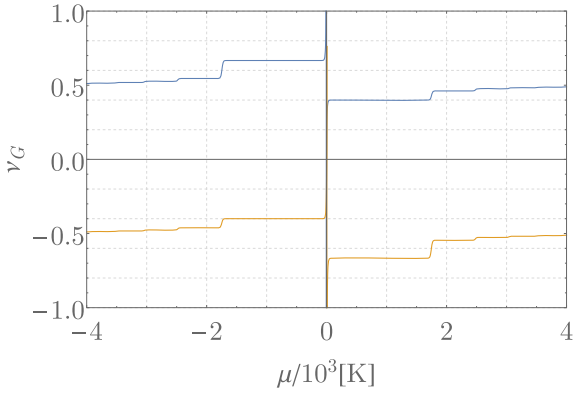


FIG. 3. Total filling fraction $\nu_G = \frac{4\nu}{2k-4\nu+1}$ as a function of the chemical potential μ at $B_{\text{eff}} = 15$ T and $T = 10$ K for $k = +1$ (blue) and $k = -1$ (orange). The finite temperature smears out the transitions from one Hall plateau to another, similar to the noninteracting case, cf. Fig. 2. Note that the plateaus occur in pairs, lying symmetrically around the charge neutrality point $\nu_G = 0$. In this simple case, one can construct a manifestly particle-hole symmetric filling fraction by considering the regimes $\mu < 0$ and $\mu > 0$ and flip the sign of k at $\mu = 0$, see Fig. 4, which yields the two branches $|\nu_G| < |1/2k|$ and $|\nu_G| > |1/2k|$.

obtained in Ref. [62]. This total filling fraction as a function of the chemical potential μ is shown in Fig. 3 at the effective magnetic field $B_{\text{eff}} = 15$ T and temperature $T = 10$ K for $k = \pm 1$. We remind the reader that, if one wishes to change the charge carrier density via the chemical potential, but keep the effective magnetic field B_{eff} to be constant, then, according to the mean-field equation (28), one has to change the external magnetic field B as well.

For a fixed flux attachment prescribed by the integer k , it is obvious that the filling fraction ν_G is not manifestly particle-hole symmetric. Yet, the Hall plateaus occur in particle-hole symmetric pairs, when considering k and $-k$ simultaneously. This observation suggests that one can construct a manifestly particle-hole symmetric filling fraction by distinguishing the two regimes $\mu < 0$ and $\mu > 0$, and flip the sign of k at $\mu = 0$, which yields the two branches

$$\nu_G^{\text{ph}} = \frac{4\nu}{-2|k|4\nu+1}\Theta(-\mu) + \frac{4\nu}{2|k|4\nu+1}\Theta(\mu), \quad (53a)$$

$$\nu_G^{\text{ph}*} = \frac{4\nu}{2|k|4\nu+1}\Theta(-\mu) + \frac{4\nu}{-2|k|4\nu+1}\Theta(\mu), \quad (53b)$$

where $|\nu_G^{\text{ph}}| < |1/2k|$ and $|\nu_G^{\text{ph}*}| > |1/2k|$. Note that the latter branch, $\nu_G^{\text{ph}*}$, appears to have the wrong overall sign. (Naively, one would expect the sign of the total filling fraction ν_G to coincide with the sign of μ .) But recall that we absorbed the sign of the effective magnetic field into the composite Dirac fermion filling fractions ν_α , meaning that this “wrong sign” should be interpreted as an effective magnetic field being antiparallel to the external one. In Fig. 4, we show the branch (53a) for $|k| = 1, \dots, 4$, as well as a generalization of Eq. (53a) when a finite spin Zeeman coupling is present, with Zeeman energies $E_Z = 0.1, \dots, 0.4 \times \hbar\omega_c^{\text{eff}}$ for $|k| = 1$. We have chosen such large Zeeman energy scales, which vastly exceed the ones found in a realistic graphene sample [6,8],

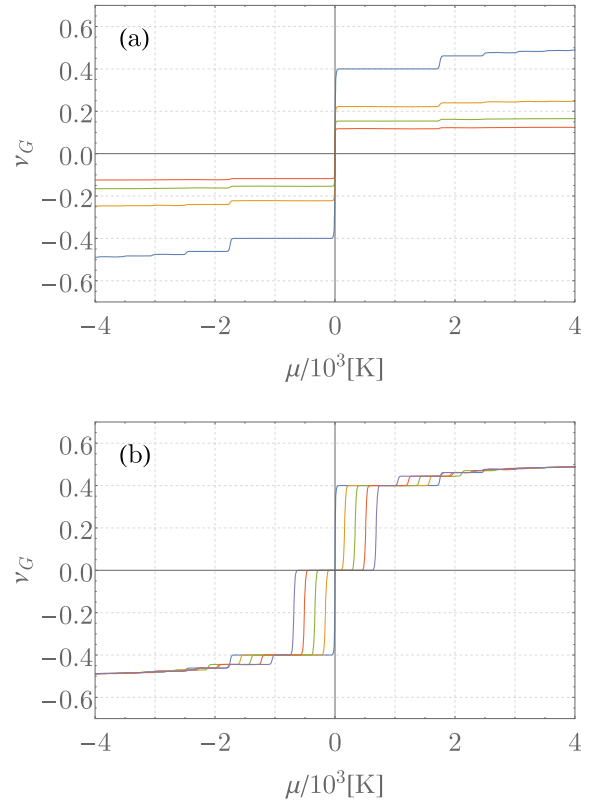


FIG. 4. Particle-hole symmetric total filling fractions for $\nu_G = \frac{\nu_\uparrow + \nu_\downarrow}{2k - (\nu_\uparrow + \nu_\downarrow) + 1}$, with $\nu_\uparrow = \nu_1 + \nu_2, \nu_\downarrow = \nu_3 + \nu_4$, as a function of the chemical potential μ at $B_{\text{eff}} = 15$ T and $T = 10$ K. (a) Zero Zeeman splitting, implying $\nu_\uparrow = \nu_\downarrow = 2\nu$, for $|k| = 1, \dots, 4$. (b) Finite spin Zeeman term with Zeeman energies $E_Z = 0.0, 0.1, \dots, 0.4 \times \hbar\omega_c^{\text{eff}}$ for $|k| = 1$. The finite Zeeman term leads to the formation of new plateaus, with the $\nu_G = 0$ plateau being the most dominant one.

for demonstrational purposes to make the additional plateau structure at $\nu_G = 0$ visible.

The examples (2) and (3) of Table I are best discussed comparatively. Each of these examples comes in two variations, where the flux attachment to spin and valley degrees of freedom are interchanged. Without loss of generality we may limit our comparative discussion to the (2a) and (3b) configuration, simply referring to them as (2) and (3) if not stated otherwise.

While the (2) configuration is another important example of a singular \mathcal{K} matrix, and as such can be represented in terms of a reduced Chern-Simons theory [in this case, a $U(1)_\uparrow \otimes U(1)_\downarrow$], the (3) configuration is regular. The two \mathcal{K} -matrix configurations represent very different physical scenarios. The states associated to (2) are the analog of the nonrelativistic bilayer FQH states found in Ref. [53], where an additional *internal* degree of freedom—the valley polarization—in each “spin-layer” is present. Neglecting the Zeeman couplings in the valley subspace, that is, equating $\nu_1 = \nu_2$ and $\nu_3 = \nu_4$, restores the global valley $SU(2)$ symmetry. The states associated to the (3) configuration on the other hand, can be interpreted as two independent, decoupled “bilayers,” one for each valley degree of freedom. Once again, the bilayer structure is formed by the spin degree of freedom, but the valley now appears

as an *external* degree of freedom. [For comparison, the (3a) configuration would yield a bilayer structure formed by the valley and the spin would appear as an external degree of freedom.]

The difference of internal and external valley polarization is also reflected in the filling fraction itself, as can be seen from Table I. For simplicity we set all composite fermion filling fractions equal, $\nu_\alpha = \nu$, and, furthermore, we may also set $k_1 = k_2 = k$ for the (2) configuration, and $k_\alpha = k$, $m_1 = m_2 = m$ for the (3) configuration. In those cases the \mathcal{K} -matrix configurations (2a) and (2b), respectively, (3a) and (3b) yield the same filling fraction. If the valley appears as an internal degree of freedom, we obtain

$$\nu_G^{\text{int}} = \frac{4\nu}{(2k+n)2\nu+1}, \quad (54)$$

whereas if the valley is an external degree of freedom we get

$$\nu_G^{\text{ext}} = 2 \frac{2\nu}{(2k+m)\nu+1}. \quad (55)$$

The two filling fractions coincide by setting $n = 0$ in Eq. (54) and $m = 2k$ in Eq. (55). It is this special case, which has been proposed in Ref. [61].

Manifestly particle-hole symmetric total filling fractions can be constructed for Eqs. (54) and (55) in the same way as was done before, but this time at $\nu_G = 0$ one has to flip the sign of k and n , respectively, m , simultaneously. Similarly, the other filling fractions in Table I also lead to particle-hole symmetric Hall plateaus. [In general, sending $\hat{\mathcal{K}} \rightarrow -\hat{\mathcal{K}}$ and $\nu_\alpha \rightarrow -\nu_\alpha$ results in $\nu_G \rightarrow -\nu_G$, cf. Eqs. (50) and (52).] Hence it is expected that for those filling fractions a similar, albeit more involved construction can be performed to present them in a manifestly particle-hole symmetric form.

As a final example we show how the prominent $\nu_G = \pm 1/3$ filling fraction, which has recently been observed in an experiment [7,15,16], arises in our theory. To produce such a filling fraction, there are several possible candidates for the \mathcal{K} matrix, the simplest of which is given by the configuration (1) of Table I upon choosing $\sum_\alpha \nu_\alpha = \pm 1$ and $k = \pm 1$. Note that this \mathcal{K} -matrix configuration also gives rise to the prominent filling fractions $\nu_G = \pm 2/3$ and $\nu_G = \pm 2/5$, which are obtained by setting $\sum_\alpha \nu_\alpha = \pm 2$ and $k = \pm 1$, or $k = \pm 2$, respectively. Another possible choice for the \mathcal{K} matrix is configuration (2), where n and k_2 are set to zero (one may also set $k_1 = 0$ instead). In that case, the total filling fraction simplifies to $\nu_G = \frac{\nu_1 + \nu_2}{2k_1(\nu_1 + \nu_2) + 1} + \nu_3 + \nu_4$. Choosing the composite fermion filling fractions and the remaining flux-attachment parameter k_1 appropriately, that is, $\nu_1 + \nu_2 = \pm 1$, $k_1 = \pm 1$ and $\nu_3 + \nu_4 = 0$, yields $\nu_G = \pm 1/3$ likewise.

Lastly, configuration (3) can also be employed to yield a total filling fraction of one third and it seems to us that this is the analogous configuration of the one discussed in Ref. [43], which employs the conventional wave-function approach. In this work, it was argued, that, from the four spin-valley Landau levels, two are completely filled, one is completely empty, and a last one is filled to one third. Taking this statement literally, one can interpret it as follows: while the completely filled (empty) levels each contribute to the filling fraction with $+\frac{1}{2}(-\frac{1}{2})$, the last level should be empty to a sixth ($-\frac{1}{2} + \frac{1}{3} = -\frac{1}{6}$). Setting $m_1 = m_2 = 0$, as well as $k_2 = k_3 = k_4 = 0$ in the

configuration (3) of Table I, meaning that flux is attached to one flavor only, we obtain $\nu_G = \frac{\nu_1}{2k_1\nu_1+1} + \nu_2 + \nu_3 + \nu_4$. Clearly, for $\nu_1 = \nu_2 = -\frac{1}{2}$, $\nu_3 = \nu_4 = \frac{1}{2}$, and $k_1 = -2$, we reproduce the above situation $\nu_G = -\frac{1}{6} - \frac{1}{2} + \frac{1}{2} + \frac{1}{2} = \frac{1}{3}$. However, the actual wave function proposed in Ref. [43] has an (*mmm*)-like structure, meaning the Jastrow factor contains an “off-diagonal” vortex-attachment accounting for interflavor correlations between two of the four flavors, which we believe is not realized by the above simple flux attachment. Although the precise correspondence between the \mathcal{K} matrix and the electron/hole wave function is not yet clear, since our flux-attachment scheme refers to the charge carriers rather than electrons/holes, such off-diagonal correlations between two flavors are achieved by relaxing the constraint that, say, m_1 vanishes. Referring to the (3a) configuration for definiteness, one may set $k_1 = k_2 = k$, $k_3 = k_4 = 0$, and $\nu_1 = \nu_2 = \nu$. In this special case, the total filling fraction becomes $\nu_G = \frac{2\nu}{(2k+m)\nu+1} + \nu_3 + \nu_4$. If now $k = -1$ and $m = 2k - 1 = -3$ is considered (which resembles a \mathcal{K} matrix that is used in the nonrelativistic Chern-Simons theory to describe a (333) state [54]), and $\nu = \nu_3 = \nu_4 = 1/2$, we obtain the desired filling fraction $\nu_G = -2/3 + 1 = 1/3$.

V. CONCLUSIONS AND OUTLOOK

In the present work, we developed a finite temperature theory for the pseudorelativistic fractional quantum Hall effect of monolayer graphene, employing the real-time Keldysh formalism in the functional integral approach. We considered a $U(1)^{\otimes 4}$ Chern-Simons gauge theory, which is minimally coupled to the system of interacting Dirac fermions. In this theory, each fermionic flavor interacts with any other flavor through Coulomb interactions, in addition to an individual $U(1)$ gauge field. The latter transforms ordinary into composite Dirac fermions. After integrating the fermionic degrees of freedom, we obtained an exact effective action for the gauge fields that has been analyzed in the random phase approximation. We derived the electromagnetic response tensor from which the dc Hall conductivities have been extracted.

Our research could be extended into several different directions. One obvious extension concerns a more detailed analysis of the electromagnetic response tensor for the various FQH states as presented here. The density-density response, given by $K_{\alpha\beta}^{00}$, allows for an investigation of the dynamical screening properties of the system together with the spectrum of collective modes. The current-current response, given by $K_{\alpha\beta}^{ij}$, may be studied beyond the static case, which gives information about the optical conductivity $\sigma_{ij}(\omega)$. In this context, we also want to mention the straightforward generalizations of the response tensor, which result from modifications of the linear and isotropic Dirac spectrum. Here we only considered a non-vanishing (generalized) Zeeman term implicitly through the flavor dependent chemical potentials μ_α . Other modifications, such as trigonal warping, anisotropies in strained graphene, or finite mass terms (gaps), could lead to interesting effects and can be obtained by adding the respective term to the noninteracting Dirac action (11). Note that such alterations do not invalidate our general result given by Eqs. (47) and (48), if the analysis is restricted to the Gaussian approximation,

but would enter via a modification of the kernels $\Pi_{\alpha\beta}^{0/1/2}$. [The kernel expansion of $K_{\alpha\beta}^{\mu\nu}$ is based on gauge invariance and therefore exact, but a higher-order expansion in gauge fluctuations prior to integration may not only be manifested in a modification of the Π kernels, but also in the form of the \tilde{K} kernels, Eqs. (47) and (48).] Only minor modifications are involved to describe spin- or valley-polarized bilayer graphene, in the limit of weak interlayer coupling.

Once the Gaussian theory and, especially, the associated collective excitations are fully understood, the next logical step would be to consider a higher-order expansion in the fluctuating gauge fields. Such a calculation requires a great amount of effort and, therefore, needs to be properly motivated. While the renormalization of the collective modes in a nonrelativistic system is constrained to some degree by virtue of Kohn's theorem [81], this is not the case for (pseudo)relativistic systems like graphene. Kohn's theorem only applies to Galilei invariant systems, stating that in the long wavelength limit the entire electron system performs a cyclotron motion with the bare cyclotron frequency $\omega_c = eB/m$, where m is the band mass. In other words, in the limit $\vec{q} \rightarrow 0$, the spectra of the collective modes in the IQH and FQH system converge to the gap ω_c , which is not renormalized by Coulomb interactions [51,53,54,80]. The breakdown of Kohn's theorem in graphene and the associated renormalization of cyclotron resonances may be understood intuitively by considering the renormalization of the spectrum due to Coulomb interactions in the absence of external magnetic fields. In this case the Coulomb interaction leads to logarithmic momentum corrections to the Fermi velocity, which renormalize the linear spectrum and diverge in the infrared regime at zero temperature [6,7,82–85]. Such deviations from linearity should influence the Landau level spectrum when finite magnetic fields are considered, even for large fields in the IQH regime. Indeed, perturbative calculations of the self-energy at finite B lead to similar logarithmic corrections, which, in turn, renormalize the noninteracting cyclotron resonances [7,73–76], showing the breakdown of Kohn's theorem. Since here the FQHE is viewed as an IQHE of composite Dirac fermions for which Kohn's theorem does not hold, it is natural to expect that self-energy corrections to the composite Dirac fermions also lead to observational consequences in the FQH regime.

The analysis of such corrections and their impact on the electromagnetic response in particular, would require more elaborate calculations that are going beyond the RPA of the present paper. Recall that within the RPA the polarization tensor $\tilde{\Pi}$ is computed with noninteracting Green functions, which take into account the finite gauge field expectation values but neglect exchange self-energy contributions. One way to include self-energy effects would be to expand the tracelog in Eq. (22) to higher orders in the fluctuations as stated above. The resulting effective action (31) would then contain non-Gaussian contributions, which renormalize the propagator of gauge fluctuations as well as the electromagnetic response tensor \tilde{K} , Eq. (44). Alternatively, one may reintroduce fermionic degrees of freedom by writing the exponentiated tracelog in Eq. (22) as a fermionic functional integral. Such a Fermi-Bose theory allows for a more systematic approach to study the

mutual effects of gauge fluctuations on the fermionic self-energy, and, vice versa, self-energy effects on the bosonic polarization tensor, even beyond perturbation theory [83–85].

An important aspect in the study of the integer and fractional quantum Hall effect constitutes the role of disorder [2]. As is well-known, scalar potential disorder leads to a broadening of the noninteracting Landau levels, which enter the calculation of the fermionic polarization tensor and, in turn, lead to observable consequences in the electromagnetic response spectrum, such as new kinds of collective modes (typically, diffusion modes). Apart from the simple scalar potential disorder, there are other types of disorder potentials, which allow scattering processes between different flavors, causing the fermionic propagators to be nondiagonal in flavor space and may even lead to another set of collective diffusion modes [86–89]. Given the large variety of possible microscopic scattering channels among the different flavors of Dirac particles and the mutual interactions between the possible collective modes, the study of disorder in graphene is a highly nontrivial task. The Keldysh formulation we employed here has proven to be an efficient computational tool for these kinds of problems, as one can perform a disorder average directly on the level of the partition function, assuming that the disorder potentials are delta correlated, which results in a fermionic pseudointeraction [64,78,79]. In contrast to the Matsubara formulation, there is no need of the replica trick and a subsequent analytical continuation. The pseudointeraction term may then be analyzed by standard techniques, such as Hubbard-Stratonovich bosonization and/or the Wilsonian/functional renormalization group [64,78,79].

Another particularly interesting research direction concerns the gauge group of the Chern-Simons field itself. Here we formulated an Abelian $U(1)^{\otimes 4}$ CS theory, where $SU(2)^{\otimes 2}$ and $SU(4)$ invariant states only arise as a subset of all possible FQH states obtained from the $U(1)^{\otimes 4}$ theory. The symmetry of the exact theory may only be generated as a dynamical symmetry in a more elaborate calculation, going well beyond the Gaussian fluctuations around a mean-field solution. An alternative route, where the non-Abelian $SU(2)^{\otimes 2}$, respectively $SU(4)$ symmetry is manifest, would be to formulate a corresponding non-Abelian gauge theory in analogy to the one proposed in Refs. [52,54]. In these works the electron is regarded as a compound object, consisting of a charge carrying holon and a charge neutral spinon that carries the spin degree of freedom, which are bound together by an RVB (resonating valence bond) gauge field. The holon interacts with a $U(1)$ Chern-Simons gauge field (in addition to the charge density–charge density Coulomb interaction) which is responsible for the actual FQHE and yields the allowed filling fractions, whereas the spinon interacts with a non-Abelian $SU(2)$ Chern-Simons gauge field assigning the correct spin structure to the respective states at each filling fraction. As a consequence, the states for each filling fraction naturally form irreducible representations of the non-Abelian gauge group [90]. It should be possible to apply these ideas also for graphene and it is expected that analogous features will arise in this pseudorelativistic framework. The spin sector of such theories, however, would be much more difficult to analyze than the corresponding Abelian theory, in particular beyond a mean-field approximation, due to the additional

cubic gauge field term required by gauge invariance, and propagating Fadeev-Popov ghosts, arising from gauge fixing [68]. Nevertheless, such a model is worth studying as it may lead to interesting insights in the fractional quantum Hall effect in graphene.

As a last remark, we want to point out that our Chern-Simons theory may be of use in the conventional nonrelativistic FQHE. In this context we remind the reader of Son's proposal of a pseudorelativistic theory to explain the physics of a half-filled Landau level, Ref. [49]. Naively applying our framework for a single Dirac flavor under the assumption that charge neutrality of this relativistic model maps to half-filling of the nonrelativistic one, $\nu_{\text{NR}} = \frac{1}{2} + \frac{\nu_{\text{CDF}}}{2k\nu_{\text{CDF}}+1}$, we made an interesting observation: not only this formula reproduces all the particle-hole symmetric filling fractions of Jain's primary sequence around half-filling, but also those filling fractions that are found in the Haldane-Halperin hierarchy and/or Jains secondary sequence (such as 5/13, 4/11, and 7/11, for example) [36,92,93], as long as k is restricted to be an even integer. Of course, it could very well be the case that this feature is a mere accident, but the more appealing possibility is that there is a deeper connection between our Chern-Simons framework and Son's idea than expected. In any case, it is worthwhile investigating this issue.

ACKNOWLEDGMENTS

The author wants to thank Piet Brouwer and Zhao Liu for helpful discussions and Piet Brouwer for support in the preparation of the manuscript. This work is supported by the German Research Foundation (DFG) in the framework of the Priority Program 1459 "Graphene."

APPENDIX A: FERMION PROPAGATOR IN EXTERNAL MAGNETIC FIELD

In this first Appendix, we derive the noninteracting propagator of two-dimensional Dirac particles in graphene, moving in a homogeneous magnetic field at finite temperature in

Keldysh basis. This propagator has already been calculated by several authors using different methods, see, for example, the Refs. [94–96], but in order to make the article self-contained, we present one of those calculations, adapted to our notational conventions, here again.

The problem of inverting the operator \hat{G}_0^{-1} in the quadratic form (11) is simplified by the fact that it is diagonal in flavor space [see Eq. (12)]. Therefore the propagator itself has to be flavor diagonal,

$$\hat{G} = \text{diag}(G_{+\uparrow}, G_{-\uparrow}, G_{+\downarrow}, G_{-\downarrow}), \quad (\text{A1})$$

with $G_\alpha = (G_\alpha^{-1})^{-1}$. Thus the problem is reduced to finding the inverse of G_α^{-1} , which describes the propagation of a single flavor. Slightly abusing language, we refer to the propagator for each individual flavor G_α as "the propagator" in what follows. Based on the results of the mean-field approximation, Eqs. (27) and (28), we assume that each of the flavors is subject to an individual magnetic field $B_{\text{eff}}^\alpha = B + b^\alpha$, and we allow each flavor to be doped individually. The propagator we obtain here occurs in the derivation of the one-loop polarization tensor (32). The latter will be derived in detail in Appendix B. In order to lighten the notation, a repeated flavor space index does not imply summation. Furthermore, calculations are performed in the mixed frequency-position space.

After mapping from contour to physical time and rotating to Keldysh basis, the propagator obeys the triangular Keldysh structure

$$G_\alpha(\vec{r}, \vec{r}', \varepsilon) = \begin{pmatrix} G_\alpha^K(\vec{r}, \vec{r}', \varepsilon) & G_\alpha^R(\vec{r}, \vec{r}', \varepsilon) \\ G_\alpha^A(\vec{r}, \vec{r}', \varepsilon) & 0 \end{pmatrix}. \quad (\text{A2})$$

As mentioned in the main text, we are only interested in the linear response regime at finite temperature. Hence the fluctuation-dissipation theorem can be employed to express the Keldysh propagator as

$$G_\alpha^K(\vec{r}, \vec{r}', \varepsilon) = \tanh\left(\frac{\varepsilon}{2T}\right) (G_\alpha^R(\vec{r}, \vec{r}', \varepsilon) - G_\alpha^A(\vec{r}, \vec{r}', \varepsilon)). \quad (\text{A3})$$

The retarded and advanced propagators will be constructed from the exact solutions of the stationary Dirac equation. Working in Landau gauge with the effective vector potential $\vec{A}_{\text{eff}}^\alpha(\vec{r}) = (-B_{\text{eff}}^\alpha y, 0)^\top$, these solutions read

$$\Psi_{\alpha, k_x}^0(x, \xi) = e^{ik_x x} \begin{pmatrix} 0 \\ \psi_0(\xi) \end{pmatrix}, \quad \Psi_{\alpha, k_x, n}^\lambda(x, \xi) = \frac{1}{\sqrt{2}} e^{ik_x x} \begin{pmatrix} -\lambda \kappa_\alpha \psi_n(\xi) \\ \psi_{n+1}(\xi) \end{pmatrix} \quad \text{if } eB_{\text{eff}}^\alpha < 0, \quad (\text{A4a})$$

$$\Psi_{\alpha, k_x}^0(x, \xi) = e^{ik_x x} \begin{pmatrix} \psi_0(\xi) \\ 0 \end{pmatrix}, \quad \Psi_{\alpha, k_x, n}^\lambda(x, \xi) = \frac{1}{\sqrt{2}} e^{ik_x x} \begin{pmatrix} \psi_{n+1}(\xi) \\ +\lambda \kappa_\alpha \psi_n(\xi) \end{pmatrix} \quad \text{if } eB_{\text{eff}}^\alpha > 0, \quad (\text{A4b})$$

where k_x is a momentum quantum number, n is a positive integer including zero, $\xi = \frac{y}{\ell_\alpha} + \text{sign}(eB_{\text{eff}}^\alpha) k_x \ell_\alpha$ is a dimensionless real-space coordinate, and $\ell_\alpha = \frac{1}{\sqrt{|eB_{\text{eff}}^\alpha|}}$ is the magnetic length associated to the effective magnetic field B_{eff}^α . The spinor $\Psi_{\alpha, k_x}^0(x, \xi)$ is the zero-energy Landau level located at the Dirac point, and $\Psi_{\alpha, k_x, n}^\lambda(x, \xi)$ are Landau levels in the conduction ($\lambda = +1$) and valence band ($\lambda = -1$), respectively, whose spectrum is symmetric around the Dirac point. Recall that $\kappa_\alpha = \pm 1$ in the definition of the above spinors refers to the valleys K_\pm . Furthermore, $\psi_n(\xi)$ are the normalized harmonic oscillator wave functions

$$\psi_n(\xi) = \frac{1}{\sqrt{2^n n!}} \frac{1}{\pi^{1/4}} e^{-\frac{1}{2}\xi} H_n(\xi), \quad (\text{A5})$$

with $H_n(\xi)$ being the Hermite polynomial of degree n .

In terms of the above exact solution the retarded and advanced propagators admit the following spectral decomposition:

$$G_\alpha^{R/A}(\vec{r}, \vec{r}', \varepsilon) = \frac{1}{\ell_\alpha} \int \frac{dk_x}{2\pi} \left[\frac{\Psi_{\alpha, k_x}^0(x, \xi) \Psi_{\alpha, k_x}^{0\dagger}(x', \xi')}{\varepsilon + \mu_\alpha \pm i0} + \sum_{\lambda=\pm 1} \sum_{n=0}^{\infty} \frac{\Psi_{\alpha, k_x n}^\lambda(x, \xi) \Psi_{\alpha, k_x n}^{\lambda\dagger}(x', \xi')}{(\varepsilon + \mu_\alpha \pm i0) - \lambda \sqrt{n+1} \omega_c^\alpha} \right], \quad (\text{A6})$$

with the cyclotron frequency $\omega_c^\alpha = \frac{\sqrt{2}v_F}{\ell_\alpha}$. The momentum integration therein can be performed analytically with the help of the integral identity (Ref. [97], Eq. 7.377),

$$\int_x e^{-x^2} H_m(y+x) H_n(z+x) = 2^n \sqrt{\pi} m! z^{n-m} L_m^{n-m}(-2yz), \quad m \leq n. \quad (\text{A7})$$

Here, $L_n^k(x)$ are the associated Laguerre polynomials of degree n . As a result of the momentum integration, we find that the propagators can be written as a product of a translation- and gauge noninvariant phase $\chi_\alpha(\vec{r}, \vec{r}') = -e \int_{\vec{r}'}^{\vec{r}} \vec{A}_\alpha(\vec{r}'') \cdot d\vec{r}''$ —which is nothing but a Wilson line—and a translation- and gauge-invariant part $S_\alpha^{R/A}(\vec{r} - \vec{r}', \varepsilon)$,

$$G_\alpha^{R/A}(\vec{r}, \vec{r}', \varepsilon) = e^{i\chi_\alpha(\vec{r}, \vec{r}')} S_\alpha^{R/A}(\vec{r} - \vec{r}', \varepsilon). \quad (\text{A8})$$

Introducing the relative coordinate $\Delta\vec{r} = \vec{r} - \vec{r}'$, and the projection operators

$$\mathcal{P}_\pm = \frac{1}{2}(\sigma_0 \pm \text{sign}(eB_\alpha^{\text{eff}})\sigma_3), \quad (\text{A9})$$

the translation- and gauge-invariant part of the propagators can be written compactly as

$$S_\alpha^{R/A}(\Delta\vec{r}, \varepsilon) = \frac{\exp(-\frac{\Delta\vec{r}^2}{4\ell_\alpha^2})}{4\pi\ell_\alpha^2} \sum_{n=0}^{\infty} \sum_{\lambda=\pm 1} \left[\mathcal{P}_+ L_n^0\left(\frac{\Delta\vec{r}^2}{2\ell_\alpha^2}\right) + \mathcal{P}_- L_{n-1}^0\left(\frac{\Delta\vec{r}^2}{2\ell_\alpha^2}\right) + i \frac{\lambda\kappa}{\sqrt{2}\ell_\alpha} \frac{\vec{\sigma} \cdot \Delta\vec{r}}{\sqrt{n}} L_{n-1}^1\left(\frac{\Delta\vec{r}^2}{2\ell_\alpha^2}\right) \right] S_{\alpha, \lambda n}^{R/A}(\varepsilon), \quad (\text{A10})$$

with

$$S_{\alpha, \lambda n}^{R/A}(\varepsilon) = \frac{1}{(\varepsilon + \mu_\alpha \pm i0) - \lambda \sqrt{n} \omega_c^\alpha}. \quad (\text{A11})$$

Here we have defined $L_{-1}^0, L_{-1}^1 \equiv 0$.

The charge carrier 3-current per flavor, \vec{j}_α^μ , is given by

$$\vec{j}_\alpha^\mu(\vec{r}, t) = -\frac{i}{2} \text{tr} \sigma_\alpha^\mu G_\alpha^K(\vec{r}, t, \vec{r}, t) = -\frac{i}{2} \int_\varepsilon \tanh\left(\frac{\varepsilon}{2T}\right) \text{tr} \sigma_\alpha^\mu (G_\alpha^R(\vec{r}, \vec{r}, \varepsilon) - G_\alpha^A(\vec{r}, \vec{r}, \varepsilon)). \quad (\text{A12})$$

In thermal equilibrium, only its zero component, being the charge carrier density, $\vec{j}_\alpha^0 \equiv \bar{n}_\alpha$, acquires a finite value

$$\bar{n}_\alpha(\vec{r}, t) = \frac{1}{2\pi\ell_\alpha^2} v_\alpha. \quad (\text{A13})$$

Here, v_α defines the filling fraction per flavor as a function of the chemical potential μ_α , the effective magnetic field B_α^{eff} , and temperature T :

$$v_\alpha = \frac{1}{2} \left[\tanh\left(\frac{\mu_\alpha}{2T}\right) + \sum_{n=1}^{\infty} \left(\tanh\left(\frac{\sqrt{n}\omega_c^\alpha + \mu_\alpha}{2T}\right) + \tanh\left(\frac{-\sqrt{n}\omega_c^\alpha + \mu_\alpha}{2T}\right) \right) \right]. \quad (\text{A14})$$

Near absolute zero temperature the filling fraction is quantized into plateaus of half-integers $v_\alpha = \pm(n_\alpha + \frac{1}{2}), n_\alpha = 0, 1, 2, \dots$, see Fig. 2. The anomalous additional fraction occurs due to the presence of a Landau level at charge neutrality ($\mu_\alpha = 0$).

APPENDIX B: FERMIONIC ONE-LOOP POLARIZATION TENSOR

In this second Appendix, we derive the one-loop polarization tensor for Dirac fermions experiencing a homogeneous, flavor-dependent effective magnetic field $B_\alpha^{\text{eff}} = B + b^\alpha$. See also Ref. [98] for a calculation of the polarization function [the 00 component of Eq. (B1)], with which our result coincides. Displaying the Keldysh structure explicitly, Eq. (32) reads

$$\Pi_{\alpha\beta}^{\mu\nu}(x, y) = -\frac{i}{2} \frac{\delta^2}{\delta a_\nu^\beta(y) \delta a_\mu^\alpha(x)} \text{tr} \ln \left(\begin{array}{cc} 0 & (\hat{G}_0^A)^{-1} \\ (\hat{G}_0^R)^{-1} & -(\hat{G}_0^R)^{-1} (\hat{G}_0^K) (\hat{G}_0^A)^{-1} \end{array} \right) \Big|_{a=\bar{a}} [e\mathbf{A}_\mu + \mathbf{a}_\mu^\alpha]. \quad (\text{B1})$$

Recall that \bar{a} is the field expectation value of the statistical gauge field, which possesses a classical component only. Performing the functional derivatives and evaluating the result at the mean-field values of the statistical gauge fields, we obtain the following

retarded, advanced, and Keldysh components:

$$(\Pi^{R/A})_{\alpha\beta}^{\mu\nu}(x-y) = \frac{i}{2} \text{tr}(\sigma_\alpha^\mu S_\alpha^{R/A}(x-y) \sigma_\alpha^\nu S_\alpha^K(y-x) + \sigma_\alpha^\mu S_\alpha^K(x-y) \sigma_\alpha^\nu S_\alpha^{A/R}(y-x)) \delta_{\alpha\beta}, \quad (\text{B2a})$$

$$(\Pi^K)_{\alpha\beta}^{\mu\nu}(x-y) = \frac{i}{2} \text{tr}(\sigma_\alpha^\mu S_\alpha^R(x-y) \sigma_\alpha^\nu S_\alpha^A(y-x) + \sigma_\alpha^\mu S_\alpha^A(x-y) \sigma_\alpha^\nu S_\alpha^R(y-x) + \sigma_\alpha^\mu S_\alpha^K(x-y) \sigma_\alpha^\nu S_\alpha^K(y-x)) \delta_{\alpha\beta}. \quad (\text{B2b})$$

The repeated flavor space index α does *not* imply summation, as was the case in Appendix A. Recall that the Pauli 3-vector therein is given by $\sigma_\alpha^\mu \equiv (\sigma_0, \kappa_\alpha v_F \sigma_1, \kappa_\alpha v_F \sigma_2)$. First, observe that the polarization tensor is diagonal in flavor space, $\Pi_{\alpha\beta}^{\mu\nu} = \Pi_\alpha^{\mu\nu} \delta_{\alpha\beta}$, which is a consequence of the free propagator being diagonal, see Eq. (A1). Second, note that the gauge- and translation-noninvariant phase $\chi_\alpha(\vec{r}, \vec{r}')$ drops out, such that the polarization tensor can be expressed solely in terms of the propagators $S_\alpha^{R/A/K}$, proving its manifest gauge and translation invariance. In Fourier space, the above equations for the flavor diagonal components Π_α become

$$(\Pi^{R/A})_\alpha^{\mu\nu}(\omega, \vec{q}) = \frac{i}{2} \int_{\Delta\vec{r}} e^{-i\vec{q}\cdot\Delta\vec{r}} \int_\varepsilon \text{tr}(\sigma_\alpha^\mu S_\alpha^{R/A}(\Delta\vec{r}, \varepsilon + \omega) \sigma_\alpha^\nu S_\alpha^K(-\Delta\vec{r}, \varepsilon) + \sigma_\alpha^\mu S_\alpha^K(\Delta\vec{r}, \varepsilon) \sigma_\alpha^\nu S_\alpha^{A/R}(-\Delta\vec{r}, \varepsilon - \omega)), \quad (\text{B3a})$$

$$(\Pi^K)_\alpha^{\mu\nu}(\omega, \vec{q}) = \coth\left(\frac{\omega}{2T}\right) ((\Pi^R)_\alpha^{\mu\nu}(\omega, \vec{q}) - (\Pi^A)_\alpha^{\mu\nu}(\omega, \vec{q})). \quad (\text{B3b})$$

Equation (B3b) is a manifestation of the (bosonic) fluctuation-dissipation theorem. In order to arrive at this form, one has to rewrite the first line of Eq. (B2b) according to $\sigma^\mu S_{xy}^R \sigma^\nu S_{yx}^A + \sigma^\mu S_{xy}^A \sigma^\nu S_{yx}^R = -\sigma^\mu (S_{xy}^R - S_{xy}^A) \sigma^\nu (S_{yx}^R - S_{yx}^A)$, which holds true because of the causality properties of the retarded and advanced propagators, cf. Ref. [64]. Next, one has to employ Eq. (A3) and finally make use of the identity $\tanh(x)\tanh(y) - 1 = \coth(x-y)(\tanh(y) - \tanh(x))$.

By substituting the propagators (A3) and (A10) into Eq. (B3a), the polarization tensor acquires the form

$$(\Pi^{R/A})_\alpha^{\mu\nu}(\omega, \vec{q}) = \frac{1}{32\pi^2 \ell_\alpha^4} \sum_{n,n'} \sum_{\lambda,\lambda'} \frac{\mathcal{F}_{nn'}^{\lambda\lambda'}(T, \mu_\alpha)}{(\omega \pm i0) - \lambda\sqrt{n}\omega_\alpha^c + \lambda'\sqrt{n'}\omega_\alpha^c} \int_{\Delta\vec{r}} e^{-i\vec{q}\cdot\Delta\vec{r}} e^{-\frac{\Delta\vec{r}^2}{2\ell_\alpha^2}} \text{tr}(\sigma_\alpha^\mu M_n^\alpha(\lambda\Delta\vec{r}) \sigma_\alpha^\nu M_{n'}^\alpha(-\lambda'\Delta\vec{r}')), \quad (\text{B4})$$

with

$$\mathcal{F}_{nn'}^{\lambda\lambda'}(T, \mu_\alpha) = \tanh\left(\frac{\lambda'\sqrt{n'}\omega_\alpha^c - \mu_\alpha}{2T}\right) - \tanh\left(\frac{\lambda\sqrt{n}\omega_\alpha^c - \mu_\alpha}{2T}\right) \quad (\text{B5})$$

and

$$M_n^\alpha(\lambda\Delta\vec{r}) = \mathcal{P}_+ L_n^0\left(\frac{\Delta\vec{r}^2}{2\ell_\alpha}\right) + \mathcal{P}_- L_{n-1}^0\left(\frac{\Delta\vec{r}^2}{2\ell_\alpha}\right) + i \frac{\lambda\kappa}{\sqrt{2}\ell_\alpha} \frac{\vec{\sigma} \cdot \Delta\vec{r}}{\sqrt{n}} L_{n-1}^1\left(\frac{\Delta\vec{r}^2}{2\ell_\alpha}\right). \quad (\text{B6})$$

Performing the trace for each tensor component and comparing the resulting expressions with the kernel expansion (35), we can extract the following scalar quantities:

$$(\Pi^{R/A})_\alpha^0(\omega, \vec{q}) = -\frac{1}{32\pi^2 \ell_\alpha^4} \frac{1}{\vec{q}^2} \sum_{n,n'} \sum_{\lambda,\lambda'} \frac{\mathcal{F}_{nn'}^{\lambda\lambda'}(T, \mu_\alpha)}{(\omega \pm i0) - \lambda\sqrt{n}\omega_\alpha^c + \lambda'\sqrt{n'}\omega_\alpha^c} \left(I_{n-1,n'}^0(Q_\alpha) + I_{n,n'-1}^0(Q_\alpha) + \frac{2\lambda\lambda'}{\sqrt{nn'}} I_{n-1,n'-1}^1(Q_\alpha) \right), \quad (\text{B7a})$$

$$(\Pi^{R/A})_\alpha^1(\omega, \vec{q}) = -\frac{\text{sign}(B_\alpha^{\text{eff}}) v_F^2}{32\pi^2 \ell_\alpha^4} \frac{1}{\omega} \sum_{n,n'} \sum_{\lambda,\lambda'} \frac{\mathcal{F}_{nn'}^{\lambda\lambda'}(T, \mu_\alpha)}{(\omega \pm i0) - \lambda\sqrt{n}\omega_\alpha^c + \lambda'\sqrt{n'}\omega_\alpha^c} (I_{n-1,n'}^0(Q_\alpha) - I_{n,n'-1}^0(Q_\alpha)), \quad (\text{B7b})$$

$$(\Pi^{R/A})_\alpha^2(\omega, \vec{q}) = +\frac{1}{32\pi^2} \sum_{n,n'} \sum_{\lambda,\lambda'} \frac{\mathcal{F}_{nn'}^{\lambda\lambda'}(T, \mu_\alpha)}{(\omega \pm i0) - \lambda\sqrt{n}\omega_\alpha^c + \lambda'\sqrt{n'}\omega_\alpha^c} \left(\frac{2\lambda\lambda'}{\sqrt{nn'}} \frac{v_F^2}{\ell_\alpha^2} \partial_{Q_\alpha}^2 \tilde{I}_{n-1,n'-1}^1(Q_\alpha) \right). \quad (\text{B7c})$$

Here we have defined the integral expressions

$$\begin{aligned} I_{n,n'}^k(Q_\alpha) &= \int_{\Delta\vec{r}} e^{-i\vec{q}\cdot\Delta\vec{r}} e^{-\frac{\Delta\vec{r}^2}{2\ell_\alpha^2}} \left(\frac{\Delta\vec{r}^2}{2\ell_\alpha^2}\right)^k L_n^k\left(\frac{\Delta\vec{r}^2}{2\ell_\alpha^2}\right) L_{n'}^k\left(\frac{\Delta\vec{r}^2}{2\ell_\alpha^2}\right) \\ &= 2\pi \ell_\alpha^2 Q_\alpha^{n_>-n_<} e^{-Q_\alpha} \frac{(n_<+k)!}{n_>!} L_{n_<}^{n_>-n_<}(Q_\alpha) L_{n_<+k}^{n_>-n_<}(Q_\alpha), \quad k=0,1, \end{aligned} \quad (\text{B8a})$$

$$\tilde{I}_{n,n'}^1(Q_\alpha) = \int_{\Delta\vec{r}} e^{-i\vec{q}\cdot\Delta\vec{r}} e^{-\frac{\Delta\vec{r}^2}{2\ell_\alpha^2}} L_n^1\left(\frac{\Delta\vec{r}^2}{2\ell_\alpha^2}\right) L_{n'}^1\left(\frac{\Delta\vec{r}^2}{2\ell_\alpha^2}\right) = \sum_{m=0}^n \sum_{m'=0}^{n'} I_{m,m'}^0(Q_\alpha), \quad (\text{B8b})$$

where $Q_\alpha = \frac{\tilde{q}^2 \ell_\alpha^2}{2}$ is a dimensionless momentum variable, and $n_> = \max\{n, n'\}$, $n_< = \min\{n, n'\}$. Note that both $I_{n, n'}^k$ and $\tilde{I}_{n, n'}^1$ are symmetric in their Landau indices n, n' . Hence, without loss of generality, we can assume $n \leq n'$ in the following proof.

First, let us show how $\tilde{I}_{n, n'}^1(Q_\alpha)$ can be reduced to a sum of $I_{n, n'}^0(Q_\alpha)$. In order to prove this equality, we only have to make use of the property $L_n^{k+1}(x) = \sum_{m=0}^n L_m^k(x)$, see Ref. [97], Eq. 8.974.3, and interchange integration and summation. We immediately arrive at the second line of Eq. (B8b). The proof of Eq. (B8a) is more involved. First of all, one has to work in polar coordinates, substituting $t = \frac{\Delta F^2}{2\ell_\alpha^2}$, and perform the angle integration, which yields the Bessel function of the first kind J_0 :

$$I_{n, n'}^k(Q_\alpha) = 2\pi \ell_\alpha^2 \int_0^\infty dt e^{-t} t^k J_0(2\sqrt{Q_\alpha t}) L_{n_>}^k(t) L_{n_<}^k(t). \quad (\text{B9})$$

Next, we rewrite $L_{n_<}^k(t) = (-t)^{-k} \frac{(n_<+k)!}{n_<!} L_{n_<+k}^{-k}(t)$, see Ref. [98], resulting in

$$I_{n, n'}^k(Q_\alpha) = 2\pi \ell_\alpha^2 (-1)^k (n_< + 1)^k \int_0^\infty dt e^{-t} J_0(2\sqrt{Q_\alpha t}) L_{n_>}^k(t) L_{n_<+k}^{-k}(t). \quad (\text{B10})$$

The residual integration can be performed by making use of the integral identity (Ref. [97], Eq. 7.422.2)

$$\int_0^\infty dt e^{-t} J_0(2\sqrt{Q_\alpha t}) L_{n_>}^k(t) L_{n_<+k}^{-k}(t) = (-1)^{n_>+n_<+k} e^{-Q_\alpha} L_{n_>}^{n_<-n_>}(Q_\alpha) L_{n_<+k}^{n_>-n_<}(Q_\alpha). \quad (\text{B11})$$

After straightforward manipulation of the result, we find Eq. (B8a) eventually.

-
- [1] K. v. Klitzing, G. Dorda, and M. Pepper, *Phys. Rev. Lett.* **45**, 494 (1980).
- [2] J. K. Jain, *Composite Fermions* (Cambridge University Press, Cambridge, 2007).
- [3] P. R. Wallace, *Phys. Rev.* **71**, 622 (1947).
- [4] G. W. Semenoff, *Phys. Rev. Lett.* **53**, 2449 (1984).
- [5] V. P. Gusynin, S. G. Sharapov, and J. P. Carbotte, *Int. J. Mod. Phys. B* **21**, 4611 (2007).
- [6] A. H. Castro Neto, F. Guinea, N. M. R. Peres, K. S. Novoselov, and A. K. Geim, *Rev. Mod. Phys.* **81**, 109 (2009).
- [7] S. Das Sarma, S. Adam, E. H. Hwang, and E. Rossi, *Rev. Mod. Phys.* **83**, 407 (2011).
- [8] M. O. Goerbig, *Rev. Mod. Phys.* **83**, 1193 (2011).
- [9] E. V. Gorbar, V. P. Gusynin, V. A. Miransky, and I. A. Shovkovy, *Phys. Rev. B* **66**, 045108 (2002).
- [10] V. P. Gusynin and S. G. Sharapov, *Phys. Rev. Lett.* **95**, 146801 (2005).
- [11] Y. Zhang, Y.-W. Tan, H. L. Stormer, and P. Kim, *Nature (London)* **438**, 201 (2005).
- [12] K. S. Novoselov, Z. Jiang, Y. Zhang, S. V. Morozov, H. L. Stormer, U. Zeitler, J. C. Maan, and G. S. Boebinger, *Science* **315**, 1379 (2007).
- [13] D. C. Tsui, H. L. Stormer, and A. C. Gossard, *Phys. Rev. Lett.* **48**, 1559 (1982).
- [14] W. Pan, H. L. Stormer, D. C. Tsui, L. N. Pfeiffer, K. W. Baldwin, and K. W. West, *Phys. Rev. Lett.* **88**, 176802 (2002).
- [15] X. Du, I. Skachko, F. Duerr, A. Luican, and E. Y. Andrei, *Nature (London)* **462**, 192 (2009).
- [16] K. I. Bolotin, F. Ghahari, M. D. Shulman, H. L. Stormer, and P. Kim, *Nature (London)* **462**, 196 (2009).
- [17] C. R. Dean, A. F. Young, P. Cadden-Zimansky, L. Wang, H. Ren, K. Watanabe, T. Taniguchi, P. Kim, J. Hone, and K. L. Shepard, *Nat. Phys.* **7**, 693 (2011).
- [18] R. B. Laughlin, *Phys. Rev. Lett.* **50**, 1395 (1983).
- [19] J. K. Jain, *Phys. Rev. Lett.* **63**, 199 (1989).
- [20] O. Heinonen, *Composite Fermions* (World Scientific, Singapore, 1998).
- [21] R. R. Du, H. L. Stormer, D. C. Tsui, L. N. Pfeiffer, and K. W. West, *Phys. Rev. Lett.* **70**, 2944 (1993).
- [22] R. L. Willett, R. R. Ruel, K. W. West, and L. N. Pfeiffer, *Phys. Rev. Lett.* **71**, 3846 (1993).
- [23] W. Kang, H. L. Stormer, L. N. Pfeiffer, K. W. Baldwin, and K. W. West, *Phys. Rev. Lett.* **71**, 3850 (1993).
- [24] H. C. Manoharan, M. Shayegan, and S. J. Klepper, *Phys. Rev. Lett.* **73**, 3270 (1994).
- [25] V. J. Goldman, B. Su, and J. K. Jain, *Phys. Rev. Lett.* **72**, 2065 (1994).
- [26] R. Du, H. Stormer, D. Tsui, L. Pfeiffer, and K. West, *Solid State Commun.* **90**, 71 (1994).
- [27] D. R. Leadley, R. J. Nicholas, C. T. Foxon, and J. J. Harris, *Phys. Rev. Lett.* **72**, 1906 (1994).
- [28] J. H. Smet, D. Weiss, R. H. Blick, G. Lütjering, K. von Klitzing, R. Fleischmann, R. Ketzmerick, T. Geisel, and G. Weimann, *Phys. Rev. Lett.* **77**, 2272 (1996).
- [29] J. H. Smet, K. von Klitzing, D. Weiss, and W. Wegscheider, *Phys. Rev. Lett.* **80**, 4538 (1998).
- [30] J. H. Smet, S. Jobst, K. von Klitzing, D. Weiss, W. Wegscheider, and V. Umansky, *Phys. Rev. Lett.* **83**, 2620 (1999).
- [31] R. L. Willett, K. W. West, and L. N. Pfeiffer, *Phys. Rev. Lett.* **83**, 2624 (1999).
- [32] S. Melinte, N. Freytag, M. Horvatić, C. Berthier, L. P. Lévy, V. Bayot, and M. Shayegan, *Phys. Rev. Lett.* **84**, 354 (2000).
- [33] I. V. Kukushkin, J. H. Smet, D. Schuh, W. Wegscheider, and K. von Klitzing, *Phys. Rev. Lett.* **98**, 066403 (2007).
- [34] D. Kamburov, M. Shayegan, L. N. Pfeiffer, K. W. West, and K. W. Baldwin, *Phys. Rev. Lett.* **109**, 236401 (2012).
- [35] D. Kamburov, Y. Liu, M. Shayegan, L. N. Pfeiffer, K. W. West, and K. W. Baldwin, *Phys. Rev. Lett.* **110**, 206801 (2013).
- [36] J. K. Jain, *Indian J. Phys.* **88**, 915 (2014).
- [37] C. Töke, P. E. Lammert, V. H. Crespi, and J. K. Jain, *Phys. Rev. B* **74**, 235417 (2006).

- [38] C. Töke and J. K. Jain, *Phys. Rev. B* **75**, 245440 (2007).
- [39] V. M. Apalkov and T. Chakraborty, *Phys. Rev. Lett.* **97**, 126801 (2006).
- [40] B. I. Halperin, *Helv. Phys. Acta* **56**, 75 (1983).
- [41] V. W. Scarola and J. K. Jain, *Phys. Rev. B* **64**, 085313 (2001).
- [42] Z. Papić, M. O. Goerbig, and N. Regnault, *Solid State Commun.* **149**, 1056 (2009).
- [43] Z. Papić, M. O. Goerbig, and N. Regnault, *Phys. Rev. Lett.* **105**, 176802 (2010).
- [44] M. O. Goerbig and N. Regnault, *Phys. Rev. B* **75**, 241405 (2007).
- [45] I. Sodemann and A. H. MacDonald, *Phys. Rev. B* **87**, 245425 (2013).
- [46] M. R. Peterson and C. Nayak, *Phys. Rev. B* **87**, 245129 (2013).
- [47] M. R. Peterson and C. Nayak, *Phys. Rev. Lett.* **113**, 086401 (2014).
- [48] M. I. Dyakonov, [arXiv:cond-mat/0209206](https://arxiv.org/abs/cond-mat/0209206).
- [49] D. T. Son, *Phys. Rev. X* **5**, 031027 (2015).
- [50] B. I. Halperin, P. A. Lee, and N. Read, *Phys. Rev. B* **47**, 7312 (1993).
- [51] A. Lopez and E. Fradkin, *Phys. Rev. B* **44**, 5246 (1991).
- [52] A. Balatsky and E. Fradkin, *Phys. Rev. B* **43**, 10622 (1991).
- [53] A. Lopez and E. Fradkin, *Phys. Rev. B* **47**, 7080 (1993).
- [54] A. Lopez and E. Fradkin, *Phys. Rev. B* **51**, 4347 (1995).
- [55] L. Zhang, *Phys. Rev. B* **51**, 4645 (1995).
- [56] S. C. Zhang, T. H. Hansson, and S. Kivelson, *Phys. Rev. Lett.* **62**, 82 (1989).
- [57] S. Modak, S. S. Mandal, and K. Sengupta, *Phys. Rev. B* **84**, 165118 (2011).
- [58] D. V. Khveshchenko, *Phys. Rev. B* **75**, 153405 (2007).
- [59] E. Fradkin, *Field Theories of Condensed Matter Physics* (Cambridge University Press, Cambridge, 2013).
- [60] The Hall conductivity that has been obtained in Ref. [58] appears to be formally identical to our result, but a close inspection of the discussed examples reveals that therein the Hall conductivities of the composite fermions $\sigma_{0,xy}^\alpha$ are integer quantized as opposed to the half-integer quantized values that enter our formula. This fact is a consequence of the flux attachment to the physical electrons measured from the bottom of the lowest Landau level.
- [61] N. M. R. Peres, F. Guinea, and A. H. Castro Neto, *Phys. Rev. B* **73**, 125411 (2006).
- [62] A. Jellal and B. Malika, *Int. J. Geom. Method. Mod. Phys.* **07**, 143 (2010).
- [63] K.-c. Chou, Z.-b. Su, B.-l. Hao, and L. Yu, *Phys. Rep.* **118**, 1 (1985).
- [64] A. Kamenev, *Field Theory of Non-Equilibrium Systems* (Cambridge University Press, Cambridge, 2011).
- [65] P. Danielewicz, *Ann. Phys.* **152**, 239 (1984).
- [66] E. Calzetta and B. L. Hu, *Phys. Rev. D* **37**, 2878 (1988).
- [67] J. W. Negele and H. Orland, *Quantum Many-Particle Systems* (Westview Press, Boulder, Colorado, 1998).
- [68] M. E. Peskin and D. V. Schroeder, *An Introduction to Quantum Field Theory* (Westview Press, Boulder, Colorado, 1995).
- [69] Additionally, one obtains a similar equation for the first variational derivative with respect to the classical components of the gauge fields. Such equations, however, would be trivial, since their solutions for the quantum components of the gauge fields are constrained to vanish [63].
- [70] Note that the magnetic field in the Zeeman term is not affected by the statistical magnetic field.
- [71] That means the Keldysh components can be parametrized by the respective retarded and advanced components as
- $$(\Pi^K)_{\alpha\beta}^{\mu\nu}(\omega, \vec{q}) = \coth\left(\frac{\omega}{2T}\right)((\Pi^R)_{\alpha\beta}^{\mu\nu} - (\Pi^A)_{\alpha\beta}^{\mu\nu})(\omega, \vec{q}),$$
- $$(C^K)_{\alpha\beta}^{\mu\nu}(\omega, \vec{q}) = \coth\left(\frac{\omega}{2T}\right)((C^R)_{\alpha\beta}^{\mu\nu} - (C^A)_{\alpha\beta}^{\mu\nu})(\omega, \vec{q}).$$
- [72] We have to mention here that interactions may nevertheless lead to interesting observable consequences in the realm of the integer quantum Hall effect. A possible scenario is a degeneracy breaking of certain, if not all noninteracting Landau levels of the multicomponent quantum Hall system. The lifted degeneracy, in turn, would lead to the formation of additional plateaus in the Hall spectrum. This kind of interaction effect clearly has to be distinguished from the fractional quantum Hall effect, as the underlying physical mechanisms for both phenomena vastly differ. We do not consider interaction effects of this kind in the present paper, and refer to Refs. [7,8] and references therein for a more elaborate discussion (see also Refs. [73–76]).
- [73] Y. A. Bychkov and G. Martinez, *Phys. Rev. B* **77**, 125417 (2008).
- [74] R. Roldán, J.-N. Fuchs, and M. O. Goerbig, *Phys. Rev. B* **82**, 205418 (2010).
- [75] K. Shizuya, *Phys. Rev. B* **81**, 075407 (2010).
- [76] A. A. Sokolik, A. D. Zabolotskiy, and Y. E. Lozovik, *Phys. Rev. B* **95**, 125402 (2017).
- [77] To be exact, the Fadeev-Popov determinant can be absorbed into the normalization constant only, if it does not depend on the gauge field itself. This is not always the case, specifically in non-Abelian gauge theories, or if the gauge fixing function $G(\Delta a_\mu^\alpha)$ contains powers of the gauge field larger than or equal to two. In that case, the Fadeev-Popov determinant leads to an additional contribution to the action known as Fadeev-Popov ghosts [68]. In the present paper, however, we are dealing with an Abelian gauge theory and consider linear gauge fixing functions only, such that the above mentioned problems are avoided.
- [78] G. Schwiete and A. M. Finkel'stein, *Phys. Rev. B* **89**, 075437 (2014).
- [79] G. Schwiete and A. M. Finkel'stein, *Phys. Rev. B* **90**, 155441 (2014).
- [80] A. Lopez and E. Fradkin, *Phys. Rev. Lett.* **69**, 2126 (1992).
- [81] W. Kohn, *Phys. Rev.* **123**, 1242 (1961).
- [82] D. C. Elias, R. V. Gorbachev, A. S. Mayorov, S. V. Morozov, A. A. Zhukov, P. Blake, L. A. Ponomarenko, I. V. Grigorieva, K. S. Novoselov, F. Guinea, and A. K. Geim, *Nat. Phys.* **7**, 701 (2011).
- [83] C. Popovici, C. S. Fischer, and L. von Smekal, *Phys. Rev. B* **88**, 205429 (2013).
- [84] C. Bauer, A. Rückriegel, A. Sharma, and P. Kopietz, *Phys. Rev. B* **92**, 121409 (2015).
- [85] C. Fräßdorf and J. E. M. Mosig, *Phys. Rev. B* **95**, 125412 (2017).
- [86] I. L. Aleiner and K. B. Efetov, *Phys. Rev. Lett.* **97**, 236801 (2006).
- [87] P. M. Ostrovsky, I. V. Gornyi, and A. D. Mirlin, *Phys. Rev. B* **74**, 235443 (2006).
- [88] E. McCann, K. Kechedzhi, V. I. Fal'ko, H. Suzuura, T. Ando, and B. L. Altshuler, *Phys. Rev. Lett.* **97**, 146805 (2006).
- [89] K. Kechedzhi, O. Kashuba, and V. I. Fal'ko, *Phys. Rev. B* **77**, 193403 (2008).

- [90] Note that, although the spin sector features a non-Abelian gauge field, this fact does not imply that the corresponding FQH states are indeed “truly” non-Abelian, in the sense that their excitations feature non-Abelian braiding statistics. For a review about such non-Abelian anyons see Ref. [91] and references therein.
- [91] C. Nayak, S. H. Simon, A. Stern, M. Freedman, and S. Das Sarma, *Rev. Mod. Phys.* **80**, 1083 (2008).
- [92] F. D. M. Haldane, *Phys. Rev. Lett.* **51**, 605 (1983).
- [93] B. I. Halperin, *Phys. Rev. Lett.* **52**, 1583 (1984).
- [94] J. Schwinger, *Phys. Rev.* **82**, 664 (1951).
- [95] N. J. M. Horing and S. Y. Liu, *J. Phys. A* **42**, 225301 (2009).
- [96] T. M. Rusin and W. Zawadzki, *J. Phys. A* **44**, 105201 (2011).
- [97] I. S. Gradshteyn and I. M. Ryzhik, *Table of Integrals, Series, and Products* (Academic, Burlington, MA, 2007).
- [98] P. K. Pyatkovskiy and V. P. Gusynin, *Phys. Rev. B* **83**, 075422 (2011).

Chapter 5

Disordered Dirac fermions

In this final chapter we consider noninteracting Dirac fermions in a random environment. First, we discuss how disorder is treated in quantum many-body theory. Afterwards, we sketch how the most general disorder potential in the continuum Dirac theory arises from the tight-binding model in the presence of impurities and random lattice deformations. This model serves as the starting point for the two papers that are included here. Next, we present a paper where we consider the chiral modes that form at the interface of a graphene pn junction in a uniform magnetic field. We derive the influence of bulk disorder on those interface modes and analyze the effective one dimensional model by a scattering matrix approach, which yields the full conductance distribution for arbitrary disorder strengths. Lastly, we include a manuscript for a paper, which employs field-theoretical techniques to calculate the disorder induced self-energy for graphene and other paradigmatic semimetals at nodal-point filling and zero temperature.

Included papers/manuscripts

Pages 151-161	“Graphene pn junction in a quantizing magnetic field: Conductance at intermediate disorder strength”
Pages 163-175	“Strong disorder in nodal semimetals: Schwinger-Dyson–Ward approach”

5.1 Statistical field theory and disorder

In this section we briefly explain how disorder is accounted for in quantum many-body theory. For now we consider a single fermion flavour that has no spinor structure as it is realized in spin-polarized metals. The generalization to Dirac electrons will be discussed in the next section, once we introduced the relevant notions for this simpler case and identified the general strategy to pursue.

It should be a given that the assumption of absolutely clean and perfectly ordered crystals is a highly idealized abstraction of physical reality. In a realistic macroscopic sample there are always impurities and imperfections in the lattice structure at which the electrons can scatter. To some extent such deviations from the perfect lattice structure can be modeled by a complicated time-independent potential landscape – the disorder potential – in which the electrons move. Here we consider a simple linear coupling of the disorder potential to the electron density in

analogy to an external electric potential [1–6]

$$H_{dis} = \int_{\vec{r}} \psi^\dagger(\vec{r}) V(\vec{r}) \psi(\vec{r}). \quad (5.1.1)$$

This disorder term adds to the Hamiltonian of the clean system. Their sum generates the time evolution of the disordered system for a single realization of the disorder potential. Given a particular realization of the disorder field, one can use the techniques of chapter 3 to calculate the n -point Green functions. Since we are considering noninteracting fermions in this chapter, all we need to calculate is the connected two-point correlator. According to Secs. 3.1 and 3.2, the other $2n$ -point functions with $n > 2$ are just algebraic products of this fundamental correlator. To find the connected two-point function for a fixed disorder field configuration $V(\vec{r})$ we need to solve the Dyson-like equation

$$\int_z (G_0^{-1} - V)(x, z) G_c(z, y|V) = \delta(x - y). \quad (5.1.2)$$

This equation is just an ordinary differential equation written in a distributional matrix form. The inverse propagator of the clean system is denoted by G_0^{-1} and the disorder potential is elevated to a matrix defined as $V(x_1, x_2) \equiv V(\vec{r}_1) \delta(\vec{r}_1 - \vec{r}_2) \delta(t_1 - t_2)$. The connected two-point correlator $G_c(x, y|V)$ is understood as both a function of two space-time coordinates and a functional of the disorder field. (Compare the notation with Eq. (3.A.1). Furthermore, recall that the time arguments are defined on the Schwinger-Keldysh contour.)

To proceed let us consider a concrete disorder field configuration. Possibly the first idea that comes to mind is to model the disorder potential as a sum of N individual impurity potentials $u_i(\vec{r} - \vec{r}_i)$ that are randomly distributed at the points \vec{r}_i [1],

$$V(\vec{r}) = \sum_{i=1}^N u_i(\vec{r} - \vec{r}_i). \quad (5.1.3)$$

A single impurity potential could be a screened Coulomb potential, a Gaussian, a Lorentzian or anything else that falls off fast enough away from the center of the impurity. The precise form is not relevant for our discussion. What matters is that the superposition of the individual contributions results in a random function with a countless number of hills and valleys. It should be obvious that for such a complicated potential landscape it is impossible to calculate the correlator $G_c(x, y|V)$ analytically exactly. But even if we ignore that fact for the moment, there is yet another problem: we simply do not know the precise positions of the individual impurities. Experimentally there is no way to precisely determine, let alone control the exact disorder potential. Variations of certain experimental control parameters, such as temperature and pressure, may even cause the microscopic disorder potential to change. Therefore it is not only hopeless, but also meaningless to calculate any physical observable in the presence of a random potential. It is at this point where the disorder average comes into play and where we turn our ignorance about the microscopic details of the disorder potential into an advantage. Instead of trying to find the two-point function or any other disorder dependent quantity for one particular disorder realization, we consider a statistical ensemble of samples – each of which featuring some realization of the disorder field – and we calculate statistically averaged quantities. This way we do not have to worry about the inaccessible microscopic details of disorder and we can still study its effect on physical observables.

The implementation of this idea is straightforward. Since there is no way to know the precise positions of the individual impurities, we have to take into account all possibilities weighted by

a certain normalized probability distribution $\mathcal{P}(\vec{r}_1, \dots, \vec{r}_N)$ [1]

$$\langle \dots \rangle_{dis} = \int \prod_{i=1}^N d^2 \vec{r}_i \dots \mathcal{P}(\vec{r}_1, \dots, \vec{r}_N). \quad (5.1.4)$$

A natural choice for $\mathcal{P}(\vec{r}_1, \dots, \vec{r}_N)$ is to assume, that each impurity is statistically independent of any other impurity and that they are uniformly distributed over the sample volume \mathcal{V} . These assumptions lead to $\mathcal{P}(\vec{r}_1, \dots, \vec{r}_N) = 1/\mathcal{V}^N$. Given a set of impurity potentials $u_i(\vec{r})$ one can then calculate the fundamental disorder correlators. For simplicity we further assume that all impurities are identical, $u_i(\vec{r}) = u(\vec{r})$. In that case we obtain for the first two correlators

$$\langle V(\vec{r}) \rangle_{dis} = \frac{1}{\mathcal{V}} \sum_{\vec{q}} u_{\vec{q}} N \delta_{\vec{q},0} e^{i\vec{q} \cdot \vec{r}} = \frac{N}{\mathcal{V}} u_{\vec{q}=0}, \quad (5.1.5a)$$

$$\begin{aligned} \langle V(\vec{r}) V(\vec{r}') \rangle_{dis} &= \frac{1}{\mathcal{V}^2} \sum_{\vec{q}_1, \vec{q}_2} u_{\vec{q}_1} u_{\vec{q}_2} [N(N-1) \delta_{\vec{q}_1,0} \delta_{\vec{q}_2,0} + N \delta_{\vec{q}_1 + \vec{q}_2,0}] e^{i\vec{q}_1 \cdot \vec{r} + i\vec{q}_2 \cdot \vec{r}'} \\ &= \frac{N(N-1)}{\mathcal{V}^2} u_{\vec{q}=0}^2 + \frac{N}{\mathcal{V}^2} \sum_{\vec{q}} u_{\vec{q}} u_{-\vec{q}} e^{i\vec{q} \cdot (\vec{r} - \vec{r}')}, \end{aligned} \quad (5.1.5b)$$

where $u_{\vec{q}}$ are the Fourier amplitudes of a single impurity potential. We emphasize that the higher moments are nontrivial. Their calculation is straightforward, but the resulting analytical expressions become more and more involved. Furthermore, note that the disorder average with respect to a uniform probability distribution restores translation invariance. In general this is not the case, see also the discussion below. To actually calculate the average of a disorder dependent quantity $Q[V]$ one has to expand its functional dependence on the disorder field in a power series. This step is necessary as it allows us to use the above disorder correlators, otherwise we would have to perform N spatial integrations. It goes without saying that this is not feasible. So, even if we would have been able to calculate $G_c(x, y|V)$ analytically exactly, it would be of no use as it is impossible to perform the subsequent integrations involved in the averaging procedure. Fortunately, the series expansion of $G_c(x, y|V)$ is easy to find. According to Eq. (5.1.2) it can be formally written as $(G_0^{-1} - V)^{-1}$. When expanded in powers of V we find the structure of a geometric series. Subsequently performing the disorder average for each term using the fundamental disorder correlators then yields a complicated series expression for the disorder averaged two-point function. This series cannot be calculated exactly, but each term can be disassembled into its reducible and irreducible parts. This topological classification allows for a definition of the disorder induced self-energy as the sum of all irreducible terms. After rearranging the original series in powers of the self-energy one finds the same structure as in an interacting field theory, almost as if disorder causes the free fermions to interact (cf. Eq. (3.3.19) and the footnote on that page). However, the outline of this approach reveals its fundamental drawback. It is inherently perturbative. The so-defined self-energy is obtained as a perturbation series and the best one can do to obtain nonperturbative approximations is to use resummation techniques. As we have argued in the introduction, such techniques are insufficient for disordered graphene at charge neutrality. Therefore we have to improve upon our strategy to calculate the disorder average.

In a nutshell, performing the disorder average in the way described above is rather impractical and one is constrained to resummation techniques. This raises the question: how can we do better? Is there an alternative way to perform the disorder average, which allows for truly nonperturbative calculations? It turns out there is. Instead of summing over all possible position configurations of individual impurity potentials, we may simply sum over all possible

configurations of the disorder field as a whole. In other words, we define the disorder average to be a functional integral [2–6]

$$\langle \cdots \rangle_{dis} = \int \mathcal{D}V \cdots \mathcal{P}[V], \quad (5.1.6)$$

where, similar to Eq. (5.1.4), each field configuration $V(\vec{r})$ is weighted by a normalized probability distribution $\mathcal{P}[V]$. To further motivate – at least on a heuristic level – why such an averaging prescription should be equally valid, we remind the reader of the different formulations of many-body quantum mechanics. Using the language of second quantization, which is just a clever reformulation of the theory, it is easy to see that the quantum mechanics of many particles is equivalent to a quantum field theory.¹ In the present case the relation between the two different disorder-average prescriptions is analogous. The statistical mechanics of many impurities is equivalent to a statistical field theory.² At first glance it seems we have not gained any advantage over the previous averaging prescription. Performing a functional integral is by no means simpler than performing multiple ordinary integrals, especially if the integrand is a nonpolynomial functional of the disorder field (as it is the case for $G_c(x, y|V)$). Yet, appearances are deceptive. Instead of averaging the two-point correlator and its products one at a time, we can average the generating functional to obtain a new functional that generates disorder averaged correlation functions [2–6].³ Since now the disorder field appears on an equal footing with the fermionic fields, we arrive at a Fermi-Bose field theory, which is much more flexible to analyze and even allows us to employ truly nonperturbative techniques of quantum field theory.

Of particular relevance in this thesis is the Gaussian probability distribution

$$\mathcal{P}[V] = \mathcal{N} \exp \left\{ -\frac{1}{2} \int_{\vec{r}, \vec{r}'} V(\vec{r}) K^{-1}(\vec{r} - \vec{r}') V(\vec{r}') \right\}, \quad (5.1.7)$$

with the correlation profile

$$\langle V(\vec{r}) \rangle_{dis} = 0, \quad \langle V(\vec{r}) V(\vec{r}') \rangle_{dis} = K(\vec{r} - \vec{r}'). \quad (5.1.8)$$

All the odd moments vanish identically and the even moments are expressible as products of $K(\vec{r} - \vec{r}')$, being the only nonvanishing cumulant, see Sec. 3.1. Since the disorder term (5.1.1) is linear in $V(\vec{r})$, the disorder average of the generating functional is reduced to an ordinary Gaussian integral. According to the rules of Gaussian integration, the average will lead to a quartic term in the action that is similar to an interaction term [2–6]. It describes the nontrivial influence of the ensemble average on the electron dynamics, but it should be distinguished from a true interaction process as there is only momentum transfer and no frequency transfer. Another peculiarity of this pseudo-interaction shows up in its perturbative analysis in terms of Feynman

¹From a field theorist’s viewpoint the term “second quantization” is inappropriate, since a classical field is quantized only once. In that viewpoint, which is shared by the author, the single-particle Schrödinger equation is just the equation of motion of a non-quantized, complex number-valued field. Hence, Schrödinger theory is actually just a classical field theory, just like Maxwell’s electrodynamics, but where the field itself has a certain quantum mechanical interpretation. Quantizing the Schrödinger field, that is, elevating the field to be operator-valued, automatically results in a quantum theory of many particles.

²This last statement is not entirely correct. The disorder average (5.1.4) only sums all possible impurity position configurations and keeps the amplitudes of the individual impurity potentials u_i fixed. In contrast, the functional average (5.1.6) covers all static field configurations, which includes the summation over different amplitudes. On the other hand, it is straightforward to generalize Eq. (5.1.4) to contain such a summation.

³In principle we could try the same with the average prescription (5.1.4), but then we would be stuck. Since it is not possible to perform the multiple ordinary integrations, we would have to resort to perturbation theory again to evaluate the averaged functional.

diagrams. The disorder induced self-energy and the vertex functions do not feature closed fermion loops in stark contrast to a generic interacting theory. This is a serious simplification compared to the Fermi-Bose theory for Coulomb interactions we studied in chapter 4. (If the theory would contain both a true interaction and a disorder generated pseudo-interaction, there would of course be fermionic loops. But all those diagrams, where a loop is connected to the remainder of the diagram by disorder lines only would not contribute to a physical amplitude.) Apart from these differences the pseudo-interacting field theory is open to the whole machinery of nonperturbative quantum field theory. In particular, it is possible to derive exact equations for the self-energy and the other vertex functions, which go beyond perturbative resummation techniques. This set of equations together with the simplifications implied by the absence of closed fermion loops will be the key to access disordered graphene at charge neutrality.

Before we move to the next section a few remarks are in order. First, we note that the translation invariance of the two-point correlator $K(\vec{r} - \vec{r}')$ in Eqs. (5.1.7) and (5.1.8) is a particular choice on the statistical properties of the ensemble. As mentioned before, a statistical ensemble does not need to be translation invariant on average in general. It depends on the experimental setup and the preparation of the ensemble of samples whether such a generalized correlation should be considered. Furthermore, we stress that the statistical description of a realistic disorder ensemble requires more than a single cumulant as we have seen above using the microscopic disorder potential (5.1.3) and the average prescription (5.1.4). The Gaussian ensemble we consider in this thesis is only a simplified model, but it is very convenient for practical analytical calculations and it captures the essence of disorder physics. Nonetheless, non-Gaussian ensembles can be described rather easily by considering “interaction terms” in the exponent of Eq. (5.1.7) – polynomials in $V(\vec{r})$ of a degree higher than two. In that case one would lose the ability to integrate the disorder field analytically exactly, but the Fermi-Bose field theory could still be treated by nonperturbative techniques. Lastly, we want to mention the possibility to modify the coupling of the disorder potential to the fermions from a linear to a quadratic coupling. This variation is motivated by cold-atom experiments, where the influence of disorder on the single-particle dynamics can be studied systematically using laser speckles [7–10]. Here, the light field passing through a diffusive plate to create the speckle pattern is considered a random variable – typically assumed to be Gaussian distributed – but it is the intensity of the laser light – the absolute-value square of the light field – that couples to the particle degrees of freedom. As a result, the atoms effectively feel an attractive or repulsive potential that is (unilaterally) exponentially distributed [7, 10]. To approximately describe such a probability distribution with a linear disorder coupling would require a large number of “interaction terms” in the exponent of Eq. (5.1.7). So the quadratic coupling to fermions in disordered condensed matter systems effectively widens the range of probability distributions one can practically study.

5.2 A matrix-valued disorder potential

The way disorder couples to the Dirac fermions in graphene is no different compared to conventional Fermi gases discussed in the previous section. The only peculiarity is that here the fermionic creation and annihilation operators have a spinor structure. Hence, there is a multitude of possible disorder couplings, describing different kinds of scattering processes. Certainly, the most general disorder potential should account for all of them. (In the following discussion we exclude spin-flipping processes for brevity.) By introducing a matrix-valued disorder field

$\hat{V}(x)$ we can express these scattering processes in the concise form [11–15]

$$H_{dis} = \int_x \Psi^\dagger(x) \hat{V}(x) \Psi(x). \quad (5.2.1)$$

Hermiticity of the Hamiltonian implies hermiticity of the disorder matrix. For this reason it may be expanded in terms of Pauli matrices, $\hat{V}(x) = \sum_{\mu,\nu=0}^3 V_{\mu\nu}(x) \tau_\mu \otimes \sigma_\nu$, with sixteen real amplitudes $V_{\mu\nu}(x)$ and τ and σ acting in valley and sublattice space respectively. Although all of these sixteen amplitudes are necessary to describe the possible scattering processes for spin polarized Dirac fermions, not all of them are statistically independent. After disorder averaging, the spatial symmetries (translation, rotation and reflection) of the clean system have to be restored [11, 12], which leads to certain constraints for the allowed probability distribution of the disorder amplitudes. As a result, there are only nine independent correlators

$$\langle V_{\mu\nu}(\vec{r}) \rangle_{dis} = 0, \quad \langle V_{\mu\nu}(\vec{r}) V_{\mu'\nu'}(\vec{r}') \rangle_{dis} = K_{\mu\nu} \delta_{\mu\mu'} \delta_{\nu\nu'} \delta(\vec{r} - \vec{r}'), \quad (5.2.2)$$

with

$$K_{\mu\nu} = \begin{pmatrix} \alpha_0 & \gamma_\perp & \gamma_\perp & \alpha_z \\ \beta_z & \beta_\perp & \beta_\perp & \beta_0 \\ \beta_z & \beta_\perp & \beta_\perp & \beta_0 \\ \gamma_0 & \alpha_\perp & \alpha_\perp & \gamma_z \end{pmatrix}. \quad (5.2.3)$$

Here, we used the notation of Ref. [12] for the individual disorder strengths. The disorder terms associated to the parameters $\alpha_0, \beta_\perp, \beta_z, \gamma_\perp, \gamma_z$ preserve time-reversal symmetry and the disorder terms associated to the parameters $\alpha_\perp, \alpha_z, \beta_\perp, \beta_0, \gamma_0$ break it. For a complete analysis of all the disorder structures and their symmetries we refer to Ref. [12].

Up until this point the matrix-valued disorder structure for Dirac electrons in graphene was mainly motivated by heuristic arguments. In order to properly interpret the physical content of the amplitudes $V_{\mu\nu}(x)$, we have to go back to the tight-binding model to trace their microscopic origin. We emphasize that the following analysis does not claim to be complete. The full treatment of disorder in graphene is beyond the purpose of this section, and the upcoming calculations shall mainly serve as a motivation for the form of Eq. (5.2.1) beyond heuristic arguments. That being said, let us recall the hopping part of the tight-binding Hamiltonian

$$H_{hop} = - \sum_{i,j} t_{\vec{R}_{0i}\vec{R}_{0j}} c_{\vec{R}_{0i}}^\dagger c_{\vec{R}_{0j}}. \quad (5.2.4)$$

We organized the individual terms into a series of successively decreasing hopping amplitudes (nearest-neighbor, next-nearest-neighbor and so on), assuming the hopping to be isotropic and translation invariant. Clearly, the latter assumption would only be justified for a perfect static crystal. As stated before, in a realistic sample there may be imperfections in the lattice structure and impurities. To some extent such deviations from the perfect lattice structure can be incorporated into the model by allowing nonisotropic and nontranslation invariant distortions of the hopping amplitude δt_{ij} . In addition, impurities may lead to finite on-site energies $V_i^{A/B}$, that can be distinct for the two sublattices A and B and may vary from lattice site to lattice site. The Hamilton operator associated to such kinds of distortions assumes the form

$$H_{dis} = - \sum_{\langle i,j \rangle} (\delta t_{ij} a_i^\dagger b_j + \text{h.c.}) - \sum_i (U_i^A a_i^\dagger a_i + U_i^B b_i^\dagger b_i). \quad (5.2.5)$$

We emphasize that this disorder Hamiltonian is not the most general single-particle perturbation one could possibly imagine. There may be distortions of the hopping amplitude/nonlocal

potentials beyond the nearest-neighbor approximation, but for now such a disorder model is sufficient to prove the points we want to make. In Fourier space this Hamiltonian can be written as

$$H_{dis} = - \sum_{\vec{k}_1, \vec{k}_2 \in \text{1.BZ}} \begin{pmatrix} a_{\vec{k}_1}^\dagger & b_{\vec{k}_1}^\dagger \end{pmatrix} \begin{pmatrix} U_{\vec{k}_1 - \vec{k}_2}^A & \delta\gamma_{\vec{k}_1 \vec{k}_2} \\ \delta\gamma_{\vec{k}_2 \vec{k}_1}^* & U_{\vec{k}_1 - \vec{k}_2}^B \end{pmatrix} \begin{pmatrix} a_{\vec{k}_2} \\ b_{\vec{k}_2} \end{pmatrix}, \quad (5.2.6)$$

with

$$U_{\vec{k}}^{A/B} = \frac{1}{N} \sum_{\vec{R}_{A/B}} e^{-i\vec{k} \cdot \vec{R}_{A/B}} U_{\vec{R}_{A/B}}^{A/B}, \quad (5.2.7a)$$

$$\delta\gamma_{\vec{k}_1 \vec{k}_2} = \frac{1}{N} \sum_{\vec{R}_A} e^{-i(\vec{k}_1 - \vec{k}_2) \cdot \vec{R}_A} \left(\delta t_{1, \vec{R}_A} e^{i\vec{k}_2 \cdot \vec{\delta}_1} + \delta t_{2, \vec{R}_A} e^{i\vec{k}_2 \cdot \vec{\delta}_2} + \delta t_{3, \vec{R}_A} e^{i\vec{k}_2 \cdot \vec{\delta}_3} \right). \quad (5.2.7b)$$

Note that random lattice deformations not only modify the hoppings, but also the lattice basis and shift vectors, $\vec{a}_{1/2}$ and $\vec{\delta}_{1/2/3}$. In a complete first principle calculations such contributions should be taken into account, but here we already neglected them, since the main features we want to obtain are already present. In this context recall our discussion of uniaxially strained graphene in Sec. 2.A.

In contrast to the clean case, Eq. (2.2.8), the Fourier space hopping amplitudes explicitly depend on two momenta. When we expand these momenta around the two inequivalent Dirac points of the Brillouin zone, $\vec{k} = \vec{K}_\pm + \delta\vec{k}$, there will be terms that mix the two valleys. The same applies for the amplitudes $U^{A/B}$. Keeping only the momentum components close to the Dirac points we find

$$\begin{aligned} H_{dis} \approx & - \sum_{\delta\vec{k}_1, \delta\vec{k}_2} \begin{pmatrix} a_{\vec{K}_+ + \delta\vec{k}_1}^\dagger & b_{\vec{K}_+ + \delta\vec{k}_1}^\dagger \end{pmatrix} \begin{pmatrix} U_{\delta\vec{k}_1 - \delta\vec{k}_2}^A & \delta\gamma_{\vec{K}_+ + \delta\vec{k}_1, \vec{K}_+ + \delta\vec{k}_2} \\ \delta\gamma_{\vec{K}_+ + \delta\vec{k}_2, \vec{K}_+ + \delta\vec{k}_1}^* & U_{\delta\vec{k}_1 - \delta\vec{k}_2}^B \end{pmatrix} \begin{pmatrix} a_{\vec{K}_+ + \delta\vec{k}_2} \\ b_{\vec{K}_+ + \delta\vec{k}_2} \end{pmatrix} \\ & - \sum_{\delta\vec{k}_1, \delta\vec{k}_2} \begin{pmatrix} a_{\vec{K}_+ + \delta\vec{k}_1}^\dagger & b_{\vec{K}_+ + \delta\vec{k}_1}^\dagger \end{pmatrix} \begin{pmatrix} U_{\vec{K}_+ + \delta\vec{k}_1 - \vec{K}_- - \delta\vec{k}_2}^A & \delta\gamma_{\vec{K}_+ + \delta\vec{k}_1, \vec{K}_- + \delta\vec{k}_2} \\ \delta\gamma_{\vec{K}_- + \delta\vec{k}_2, \vec{K}_+ + \delta\vec{k}_1}^* & U_{\vec{K}_+ + \delta\vec{k}_1 - \vec{K}_- - \delta\vec{k}_2}^B \end{pmatrix} \begin{pmatrix} a_{\vec{K}_- + \delta\vec{k}_2} \\ b_{\vec{K}_- + \delta\vec{k}_2} \end{pmatrix} \\ & - \sum_{\delta\vec{k}_1, \delta\vec{k}_2} \begin{pmatrix} a_{\vec{K}_- + \delta\vec{k}_1}^\dagger & b_{\vec{K}_- + \delta\vec{k}_1}^\dagger \end{pmatrix} \begin{pmatrix} U_{\vec{K}_- + \delta\vec{k}_1 - \vec{K}_+ - \delta\vec{k}_2}^A & \delta\gamma_{\vec{K}_- + \delta\vec{k}_1, \vec{K}_+ + \delta\vec{k}_2} \\ \delta\gamma_{\vec{K}_+ + \delta\vec{k}_2, \vec{K}_- + \delta\vec{k}_1}^* & U_{\vec{K}_- + \delta\vec{k}_1 - \vec{K}_+ - \delta\vec{k}_2}^B \end{pmatrix} \begin{pmatrix} a_{\vec{K}_+ + \delta\vec{k}_2} \\ b_{\vec{K}_+ + \delta\vec{k}_2} \end{pmatrix} \\ & - \sum_{\delta\vec{k}_1, \delta\vec{k}_2} \begin{pmatrix} a_{\vec{K}_- + \delta\vec{k}_1}^\dagger & b_{\vec{K}_- + \delta\vec{k}_1}^\dagger \end{pmatrix} \begin{pmatrix} U_{\delta\vec{k}_1 - \delta\vec{k}_2}^A & \delta\gamma_{\vec{K}_- + \delta\vec{k}_1, \vec{K}_- + \delta\vec{k}_2} \\ \delta\gamma_{\vec{K}_- + \delta\vec{k}_2, \vec{K}_- + \delta\vec{k}_1}^* & U_{\delta\vec{k}_1 - \delta\vec{k}_2}^B \end{pmatrix} \begin{pmatrix} a_{\vec{K}_- + \delta\vec{k}_2} \\ b_{\vec{K}_- + \delta\vec{k}_2} \end{pmatrix}. \end{aligned} \quad (5.2.8)$$

We may now proceed as in Sec. 2.2.2 to obtain the compact form

$$H_{dis} \approx - \sum_{\delta\vec{k}_1, \delta\vec{k}_2} \Psi_{\delta\vec{k}_1}^\dagger \hat{V}_{\delta\vec{k}_1 \delta\vec{k}_2} \Psi_{\delta\vec{k}_2}, \quad (5.2.9a)$$

$$\hat{V}_{\delta\vec{k}_1 \delta\vec{k}_2} \equiv \begin{pmatrix} U_{\delta\vec{k}_1 - \delta\vec{k}_2}^A & \delta\gamma_{\vec{K}_+ + \delta\vec{k}_1, \vec{K}_+ + \delta\vec{k}_2} & \delta\gamma_{\vec{K}_+ + \delta\vec{k}_1, \vec{K}_- + \delta\vec{k}_2} & U_{2\vec{K}_+ + \delta\vec{k}_1 - \delta\vec{k}_2}^A \\ \delta\gamma_{\vec{K}_+ + \delta\vec{k}_2, \vec{K}_+ + \delta\vec{k}_1}^* & U_{\delta\vec{k}_1 - \delta\vec{k}_2}^B & U_{2\vec{K}_+ + \delta\vec{k}_1 - \delta\vec{k}_2}^B & \delta\gamma_{\vec{K}_- + \delta\vec{k}_2, \vec{K}_+ + \delta\vec{k}_1}^* \\ \delta\gamma_{\vec{K}_+ + \delta\vec{k}_2, \vec{K}_- + \delta\vec{k}_1}^* & U_{2\vec{K}_- + \delta\vec{k}_1 - \delta\vec{k}_2}^B & U_{\delta\vec{k}_1 - \delta\vec{k}_2}^B & \delta\gamma_{\vec{K}_- + \delta\vec{k}_1, \vec{K}_- + \delta\vec{k}_2}^* \\ U_{2\vec{K}_- + \delta\vec{k}_1 - \delta\vec{k}_2}^A & \delta\gamma_{\vec{K}_- + \delta\vec{k}_1, \vec{K}_+ + \delta\vec{k}_2} & \delta\gamma_{\vec{K}_- + \delta\vec{k}_1, \vec{K}_- + \delta\vec{k}_2} & U_{\delta\vec{k}_1 - \delta\vec{k}_2}^A \end{pmatrix}. \quad (5.2.9b)$$

5.2. A matrix-valued disorder potential

Here the disorder matrix still depends on two momenta. To obtain a local potential in real space only the difference $\delta\vec{k}_1 - \delta\vec{k}_2$ should appear as an argument. So the next-to-last step is to introduce relative and center-of-mass coordinates and consider a lowest order gradient approximation in the center-of-mass coordinate. Finally, one has to perform the continuum limit as done in Sec. 2.2.2 and Fourier transform to real space, which yields Eq. (5.2.1).

5.3. Paper: *“Graphene pn junction in a quantizing magnetic field: Conductance at intermediate disorder strength”*

5.3 Paper: *“Graphene pn junction in a quantizing magnetic field: Conductance at intermediate disorder strength”*

5.3. Paper: “Graphene pn junction in a quantizing magnetic field: Conductance at intermediate disorder strength”

Graphene pn junction in a quantizing magnetic field: Conductance at intermediate disorder strength

Christian Fräßdorf, Luka Trifunovic, Nils Bogdanoff, and Piet W. Brouwer

Dahlem Center for Complex Quantum Systems and Institut für Theoretische Physik, Freie Universität Berlin, Arnimallee 14, 14195 Berlin, Germany

(Received 26 July 2016; revised manuscript received 2 November 2016; published 28 November 2016)

In a graphene pn junction at high magnetic field, unidirectional “snake states” are formed at the pn interface. In a clean pn junction, each snake state exists in one of the valleys of the graphene band structure, and the conductance of the junction as a whole is determined by microscopic details of the coupling between the snake states at the pn interface and quantum Hall edge states at the sample boundaries [Tworzydło *et al.*, *Phys. Rev. B* **76**, 035411 (2007)]. Disorder mixes and couples the snake states. We here report a calculation of the full conductance distribution in the crossover between the clean limit and the strong-disorder limit, in which the conductance distribution is given by random matrix theory [Abanin and Levitov, *Science* **317**, 641 (2007)]. Our calculation involves an exact solution of the relevant scaling equation for the scattering matrix, and the results are formulated in terms of parameters describing the microscopic disorder potential in bulk graphene.

DOI: [10.1103/PhysRevB.94.195439](https://doi.org/10.1103/PhysRevB.94.195439)

I. INTRODUCTION

Many of the unique electronic properties of graphene, a single layer of carbon atoms as they occur in graphite, can be traced back to its pseudorelativistic band structure, in which quasiparticles behave as massless relativistic Dirac particles, be it with the Fermi velocity v_F instead of the speed of light c [1–3]. Examples of such “relativistic” effects in graphene are Klein tunneling through potential barriers [4–7], the Zitterbewegung in confining potentials [6,8], the anomalous integer quantum Hall effect [9–15], or the breakdown of Landau quantization in crossed electric and magnetic fields [16,17].

The integer quantum Hall effect in graphene is called “anomalous” because the number of chiral edge states at the boundary of a graphene flake in a large perpendicular magnetic field is a multiple of 4 plus 2, whereas the Dirac bands are fourfold degenerate because of the combined spin and valley degeneracies. The presence of a “half” edge mode per valley degree of freedom has a direct explanation once it is taken into account that the valley degeneracy is necessarily lifted at a graphene flake’s outer boundaries [18]. Chiral states need not only occur at a flake’s outer boundaries, but they may also occur in the sample’s interior, separating regions with different electron density. At such an interface valley degeneracy is usually preserved, and the number of chiral interface states is always a multiple of 4.

A particularly interesting realization of such an interface occurs at a pn junction in a perpendicular magnetic field, separating hole-doped (p -type) and electron-doped (n -type) graphene regions [19–21]. The edge states at the pn interface are referred to as “snake states” because, at least in a semiclassical picture, such states propagate alternately at the p and n sides of the junction [22–25], similar to the behavior of the states that propagate along zero-field contours in the quantum Hall insulators in an inhomogeneous magnetic field [26–29]. A graphene pn junction also has edge states at the sample boundaries, which move in opposite directions in the p - and n -type regions (see Fig. 1), and feed into/flow out of the snake states at the pn interface.

The minimal number of chiral edge and interface states is realized for a pn junction with filling fractions 2 and -2 . In this case there are two edge modes, one for each spin direction and four chiral interface modes. The two-terminal conductance G of such a pn junction is determined by the probability T that an electron that enters the common edge at the pn interface from the source reservoir is transmitted to the drain reservoir:

$$G = \frac{2e^2}{h} T. \quad (1)$$

In the limit of a strongly disordered pn interface, Abanin and Levitov predicted that the probability T itself is subject to mesoscopic fluctuations [30], with average $\langle T \rangle = 1/2$ and variance $\text{var } T = 1/12$.¹ In the opposite limit of an ideal graphene sheet, Tworzydło *et al.* found [31]

$$T = \frac{1}{2}(1 - \mathbf{v}_T \cdot \mathbf{v}_B), \quad (2)$$

where the “isospin” vectors \mathbf{v}_T and \mathbf{v}_B describe the precise way in which the valley degeneracy is broken at the sample boundaries (see Fig. 1). Subsequent theoretical work involved a semiclassical analysis [32,33], numerical simulations of the effect of disorder [34,35], and a phenomenological inclusion of dephasing [36]. Several experimental groups have performed measurements of the two-terminal conductance of graphene pn junctions in a large perpendicular magnetic field [19–21,23,37–41]. The measured conductance follows the ensemble average of the strongly disordered limit of Ref. [30], although the experimentally observed mesoscopic fluctuations remain significantly below the theoretical prediction. Measurements of the shot noise power find a value that approaches the theoretical prediction for the shortest interface lengths [42,43].

In this article we present a theory of the transmission probability T for a graphene pn junction with generic disorder.

¹Abanin and Levitov predict $\text{var } T = 1/15$ for $(v_n, v_p) = (2, -2)$ if spin-orbit coupling is strong enough that the spin degeneracy is lifted [30]. The result quoted in the main text is valid in the presence of spin degeneracy.

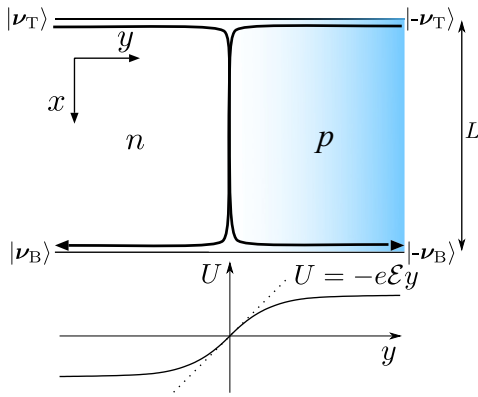


FIG. 1. Schematic experimental setup of a graphene pn junction in a quantizing magnetic field, such that the n region has filling fraction 2 (left) and the p region has filling fraction -2 (right). At the pn interface there is a fourfold degenerate chiral interface state; there are twofold degenerate chiral edge states at the sample's top and bottom edge.

We focus on the case of filling fractions $(\nu_n, \nu_p) = (2, -2)$, for which we give an exact solution for the distribution of the transmission probability T , thus bridging the gap between the clean limit of Ref. [31] and the strong-disorder limit of Ref. [30]. Knowledge of the distribution of T allows us to calculate the average conductance G , its variance, and the Fano factor F throughout the weak-to-strong-disorder crossover. There are two reasons why we focus on the case $(\nu_n, \nu_p) = (2, -2)$ for our exact solution. First, as we show below, two length scales suffice to describe the effect of generic disorder on the edge states, which is an essential simplification that makes our exact solution possible. Second, quantum interference effects are strongest in this case, so that the need for an exact treatment is maximal. Our results for the case $(\nu_n, \nu_p) = (2, -2)$ also apply to higher filling fractions if the mixing of interface states occurs for the lowest Landau level only [41].

The problem we consider here is related to two different problems that have been studied in the literature, and we wish to comment on both. First, the study is reminiscent of that of transport in coupled one-dimensional channels with disorder, a problem that was solved exactly already in the 1950s, in the context of wave propagation through random media [44,45]. A crucial difference between the two problems is, however, that all one-dimensional modes at the pn interface propagate in the same direction, whereas a normal metal wire has equal numbers of modes propagating in both directions. This difference leads to a rather different phenomenology. Whereas transmission is exponentially suppressed for sufficiently strong disorder or long length in the standard case [46], for the chiral interface states at a pn junction the probability that electrons are transmitted along the interface is always 1. The question is whether they are fed into an edge state that transfers them back to the source reservoir, or into the edge that leads to the drain.

The second related problem is that of the parametric dependence of transport properties in mesoscopic samples. Traditionally (and correctly), it is the Hamiltonian that is taken

to depend on an external parameter, such as the magnetic field or a gate voltage, either by modeling the perturbation directly or in a stochastic manner through a ‘‘Brownian motion’’ process. In a second step the transport properties are then calculated from the Hamiltonian. There have been theoretical attempts to make a theory directly for the parameter dependence of the scattering matrix, e.g., through a modification of Dyson’s Brownian motion model, but such an approach could not be made to agree with the Hamiltonian-based approach if the dimension of the scattering matrix is small [47–50]. Interestingly, we find that the dependence of the scattering matrix of the interface states on the interface length is *precisely* described by the Dyson Brownian motion model. To our knowledge, this constitutes the first application of this model to a quantum transport problem.

The article is organized as follows. In Sec. II we outline the microscopic model of a disordered graphene pn junction and derive an effective one-dimensional Hamiltonian for the chiral interface states in the presence of generic disorder. In Sec. III, we then derive and solve the Fokker-Planck equation describing the diffusive transport through the pn junction. Using the probability distribution of the scattering matrix, we obtain an expression for the conductance and its variance, being valid for an arbitrary disorder strengths as long as the mean-free path is much larger compared to the lattice constant and the magnetic length. We conclude in Sec. IV.

II. MICROSCOPIC MODEL

We choose coordinates such that the pn interface is along the x direction (see Fig. 1). At low energies conduction electrons in the graphene pn junction are described by a 4×4 matrix Hamiltonian,

$$\hat{H} = \hat{H}_0 + \hat{V}(\mathbf{r}), \quad (3)$$

in which $\hat{V}(\mathbf{r})$ in Eq. (3) is a matrix-valued potential representing the disorder and

$$\hat{H}_0 = \tau_0 \otimes \sigma_0 U(y) + v_F \tau_3 \otimes [\sigma_1 \pi_1(\mathbf{r}) + \sigma_2 \pi_2(\mathbf{r})]. \quad (4)$$

Here the τ_μ and σ_μ are Pauli matrices acting in valley and sublattice space, respectively, $U(y)$ is a gate potential that defines the p - and n -type regions, and $\pi_1(\mathbf{r})$ and $\pi_2(\mathbf{r})$ are the in-plane components of the kinematic momentum,

$$\begin{aligned} \pi_1(\mathbf{r}) &= -i\hbar\partial_x - eA_x(\mathbf{r}), \\ \pi_2(\mathbf{r}) &= -i\hbar\partial_y - eA_y(\mathbf{r}). \end{aligned} \quad (5)$$

Since spin-orbit coupling is weak in graphene, the spin degree of freedom will be suppressed throughout.

For the vector potential we take the asymmetric gauge

$$A_1(\mathbf{r}) = -\mathcal{B}y, \quad A_2(\mathbf{r}) = 0, \quad (6)$$

with $\mathcal{B} > 0$ the perpendicular magnetic field. The magnetic field defines the length scale $\ell = (e\mathcal{B})^{-1/2}$. The gate potential $U(y)$ is negative for $y < 0$, zero for $y = 0$, and positive for $y > 0$, so that the pn interface is at $y = 0$ precisely (see Fig. 1). In the limit of a large magnetic field, it is sufficient to expand $U(y)$ to linear order in y for $|y| \lesssim \ell$, and we set

$$U(y) = -e\mathcal{E}y. \quad (7)$$

In order to describe graphene with generic disorder, we expand the matrix-valued disorder potential $\hat{V}(\mathbf{r})$ as [51–53]

$$\hat{V}(\mathbf{r}) = \sum_{\mu, \nu=0}^3 V_{\mu\nu}(\mathbf{r}) \tau_{\mu} \otimes \sigma_{\nu}, \quad (8)$$

with real amplitudes $V_{\mu\nu}(\mathbf{r})$. We assume these amplitudes to be Gaussian correlated with vanishing mean and with correlation function

$$\langle V_{\mu\nu}(\mathbf{r}) V_{\mu'\nu'}(\mathbf{r}') \rangle = \Gamma_{\mu\nu} \delta_{\mu\mu'} \delta_{\nu\nu'} \delta(\mathbf{r} - \mathbf{r}'), \quad (9)$$

where the absence of correlations between different amplitudes is a consequence of translation and rotation symmetry on the average [53]. The same symmetry considerations reduce the number of independent correlators to nine,

$$\Gamma_{\mu\nu} = \begin{pmatrix} \alpha_0 & \gamma_{\perp} & \gamma_{\perp} & \alpha_z \\ \beta_z & \beta_{\perp} & \beta_{\perp} & \beta_0 \\ \beta_z & \beta_{\perp} & \beta_{\perp} & \beta_0 \\ \gamma_0 & \alpha_{\perp} & \alpha_{\perp} & \gamma_z \end{pmatrix}, \quad (10)$$

such that the five parameters α_0 , β_{\perp} , β_z , γ_{\perp} , and γ_z represent disorder contributions respecting time-reversal symmetry [51,52], whereas the remaining four parameters α_{\perp} , α_z , β_0 , and γ_0 represent time-reversal symmetry-breaking disorder. The coefficient α_0 represents potential disorder that is smooth on the scale of the lattice spacing; the coefficients β_{\perp} and γ_z appear if the potential disorder is short range, so that it couples to the valley and sublattice degrees of freedom. The other coefficients are associated with a (random) magnetic field, strain, or lattice defects (see Ref. [53]). Since time-reversal symmetry is broken by the large magnetic field \mathcal{B} , we will consider all nine contributions.

With a large magnetic field \mathcal{B} the low-energy degrees of freedom of the Hamiltonian (3) are the two chiral one-dimensional modes at the pn interface (per spin direction). They are described by an effective Hamiltonian,

$$H_s = -i\hbar v_s \tau_0 \partial_x + \sum_{\mu=0}^3 V_{s,\mu}(x) \tau_{\mu}, \quad (11)$$

where v_s is the velocity of the interface modes and the $V_{s,\mu}(x)$ are effective disorder potentials representing the effect of the bulk disorder potential $\hat{V}(\mathbf{r})$ on the interface states. In the limit of a large magnetic field, we can find exact expressions for v_s and for the correlation functions of the disorder potential V_s in terms of the parameters of the underlying a two-dimensional Hamiltonian (3). The linear approximation (7) for the gate potential U allows us to make use of an exact solution for the eigenstates of the Hamiltonian H_0 of Eq. (4) [16,17]. [See Ref. [54] for an approximate solution that does not make use of the linear approximation (7).] Furthermore, for large magnetic fields the Landau-level separation is large enough that only the zeroth Landau level needs to be considered. With the help of the exact solution for the zeroth Landau level, we then find that the velocity of the interface modes is

$$v_s = \mathcal{E}/\mathcal{B}, \quad (12)$$

whereas the disorder potentials $V_{s,\mu}(x)$ have zero mean and correlation functions

$$\langle V_{s,\mu}(x) V_{s,\nu}(x') \rangle = K_{\mu} \delta_{\mu\nu} \delta(x - x'), \quad (13)$$

with, to leading order in $v_s/v_F \ll 1$,

$$K_0(\alpha_0, \alpha_z, \alpha_{\perp}) = \frac{1}{\sqrt{2\pi\ell^2}} (\alpha_0 + \alpha_z), \quad (14a)$$

$$K_{1,2}(\beta_0, \beta_z, \beta_{\perp}) = \frac{1}{\sqrt{2\pi\ell^2}} (\beta_0 + \beta_z), \quad (14b)$$

$$K_3(\gamma_0, \gamma_z, \gamma_{\perp}) = \frac{1}{\sqrt{2\pi\ell^2}} (\gamma_0 + \gamma_z). \quad (14c)$$

The microscopic amplitudes $\alpha_{\perp}, \beta_{\perp}, \gamma_{\perp}$ contribute only at higher orders in v_s/v_F . We refer to Appendix A for details of the calculation.

III. SCALING APPROACH FOR THE SCATTERING MATRIX

Disorder mixes the chiral interface modes. The effect of this disorder-induced mode mixing is described by a 2×2 scattering matrix \hat{S} . In the absence of disorder one has $\hat{S} = e^{ikL} \mathbb{1}$. With disorder \hat{S} acquires a nontrivial probability distribution $P(\hat{S})$, which we now calculate.

We parametrize the scattering matrix using four ‘‘angles,’’

$$\hat{S} = e^{i\psi\tau_0} e^{i\tau_3\varphi/2} e^{i\tau_2\theta/2} e^{i\tau_3\zeta/2}, \quad (15)$$

where $\theta \in [0, \pi]$. We will first derive a differential equation that describes the change of the joint distribution $P(\varphi, \theta, \zeta, \psi; L)$ upon changing the length L of the interface region (see Fig. 1). To this end, we consider the scattering matrix $\hat{S}_{\delta L}$ for an interface segment of length δL much smaller than the mean-free path for disorder scattering. We parametrize $\hat{S}_{\delta L}$ as

$$\hat{S}_{\delta L} = e^{ik\delta L} e^{i\hat{A}}, \quad \hat{A} = \sum_{\mu=0}^3 r_{\mu} \tau_{\mu}. \quad (16)$$

From the effective Hamiltonian (11) we find that the coefficients r_{μ} are statistically independent, with disorder averages $\langle r_{\mu} \rangle = 0$, $\mu = 0, 1, 2, 3$, and with variances

$$\langle r_{\mu}^2 \rangle = \frac{K_{\mu}}{\hbar^2 v_s^2} \delta L, \quad (17)$$

with the coefficients K_{μ} given in Eq. (14). To simplify the expressions in the remainder of this section, we replace the notation with the coefficients K_{μ} in favor of the intervalley scattering length

$$l_i = \frac{\hbar^2 v_s^2}{4K_1}, \quad (18)$$

the (antisymmetric) intravalley scattering length

$$l_a = \frac{\hbar^2 v_s^2}{4K_3}, \quad (19)$$

and the dimensionless coefficients

$$\alpha = K_0/4K_1, \quad \gamma = K_3/K_1 = l_i/l_a, \quad (20)$$

which relate inter- and intravalley scattering rates. In the case of pure potential disorder, only the disorder coefficients α_0 , β_{\perp} , and γ_z are nonzero, so that the constants α , $\gamma \sim (v_F/v_s)^2 \gg 1$. For generic disorder that scatters between the

two sublattices of the hexagonal graphene lattice, one expects that $\alpha, \gamma \sim 1$. The parameters α and γ determine symmetric and antisymmetric intravalley scattering lengths, respectively. Since intravalley scattering that is equal for the two valleys corresponds to multiplication of \hat{S} with an overall phase factor, the coefficient α will not appear in the expressions for the conductance distribution below. Antisymmetric intravalley scattering, however, does affect the transmission probability T of the pn junction.

Since the interface modes are unidirectional, the composition rule for scattering matrices is matrix multiplication. In particular, we obtain the scattering matrix $\hat{S}(L + \delta L)$ of an interface segment of length $L + \delta L$ as

$$\hat{S}(L + \delta L) = \hat{S}(L)\hat{S}_{\delta L}. \quad (21)$$

This composition rule and the known statistical distribution of the scattering matrices $\hat{S}_{\delta L}$ define a ‘‘Brownian motion’’ problem for the scattering matrix $\hat{S}(L)$. An isotropic version of the Brownian motion problem, with $\alpha = \gamma = 1$, was studied previously in the context of quantum transport through chaotic quantum dots [47–50]. Using standard methods (see Appendix B for details), we can derive a Fokker-Planck equation for the joint probability distribution $P(\varphi, \theta, \zeta, \psi; L)$ of the coefficients parametrizing the scattering matrix \hat{S} ,

$$\begin{aligned} l_i \frac{\partial P}{\partial L} = & -kl_i \frac{\partial P}{\partial \psi} + \frac{1}{2} \alpha \frac{\partial^2 P}{\partial \psi^2} + \frac{1}{2} (\gamma + \cot^2 \theta) \frac{\partial^2 P}{\partial \zeta^2} \\ & + \frac{1}{2} \frac{\partial^2 P}{\partial \theta^2} - \frac{1}{2} \cot \theta \frac{\partial P}{\partial \theta} + \frac{1}{2} \csc^2 \theta \frac{\partial^2 P}{\partial \varphi^2} \\ & - \cot \theta \csc \theta \frac{\partial^2 P}{\partial \varphi \partial \zeta} + \frac{1}{2} \csc^2 \theta P. \end{aligned} \quad (22)$$

The Fokker-Planck equation, Eq. (22), for the L dependence of the scattering matrix of two copropagating modes can be solved exactly by adapting Ancliff’s method to solve the corresponding problem for a pair of counterpropagating modes [55]. After separating variables

$$P(L, \varphi, \theta, \zeta, \psi) = e^{-\lambda L/l_i} P(\varphi, \theta, \zeta, \psi), \quad (23)$$

Eq. (22) can be cast in the form of an eigenvalue problem, which, following Ref. [55], can be solved exactly by noticing that its right-hand side can be expressed through the operator \hat{A} defined in Eq. (16), seen as a differential operator acting in the Hilbert space of functions $f(\hat{S})$,

$$\langle \hat{A}^2 \rangle = -(\hat{L}_x^2 + \hat{L}_y^2 + \hat{L}_z^2 + (\gamma - 1)\hat{L}_z^2 + \alpha\hat{L}_0^2), \quad (24)$$

in which the operators \hat{L}_μ are the generators of the Lie algebra $u(2)$. The Lie algebra $u(2)$ has two Casimir operators, \hat{L}_0 and $\hat{L}^2 = \hat{L}_x^2 + \hat{L}_y^2 + \hat{L}_z^2$, that act as scalars K and $l(l + 1)$ (l being integer or half-integer, K being a real number), respectively, within each irreducible representation of $U(2)$. Thus we can conclude immediately that the eigenvalues associated to the eigenvalue problem obtained from Eq. (22) are of the form

$$-\lambda_{Klm} = l(l + 1) + (\gamma - 1)m^2 + \alpha K^2 + 2ikl_i K, \quad (25)$$

where $m = -l, -l + 1, \dots, l$ and we included the drift term for ψ being proportional to kl_i , which is not contained in Eq. (24). The eigenfunctions can be expressed [56] in terms of

Jacobi polynomials $P_n^{(a,b)}$ ($|m| \leq l$)

$$\begin{aligned} P_{Klmn} = & \sqrt{\frac{(l+m)!(l-m)!}{(l+n)!(l-n)!}} e^{iK\psi} e^{im\varphi + in\zeta} \sin \theta \\ & \times \sin^{m-n}(\theta/2) \cos^{m+n}(\theta/2) P_{j-m}^{(m-n, m+n)}(\cos \theta). \end{aligned} \quad (26)$$

For $m = n = 0$ these eigenfunctions match the ones previously obtained by Frahm and Pichard for the isotropic scattering matrix Brownian motion problem [49]. It can be readily checked that the above functions for arbitrary K, l, m , and n are simultaneously eigenfunctions of \hat{L}^2 , \hat{L}_z , and \hat{L}_0 and that they satisfy the eigenvalue equation derived from Eq. (22) with eigenvalues given by Eq. (25).

As the initial condition at $L = 0$ we take $\hat{S}(0) = \mathbb{1}$, which corresponds to

$$P(\varphi, \theta, \zeta, \psi; 0) = \delta(\varphi + \zeta) \delta(\theta) \delta(\psi). \quad (27)$$

With this initial condition the solution for the probability distribution is

$$\begin{aligned} P(\varphi, \theta, \zeta, \psi; L) = & \sqrt{\frac{l_i}{2\pi\alpha L}} e^{-\frac{l_i(\psi - kL)^2}{2\alpha L}} \sum_l \frac{2l + 1}{8\pi^2} \sin \theta \\ & \times \sum_{m=-l}^l e^{-[l(l+1) + (\gamma-1)m^2]L/l_i + im(\varphi + \zeta)} \\ & \times \cos^{2m}(\theta/2) P_{l-m}^{(0, 2m)}(\cos \theta). \end{aligned} \quad (28)$$

The scattering matrix \hat{S} is related to the transmission probability T of a graphene pn junction through the relation [31]

$$T = |\langle \mathbf{v}_T | \hat{t}_T \hat{S} \hat{t}_B | -\mathbf{v}_B \rangle|^2, \quad (29)$$

in which \hat{t}_T (\hat{t}_B) is the scattering matrix describing how the edge modes at the top (bottom) edges of the pn junction feed into/originate from the interface modes and $|\pm \mathbf{v}_T\rangle$ ($|\pm \mathbf{v}_B\rangle$) are valley isospin Bloch vectors for the top (bottom) edges of the n (+) and p -doped (−) regions (see Fig. 1). The isospin vectors $|\mathbf{v}_X\rangle$ are superpositions of the vectors $|1\rangle$ and $|-1\rangle$ representing the two valleys,

$$|\mathbf{v}_X\rangle = \cos \frac{\theta_X}{2} |1\rangle + e^{i\phi_X} \sin \frac{\theta_X}{2} |-1\rangle, \quad (30)$$

$$|-\mathbf{v}_X\rangle = \sin \frac{\theta_X}{2} |1\rangle - e^{i\phi_X} \cos \frac{\theta_X}{2} |-1\rangle,$$

with polar angles θ_X and ϕ_X , $X = T, B$. The scattering matrices \hat{t}_T and \hat{t}_B , in the absence of intervalley scattering,² express isospin conservation at the point where the valley-nondegenerate edge states merge into/evolve out of the valley-degenerate interface state [31],

$$\hat{t}_X = e^{i\tilde{\varphi}_X} |\mathbf{v}_X\rangle \langle \mathbf{v}_X| + e^{i\tilde{\varphi}'_X} |-\mathbf{v}_X\rangle \langle -\mathbf{v}_X|, \quad (31)$$

with $\tilde{\varphi}_X$ and $\tilde{\varphi}'_X$ arbitrary phases that do not need to be specified. Combination of Eqs. (29) and (31) gives [31]

$$T = |\langle \mathbf{v}_T | \hat{S} | -\mathbf{v}_B \rangle|^2. \quad (32)$$

²For a zigzag edge the intravalley scattering is always present.

Using Eq. (15) as well as the fact that the phase difference $\varphi - \zeta$ is uniformly distributed for all L , we find that the disorder average $\langle T \rangle$ is given by

$$\begin{aligned} \langle T \rangle = & \frac{1}{2} [1 - \cos \theta_T \cos \theta_B \langle \cos \theta \rangle \\ & - \sin \theta_T \sin \theta_B \langle \cos \theta \cos(\varphi + \phi_T) \cos(\zeta - \phi_B) \rangle \\ & + \sin \theta_T \sin \theta_B \langle \sin(\varphi + \phi_T) \sin(\zeta - \phi_B) \rangle]. \end{aligned} \quad (33)$$

Using the probability distribution (28) one then finds the remarkably simple result

$$\begin{aligned} \langle T \rangle = & \frac{1}{2} [1 - e^{-2L/l_i} \cos \theta_T \cos \theta_B \\ & - e^{-L/l_i - L/l_a} \sin \theta_T \sin \theta_B \cos(\phi_T - \phi_B)]. \end{aligned} \quad (34)$$

Similarly, we obtain the variance of the transmission probability

$$\begin{aligned} \text{var } T = & \frac{1}{12} - \frac{1}{4} e^{-4L/l_i} \cos^2 \theta_T \cos^2 \theta_B \\ & + \frac{1}{24} e^{-6L/l_i} (3 \cos^2 \theta_T - 1)(3 \cos^2 \theta_B - 1) \\ & - \frac{1}{4} e^{-2L/l_i - 2L/l_a} \cos^2(\phi_T - \phi_B) \sin^2 \theta_T \sin^2 \theta_B \\ & + \frac{1}{8} e^{-2L/l_i - 4L/l_a} \cos 2(\phi_T - \phi_B) \sin^2 \theta_T \sin^2 \theta_B \\ & + \frac{1}{8} e^{-5L/l_i - L/l_a} \cos(\phi_T - \phi_B) \sin(2\theta_T) \sin(2\theta_B) \\ & - \frac{1}{8} e^{-3L/l_i - L/l_a} \cos(\phi_T - \phi_B) \sin(2\theta_T) \sin(2\theta_B). \end{aligned} \quad (35)$$

In the isotropic case, $\gamma = l_i/l_a = 1$, these expressions can be further simplified such that $\langle T \rangle$ and $\text{var } T$ depend on the scalar product $\mathbf{v}_T \cdot \mathbf{v}_B$ of the isospin vectors only:

$$\langle T \rangle = \frac{1}{2} (1 - e^{-2L/l_i} \mathbf{v}_T \cdot \mathbf{v}_B), \quad (36)$$

$$\begin{aligned} \text{var } T = & \frac{1}{12} - \frac{1}{4} e^{-4L/l_i} (\mathbf{v}_T \cdot \mathbf{v}_B)^2 \\ & + \frac{1}{4} e^{-6L/l_i} \left((\mathbf{v}_T \cdot \mathbf{v}_B)^2 - \frac{1}{3} \right). \end{aligned} \quad (37)$$

In the limiting cases $L \ll l_i, l_a$ and $L \gg l_i, l_a$, Eqs. (34) and (35) [or (37)] agree with the known results for the clean and dirty limits, respectively (see Refs. [30] and [31]).

Figure 2 shows the ensemble average $\langle T \rangle$ and the variance $\text{var } T$ for armchair terminations at the top and bottom edges of the pn junction. For armchair termination one has $\mathbf{v}_X \cdot \mathbf{e}_z = 0$, so that $\theta_T = \theta_B = 0$. The difference $\phi_T - \phi_B$ of the azimuthal angles can take the three values π and $\pm\pi/3$, depending on the number of hexagons along the interface length L modulo 3. We observe that the characteristic length scale for armchair nanoribbon termination is l_a .

Additional information on the mixing of interface states can be obtained from a measurement of the Fano factor $F = P/2eI$, the ratio of the shot noise power P , and the

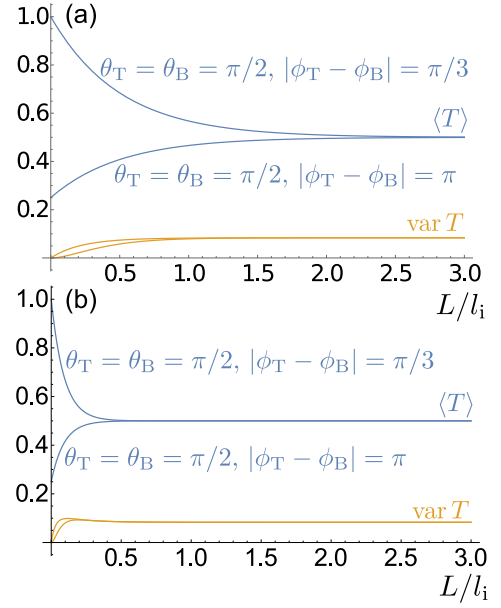


FIG. 2. Mean $\langle T \rangle$ and variance $\text{var } T$ of the transmission T , as a function of the interface length L , for $\gamma = l_i/l_a = 1$ (panel a) and $\gamma = 10$ (panel b); the armchair termination is assumed. The top curve for $\text{var } T$ is for $|\phi_T - \phi_B| = \pi/3$; the bottom variance curve is for $|\phi_T - \phi_B| = \pi$.

current I . For the case we consider here, one has (at zero temperature) [57]

$$F = 1 - T, \quad (38)$$

so that the ensemble average of the Fano factor F directly follows from our expression Eq. (34) for the disorder-averaged transmission probability T . In particular, in the limit of a clean junction ($L \ll l_i, l_a$), one finds $F = (1 + \mathbf{v}_T \cdot \mathbf{v}_B)/2$, whereas in the limit of a dirty junction one has

$$\langle F \rangle = 1/2. \quad (39)$$

A finite temperature leads, first and foremost, to a smearing of the electron energy. Since thermal smearing effectively amounts to taking an ensemble average, thermal smearing has no effect on the ensemble average $\langle T \rangle$ but it strongly suppresses the transmission fluctuations. In the limit of large temperatures ($k_B T$ much larger than the Thouless energy of the interface) the Fano factor becomes [57] $F = \langle T(1 - T) \rangle / \langle T \rangle$, which may be easily evaluated by combining Eqs. (34) and (35). In the limit of a clean junction one then finds the same Fano factor as in the zero temperature limit, whereas in the strong-disorder limit $L \gg l_i, l_a$ the high-temperature limit is

$$\langle F \rangle = 1/3. \quad (40)$$

Note that this value for $\langle F \rangle$, as well as the zero-temperature limit Eq. (39) mentioned above, differs from the Fano factor reported in Ref. [30]. The difference arises because Ref. [30] takes the semiclassical expression for the shot noise power, whereas quantum effects are strong in the limit of low filling fractions we consider here and the semiclassical

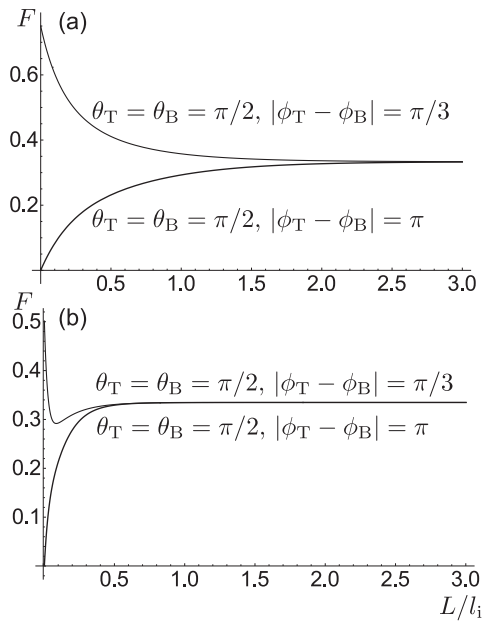


FIG. 3. The Fano factor F versus interface length L in the high-temperature limit for $\gamma = l_i/l_a = 1$ (panel a) and $\gamma = 10$ (panel b) and armchair termination of the top and bottom edges.

approximation is no longer quantitatively correct.

Figure 3 shows the high-temperature limit of the Fano factor F for the armchair edge terminations. For armchair termination we find that the Fano factor dependence can be nonmonotonic (for $\gamma \gg 1$), and the characteristic length scale is l_a . In the isotropic limit $\gamma = l_i/l_a = 1$ there is a monotonic dependence on L [Fig. 3(a)].

IV. CONCLUSION

We calculated the conductance distribution of a graphene pn junction in a quantizing magnetic field. Our theory captures the entire crossover between the limit of a clean pn junction and that of a strongly disordered junction. In the former case, the conductance is a known function of the isospin vectors $|\nu_T\rangle$ and $|\nu_B\rangle$ for the chiral states at the edges of the pn junction [31]. In the latter case the conductance has a probability distribution that is universal and independent of the details of the edges [30]. Our solution for the intermediate regime combines features of both extremes. On the one hand, the conductance has finite sample-to-sample fluctuations, on the other hand, mean and variance of the conductance depend on the isospin vectors $|\nu_T\rangle$ and $|\nu_B\rangle$.

A special feature of our solution is that we are able to relate the mean free paths for transport along the one-dimensional interface to the coefficients describing the random potential in the two-dimensional graphene sheet. Even after translation and rotation invariance are taken into account, generic disorder in graphene is still characterized by five independent constants. Some information on these constants can be obtained from measurements of a two-dimensional graphene sheet. For example, pure potential disorder gives rise to weak antilocalization, whereas disorder terms that couple the valleys cause weak

localization [58–60]. Complementary information can be obtained from the carrier-density dependence of the conductivity [61]. Our theory links the conductance distribution of a pn junction in a large magnetic field to the same set of coefficients and, thus, provides an additional and independent method to determine these.

A central observation of the many conductance experiments [19–21,23,37–41] is that the measured conductance in the case $(\nu_n, \nu_p) = (2, -2)$ consistently agrees with the ensemble average $\langle T \rangle = 1/2$ of the strong-disorder limit [30], but the experiments do not show any signatures of the large mesoscopic fluctuations that are expected in the limit of zero temperature. These experiments are not consistent with the clean-limit predictions, since none of the standard nanoribbon terminations (armchair or zigzag) give a conductance G consistent with $T = 1/2$ [31]. The Fano factors observed in Refs. [43] and [42] are slightly below the theoretical predictions of Eqs. (39) and (40) for the strong-disorder limit (assuming spin degeneracy), but they are not far from it when extrapolating the observation of Ref. [43] to zero interface length. Our theory for the crossover between the clean and strong-disorder limits shows that the approach to the average value $T = 1/2$ and the development of large mesoscopic fluctuations occur at the same length scale l_a for armchair nanoribbon termination, irrespective of the form of the microscopic disorder (see Fig. 2). We note that for nonstandard nanoribbon termination with $|\phi_T - \phi_B| = \pi/2$ it is possible to approach the mean value $T = 1/2$ on length scale l_i while the mesoscopic fluctuations are developed on the length scale l_a . The opposite scenario, which would offer an explanation for the experimental observations, is not possible within our theory. Thus the experimentally observed absence of mesoscopic fluctuations cannot be explained by an incomplete transition to the strong-disorder limit. Other causes of suppressed mesoscopic fluctuations that have been mentioned in the literature are thermal smearing, slow time-dependent fluctuations of system parameters, or inelastic processes contributing to the mixing between the interface states [30]. The observed suppression of shot noise for long interface lengths in Ref. [43] clearly hints at a role of inelastic processes for large interface lengths L , whereas the observation of a finite shot noise power at short junction lengths is consistent with the first two explanations. A quantitative theory of thermal smearing effects requires the extension of the present theory to the energy dependence of the scattering matrix, a considerable theoretical challenge that is left to future work.

ACKNOWLEDGMENTS

This work is supported by the German Research Foundation (DFG) in the framework of the Priority Program SPP 1459 “Graphene.”

APPENDIX A: EFFECTIVE HAMILTONIAN FOR CHIRAL INTERFACE STATES

In this Appendix we derive the effective one-dimensional Hamiltonian H_s for the chiral states at the pn interface [see Eq. (11)]. Hereto we need the explicit form of the

eigenfunctions of the Hamiltonian H_0 for the clean system. These eigenfunctions are known from the exact solution of Refs. [16] and [17]. They have a linear energy-momentum dispersion $\varepsilon_k = v_s k$ with v_s given by Eq. (12), and the δ -function normalized spinor-valued wave functions for the zeroth Landau level read [16,17]

$$|\Psi_{k\kappa}^0(\mathbf{r})\rangle = e^{ikx} \phi_0(y - k\ell^2) |\kappa\rangle \otimes |\xi_\kappa\rangle, \quad (\text{A1})$$

where $\kappa = \pm 1$ is the valley index, $|\kappa\rangle$ are the basis spinors with respect to the valley degree of freedom, and $|\xi_\kappa\rangle$ represents a two-component spinor with respect to the sublattice degree of freedom. Further,

$$\phi_0(y) = \left(\frac{\beta}{\pi\ell^2}\right)^{1/4} e^{-\beta y^2/2\ell^2}, \quad (\text{A2})$$

where we abbreviated

$$\beta = \sqrt{1 - \left(\frac{\mathcal{E}}{v_F \mathcal{B}}\right)^2}. \quad (\text{A3})$$

(Note that the validity of this exact solution requires $|\mathcal{E}| < v_F \mathcal{B}$.) The spinor $|\xi_\kappa\rangle$ reads

$$|\xi_\kappa\rangle \equiv \sqrt{\frac{|\mathcal{E}|}{2v_F \mathcal{B}}} \begin{pmatrix} \text{sgn}(\mathcal{E}) \kappa C^{1/2} \\ C^{-1/2} \end{pmatrix}, \quad (\text{A4})$$

with

$$C = \frac{v_F \mathcal{B}}{|\mathcal{E}|} (1 - \beta). \quad (\text{A5})$$

One verifies that in the limit of a vanishing electric field the solutions Eq. (A1) reduce to the well-known results for graphene in a homogeneous external magnetic field.

As explained in the main text, for large magnetic fields it is sufficient to restrict to the zeroth Landau level. We may obtain an effective Hamiltonian for the interface states by projecting the Hamiltonian H_0 to the states spanned by the wave functions (A1). Using the Fourier representation of Eq. (A1), this projection takes the simple diagonal form

$$H_{s,0} = v_s k \tau_0. \quad (\text{A6})$$

Fourier transformation with respect to k gives the first term of the Hamiltonian H_s of Eq. (11).

To incorporate the disorder potential we need to evaluate the matrix elements

$$\begin{aligned} V_{s,\kappa\kappa'}(k,k') &= \int d\mathbf{r} \langle \Psi_{k\kappa}^0(\mathbf{r}) | \hat{V}(\mathbf{r}) | \Psi_{k'\kappa'}^0(\mathbf{r}) \rangle \\ &= \int d\mathbf{r} e^{-i(k-k')x} \phi_0(y - k\ell^2) \phi_0(y - k'\ell^2) \\ &\quad \times (\langle \kappa | \otimes \langle \xi_\kappa |) \hat{V}(\mathbf{r}) (| \kappa' \rangle \otimes | \xi_{\kappa'} \rangle). \end{aligned} \quad (\text{A7})$$

In the limit of a large magnetic field and for small momenta k, k' , we may neglect the shifts $k\ell^2$ and $k'\ell^2$ in the arguments of the functions ϕ_0 . With this approximation, $V_{s,\kappa\kappa'}(k,k')$ becomes a function of the difference $k - k'$ only, so that it represents an effective disorder potential that is local in space,

$$V_{s,\kappa\kappa'}(x) = \int dy \phi_0(y)^2 (\langle \kappa | \otimes \langle \xi_\kappa |) \hat{V}(x,y) (| \kappa' \rangle \otimes | \xi_{\kappa'} \rangle). \quad (\text{A8})$$

Since the disorder potential $\hat{V}(x,y)$ has a Gaussian distribution with zero mean and with δ -function correlations, the same applies to the effective disorder potential $\hat{V}_s(x)$ for the interface states. The two-point correlation function can be calculated with the help of Eq. (9), and one finds

$$\langle V_{s,\kappa\lambda}(x) V_{s,\kappa'\lambda'}(x') \rangle = K_{\kappa\lambda\kappa'\lambda'} \delta(x - x'), \quad (\text{A9})$$

with

$$\begin{aligned} K_{++++} &= K_{----} \equiv K_0 + K_3, \\ K_{+--+} &= K_{-++-} \equiv K_0 - K_3, \\ K_{+---} &= K_{-+-+} \equiv 2K_1, \end{aligned} \quad (\text{A10})$$

where the coefficients K_μ are

$$\begin{aligned} K_0 &= \frac{1}{4} \sqrt{\frac{\beta}{2\pi\ell^2}} \left(\frac{\mathcal{E}}{v_F \mathcal{B}}\right)^2 [(C + 1/C)^2 \alpha_0 \\ &\quad + (C - 1/C)^2 \alpha_z + 4\alpha_\perp], \end{aligned} \quad (\text{A11a})$$

$$\begin{aligned} K_1 = K_2 &= \frac{1}{4} \sqrt{\frac{\beta}{2\pi\ell^2}} \left(\frac{\mathcal{E}}{v_F \mathcal{B}}\right)^2 [(C + 1/C)^2 \beta_0 \\ &\quad + (C - 1/C)^2 \beta_z + 4\beta_\perp], \end{aligned} \quad (\text{A11b})$$

$$\begin{aligned} K_3 &= \frac{1}{4} \sqrt{\frac{\beta}{2\pi\ell^2}} \left(\frac{\mathcal{E}}{v_F \mathcal{B}}\right)^2 [(C + 1/C)^2 \gamma_0 \\ &\quad + (C - 1/C)^2 \gamma_z + 4\gamma_\perp]. \end{aligned} \quad (\text{A11c})$$

Notice that each of the three coefficients depends on a different set of the disorder coefficients for the two-dimensional disorder potential $\hat{V}(x,y)$. Upon writing

$$\hat{V}_s(x) = \sum_{\mu=0}^3 V_{s,\mu}(x) \tau_\mu, \quad (\text{A12})$$

the correlation function of the form (A9) reproduces that of Eq. (13) of the main text. The expressions for the coefficients K_μ quoted in Eq. (14) of the main text follow from Eq. (A11) upon keeping the leading contribution in $(\mathcal{E}/v_F \mathcal{B})^2$.

APPENDIX B: DERIVATION OF THE FOKKER-PLANCK EQUATION FOR SCATTERING MATRIX

In this Appendix we give the details of the derivation of the Fokker-Planck equation, Eq. (22). We use the parametrization (15) of the scattering matrix in terms of Euler angles, which we combine into a four-component vector $\mathbf{p} = (\varphi, \theta, \zeta, \psi)^T$. The composition rule (21) leads to a Langevin process for the Euler angles \mathbf{p} . We can calculate the change $\delta\mathbf{p}$ from the change

$$\delta\hat{S} = \hat{S}(L + \delta L) - \hat{S}(L) \quad (\text{B1})$$

of the scattering matrix. We keep contributions to $\delta\mathbf{p}$ and $\delta\hat{S}$ up to second order in r_μ and write accordingly

$$\begin{aligned} \delta\mathbf{p} &= \delta\mathbf{p}^{(1)} + \delta\mathbf{p}^{(2)}, \\ \delta\hat{S} &= \delta\hat{S}^{(1)} + \delta\hat{S}^{(2)} + O(r_\mu^3). \end{aligned} \quad (\text{B2})$$

We can then obtain $\delta \mathbf{p}$ from $\delta \hat{S}$ using the relations

$$\delta \hat{S}^{(1)} = \sum_{\mu=0}^3 \frac{\partial \hat{S}}{\partial p_{\mu}} \delta p_{\mu}^{(1)}, \quad (\text{B3})$$

$$\delta \hat{S}^{(2)} = \frac{1}{2} \sum_{\mu, \nu=0}^3 \frac{\partial^2 \hat{S}}{\partial p_{\mu} \partial p_{\nu}} \delta p_{\mu}^{(1)} \delta p_{\nu}^{(1)} + \sum_{\mu=0}^3 \frac{\partial \hat{S}}{\partial p_{\mu}} \delta p_{\mu}^{(2)}. \quad (\text{B4})$$

The solutions of the above equations read

$$\delta \mathbf{p}^{(1)} = \frac{1}{2} \begin{pmatrix} \csc \theta (r_2 \sin \gamma + r_1 \cos \gamma) \\ r_2 \cos \gamma - r_1 \sin \gamma \\ r_3 - \cot \theta (r_2 \sin \gamma + r_1 \cos \gamma) \\ 2r_0 \end{pmatrix}, \quad (\text{B5})$$

$$\delta \mathbf{p}^{(2)} = \frac{1}{8} \begin{pmatrix} -\csc \theta (r_2 \cos \gamma - r_1 \sin \gamma) [2 \cot \theta (r_2 \sin \gamma + r_1 \cos \gamma) - r_3] \\ (r_2 \sin \gamma + r_1 \cos \gamma) (r_1 \cos \gamma \cot \theta + r_2 \sin \gamma \cot \theta - r_3) \\ (r_2 \cos \gamma - r_1 \sin \gamma) \{ [\cos(2\theta) + 3] \csc^2 \theta (r_2 \sin \gamma + r_1 \cos \gamma) - 2r_3 \cot \theta \} / 2 \\ 8k\delta L \end{pmatrix}. \quad (\text{B6})$$

These equations define the Langevin process for the parameters \mathbf{p} . To obtain the corresponding Fokker-Planck equation, we need to calculate the average of $\delta \mathbf{p}^{(2)}$ and the (co)variance of $\delta \mathbf{p}^{(1)}$. With the help of Eq. (17) we obtain

$$\langle \delta \mathbf{p}^{(2)} \rangle = \begin{pmatrix} 0 \\ \frac{1}{2} \cot \theta \\ 0 \\ k \end{pmatrix} \delta L, \quad (\text{B7})$$

$$\langle \delta \mathbf{p}^{(1)} \delta \mathbf{p}^{(1)T} \rangle = \begin{pmatrix} \csc^2 \theta & 0 & -\cot \theta \csc \theta & 0 \\ 0 & 1 & 0 & 0 \\ -\cot \theta \csc \theta & 0 & \csc^2 \theta + \gamma - 1 & 0 \\ 0 & 0 & 0 & \alpha \end{pmatrix} \delta L. \quad (\text{B8})$$

Inserting these correlators into the general form of the Fokker-Planck equation [62],

$$\frac{\partial P}{\partial L} = - \sum_{\mu=0}^3 \partial_{p_{\mu}} \left(\frac{\langle \delta p_{\mu}^{(2)} \rangle}{\delta L} P \right) + \frac{1}{2} \sum_{\mu, \nu=0}^3 \partial_{p_{\mu} p_{\nu}}^2 \left(\frac{\langle \delta p_{\mu}^{(1)} \delta p_{\nu}^{(1)} \rangle}{\delta L} P \right), \quad (\text{B9})$$

we arrive at Eq. (22) of the main text.

-
- [1] A. H. Castro Neto, F. Guinea, N. M. R. Peres, K. S. Novoselov, and A. K. Geim, *Rev. Mod. Phys.* **81**, 109 (2009).
[2] S. Das Sarma, S. Adam, E. H. Hwang, and E. Rossi, *Rev. Mod. Phys.* **83**, 407 (2011).
[3] N. M. R. Peres, *Rev. Mod. Phys.* **82**, 2673 (2010).
[4] O. Klein, *Eur. Phys. J. A* **53**, 157 (1929).
[5] V. V. Cheianov and V. I. Falko, *Phys. Rev. B* **74**, 041403(R) (2006).
[6] M. I. Katsnelson, K. S. Novoselov, and A. K. Geim, *Nat. Phys.* **2**, 620 (2006).
[7] C. W. J. Beenakker, *Rev. Mod. Phys.* **80**, 1337 (2008).
[8] T. M. Rusin and W. Zawadzki, *Phys. Rev. B* **78**, 125419 (2008).
[9] V. P. Gusynin and S. G. Sharapov, *Phys. Rev. Lett.* **95**, 146801 (2005).
[10] K. S. Novoselov, A. K. Geim, S. V. Morozov, D. Jiang, M. I. Katsnelson, I. V. Grigorieva, S. V. Dubonos, and A. A. Firsov, *Nature (London)* **438**, 197 (2005).
[11] Y. Zhang, Y.-W. Tan, H. L. Stormer, and P. Kim, *Nature (London)* **438**, 201 (2005).
[12] K. S. Novoselov, Z. Jiang, Y. Zhang, S. V. Morozov, H. L. Stormer, U. Zeitler, J. C. Maan, and G. S. Boebinger, *Science* **315**, 1379 (2007).
[13] G. Giavaras, P. A. Maksym, and M. Roy, *J. Phys.: Condens. Matter* **21**, 102201 (2009).
[14] H.-Y. Chen, V. Apalkov, and T. Chakraborty, *Phys. Rev. Lett.* **98**, 186803 (2007).
[15] A. Rozhkov, G. Giavaras, Y. P. Bliokh, V. Freilikher, and F. Nori, *Phys. Rep.* **503**, 77 (2011).
[16] V. Lukose, R. Shankar, and G. Baskaran, *Phys. Rev. Lett.* **98**, 116802 (2007).
[17] N. M. R. Peres and E. V. Castro, *J. Phys.: Condens. Matter* **19**, 406231 (2007).
[18] L. Brey and H. A. Fertig, *Phys. Rev. B* **73**, 195408 (2006).

- [19] J. R. Williams, L. DiCarlo, and C. M. Marcus, *Science* **317**, 638 (2007).
- [20] T. Lohmann, K. von Klitzing, and J. H. Smet, *Nano Lett.* **9**, 1973 (2009).
- [21] D.-K. Ki and H.-J. Lee, *Phys. Rev. B* **79**, 195327 (2009).
- [22] L. Oroszlány, P. Rakytá, A. Kormányos, C. J. Lambert, and J. Cserti, *Phys. Rev. B* **77**, 081403 (2008).
- [23] J. R. Williams and C. M. Marcus, *Phys. Rev. Lett.* **107**, 046602 (2011).
- [24] P. Rickhaus, P. Makk, M.-H. Liu, E. Tóvári, M. Weiss, R. Maurand, K. Richter, and C. Schönberger, *Nat. Commun.* **6**, 6470 (2015).
- [25] T. Taychatanapat, J. Y. Tan, Y. Yeo, K. Watanabe, T. Taniguchi, and B. Özyilmaz, *Nat. Commun.* **6**, 6093 (2015).
- [26] J. E. Müller, *Phys. Rev. Lett.* **68**, 385 (1992).
- [27] P. D. Ye, D. Weiss, R. R. Gerhardts, M. Seeger, K. von Klitzing, K. Eberl, and H. Nickel, *Phys. Rev. Lett.* **74**, 3013 (1995).
- [28] J. Reijnders and F. M. Peeters, *J. Phys.: Condens. Matter* **12**, 9771 (2000).
- [29] T. K. Ghosh, A. De Martino, W. Häusler, L. Dell'Anna, and R. Egger, *Phys. Rev. B* **77**, 081404 (2008).
- [30] D. A. Abanin and L. S. Levitov, *Science* **317**, 641 (2007).
- [31] J. Tworzydło, I. Snyman, A. R. Akhmerov, and C. W. J. Beenakker, *Phys. Rev. B* **76**, 035411 (2007).
- [32] P. Carmier, C. Lewenkopf, and D. Ullmo, *Phys. Rev. B* **81**, 241406 (2010).
- [33] P. Carmier, C. Lewenkopf, and D. Ullmo, *Phys. Rev. B* **84**, 195428 (2011).
- [34] J. Li and S.-Q. Shen, *Phys. Rev. B* **78**, 205308 (2008).
- [35] W. Long, Q.-F. Sun, and J. Wang, *Phys. Rev. Lett.* **101**, 166806 (2008).
- [36] J.-C. Chen, H. Zhang, S.-Q. Shen, and Q.-F. Sun, *J. Phys.: Condens. Matter* **23**, 495301 (2011).
- [37] D.-K. Ki, S.-G. Nam, H.-J. Lee, and B. Özyilmaz, *Phys. Rev. B* **81**, 033301 (2010).
- [38] M. Woszczyzna, M. Friedemann, T. Dziomba, T. Weimann, and F. J. Ahlers, *Appl. Phys. Lett.* **99**, 022112 (2011).
- [39] H. Schmidt, J. C. Rode, C. Belke, D. Smirnov, and R. J. Haug, *Phys. Rev. B* **88**, 075418 (2013).
- [40] S. Matsuo, S. Nakaharai, K. Komatsu, K. Tsukagoshi, T. Moriyama, T. Ono, and K. Kobayashi, *Sci. Rep.* **5**, 11723 (2015).
- [41] N. N. Klimov, S. T. Le, J. Yan, P. Agnihotri, E. Comfort, J. U. Lee, D. B. Newell, and C. A. Richter, *Phys. Rev. B* **92**, 241301 (2015).
- [42] S. Matsuo, S. Takeshita, T. Tanaka, S. Nakaharai, K. Tsukagoshi, T. Moriyama, T. Ono, and K. Kobayashi, *Nat. Commun.* **6**, 8066 (2015).
- [43] N. Kumada, F. D. Parmentier, H. Hibino, D. C. Glatli, and P. Roulleau, *Nat. Commun.* **6**, 8068 (2015).
- [44] M. E. Gertsenshtein and V. B. Vasil'ev, *Teor. Veroyatn. Primen.*, 424 (1959) [*Theor. Probab. Appl.* **4**, 391 (1959)].
- [45] M. E. Gertsenshtein and V. B. Vasil'ev, *Teor. Veroyatn. Primen.*, 3(E) (1959) [*Theor. Probab. Appl.* **5**, 340(E) (1960)].
- [46] N. F. Mott and W. D. Twose, *Adv. Phys.* **10**, 107 (1961).
- [47] A. M. S. Macêdo, *Phys. Rev. B* **49**, 16841 (1994).
- [48] A. M. S. Macêdo, *Phys. Rev. B* **53**, 8411 (1996).
- [49] K. Frahm and J.-L. Pichard, *J. Phys. I* **5**, 877 (1995).
- [50] J. Rau, *Phys. Rev. B* **51**, 7734 (1995).
- [51] I. L. Aleiner and K. B. Efetov, *Phys. Rev. Lett.* **97**, 236801 (2006).
- [52] A. Altland, *Phys. Rev. Lett.* **97**, 236802 (2006).
- [53] P. M. Ostrovsky, I. V. Gornyi, and A. D. Mirlin, *Phys. Rev. B* **74**, 235443 (2006).
- [54] Y. Liu, R. P. Tiwari, M. Brada, C. Bruder, F. V. Kusmartsev, and E. J. Mele, *Phys. Rev. B* **92**, 235438 (2015).
- [55] M. Ancliff, *J. Phys. A: Math. Theor.* **49**, 285003 (2016).
- [56] L. D. Landau and E. M. Lifshitz, *Quantum Mechanics: Non-Relativistic Theory* (Butterworth-Heinemann, Oxford, 1991).
- [57] Y. M. Blanter and M. Büttiker, *Phys. Rep.* **336**, 1 (2000).
- [58] E. McCann, K. Kechedzhi, V. I. Fal'ko, H. Suzuura, T. Ando, and B. L. Altshuler, *Phys. Rev. Lett.* **97**, 146805 (2006).
- [59] A. F. Morpurgo and F. Guinea, *Phys. Rev. Lett.* **97**, 196804 (2006).
- [60] F. V. Tikhonenko, A. A. Kozikov, A. K. Savchenko, and R. V. Gorbachev, *Phys. Rev. Lett.* **103**, 226801 (2009).
- [61] P.-L. Zhao, S. Yuan, M. I. Katsnelson, and H. De Raedt, *Phys. Rev. B* **92**, 045437 (2015).
- [62] N. G. van Kampen, *Stochastic Processes in Physics and Chemistry* (North-Holland, Amsterdam, 2007).

5.3. Paper: “Graphene pn junction in a quantizing magnetic field: Conductance at intermediate disorder strength”

5.A Appendix: Manuscript: “*Strong disorder in nodal semimetals: Schwinger-Dyson–Ward approach*”

Strong disorder in nodal semimetals: Schwinger-Dyson–Ward approach

Björn Sbierski and Christian Fräßdorf

*Dahlem Center for Complex Quantum Systems and Institut für Theoretische Physik,
Freie Universität Berlin, D-14195, Berlin, Germany*

(Dated: October 31, 2018)

Abstract

The self-consistent Born approximation quantitatively fails to capture disorder effects in semimetals. We present an alternative, simple-to-use non-perturbative approach to calculate the disorder induced self-energy. It requires a sufficient broadening of the quasiparticle pole and the solution of a differential equation on the imaginary frequency axis. We demonstrate the performance of our method for various paradigmatic semimetal Hamiltonians and compare our results to exact numerical reference data. For intermediate and strong disorder, our approach yields quantitatively correct momentum resolved results. It is thus complementary to existing RG treatments of weak disorder in semimetals.

Introduction.—Semimetals with point-like Fermi surface are by now an established research field in condensed matter physics. Well-studied examples are two-dimensional (2d) Dirac fermions in graphene [1], 3d Weyl fermions in spin-orbit coupled compounds [2], or parabolic band touching points in Bernal-stacked bilayer graphene [3]. Many experimental properties of semimetals rely on the presence of impurities or disorder, ubiquitous in solid state realizations, but under control in cold atom setups via speckle potentials [4]. For example, in undoped graphene the non-zero density-of-states is purely disorder generated [5]. Likewise, in ARPES experiments it is the disorder, which broadens the spectral function at the nodal point and modifies its dispersion away from it. Another example is a disorder driven phase transition between a semimetallic and a metallic phase in 3d Weyl fermions [6]. In the following, motivated by the observables described above, we focus on single-particle properties.

Theoretically, however, the currently available analytical methods for disordered semimetals yield unsatisfactory results. Weak disorder in semimetals can be treated using the perturbative Wilsonian momentum shell renormalization group (RG) as pioneered in the context of 2d Dirac systems by Ref. [7]. The starting point of this approach is the functional integral formalism that can be disorder averaged after the fermions have been replicated. The bosonic disorder field is then eliminated in favor of a four-fermion pseudo-interaction whose coupling constant flows as high energy shells are integrated out perturbatively. The drawback of the perturbative RG method is its inapplicability in the strong disorder regime and the difficulty to extract quantitative information about observables from the abstract RG flow. Another standard approach to disorder is the non-perturbative self-consistent Born approximation (SCBA). For metals, its validity relies on the smallness of the parameter $1/k_F l$ that quantifies the suppression of diagrams with crossed disorder lines omitted in SCBA [8]. Here, k_F is the Fermi momentum and l the mean free path. However, for semimetals with $k_F = 0$, the SCBA cannot be justified [9, 10].

In this work, we propose a novel non-perturbative

approach to disorder, systematically going beyond the SCBA but free of its above restrictions. Our approach is applicable for strong and intermediate Gaussian disorder where it yields a quantitatively accurate and momentum dependent self-energy. For semimetals, it is thus complementary to the RG approach. We start from the Fermi-Bose field theory mentioned above, but we do not integrate out the disorder field. Instead we derive an exact Schwinger-Dyson equation [11, 12] for the fermionic self-energy, which is closed by replacing the Fermi-Bose three-vertex with the help of a Ward-identity. This replacement is justified for strong disorder only. We arrive at a set of ordinary differential equations on the imaginary frequency axis that can be easily solved numerically. We apply this Schwinger-Dyson–Ward (SDW) approach for various paradigmatic semimetals and compare our results to exact numerical reference data computed with a dedicated momentum space version of the kernel polynomial method. We also compare our results to the SCBA and a semi-classical approximation for strong disorder.

Model and main result.—We consider a generic two-band semimetal Hamiltonian $H_0(\vec{k})$ with a degeneracy point at $\vec{k} = 0$ located at zero energy, $H_0(\vec{k} = 0) = 0$. For simplicity, we assume an isotropic dispersion $\pm E_0(k)$ with particle-hole symmetry. These assumptions are not crucial in the following but valid for many popular choices of $H_0(\vec{k})$ like Dirac nodes.

We add a smoothly correlated disorder potential $V(\vec{r})$ which is assumed to be diagonal in band space. Its correlation length ξ represents the disorder puddle’s typical linear extent. We define the fundamental energy scale $E_\xi = E_0(k = 1/\xi)$. For the statistical properties of V , we assert a Gaussian probability distribution $P[V]$ and define the disorder average of a quantity $Q[V]$ as $\langle Q \rangle_{dis} = \int \mathcal{D}V Q[V] P[V]$. We assume the disorder correlator $\mathcal{K}(\vec{r} - \vec{r}')$ to have a Gaussian shape

$$\mathcal{K}(\vec{r} - \vec{r}') = \langle V(\vec{r})V(\vec{r}') \rangle_{dis} = \frac{W^2 E_\xi^2}{(2\pi)^{d/2}} e^{-\frac{1}{2}|\vec{r} - \vec{r}'|^2/\xi^2}. \quad (1)$$

The dimensionless parameter W quantifies the strength of disorder. It relates the typical potential in a puddle $\sim \sqrt{\langle V(\vec{r})^2 \rangle_{dis}}$ to the kinetic energy of a particle confined to the puddle’s volume. We refer to $W \ll 1$ as

weak and $W \gg 1$ as strong disorder, respectively. We are interested in the zero-temperature retarded Green function $G_V^R(\omega) = (\omega + i\eta - H_0 - V)^{-1}$ and, in particular, in its disorder average $\langle G_V^R \rangle_{dis} \equiv G^R$,

$$G^R(\omega, \vec{k}) = \frac{1}{\omega + i\eta - H_0(\vec{k}) - \Sigma^R(\vec{k}, \omega)}, \quad (2)$$

at the nodal point energy $\omega = 0$. This defines the disorder induced self-energy $\Sigma^R(\vec{k}, \omega)$. Our main result is a self-consistency equation for the self-energy on the imaginary frequency axis,

$$\Sigma_{\sigma_1\sigma_2}(i\omega, \vec{k}) = \sum_{\vec{q}} \int_{\vec{q}} \mathcal{K}(\vec{q}) \left[\delta_{\sigma_1\sigma} - \partial_{i\omega} \Sigma_{\sigma_1\sigma}(i\omega, \vec{k}) \right] G_{\sigma\sigma_2}(i\omega, \vec{k} + \vec{q}), \quad (3)$$

from which one may calculate $\Sigma^R(\omega=0, \vec{k})$. The structure of Eq. (3) is reminiscent of the SCBA with $\partial_{i\omega}\Sigma$ as a correction term. The derivation of Eq. (3), which relies on Schwinger-Dyson equations, a Ward-identity and an approximation that is valid for a sufficient broadening of the quasiparticle pole, will be sketched after treating a few examples. We refer to Eq. (3) as the Schwinger-Dyson–Ward approximation (SDWA).

To solve Eq. (3), we parameterize the momentum dependence of $\Sigma(i\omega, \vec{k})$ using the symmetries of the clean Hamiltonian H_0 , which are restored after the disorder average. We isolate the derivative term and discretize the momentum dependence, which yields a system of first order ordinary differential equations (ODE) in ω [28]. For the boundary condition, $\lim_{\omega \rightarrow \infty} G(i\omega) = \frac{1}{i\omega}$ [13] implies an at most sublinear asymptotic of $\Sigma(i\omega)$ in $i\omega$. Hence, at $\omega = \omega_{max} \gg E_\xi$, we can approximately neglect $\partial_{i\omega}\Sigma(i\omega)$ in Eq. (3). The resulting self-consistent solution for $\Sigma(i\omega_{max})$ can be found algebraically in the limit $\omega_{max} \gg E_\xi$. We finally apply standard routines to solve the array-valued ODE numerically. We have checked that the results for $\Sigma(i\omega = i\eta)$ do not depend on (large enough) ω_{max} .

Exact numerical results from KPM.—To gauge the quality of the SDW approximation, we employ the kernel polynomial method (KPM) [14] to obtain numerically exact reference data for $\Sigma_{\sigma_1\sigma_2}^R(\omega, \vec{k})$. The standard iteration procedure of KPM repeatedly applies the Hamiltonian as $(H_0 + V)|\psi\rangle$. In contrast to recent state-of-the-art studies for disordered Weyl nodes [15], we work in momentum space $|\psi\rangle = \sum_{\vec{k}\sigma} \psi_{\vec{k}\sigma} |\vec{k}\sigma\rangle$, thus avoiding to regularize H_0 on a lattice. While H_0 is diagonal in \vec{k} , the potential V is diagonal in real space. We employ a fast Fourier transform (FFT) on $\psi_{\vec{k}\sigma}$ to get to real space, apply V and transform back to momentum space. We use an equidistant k -space grid with spacing $\Delta k \ll \xi^{-1}$ and a UV-cutoff $\Lambda \gg \xi^{-1}$. We checked the convergence of our final results with respect to the number of moments, disorder realizations and lattice points. The limitation of

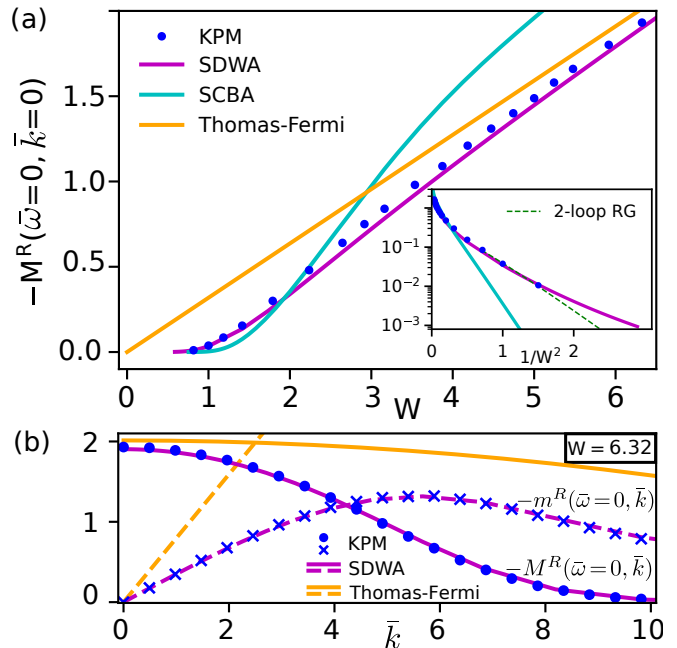


Figure 1: (a) Imaginary part of the disorder induced retarded self-energy for a 2d Dirac node at the nodal point as a function of disorder strength W . Our SDWA result (magenta line) compares well to the exact KPM data (blue dots) and asymptotically agrees with the Thomas-Fermi approximation (orange). The SCBA result is shown in cyan. Inset: For very small disorder, the SDWA deviates from the scaling found by RG (green dashed line). (b) The momentum dependence of the self-energy at $W = 6.32$ calculated from KPM (blue symbols), the SDWA (magenta lines) and Thomas-Fermi approximation (orange lines).

the KPM is in the weak disorder regime, when the finite-size energy starts to compete with the disorder induced energy scale.

Application to 2d Dirac node.—We now apply the SDWA to the case of a disordered 2d Dirac node, $H_0(\vec{k}) = \hbar v(\sigma_x k_x + \sigma_y k_y)$, with $E_0(k) = \hbar v k$ and the fundamental energy scale $E_\xi = \hbar v/\xi$. Using dimensionless variables $\vec{k} = \vec{k}/\xi$ and $\bar{\omega} = \omega/E_\xi$, the ansatz for the self-energy reads

$$\Sigma(i\bar{\omega}, \vec{k})/E_\xi = m(\bar{\omega}, \vec{k})[\sigma_x \cos \bar{\phi} + \sigma_y \sin \bar{\phi}] + iM(\bar{\omega}, \vec{k}), \quad (4)$$

where we switched to polar coordinates for \vec{k} on the right hand side. While m represents a renormalization of H_0 , M can be interpreted as a scattering rate. Using this ansatz in Eq. (3), we obtain two coupled ODEs:

$$\partial_{\bar{\omega}} M(\bar{\omega}, \vec{k}) = 1 + \frac{J_0(\bar{\omega}, \vec{k})M(\bar{\omega}, \vec{k}) + J_1(\bar{\omega}, \vec{k})m(\bar{\omega}, \vec{k})}{W^2[J_0^2(\bar{\omega}, \vec{k}) + J_1^2(\bar{\omega}, \vec{k})]}, \quad (5)$$

$$\partial_{\bar{\omega}} m(\bar{\omega}, \vec{k}) = \frac{J_0(\bar{\omega}, \vec{k})m(\bar{\omega}, \vec{k}) - J_1(\bar{\omega}, \vec{k})M(\bar{\omega}, \vec{k})}{W^2[J_0^2(\bar{\omega}, \vec{k}) + J_1^2(\bar{\omega}, \vec{k})]}, \quad (6)$$

where the functions J_0 and J_1 themselves depend on m

and M as

$$\begin{cases} J_0(\bar{\omega}, \bar{k}) \\ J_1(\bar{\omega}, \bar{k}) \end{cases} = \int_0^\infty d\bar{q} \begin{cases} \tilde{M}(\bar{\omega}, \bar{q}) I_0(\bar{k}\bar{q}) \\ \tilde{m}(\bar{\omega}, \bar{q}) I_1(\bar{k}\bar{q}) \end{cases} \frac{\bar{q} e^{-(\bar{q}^2 + \bar{k}^2)/2} / (2\pi)}{\tilde{m}^2(\bar{\omega}, \bar{q}) + \tilde{M}^2(\bar{\omega}, \bar{q})}. \quad (7)$$

Here, I_j are modified Bessel functions of the first kind [16], $\tilde{m}(\bar{\omega}, \bar{k}) = \bar{k} + m(\bar{\omega}, \bar{k})$ and $\tilde{M}(\bar{\omega}, \bar{k}) = \bar{\omega} - M(\bar{\omega}, \bar{k})$. The initial conditions for $\bar{\omega}_{max} \gg 1$ read $M(\bar{\omega}_{max}, \bar{k}) = -\frac{W^2}{2\pi\bar{\omega}_{max}}$ and $m(\bar{\omega}_{max}, \bar{k}) = 0$.

The set of ODEs (5) and (6) can be solved numerically after discretizing the \bar{k} -dependence of m and M on a geometric grid. In Fig. 1(a) we compare the resulting disorder induced self-energy at the pole of the clean Green function, $M^R(\bar{\omega} = 0, \bar{k} = 0) = M(i\bar{\omega} = i\eta, \bar{k} = 0)$ (magenta line) to the exact KPM data (blue dots), finding good agreement. This is true even for the smallest disorder strength $W \simeq 0.8$ that we can reach with KPM, see inset. Based on the above comment about the validity of SDWA, we consider this agreement for $M^R(\bar{\omega} = 0, \bar{k} = 0) \ll 1$ as coincidental. In fact the SDW solution for $M^R(\bar{\omega} = 0, \bar{k} = 0)$ does not agree asymptotically with the form $\sim \exp(-\pi/W^2)/W$, that is inferred from the scale where the 2-loop Wilsonian RG-flow crosses over to strong disorder [17] (green dashed line in the inset). In the supplemental material we show additional KPM data confirming the validity of the RG result for weak disorder, albeit using a modified uncorrelated disorder model, where even smaller M^R can be resolved.

In Fig. 1(a), we also illustrate the failure of the SCBA for all disorder strengths [9, 10] (cyan line). The data is obtained from an iterative numerical solution of the SCBA-equation, i.e. Eq. (3) without the derivative.

The momentum dependence of the self-energy at $W = 6.32$ is addressed in Fig. 1(b). Again, the SDW results (dashed and solid magenta lines) compare well with exact KPM data (blue symbols). Note that $m^R(\bar{\omega} = 0, \bar{k}) \propto -\bar{k}$ encodes a velocity suppression.

In the limit of large disorder, $W \gg 1$, the typical electron wavelength (at zero total energy) is on the order of ξ/W , thus the electron motion in the disorder potential varying on the scale ξ can be approximated as semi-classical [18–20]. This motivates the Thomas-Fermi approximation, $G^R(\omega, \vec{k}) = \int_{-\infty}^{\infty} dU P_1(U) [\omega + i\eta - H_0(\vec{k}) - U]^{-1}$ where $P_1(U) = \exp\left(-\frac{U^2}{2\mathcal{K}(\vec{r}=0)}\right) / \sqrt{2\pi\mathcal{K}(\vec{r}=0)}$ is the distribution function of the disorder potential at a single point (see supplement for details). At the nodal point, the Thomas-Fermi estimate [4, 21] $M^R(\bar{\omega} = 0, \bar{k} = 0)E_\xi = -\frac{1}{\pi P_1(0)}$ agrees with the KPM and SDWA asymptotically [orange line in Fig. 1(a)]. Consequently, this result can also be reproduced analytically from Eq. (3) after setting $H_0 \rightarrow 0$. However, for finite momentum, the Thomas-Fermi approximation fails even for strong disorder, see Fig. 1(b).

Other dispersions.—To show the flexibility of the SDWA, we now modify the clean Hamiltonian H_0 , modeling other types of nodal semimetals. First, we consider

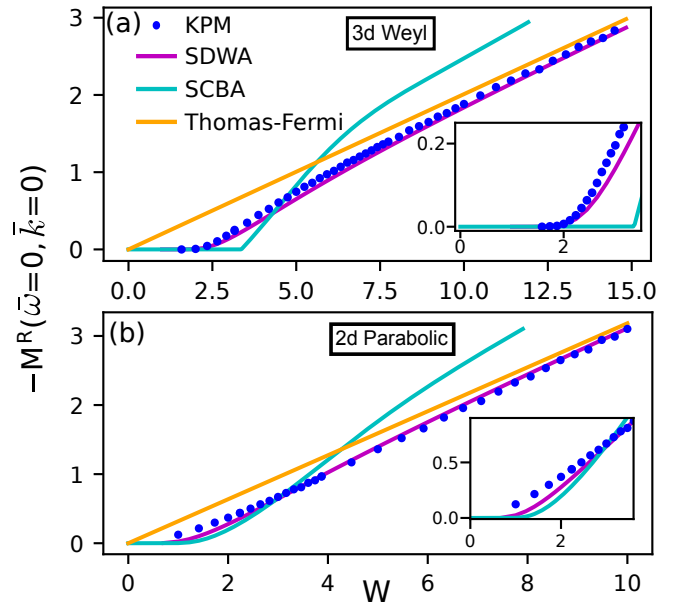


Figure 2: The same as in Fig. 1(a) but for (a) a 3d Weyl and (b) a 2d parabolic semimetal. The SDW results (magenta) compare well to the exact KPM data (blue) except for small $|M^R(\bar{\omega} = 0, \bar{k} = 0)|$, see insets.

the case of a 3d Weyl node, $H_0(\vec{k}) = \hbar v(\sigma_x k_x + \sigma_y k_y + \sigma_z k_z)$, with E_0 and E_ξ as before. The Weyl node features a disorder induced phase transition [6, 22], for W below a critical disorder strength W_c , the self-energy vanishes at $k = 0$. The ansatz for the self-energy and the resulting modifications to the ODEs (5) and (6) are detailed in the supplement. Fig. 2(a) compares the SDW results for $M^R(\bar{\omega} = 0, \bar{k} = 0)$ to KPM, SCBA and the Thomas-Fermi approximation. Again, while the SCBA fails quantitatively, our SDWA is in good agreement with the exact KPM data, except for small $|M^R(\bar{\omega} = 0, \bar{k} = 0)|$ (see inset). The Thomas-Fermi approximation clearly misses the phase transition but is valid asymptotically and we note Ref. [20] suggesting its systematic improvement for the 3d Weyl case, albeit for a different disorder model.

Second, we consider a 2d semimetal $H_0(\vec{k}) = \frac{\hbar^2 k^2}{m} [\sigma_x \cos(2\phi) + \sigma_y \sin(2\phi)]$ in polar coordinates. A similar Hamiltonian (with discrete rotation symmetry) occurs for Bernal-stacked bilayer graphene [3]. The dispersion is parabolic, $E_0(k) = \hbar^2 k^2/m$ and we have $E_\xi = \hbar^2 \xi^{-2}/m$ as the fundamental energy unit. The SDWA (see supplement for details) yields good agreement to the KPM data, see Fig. 2(b), except in the small $|M^R(\bar{\omega} = 0, \bar{k} = 0)|$ regime below $W \simeq 2$.

Derivation of main result.—In the following, we sketch the main ideas behind Eq. (3). For a detailed derivation we refer to the supplemental material. Let $\ln \mathcal{Z}_V[\bar{\eta}, \eta]$ be the generating functional for connected Green functions for a fixed disorder configuration V . The replica trick asserts that we can obtain the disorder averaged Green functions from the generating functional

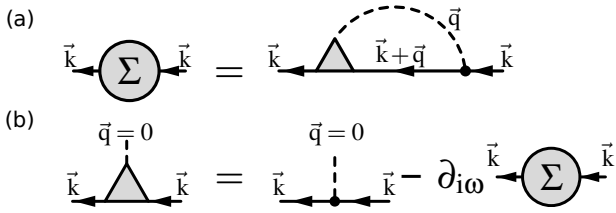


Figure 3: (a) Schwinger-Dyson equation for the fermionic self-energy Σ and (b) the Ward-identity for the Fermi-Bose vertex (triangle). Together, they form the basis of the proposed SDWA. We suppress frequency and pseudo-spin indices.

$\mathcal{Z}_R[\bar{\eta}, \eta] = \langle \mathcal{Z}_V^R[\bar{\eta}, \eta] \rangle_{dis}$ as $G_{12} = \lim_{R \rightarrow 0} \frac{1}{R} \frac{\delta^2 \mathcal{Z}_R[\bar{\eta}, \eta]}{\delta \bar{\eta}_1 \delta \eta_2} \Big|_{\eta, \bar{\eta}=0}$, where $\mathcal{Z}_V^R[\bar{\eta}, \eta]$ contains R replicated fermion species ψ^α , $\alpha = 1, 2, \dots, R$, all coupling to the same disorder potential V and the same source $\bar{\eta}$ (analogous for $\bar{\psi}^\alpha$ and η). We can now formally consider $\mathcal{Z}_R[\bar{\eta}, \eta] \rightarrow \mathcal{Z}_R[\bar{\eta}^\alpha, \eta^\alpha, J]$ such that each fermion species couples to separate sources η^α and $\bar{\eta}^\alpha$ and introduce a source J for the bosonic field V . Now, the Green function from Eq. (2) can be obtained as

$$G_{12} = \lim_{R \rightarrow 0} \frac{1}{R} \sum_{\alpha=1}^R G_{12}^{\alpha\alpha}, \quad G_{12}^{\alpha\alpha} = \frac{\delta^2 \mathcal{Z}_R[\bar{\eta}^\alpha, \eta^\alpha, J]}{\delta \bar{\eta}_1^\alpha \delta \eta_2^\alpha} \Big|_{\bar{\eta}, \eta, J=0}, \quad (8)$$

and likewise for the self-energy Σ_{12} , which is obtained as the second functional derivative of the generating functional of irreducible vertex functions [12].

Next, we consider the Schwinger-Dyson equation for the self-energy, shown diagrammatically in Fig. 3(a). In the diagram, we already anticipate the replica limit that eliminates diagrammatic contributions with internal fermion loops [23]. In this way a Hartree-like diagram, still present for $\Sigma^{\alpha\alpha}$, vanishes. Likewise, the bosonic self-energy, which contains internal fermion bubbles, is eliminated in the replica limit, such that the boson propagator $\mathcal{K}(\vec{q})$ is undressed (dashed line). Since $\mathcal{K}(\vec{q})$ is related to elastic scattering, no frequency is carried. The fermionic propagator in the loop on the right hand side does involve the fermionic self-energy from the left hand side. Finally, the triangle represents the Fermi-Bose vertex that, besides its bare part, subsumes the effect of all higher order diagrams with crossed impurity lines missing in the SCBA. In Fig. 3(b) we depict a Ward-identity for our theory \mathcal{Z}_R . It relates the Fermi-Bose vertex to the Matsubara frequency derivative of the fermionic self-energy. This relation follows from the invariance of the generating functional $\mathcal{Z}_R[\bar{\eta}^\alpha, \eta^\alpha, J]$ under a temporal gauge transformation $\psi_\sigma^\alpha(\tau, \vec{r}) = e^{+iA_\alpha(\tau)} \psi_\sigma'^\alpha(\tau, \vec{r})$ and $\bar{\psi}_\sigma^\alpha(\tau, \vec{r}) = e^{-iA_\alpha(\tau)} \bar{\psi}_\sigma'^\alpha(\tau, \vec{r})$. At an intermediate stage of the derivation, a bosonic Schwinger-Dyson equation (not shown) is used.

The idea is to eliminate the Fermi-Bose vertex in the Schwinger-Dyson equation (a) using the Ward-identity

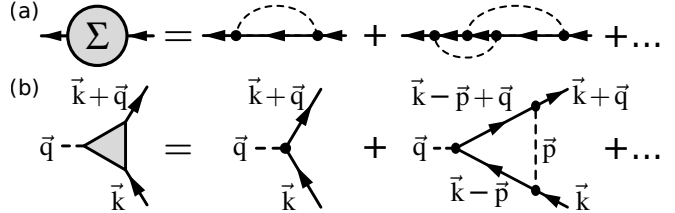


Figure 4: (a) Self-consistent perturbation theory for the disorder problem. The corresponding expansion of the Fermi-Bose vertex is shown in (b). Up to second order, it is used to argue for the validity of the $\vec{q} = 0$ approximation in the limit of strong disorder. All internal fermion lines are self-energy dressed propagators.

(b). Crucially, the Ward-identity requires vanishing bosonic momentum $\vec{q} = 0$. Thus, in order to use (b) in (a), we need to approximate the Fermi-Bose vertex with its value at $\vec{q} = 0$. Note that we keep \vec{q} everywhere else in the diagram. This yields Eq. (3).

To motivate the above approximation, note that in the diagram of Fig. 3(a), we can restrict $|\vec{q}| = q \lesssim 1/\xi$ due to the finite range of the bosonic propagator $\mathcal{K}(\vec{q}) \sim e^{-q^2 \xi^2/2}$. We argue for the validity of the approximation on the basis of the standard self-consistent expansion of the disorder self-energy [8], see Fig. 4(a). Comparing to the Schwinger-Dyson Eq. 3(a), we obtain the expansion of the Fermi-Bose vertex in Fig. 4(b). Alternatively, the expansion in Fig. 4(b) can be obtained from a Schwinger-Dyson equation for the Fermi-Bose vertex if the four-fermion vertex is treated perturbatively. The bare contribution is a constant and trivially \vec{q} -independent. The next contribution is a diagram with an internal boson line. The value of the internal (dressed) fermion propagators is dominant and nearly constant for momenta with magnitude $\lesssim 1/\gamma$, where γ is the length-scale associated to disorder broadening of the pole; a finite Matsubara frequency $\omega > 0$ only increases γ . Our approximation is valid in the regime $\gamma \lesssim \xi$, which means that the fermionic propagator with momentum $\vec{k} - \vec{p} + \vec{q}$ does not change once \vec{q} is set to zero. It is plausible that this argument holds for all higher order diagrams although we cannot give a general proof. A priori, the relation between disorder strength W and γ is not clear, but the condition $\gamma \lesssim \xi$ can be checked from the result of the SDW approach a posteriori. Note however, that keeping the full momentum dependence of $G(\vec{k} + \vec{q})$ in the diagram of Fig. 3(a) is essential, setting $\vec{q} = 0$ yields considerably worse results. *Conclusion.*—We presented a non-perturbative approach to calculate disorder averaged quasi-particle properties beyond SCBA. The SDWA for the self-energy requires a sufficient broadening of the quasiparticle pole to control the approximation involved. Systematic improvement is possible using a higher level truncation of the Schwinger-Dyson equations. This extended set may then be closed by Ward-identities. This should also allow

for the calculation of conductivities. In contrast to the numerically expensive KPM, the analytical formulation of the SDW makes this method amenable for integration in other, possibly interacting, theories. For future work, one could try to apply the SDWA to other types of disorder with non-trivial Pauli matrix structure [9, 24] or relax the particle-hole symmetry and isotropy assumption on the dispersion to study disordered tilted or anisotropic cones [25, 26]. The SDWA could also be useful for semimetals with a co-dimension of their Fermi-surface smaller than d , for example nodal-line semimetals in 3d [27].

Acknowledgments.—We thank Jörg Behrmann, Piet Brouwer, Christoph Karrasch, Georg Schwiete and Sergey Syzranov for useful discussions. Numerical computations were done on the HPC cluster of Fachbereich Physik at FU Berlin. Financial support was granted by the Deutsche Forschungsgemeinschaft through the Emmy Noether-program (KA 3360/2-1) and the CRC/Transregio 183 (Projects A02 and A03).

-
- [1] K. S. Novoselov, A. K. Geim, S. V. Morozov, D. Jiang, M. I. Katsnelson, I. V. Grigorieva, S. V. Dubonos, and A. A. Firsov, *Nature* **438**, 197 (2005).
- [2] B. A. Bernevig, *Nat. Phys.* **11**, 698 (2015).
- [3] E. McCann and M. Koshino, *Rep. Prog. Phys.* **76** (2013).
- [4] V. V. Volchkov, M. Pasek, V. Denechaud, M. Mukhtar, A. Aspect, D. Delande, and V. Josse, *Phys. Rev. Lett.* **120**, 60404 (2018).
- [5] S. Das Sarma, S. Adam, E. H. Hwang, and E. Rossi, *Rev. Mod. Phys.* **83**, 407 (2011).
- [6] S. V. Syzranov and L. Radzihovsky, *Ann. Rev. Cond. Mat. Phys.* **9**, 35 (2018).
- [7] A. W. W. Ludwig, M. P. A. Fisher, R. Shankar, and G. Grinstein, *Phys. Rev. B* **50**, 7526 (1994).
- [8] H. Bruus and K. Flensberg, *Many-Body Quantum Theory in Condensed Matter Physics* (Oxford Graduate Texts, 2004).
- [9] P. M. Ostrovsky, I. V. Gornyi, and A. D. Mirlin, *Phys. Rev. B* **74**, 235443 (2006).
- [10] I. L. Aleiner and K. B. Efetov, *Phys. Rev. Lett.* **97**, 236801 (2006).
- [11] M. E. Peskin and D. V. Schröder, *An introduction to quantum field theory* (Westview, 1995).
- [12] P. Kopietz, L. Bartosch, and F. Schütz, *Introduction to the Functional Renormalization Group* (Springer, 2010).
- [13] J. W. Negele and H. Orland, *Quantum Many-Particle Systems* (Westview, 1988).
- [14] A. Weisse, G. Wellein, A. Alvermann, and H. Fehske, *Rev. Mod. Phys.* **78**, 275 (2006).
- [15] J. H. Pixley, Y.-Z. Chou, P. Goswami, D. A. Huse, R. Nandkishore, L. Radzihovsky, and S. D. Sarma, *Phys. Rev. B* **95**, 235101 (2017).
- [16] I. Gradshteyn and I. Ryzhik, *Table of Integrals, Series, and Products*, 7th ed. (Academic Press, 2007).
- [17] A. Schuessler, P. Ostrovsky, I. Gornyi, and A. Mirlin, *Phys. Rev. B* **79**, 075405 (2009).
- [18] B. I. Shklovskii and A. L. Efros, *Electronic Properties of Doped Semiconductors* (Springer-Verlag, New-York, 1984).
- [19] B. Skinner, *Phys. Rev. B* **90**, 060202 (2014).
- [20] D. A. Pesin, E. G. Mishchenko, and A. Levchenko, *Phys. Rev. B* **92**, 174202 (2015).
- [21] M. I. Trappe, D. Delande, and C. A. Müller, *J. Phys. A: Math. Gen.* **48**, 245102 (2015).
- [22] E. Fradkin, *Phys. Rev. B* **33**, 3263 (1986).
- [23] A. Altland and B. Simons, *Condensed Matter Field Theory*, 2nd ed. (Cambridge University Press, 2006).
- [24] B. Sbierski, K. S. C. Decker, and P. W. Brouwer, *Phys. Rev. B* **94**, 22 (2016).
- [25] M. Trescher, B. Sbierski, P. W. Brouwer, and E. J. Bergholtz, *Phys. Rev. B* **91**, 115135 (2015).
- [26] M. Trescher, B. Sbierski, P. W. Brouwer, and E. J. Bergholtz, *Phys. Rev. B* **95**, 45139 (2017).
- [27] A. A. Burkov, M. D. Hook, and L. Balents, *Phys. Rev. B* **84**, 235126 (2011).
- [28] The resulting equation has a similar mathematical structure as a self-energy flow equation in a functional RG approach.

Supplemental material

for “Strong disorder in nodal semimetals: Schwinger-Dyson–Ward approach”

Weak disorder in 2d Dirac node

We now consider weak disorder in a 2d Dirac node. In Fig. 5 we prove by comparison to exact KPM data (blue dots) that the scaling $M^R(\bar{\omega} = 0, \vec{k} = 0) \sim W^{-1} \exp(-\pi/W^2)$ inferred from the 2-loop momentum shell RG flow equation [17] is correct (green dashed line). This result is obtained from the scale where the RG-flow crosses over to strong disorder. To the best of our knowledge, this scaling has never been checked numerically. Note that the RG uses a white-noise disorder correlator which cannot be implemented numerically and is responsible for the \sim sign above. To obtain converged values of small M^R over two orders of magnitude, we chose a discrete disorder model where the “correlation length” ξ equals the real-space lattice constant a , such that the disorder correlator $\xi = a$ is not smooth on the lattice scale. Thus, the SDWA formulated for the field-theory limit $\xi \gg a$ is not directly applicable. The potential at each site of the real-space lattice is uniformly distributed, $V(\vec{r}) \in [-\sqrt{3}W, \sqrt{3}W]$. This yields $\sum_{\vec{r}} \langle V(\vec{r})V(\vec{0}) \rangle_{dis} = \frac{1}{2\sqrt{3}W} \int_{-\sqrt{3}W}^{+\sqrt{3}W} dU U^2 = W^2$. We use $P = 2^{12}$ lattice points in both linear directions, such that $a = \frac{2\pi}{P\Delta k}$ and 60000 moments for convergence of the KPM. We checked that the disorder induced energy scale $M^R(\bar{\omega} = 0, \vec{k} = 0)\hbar v/a$ is always larger than the finite-size energy scale $E_{fs} = \hbar v\Delta k$.

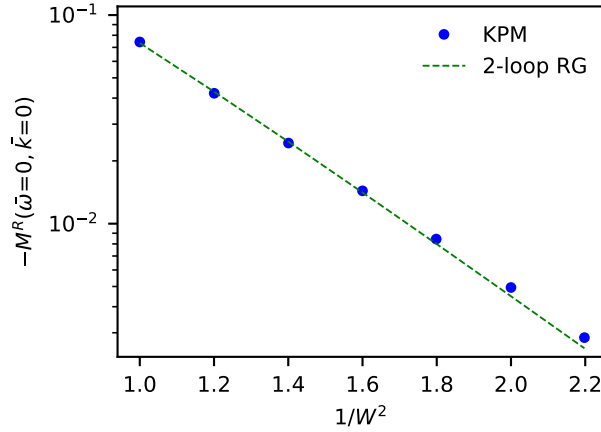


Figure 5: Imaginary part of the disorder induced retarded self-energy for a 2d Dirac node with discrete disorder as a function of disorder strength W . The exact KPM data is shown as blue dots, the RG prediction $M^R \sim W^{-1} \exp(-\pi/W^2)$ with an appropriate prefactor fitted is shown as a green dashed line.

Thomas-Fermi approximation for strong disorder

The Thomas-Fermi approximation [18, 20] amounts to approximate the disorder potential as a homogeneous effective chemical potential term. Then, the disorder averaged Green function is approximated as

$$G^R(\omega, \vec{k}) = \int_{-\infty}^{\infty} dU P_1(U) \frac{1}{\omega + i\eta - H_0(\vec{k}) - U}, \quad (9)$$

where $P_1(U)$ is the one-point distribution function, i.e. the probability that the local potential $V(\vec{r}_1)$ has the value U . This probability can be obtained as the expectation value $P_1(U) = \langle \delta(V(\vec{r}_1) - U) \rangle_{dis}$ which can be calculated by representing the δ -function as an integral over an exponential and subsequently employing the rules for functional integration over V . The result is

$$P_1(U) = \left\langle \frac{1}{2\pi} \int_{-\infty}^{+\infty} dx e^{i(V(\vec{r}_1) - U)x} \right\rangle_{dis} = \frac{1}{2\pi} \int_{-\infty}^{+\infty} dx e^{-\frac{1}{2}x^2 \langle V^2(\vec{r}_1) \rangle_{dis} - iUx} = \frac{1}{\sqrt{2\pi\mathcal{K}(\vec{0})}} e^{-\frac{U^2}{2\mathcal{K}(\vec{0})}}, \quad (10)$$

where $\mathcal{K}(\vec{0}) = \langle V^2(\vec{r}_1) \rangle_{dis} = (2\pi)^{-d/2} W^2 E_\xi^2$.

We evaluate Eq. (9) for the 2d Dirac case in the helicity basis at $\omega = 0$ and find

$$G_{\lambda,\lambda'}^R(\bar{\omega} = 0, \bar{k}) E_\xi = -\delta_{\lambda,\lambda'} \frac{\pi}{W} \left(\operatorname{erfi} \left(\frac{\lambda \bar{k}}{\sqrt{\pi W}} \right) + i \right) e^{-(\bar{k})^2/(\pi W^2)}. \quad (11)$$

Here, $\operatorname{erfi}(z)$ is the imaginary error function defined as $\operatorname{erfi}(z) = \operatorname{erf}(iz)/i$ [16]. With the ansatz

$$G_{\lambda,\lambda'}^R(\bar{\omega} = 0, \bar{k}) E_\xi = \frac{\delta_{\lambda,\lambda'}}{-\lambda [\bar{k} + m^R(\bar{\omega} = 0, \bar{k})] - i M^R(\bar{\omega} = 0, \bar{k})}, \quad (12)$$

we obtain

$$M^R(\bar{\omega} = 0, \bar{k}) = -\frac{W}{\pi} \frac{e^{\bar{k}^2/(\pi W^2)}}{\operatorname{erfi}^2 \left(\frac{\bar{k}}{\sqrt{\pi W}} \right) + 1} = -\frac{W}{\pi} + \frac{(4 - \pi) \bar{k}^2}{W \pi^3} + \mathcal{O}(\bar{k}^3), \quad (13)$$

$$m^R(\bar{\omega} = 0, \bar{k}) = -\bar{k} + \frac{W}{\pi} \frac{e^{\bar{k}^2/(\pi W^2)} \operatorname{erfi} \left(\frac{\bar{k}}{\sqrt{\pi W}} \right)}{\operatorname{erfi}^2 \left(\frac{\bar{k}}{\sqrt{\pi W}} \right) + 1} = -\underbrace{(1 - 2/\pi^2)}_{\simeq 0.8} \bar{k} + \mathcal{O}(\bar{k}^2). \quad (14)$$

Details on the SDWA for 3d Weyl and parabolic 2d semimetal

For the 3d Weyl node with $H_0(\vec{k}) = \hbar v(\sigma_x k_x + \sigma_y k_y + \sigma_z k_z)$ we consider the self-energy ansatz

$$\Sigma(\vec{k}, i\omega)/E_\xi = m(\bar{\omega}, \bar{k}) [\sin \bar{\theta} (\sigma_x \cos \bar{\phi} + \sigma_y \sin \bar{\phi}) + \sigma_z \cos \bar{\theta}] + i M(\bar{\omega}, \bar{k}). \quad (15)$$

Upon insertion into Eq. (3) we find that Eqs. (5) and (6) remain valid, but with the replacements $\{J_0, J_1\} \rightarrow \{J_0^w, J_1^w\}$ where

$$\left\{ \begin{array}{l} J_0^w(\bar{\omega}, \bar{k}) \\ J_1^w(\bar{\omega}, \bar{k}) \end{array} \right\} = \int_0^\infty d\bar{q} \left\{ \begin{array}{l} \bar{k}\bar{q} \sinh(\bar{k}\bar{q}) \tilde{M}(\bar{\omega}, \bar{q}) \\ [\bar{k}\bar{q} \cosh(\bar{k}\bar{q}) - \sinh(\bar{k}\bar{q})] \tilde{m}(\bar{\omega}, \bar{q}) \end{array} \right\} \frac{e^{-(\bar{q}^2 + \bar{k}^2)/2}/(2\pi^2 \bar{k}^2)}{\tilde{m}^2(\bar{\omega}, \bar{q}) + \tilde{M}^2(\bar{\omega}, \bar{q})}. \quad (16)$$

In addition, the initial conditions are modified to $M(\bar{\omega}_{max}, \bar{k}) = -W^2(2\pi)^{-3/2}/\bar{\omega}_{max}$ and $m(\bar{\omega}_{max}, \bar{k}) = 0$.

For the 2d parabolic semimetal, described by the clean Hamiltonian $H_0(\vec{k}) = \frac{\hbar^2 k^2}{m} [\sigma_x \cos(2\phi) + \sigma_y \sin(2\phi)]$ we use the self-energy ansatz

$$\Sigma(\vec{k}, i\omega)/E_\xi = m(\bar{\omega}, \bar{k}) [\sigma_x \cos(2\bar{\phi}) + \sigma_y \sin(2\bar{\phi})] + i M(\bar{\omega}, \bar{k}). \quad (17)$$

We arrive at Eqs. (5) and (6) with the redefinition $\tilde{m}(\bar{\omega}, \bar{k}) = \bar{k}^2 + m(\bar{\omega}, \bar{k})$ and the replacements $\{J_0, J_1\} \rightarrow \{J_0^p, J_1^p\}$, where

$$\left\{ \begin{array}{l} J_0^p(\bar{\omega}, \bar{k}) \\ J_1^p(\bar{\omega}, \bar{k}) \end{array} \right\} = \int_0^\infty d\bar{q} \left\{ \begin{array}{l} \tilde{M}(\bar{\omega}, \bar{q}) I_0(\bar{k}\bar{q}) \\ \tilde{m}(\bar{\omega}, \bar{q}) I_2(\bar{k}\bar{q}) \end{array} \right\} \frac{\bar{q} e^{-(\bar{q}^2 + \bar{k}^2)/2}/(2\pi)}{\tilde{m}^2(\bar{\omega}, \bar{q}) + \tilde{M}^2(\bar{\omega}, \bar{q})}. \quad (18)$$

The initial conditions are the same as in the 2d Dirac case, $M(\bar{\omega}_{max}, \bar{k}) = -\frac{W^2}{2\pi\bar{\omega}_{max}}$ and $m(\bar{\omega}_{max}, \bar{k}) = 0$.

Detailed derivation of the Schwinger-Dyson-Ward approximation

Within the following derivation, we mostly stick to the conventions and definitions of Ref. [12].

A. Preliminaries

For a given disorder realization $V(\vec{r})$, the generating functional for fermionic imaginary-time Green functions is given by

$$\mathcal{Z}_V[\bar{\eta}, \eta] = \int \mathcal{D}\bar{\psi} \mathcal{D}\psi e^{-S_V[\bar{\psi}, \psi] + (\bar{\eta}, \psi) + (\bar{\psi}, \eta)}, \quad (19)$$

where $S_V[\bar{\psi}, \psi]$ is the Euclidean action of the system in the presence of the disorder field V

$$S_V[\bar{\psi}, \psi] = S_0[\bar{\psi}, \psi] + \sum_{\sigma} \int_{\vec{r}, \tau} \bar{\psi}_{\sigma}(\vec{r}, \tau) V(\vec{r}) \psi_{\sigma}(\vec{r}, \tau). \quad (20)$$

The index σ plays the role of a pseudo-spin, which is necessary to describe a two band model. Its clean part, $S_0[\bar{\psi}, \psi]$, derives from the Hamiltonian $H_0(\vec{k} = -i\hbar\vec{\nabla})$ as follows [13, 23]

$$S_0[\bar{\psi}, \psi] = \sum_{\sigma\sigma'} \int_{\vec{r}, \tau} \bar{\psi}_{\sigma}(\vec{r}, \tau) \left[\partial_{\tau} + H_0(-i\hbar\vec{\nabla}) \right]_{\sigma\sigma'} \psi_{\sigma'}(\vec{r}, \tau). \quad (21)$$

For the source terms, involving the Grassmann-valued fields η and $\bar{\eta}$, we used the compact scalar product notation $(\bar{\psi}, \eta) \equiv \sum_{\sigma} \int_{\vec{r}, \tau} \bar{\psi}_{\sigma}(\vec{r}, \tau) \eta_{\sigma}(\vec{r}, \tau)$. The n -point Green functions at a fixed disorder field configuration can then be obtained as an n -fold functional derivative of \mathcal{Z}_V with respect to the sources. For the two-point Green function, for example, we have

$$G_{V, \sigma\sigma'}(\vec{r}, \tau; \vec{r}', \tau') = - \langle \psi_{\sigma}(\vec{r}, \tau) \bar{\psi}_{\sigma'}(\vec{r}', \tau') \rangle = \frac{1}{\mathcal{Z}_V[0, 0]} \frac{\delta^2 \mathcal{Z}_V[\bar{\eta}, \eta]}{\delta \bar{\eta}_{\sigma}(\vec{r}, \tau) \delta \eta_{\sigma'}(\vec{r}', \tau')} \Big|_{\eta = \bar{\eta} = 0}. \quad (22)$$

Note the appearance of the V -dependent normalization $\mathcal{Z}_V[0, 0]$. The connected n -point Green functions at fixed disorder configuration are defined as the n -fold derivative of the connected functional $\mathcal{G}_V[\bar{\eta}, \eta] = \ln \mathcal{Z}_V[\bar{\eta}, \eta]$, just as usual. Since our theory is non-interacting, the only non-vanishing connected correlator is the two-point function (22). Since we are not interested in one particular disorder realization, but in a statistical ensemble of disorder potentials, we have to perform an ensemble average. To this end, one has to specify the statistical properties of the ensemble, which are summarized in a probability distribution $P[V]$. Here, we choose the Gaussian probability distribution

$$P[V] = \mathcal{N} \exp\left(-\frac{1}{2} \int_{\vec{r}, \vec{r}'} V(\vec{r}) \mathcal{K}^{-1}(\vec{r} - \vec{r}') V(\vec{r}')\right), \quad (23)$$

where $\mathcal{K}^{-1}(\vec{r} - \vec{r}')$ is the distributional inverse of the fundamental disorder correlator $\langle V(\vec{r}) V(\vec{r}') \rangle_{dis} = \mathcal{K}(\vec{r} - \vec{r}')$, and \mathcal{N} is a normalization constant. The disorder average of a general quantity $Q[V]$ is then defined as $\langle Q \rangle_{dis} = \int \mathcal{D}V Q[V] P[V]$. To obtain disorder averaged correlation functions one would have to either average each n -point function individually, or average the normalized generating functional (19), that is $\langle \mathcal{Z}_V[\bar{\eta}, \eta] / \mathcal{Z}_V[0, 0] \rangle_{dis}$, which would serve as the generating functional of disorder averaged Green functions. However, due to the V -dependent normalization $\mathcal{Z}_V[0, 0]$ in the denominator, it is not possible to naively perform the disorder average.

To circumvent this problem and get rid of the denominator there are three possibilities [23]: (1) work in real time using the Keldysh technique; (2) rewrite the denominator as a bosonic Gaussian integral, a technique known as supersymmetry method; or (3) ‘‘replicate the system’’ and perform an analytical continuation to zero replicas at the end. Here, we choose the latter option. The trick is to rewrite the connected functional $\mathcal{G}_V[\bar{\eta}, \eta]$ as follows

$$\mathcal{G}_V[\bar{\eta}, \eta] = \ln \mathcal{Z}_V[\bar{\eta}, \eta] = \lim_{R \rightarrow 0} \frac{1}{R} \left(e^{R \ln \mathcal{Z}_V[\bar{\eta}, \eta]} - 1 \right) = \lim_{R \rightarrow 0} \frac{1}{R} \left(\mathcal{Z}_V^R[\bar{\eta}, \eta] - 1 \right), \quad (24)$$

which allows us to perform the disorder average. The disorder averaged replicated partition function then reads

$$\begin{aligned} \mathcal{Z}_R[\bar{\eta}, \eta] &\equiv \langle \mathcal{Z}_V^R[\bar{\eta}, \eta] \rangle_{dis} \\ &= \int \mathcal{D}\bar{\psi}^{\alpha} \mathcal{D}\psi^{\alpha} \mathcal{D}V \exp\left(-S_R[\bar{\psi}^{\alpha}, \psi^{\alpha}, V] + \sum_{\alpha=1}^R (\bar{\eta}, \psi^{\alpha}) + \sum_{\alpha=1}^R (\bar{\psi}^{\alpha}, \eta)\right), \end{aligned} \quad (25)$$

with the replicated action $S_R[\bar{\psi}^{\alpha}, \psi^{\alpha}, V] \equiv \sum_{\alpha=1}^R S_V[\bar{\psi}^{\alpha}, \psi^{\alpha}] + \frac{1}{2} \int_{\vec{r}, \vec{r}'} V(\vec{r}) \mathcal{K}^{-1}(\vec{r} - \vec{r}') V(\vec{r}')$. Note that there is only a single source for all replicas and only a single disorder potential coupling identically to the replica bilinears

in $S_V[\bar{\psi}^\alpha, \psi^\alpha]$. In the standard treatment one would integrate out the disorder field to obtain a quartic pseudo-interaction term for the fermions [23], but here we take another path. Instead of performing the bosonic Gaussian integral, we consider a generalization of Eq. (25), where a bosonic source J coupling to V is introduced and where the fermionic sources now carry a replica index as well

$$\mathcal{Z}_R[\bar{\eta}, \eta] \rightarrow \mathcal{Z}_R[\bar{\eta}^\alpha, \eta^\alpha, J] = \int \mathcal{D}\bar{\psi}^\alpha \mathcal{D}\psi^\alpha \mathcal{D}V \exp \left(-S_R[\bar{\psi}^\alpha, \psi^\alpha, V] + \sum_{\alpha=1}^R (\bar{\eta}^\alpha, \psi^\alpha) + \sum_{\alpha=1}^R (\bar{\psi}^\alpha, \eta^\alpha) + (J, V) \right). \quad (26)$$

Introducing the super-field vector $\Phi = (\psi^\alpha, \bar{\psi}^\alpha, V)$, the super-source vector $\mathbf{J} = (\bar{\eta}^\alpha, -\eta^\alpha, J)$, and the scalar product $(\mathbf{J}, \Phi) = \sum_{\alpha=1}^R (\bar{\eta}^\alpha, \psi^\alpha) + \sum_{\alpha=1}^R (\bar{\psi}^\alpha, \eta^\alpha) + (J, V)$, we can write this new functional in the compact form $\mathcal{Z}_R[\mathbf{J}] \equiv \int \mathcal{D}\Phi \exp(-S_R[\Phi] + (\mathbf{J}, \Phi))$. Putting everything together we find the disorder averaged connected Green function

$$\langle G_{V,12} \rangle_{dis} = \left\langle \frac{\delta^2 \ln \mathcal{Z}_V[\bar{\eta}, \eta]}{\delta \bar{\eta}_1 \delta \eta_2} \Big|_{\bar{\eta}=\eta=0} \right\rangle_{dis} \stackrel{(24)-(26)}{=} \lim_{R \rightarrow 0} \frac{1}{R} \sum_{\alpha=1}^R \frac{\delta^2 \mathcal{Z}_R[\mathbf{J}]}{\delta \bar{\eta}_1^\alpha \delta \eta_2^\alpha} \Big|_{\mathbf{J}=0} \equiv \lim_{R \rightarrow 0} \frac{1}{R} \sum_{\alpha=1}^R G_{12}^{\alpha\alpha}. \quad (27)$$

Here, the numerical indices 1 and 2 are a compact notation, which include space, imaginary-time and pseudo-spin indices. In the following we consider a finite number of replicas R – the replica limit will only be taken at the end of the calculation – and compute $G_{12}^{\alpha\alpha} = \frac{\delta^2 \mathcal{Z}_R[\mathbf{J}]}{\delta \bar{\eta}_1^\alpha \delta \eta_2^\alpha} \Big|_{\mathbf{J}=0} = -\langle \psi_1^\alpha \bar{\psi}_2^\alpha \rangle_{S_R}$. The subscript at the average is just a reminder that it has to be performed with respect to the replicated action S_R in Eq. (26).

B. Schwinger-Dyson equations

As is well-known, in classical field theory the equations of motions follow from a least action principle. Its generalization to quantum field theories and the corresponding quantum equations of motion follow from a functional analog of the fundamental theorem of calculus, stating that the functional integral over a total derivative vanishes [11, 12]

$$0 = \int \mathcal{D}\Phi \frac{\delta}{\delta \Phi_i} e^{-S_R[\Phi] + (\mathbf{J}, \Phi)} = \int \mathcal{D}\Phi \left(-\frac{\delta S_R}{\delta \Phi_i} + \zeta_i \mathbf{J}_i \right) e^{-S_R[\Phi] + (\mathbf{J}, \Phi)} \equiv \left\langle -\frac{\delta S_R}{\delta \Phi_i} + \zeta_i \mathbf{J}_i \right\rangle_{\mathbf{J}}. \quad (28)$$

Here, the index i encompasses space, imaginary time, the discrete pseudo-spin index as well as the super-field component, see our definition above. Furthermore, ζ_i is a statistical factor, which is -1 for a fermionic source and $+1$ for a bosonic one, and the subscript \mathbf{J} at the functional average indicates that it has to be performed in the presence of the source fields. We can rewrite these expectation values as functional differential equations by replacing the Φ -dependence of $\frac{\delta S_R}{\delta \Phi_i}$ with their corresponding source-derivatives

$$\left(-\frac{\delta S_R}{\delta \Phi_i} \left[\frac{\delta}{\delta \mathbf{J}} \right] + \zeta_i \mathbf{J}_i \right) \mathcal{Z}_R[\mathbf{J}] = 0. \quad (29)$$

This set of equations is known as Schwinger-Dyson equations and they serve as master equations, which can be functionally differentiated to obtain an infinite hierarchy of coupled integral equations for the one-particle irreducible vertex functions.

To obtain such equations one has to switch to the connected functional $\mathcal{G}_R[\mathbf{J}] = \ln \mathcal{Z}_R[\mathbf{J}]$, and perform a Legendre transformation to the effective action $\mathcal{L}_R[\Phi] = -\mathcal{G}_R[\mathbf{J}] + (\mathbf{J}, \Phi)$. Here, the super-field vector Φ is the quantum expectation value $\Phi = \frac{\delta \mathcal{G}_R[\mathbf{J}]}{\delta \mathbf{J}}$ in the presence of the source fields \mathbf{J} . It shall not be confused with the integration variables in Eqs. (26) and (28). Following Ref. [12], we write $\mathcal{L}_R[\Phi] = S_0[\Phi] + \Gamma_R[\Phi]$, where $S_0[\Phi] \equiv \sum_{\alpha=1}^R S_{V=0}[\bar{\psi}^\alpha, \psi^\alpha] + \frac{1}{2} \int_{\vec{r}, \vec{r}'} V(\vec{r}) \mathcal{K}^{-1}(\vec{r} - \vec{r}') V(\vec{r}')$ is the bare quadratic action and $\Gamma_R[\Phi]$ is the generating functional of one-particle irreducible vertex functions, or vertex functional for short. As a result, we find the Schwinger-Dyson equations in the form

$$\frac{\delta \Gamma_R[\Phi]}{\delta \bar{\psi}_\sigma^\alpha(\vec{r}, \tau)} = V(\vec{r}) \psi_\sigma^\alpha(\vec{r}, \tau) + \frac{\delta^2 \mathcal{G}_R[\mathbf{J}]}{\delta J(\vec{r}) \delta \bar{\eta}_\sigma^\alpha(\vec{r}, \tau)}, \quad (30)$$

$$\frac{\delta \Gamma_R[\Phi]}{\delta \psi_\sigma^\alpha(\vec{r}, \tau)} = -\bar{\psi}_\sigma^\alpha(\vec{r}, \tau) V(\vec{r}) + \frac{\delta^2 \mathcal{G}_R[\mathbf{J}]}{\delta \eta_\sigma^\alpha(\vec{r}, \tau) \delta J(\vec{r})}, \quad (31)$$

$$\frac{\delta \Gamma_R[\Phi]}{\delta V(\vec{r})} = \sum_{\alpha=1}^R \sum_{\sigma} \int_{\tau} \bar{\psi}_\sigma^\alpha(\vec{r}, \tau) \psi_\sigma^\alpha(\vec{r}, \tau) - \sum_{\alpha=1}^R \sum_{\sigma} \int_{\tau} \frac{\delta^2 \mathcal{G}_R[\mathbf{J}]}{\delta \eta_\sigma^\alpha(\vec{r}, \tau) \delta \bar{\eta}_\sigma^\alpha(\vec{r}, \tau)}. \quad (32)$$

On the right hand side, the second functional derivatives of \mathcal{G}_R still have to be replaced by second functional derivatives of Γ_R , using the inversion relation between the Hesse matrices of \mathcal{G}_R and \mathcal{L}_R , see Refs. [12, 13]. This substitution eliminates the remaining source field dependence, but it leads to rather complex expressions. For this reason we leave the above equations in this compact mixed form. To obtain the infinite hierarchy of integral equations for the one-particle irreducible vertex functions as advertised above, one has to expand the vertex functional Γ_R in a Taylor series in terms of fields, insert the expression on the left and right hand sides and compare coefficients. Alternatively one may simply apply a corresponding amount of field derivatives $\frac{\delta}{\delta\Phi}$ to the above set of equations and set the sources \mathbf{J} to zero afterwards. When the sources \mathbf{J} are set to zero, the fields in Γ_R are set to their possibly finite expectation value $\Phi_c = \Phi|_{\mathbf{J}=0} = \frac{\delta\mathcal{G}[\mathbf{J}]}{\delta\mathbf{J}}|_{\mathbf{J}=0}$ [12]. (In the present case only the bosonic field may develop a finite expectation value.) In the Taylor expansion of Γ_R one should account for that fact by expanding around $\Phi = \Phi_c$, instead of $\Phi = 0$, such that the vertex functions are defined as field-derivatives of Γ_R evaluated at $\Phi = \Phi_c$.

The Schwinger-Dyson equation for the fermionic self-energy, which is defined by $\Sigma_{12} = -\delta^2\Gamma_R/\delta\bar{\psi}_1\delta\psi_2|_{\Phi=\Phi_c}$, may be obtained from Eq. (30) after applying the derivative $\frac{\delta}{\delta\bar{\psi}}$. A short calculation yields the following equation in Fourier space

$$\begin{aligned} \Sigma_{\sigma_1\sigma_2}^{\alpha\alpha}(i\omega, \vec{k}) &= \delta_{\sigma_1, \sigma_2} \mathcal{K}(0) \sum_{\beta=1}^R \sum_{\sigma} \int_{\vec{k}', \omega'} G_{\sigma\sigma}^{\beta\beta}(i\omega', \vec{k}') \\ &\quad - \sum_{\sigma} \int_{\vec{q}} F(\vec{q}) \frac{\delta^3\Gamma}{\delta\bar{\psi}_{\sigma_1}^{\alpha}(i\omega, \vec{k})\delta\psi_{\sigma}^{\alpha}(i\omega, \vec{k} + \vec{q})\delta V(-\vec{q})} \Big|_{\Phi=\Phi_c} G_{\sigma\sigma_2}^{\alpha\alpha}(i\omega, \vec{k} + \vec{q}), \end{aligned} \quad (33)$$

with $\int_{\vec{q}} = \int \frac{d^d q}{(2\pi)^d}$. The term in the first line, involving a closed fermion loop and the bare disorder propagator at vanishing momentum, is the Hartree contribution to the self-energy. It represents the influence of a finite expectation value of V on the fermions, and has been obtained by employing Eq. (32) at $\mathbf{J} = 0$. The term in the second line represents the Fock exchange self-energy, where the third derivative of Γ_R is the full Fermi-Bose three vertex. Furthermore, $G_{\sigma_1\sigma_2}^{\alpha\alpha}(i\omega, \vec{k})$ and $F(\vec{q})$ are the full fermionic and bosonic propagators, respectively. The former involves the fermionic self-energy, which makes Eq. (33) a self-consistency equation, while the latter involves the bosonic self-energy – polarization bubbles, for which there exists a separate equation, that derives from Eq. (32) after applying $\frac{\delta}{\delta V}$. We emphasize that the closed fermion loops in the Hartree term and the polarization bubbles are finite prior to taking the replica limit. They only vanish in the replica limit, which we will discuss at the end, see Sec. D. Anticipating the replica limit, Eq. (33) is depicted in Fig. 3(a).

C. Ward identity

According to Noether's theorem a continuous symmetry in a classical field theory leads to conservation laws. In a quantum field theory such symmetries lead to Ward identities, which connect various vertex functions to one another [12]. In the present case the fermions obey a global $U(1)^{\otimes R}$ symmetry, which formally expresses the fact that the particle number for each replica is conserved. To obtain a relation between different correlation functions we have to consider a local $U(1)^{\otimes R}$ symmetry transformation

$$\psi_{\sigma}^{\alpha}(\tau, \vec{r}) = e^{+iA^{\alpha}(\tau)} \psi'_{\sigma}{}^{\alpha}(\tau, \vec{r}), \quad \bar{\psi}_{\sigma}^{\alpha}(\tau, \vec{r}) = \bar{\psi}'_{\sigma}{}^{\alpha}(\tau, \vec{r}) e^{-iA^{\alpha}(\tau)}. \quad (34)$$

(Here, we took the phase field A^{α} to be local in imaginary time only. Spatial locality is not relevant, but could be incorporated without problems.) This transformation leads to an additional term in the action,

$$S_R[\bar{\psi}^{\alpha}, \psi^{\alpha}, V] = S_R[\bar{\psi}'^{\alpha}, \psi'{}^{\alpha}, V] + \sum_{\sigma} \int_{\vec{r}, \tau} \bar{\psi}'_{\sigma}{}^{\alpha}(\tau, \vec{r}) \{\partial_{\tau} iA^{\alpha}(\tau, \vec{r})\} \psi'_{\sigma}{}^{\alpha}(\tau, \vec{r}), \quad (35)$$

but it leaves the functional integral measure and the partition function itself invariant. As a consequence of the latter fact we obtain the following relation

$$0 = \int \mathcal{D}\Phi \left(e^{(\bar{\eta}, \psi) + (\bar{\psi}, \eta)} - e^{-\sum_{\sigma} \int_{\vec{r}, \tau} \bar{\psi}_{\sigma}^{\alpha}(\tau, \vec{r}) \{\partial_{\tau} iA^{\alpha}(\tau, \vec{r})\} \psi_{\sigma}^{\alpha}(\tau, \vec{r}) + (\bar{\eta}, e^{iA} \psi) + (\bar{\psi} e^{-iA}, \eta)} \right) e^{-S_R[\Phi] + (J, V)}. \quad (36)$$

Considering only an infinitesimal phase transformation this identity becomes

$$0 = \left\langle \sum_{\alpha=1}^R \sum_{\sigma} \int_{\vec{r}, \tau} \left(-\bar{\psi}_{\sigma}^{\alpha}(\tau, \vec{r}) \{\partial_{\tau} A^{\alpha}(\tau)\} \psi_{\sigma}^{\alpha}(\tau, \vec{r}) + \bar{\eta}_{\sigma}^{\alpha}(\tau, \vec{r}) A^{\alpha}(\tau) \psi_{\sigma}^{\alpha}(\tau, \vec{r}) - \bar{\psi}_{\sigma}^{\alpha}(\tau, \vec{r}) A^{\alpha}(\tau) \eta_{\sigma}^{\alpha}(\tau, \vec{r}) \right) \right\rangle_{\mathbf{J}}. \quad (37)$$

The phase field A^α may be eliminated entirely by taking the derivative $\frac{\delta}{\delta A^\alpha(\tau)}$. After performing a Fourier transform we find

$$0 = \left\langle \sum_{\sigma} \int_{\vec{k}, \omega} \left(i\nu \bar{\psi}_{\sigma}^{\alpha}(i\omega + i\nu, \vec{k}) \psi_{\sigma}^{\alpha}(i\omega, \vec{k}) + \bar{\eta}_{\sigma}^{\alpha}(i\omega + i\nu, \vec{k}) \psi_{\sigma}^{\alpha}(i\omega, \vec{k}) - \bar{\psi}_{\sigma}^{\alpha}(i\omega + i\nu, \vec{k}) \eta_{\sigma}^{\alpha}(i\omega, \vec{k}) \right) \right\rangle_{\mathbf{J}}. \quad (38)$$

Performing the same steps as in the previous section, that is, write the above equation as a functional differential equation for \mathcal{Z}_R , switch to \mathcal{G}_R and finally perform a Legendre transform, we find

$$\sum_{\sigma} \int_{\vec{k}, \omega} \left\{ i\nu \frac{\delta^2 \mathcal{G}_R[\mathbf{J}]}{\delta \eta_{\sigma}^{\alpha}(i\omega + i\nu, \vec{k}) \delta \bar{\eta}_{\sigma}^{\alpha}(i\omega, \vec{k})} + \frac{\delta \Gamma_R}{\delta \psi_{\sigma}^{\alpha}(i\omega + i\nu, \vec{k})} \psi_{\sigma}^{\alpha}(i\omega, \vec{k}) + \bar{\psi}_{\sigma}^{\alpha}(i\omega + i\nu, \vec{k}) \frac{\delta \Gamma_R}{\delta \bar{\psi}_{\sigma}^{\alpha}(i\omega, \vec{k})} \right\} = 0. \quad (39)$$

Once again, the second functional derivative of \mathcal{G}_R should be replaced by second functional derivatives of Γ_R . In analogy to the Schwinger-Dyson equations found above one may obtain the symmetry relations between different vertex functions by applying derivatives with respect to the fields.

Here, we want to obtain a relation between the fermionic self-energy and the Fermi-Bose three-vertex. To this end, we divide Eq. (39) by $i\nu$, sum over the replica index and apply the derivative $\delta^2 / \delta \bar{\psi}_{\sigma_1}^{\alpha}(i\omega + i\nu, \vec{k}) \delta \psi_{\sigma_2}^{\alpha}(i\omega, \vec{k})$. In the limit $\nu \rightarrow 0$, we find

$$\begin{aligned} & \frac{\delta^2}{\delta \bar{\psi}_{\sigma_1}^{\alpha}(i\omega + i\nu, \vec{k}) \delta \psi_{\sigma_2}^{\alpha}(i\omega, \vec{k})} \sum_{\beta=1}^R \sum_{\sigma} \int_{\vec{k}', \omega'} \frac{\delta^2 \mathcal{G}_R[\mathbf{J}]}{\delta \eta_{\sigma}^{\beta}(i\omega', \vec{k}') \delta \bar{\eta}_{\sigma}^{\beta}(i\omega', \vec{k}')} \\ &= \lim_{\nu \rightarrow 0} \frac{1}{i\nu} \left[\frac{\delta^2 \Gamma_R}{\delta \bar{\psi}_{\sigma_1}^{\alpha}(i\omega + i\nu, \vec{k}) \delta \psi_{\sigma_2}^{\alpha}(i\omega + i\nu, \vec{k})} - \frac{\delta^2 \Gamma_R}{\delta \bar{\psi}_{\sigma_1}^{\alpha}(i\omega, \vec{k}) \delta \psi_{\sigma_2}^{\alpha}(i\omega, \vec{k})} \right] + \dots \end{aligned} \quad (40)$$

The remaining terms, indicated as dots “...”, vanish after the sources have been set to zero. Next, we need to invoke the Fourier transformed bosonic Schwinger-Dyson equation (32) at vanishing boson momentum $\vec{q} = 0$ and insert it into the left hand side of Eq. (40) to replace the second functional derivative of \mathcal{G}_R . Finally, we set the source fields to zero, which yields the Ward-identity presented in Fig. 3(b) of the main text

$$\begin{aligned} & \left. \frac{\delta^3 \Gamma_R}{\delta \bar{\psi}_{\sigma_1}^{\alpha}(i\omega, \vec{k}) \delta \psi_{\sigma_2}^{\alpha}(i\omega, \vec{k}) \delta V(0)} \right|_{\Phi=\Phi_c} = \delta_{\sigma_1, \sigma_2} - \lim_{\nu \rightarrow 0} \frac{1}{i\nu} \left[\Sigma_{\sigma_1 \sigma_2}^{\alpha\alpha}(i\omega + i\nu, \vec{k}) - \Sigma_{\sigma_1 \sigma_2}^{\alpha\alpha}(i\omega, \vec{k}) \right] \\ &= \delta_{\sigma_1, \sigma_2} - \partial_{i\omega} \Sigma_{\sigma_1 \sigma_2}^{\alpha\alpha}(i\omega, \vec{k}). \end{aligned} \quad (41)$$

D. Replica limit

To make use of the Ward identity (41) within the Schwinger-Dyson equation (33), we have to make the crucial approximation

$$\left. \frac{\delta^3 \Gamma_R}{\delta \bar{\psi}_{\sigma_1}^{\alpha}(i\omega, \vec{k}) \delta \psi_{\sigma_2}^{\alpha}(i\omega, \vec{k} + \vec{q}) \delta V(-\vec{q})} \right|_{\Phi=\Phi_c} \longrightarrow \left. \frac{\delta^3 \Gamma_R}{\delta \bar{\psi}_{\sigma_1}^{\alpha}(i\omega, \vec{k}) \delta \psi_{\sigma_2}^{\alpha}(i\omega, \vec{k}) \delta V(0)} \right|_{\Phi=\Phi_c}, \quad (42)$$

whose range of validity has been discussed in the main text. Within this approximation the self-energy (33) becomes

$$\Sigma_{\sigma_1 \sigma_2}^{\alpha\alpha}(i\omega, \vec{k}) = \delta_{\sigma_1, \sigma_2} \mathcal{K}(0) \sum_{\beta=1}^R \sum_{\sigma} \int_{\vec{k}', \omega'} G_{\sigma\sigma}^{\beta\beta}(i\omega', \vec{k}') + \sum_{\sigma} \int_{\vec{q}} F(\vec{q}) \left[\delta_{\sigma_1, \sigma} - \partial_{i\omega} \Sigma_{\sigma_1 \sigma}^{\alpha\alpha}(i\omega, \vec{k}) \right] G_{\sigma\sigma_2}^{\alpha\alpha}(i\omega, \vec{k} + \vec{q}). \quad (43)$$

The physical self-energy is given by the replica limit $\Sigma = \lim_{R \rightarrow 0} \frac{1}{R} \sum_{\alpha=1}^R \Sigma^{\alpha\alpha}$. In this limit the Hartree term vanishes, since it comes with an excess factor of R . (Note that the Hartree self-energy for a single replica α already contains a summation over a replica index β , and thus is proportional to R .) Likewise, the bosonic self-energy, which involves internal fermion loops as well, vanishes, such that the full bosonic propagator $F(\vec{q})$ is replaced by the bare propagator $\mathcal{K}(\vec{q})$. Thus, we arrive at Eq. (3) of the main paper,

$$\Sigma_{\sigma_1 \sigma_2}(i\omega, \vec{k}) = \sum_{\sigma} \int_{\vec{q}} \mathcal{K}(\vec{q}) \left[\delta_{\sigma_1, \sigma} - \partial_{i\omega} \Sigma_{\sigma_1 \sigma}(i\omega, \vec{k}) \right] G_{\sigma\sigma_2}(i\omega, \vec{k} + \vec{q}). \quad (44)$$

Bibliography

- [1] H. Bruus and K. Flensberg, *Many-body quantum theory in condensed matter physics*. Oxford University Press, 2009.
- [2] K.-c. Chou, Z.-b. Su, B.-l. Hao, and L. Yu, “Equilibrium and Nonequilibrium Formalisms Made Unified,” *Phys. Rept.*, vol. 118, p. 1, 1985.
- [3] Altland, A. and Simons, B., *Condensed Matter Field Theory*. Cambridge University Press, 2010.
- [4] A. Kamenev, *Field Theory of Non-Equilibrium Systems*. Cambridge University Press, 2011.
- [5] G. Schwiete and A. M. Finkel’stein, “Keldysh approach to the renormalization group analysis of the disordered electron liquid,” *Phys. Rev. B*, vol. 89, p. 075437, Feb. 2014.
- [6] G. Schwiete and A. M. Finkel’stein, “Renormalization group analysis of thermal transport in the disordered Fermi liquid,” *Phys. Rev. B*, vol. 90, p. 155441, Oct. 2014.
- [7] D. Clément, A. F. Varón, J. A. Retter, L. Sanchez-Palencia, A. Aspect, and P. Bouyer, “Experimental study of the transport of coherent interacting matter-waves in a 1D random potential induced by laser speckle,” *New Journal of Physics*, vol. 8, no. 8, p. 165, 2006.
- [8] V. V. Volchkov, M. Pasek, V. Denechaud, M. Mukhtar, A. Aspect, D. Delande, and V. Josse, “Measurement of Spectral Functions of Ultracold Atoms in Disordered Potentials,” *Phys. Rev. Lett.*, vol. 120, p. 060404, Feb 2018.
- [9] J. Richard, L.-K. Lim, V. Denechaud, V. V. Volchkov, B. Lecoutre, M. Mukhtar, F. Jendrzejewski, A. Aspect, A. Signoles, L. Sanchez-Palencia, and V. Josse, “Elastic Scattering Time of Matter-Waves in Disordered Potentials,” *ArXiv e-prints*, Oct. 2018.
- [10] J. W. Goodman, *Speckle Phenomena in Optics: Theory and Applications*. Roberts and Company, 2007.
- [11] I. L. Aleiner and K. B. Efetov, “Effect of Disorder on Transport in Graphene,” *Physical Review Letters*, vol. 97, p. 236801, Dec. 2006.
- [12] P. M. Ostrovsky, I. V. Gornyi, and A. D. Mirlin, “Electron transport in disordered graphene,” *Phys. Rev. B*, vol. 74, p. 235443, Dec 2006.
- [13] E. McCann, K. Kechedzhi, V. I. Fal’ko, H. Suzuura, T. Ando, and B. L. Altshuler, “Weak-Localization Magnetoresistance and Valley Symmetry in Graphene,” *Phys. Rev. Lett.*, vol. 97, p. 146805, Oct 2006.

- [14] P. M. Ostrovsky, I. V. Gornyi, and A. D. Mirlin, “Quantum Criticality and Minimal Conductivity in Graphene with Long-Range Disorder,” *Physical Review Letters*, vol. 98, p. 256801, June 2007.
- [15] K. Kechedzhi, O. Kashuba, and V. I. Fal’ko, “Quantum kinetic equation and universal conductance fluctuations in graphene,” *Phys. Rev. B*, vol. 77, p. 193403, May 2008.

Chapter 6

Conclusions

In this thesis we dealt with two important aspects in the theory of Dirac fermions in graphene, Coulomb interactions and disorder. Both of them require the heavy machinery of nonperturbative quantum field theory, but for very different reasons. The fine-structure constant in graphene – the dimensionless interaction strength of the Coulomb interaction – depends on the background dielectric constant of the substrate/surrounding medium. In principle it can be made small, but the experimentally most relevant substrates yield a value for the fine structure constant of the order one. Even if one would be satisfied with a very limited set of substrates, for the sake of using perturbation theory, there are fundamental limitations to this technique. For one the asymptotic divergence of the perturbative series and for another the incapability of accounting for nonanalytic functions, such as $e^{1/\lambda}$, which frequently appear as solutions in more ambitious nonperturbative calculations. In disorder physics the standard field theory approach is already nonperturbative. The disorder induced fermionic self-energy and the collective transport modes (diffusons and cooperons) are typically calculated in the self-consistent Born approximation (SCBA), a resummation of all Feynman diagrams without crossing disorder lines. The crossing diagrams come with a dimensionless factor $1/k_F\ell$ compared to the non-crossing ones. For ordinary metals this parameter is indeed small, justifying such an approximation, but for graphene the Fermi momentum k_F vanishes at charge neutrality. Hence, the crossing diagrams cannot be neglected. The ultimate goal would be to combine these two branches of Dirac physics into a single theory. After all, taken individually neither of them is realistic, but to address the above problems properly, we considered the cases of Coulomb interactions and disorder separately.

In the first part of this thesis, starting with Coulomb interactions, we developed a nonperturbative framework to calculate the one-particle irreducible vertex functions in- and out-of-equilibrium by combining the functional renormalization group (fRG) with the Keldysh formalism. We obtained quantum kinetic equations and a hierarchical set of flow equations for the one-particle irreducible (1PI) vertex functions. We used this formalism for the important case of thermal equilibrium to calculate the renormalization of the Fermi velocity and static dielectric function at nodal point filling for several finite temperatures. This first application certainly shows the capabilities of the Keldysh-fRG, but its true potential, nonequilibrium physics, awaits to be explored. To extend our calculations to finite densities we explored a variation of the Keldysh-fRG, where the chemical potential is interpreted as a flow parameter. Although we formulated the Keldysh-fRG to deal with finite densities as well, one would have to repeatedly solve the entire set of flow equations for different values of the chemical potential, just like we did for different temperatures. Since only the end point of the flow – where the artificial infrared cutoff scale Λ is removed – is of physical relevance, this strategy is inefficient. In contrast to the

fRG in its standard formulation, the chemical-potential flow is physical. The hierarchical set of chemical-potential flow equations for 1PI vertex functions is structurally (almost) identical to the standard-fRG hierarchy, but their solution directly gives access to the chemical potential dependence of those vertices. In other words, it is not only the end point of the flow that matters, but the entire flow. Using this framework we calculated the chemical-potential dependence of the renormalized Fermi velocity and static dielectric function for different temperatures, admittedly in a rather crude truncation that leaves room for improvement.

Although we formulated the Keldysh-fRG in very general terms, allowing for external electromagnetic fields, possibly even time-dependent ones, the case of large static magnetic fields is somewhat problematic. Electrons confined to a two-dimensional plane and subjected to an external magnetic field form Landau levels, giving rise to the quantum Hall effect. Here, one has to distinguish the integer and the fractional quantum Hall effect. The former occurs whenever an integer number of Landau levels is occupied by electrons, whereas the latter occurs at certain partial fillings. The integer quantum Hall regime can be accessed directly and rather easily with the Keldysh-fRG in its current formulation, but the fractional quantum Hall effect requires correlations that are difficult to describe by the fRG. To be clear, the problem is not the fRG itself, but rather the low-level truncations that are typically employed to approximately solve the flow equations. They simply do not account for the nontrivial correlations necessary to access the fractional quantum Hall regime. For this reason we considered a modified field theory, where these correlations are implemented “by hand” via a Chern-Simons gauge field. Of course, one could immediately apply the full machinery of the fRG for such a modified field theory, but it is advisable to perform a perturbative analysis first. Recall, that the exact fRG flow equation has a one-loop structure, so the features of one-loop perturbation theory are a good starting point to develop some physical intuition. For this reason we analyzed this modified field theory in a stationary phase approximation with Gaussian fluctuations and we calculated the electromagnetic response tensor as well as the Hall conductivities. Although first interesting results have been obtained, the analysis has actually just started, as a plenitude of questions remained unanswered. Therefore, we propose the following research program: First, calculate the spectrum of collective excitations, which can be done immediately by analyzing the poles of the response tensor given in the paper. Next, a perturbative treatment of the composite fermion self-energy is in order. To this end, one may either go beyond the Gaussian fluctuations considered in the paper, or one may avoid integrating fermions in the first place. The latter strategy would yield a Fermi-Bose theory similar to the one we considered in Secs. 4.1 and 4.2. Once such a perturbative analysis is complete, one can think about setting up a full nonperturbative treatment, either via Schwinger-Dyson equations or the fRG. With the one-loop calculations as a proper guideline, this construction should be straightforward. And finally it would be desirable to get rid of the Chern-Simons field altogether. This last part certainly requires creativity, as the standard vertex expansion of the effective action without Chern-Simons fields, combined with the typical low-level truncation schemes is just incapable of describing the fractional quantum Hall regime. A particularly interesting option would be to explore another variant of the fRG, where the magnetic field is interpreted as a flow parameter. Similar to the chemical potential flow, such a framework requires nontrivial input at the initial point of the flow. However, if a large magnetic field is chosen as the starting point of the flow one already knows a good candidate groundstate, the Laughlin wavefunction, with respect to which the initial vertices can be calculated.

In the second part of this thesis we considered disordered Dirac fermions in the absence of two-particle interactions. In a first project we considered an explicit experimental scenario, a graphene pn junction in a quantizing magnetic field perpendicular to the sheet. In particular,

we focussed on the chiral modes that are propagating along the junction interface, for which we derived an effective one-dimensional model and calculated the effect of bulk disorder on the interface states. We avoided the problems of the field theory approach – most notably the necessity to treat crossing and non-crossing diagrams on equal footing – by analyzing this model in a scattering matrix approach. We obtained a Fokker-Planck equation for the probability distribution of the scattering angles of the parametrized scattering matrix, with the length of the scattering region as the evolution parameter. Remarkably, this differential equation could be solved exactly, resulting in an exact calculation of the conductance distribution in the crossover between the clean and strong disorder limits. Unfortunately, however, the predictions of our simple model are not consistent with the current experiments, requiring some modification of the model itself. One possibility to resolve this mismatch is to include two-particle interactions. In one spatial dimension a large class of interacting models can be solved exactly by a very powerful method called (operator) bosonization. Here the fermionic Hilbert space is transformed into a bosonic one and the interacting fermionic Hamiltonian is transformed into a noninteracting bosonic Hamiltonian. As soon as disorder is taken into account even this method reaches its limits, since the bosonic Hamiltonian would no longer be quadratic in the boson fields. Instead, it is of a sine-Gordon form with a nonpolynomial interaction term. In the present case of co-propagating chiral modes, however, it is possible to “gauge away” the disorder field before performing the boson transformation. This way one can solve certain classes of interactions analytically exactly and reintroduce the effect of disorder by reverting the gauge transformation once the gauged correlation functions have been obtained. Regarding such a research program, at the time of this writing there is already work in progress and we obtained first results, but it is an open question how to perform the disorder average at the end of the calculation.

Finally, we presented a manuscript for a paper, where we investigated the disorder problem for Dirac fermions in graphene and other nodal semimetals (for instance Weyl semimetals, the three-dimensional analog of graphene) by field theoretical methods. The main problem in such a framework is to find a strategy that goes beyond the already-nonperturbative SCBA in a consistent and systematic way. By combining the Schwinger-Dyson equation for the fermionic self-energy with a Ward identity, we were able to eliminate the three-vertex approximately and obtain a closed equation for the self-energy. Solving this equation and comparing the results to exact reference data obtained by the kernel polynomial method we could show that our approach is applicable for intermediate to large disorder strengths, which makes it complementary to the Wilson RG. The latter method only works for weak disorder reliably. Admittedly, we were only able to incorporate band-diagonal disorder so far, but the spinor structure of two-band models allows for more general types of disorder scattering processes. One possible extension of our approach concerns those disorder types with non-trivial Pauli matrix structure. Another interesting research direction is the extension of our calculations to higher level vertex functions, which should not only improve our results for the self-energy in the weak disorder regime but also give access to collective transport modes. Both of these extensions should be straightforward to implement, but especially the latter project requires substantially more numerical effort as a higher level truncation yields rather complex equations with nontrivial momentum and frequency structures for the vertices.



Acknowledgements

On this page I want to express my deep gratitude to all the people who accompanied and supported me within these eventful past years.

First and foremost I would like to express my sincere gratitude to Prof. Dr. Piet W. Brouwer for giving me the opportunity to be a part of his group, his continuous support, encouragement and shared insights. I enjoyed an exceptional amount of freedom to explore different areas of research, pursue my own ideas and come up with research projects that define me as a scientist. It was because of this freedom and the trust he showed towards me that I could become the scientist I am right now and I will be forever thankful for that.

A special thanks goes to Prof. Dr. Georg Schwiete as the supervisor of my Master thesis for the plenitude of discussions, his patience and his guidance back in the day. He always pushed me further and was probably my most influential and demanding teacher.

I want to thank especially my long term office mate and good friend Jörg Behrmann not only for discussions, help in typesetting and proofreading of this thesis, but mostly for his moral support and all the fun and fights we had in the last few years. I cannot think of a better office mate than him. In the same breath I want to thank Maria Laura Baez, who became a dear friend during the time of the PhD and was to a great extent responsible for my sanity.

Furthermore, I want to say thank you to all members of the group and my collaborators, most importantly Johannes Mosig and Björn Sbierski. I enjoyed the plenitude of discussions and the great experience of working together.

Lastly, I want to thank my family and friends. Their support and encouragement was and is invaluable for me and a few words by far cannot express my gratitude. A special thanks goes to my girlfriend Natascha. She stood by me for a long time now with love, support and encouragement. Her good spirit cheered me up in hard times and stimulated me to keep going.



Curriculum Vitae

For reasons of data protection,
the curriculum vitae is not included in the online version of this thesis.

For reasons of data protection,
the curriculum vitae is not included in the online version of this thesis.

For reasons of data protection,
the curriculum vitae is not included in the online version of this thesis.



Selbstständigkeitserklärung

Ich, Christian Fräßdorf, erkläre hiermit, dass die vorliegende Dissertation mit dem Titel “Field Theories of Interacting and Disordered Dirac Fermions in Graphene” und die darin präsentierte Arbeit selbstständig verfasst wurde. Darüber hinaus werden folgende Punkte bestätigt:

- Diese Arbeit wurde angefertigt zur Erlangung des akademischen Grades eines Doktors der Naturwissenschaften auf Grundlage eines Promotionsverfahrens entsprechend der Promotionsordnung vom 2. September 2013 an der Freien Universität Berlin.
- Diese Dissertation wurde in keinem früheren Promotionsverfahren oder zur Erlangung irgendeines anderen akademischen Grades bereits angenommen oder als ungenügend beurteilt, weder an dieser Universität noch an irgendeiner anderen Institution.
- Die publizierte Arbeit Dritter, die ich während der Anfertigung dieser Dissertation konsultiert habe, ist deutlich gekennzeichnet.
- Die Quelle von Zitaten aus der Arbeit Dritter ist stets angegeben. Mit Ausnahme solcher Zitate beruht diese Dissertation vollständig auf meiner eigenen Arbeit.
- Alle Hilfsmittel und Hilfen sind angegeben.
- Die Publikationen auf denen diese Dissertation beruht sind unten aufgeführt. In denjenigen Publikationen, die in Zusammenarbeit mit anderen Wissenschaftlern entstanden sind, wird mein individueller Anteil bei Konzeption, Durchführung und Berichtabfassung dargestellt.

Berlin, 22. November 2018

Christian Fräßdorf